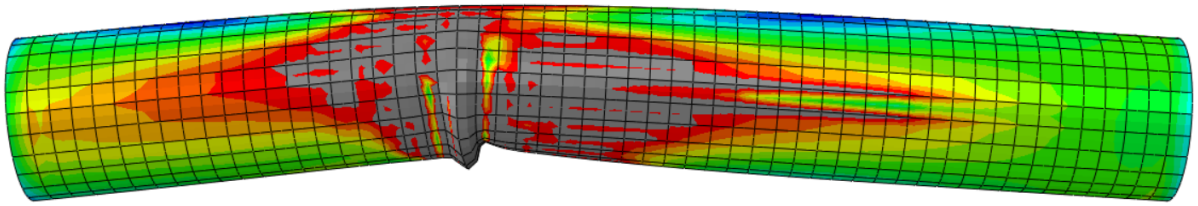

Interactive Buckling and Design Evaluation of Circular Hollow Sections

Assessment of Design Guidelines and Buckling Mode Interaction Through Numerical Analysis and Parametric Study of Buckling Resistance of Circular Hollow Steel Sections

Master's thesis in Structural Engineering & Building Technology

Sebastian Knutsson

Hossein Nabavi

Department of Architecture and Civil Engineering

CHALMERS UNIVERSITY OF TECHNOLOGY
Gothenburg, Sweden 2025
www.chalmers.se

Master's thesis 2025

Interactive Buckling and Design Evaluation of Circular Hollow Sections

Assessment of Design Guidelines and Buckling Mode Interaction Through Numerical Analysis and Parametric Study of Buckling Resistance of Circular Hollow Steel Sections

Sebastian Knutsson
Hossein Nabavi

CHALMERS
UNIVERSITY OF TECHNOLOGY

Department of Architecture and Civil Engineering
Division of Structural Engineering
Research Group of Lightweight Structures
Chalmers University of Technology
Gothenburg, Sweden 2025

Interactive Buckling and Design Evaluation of Circular Hollow Sections

Assessment of Design Guidelines and Buckling Mode Interaction Through Numerical Analysis and Parametric Study of Buckling Resistance of Circular Hollow Steel Sections

Sebastian Knutsson
Hossein Nabavi

Supervisor: Jincheng Yang, Experienced Structural Engineer ,WSP
Supervisor: Fatima Hlal, Doctoral Student, Department of Architecture and Civil Engineering
Examiner: Mohammad al-Emrani, Full professor, Department of Architecture and Civil Engineering

Master's Thesis 2025
Department of Architecture and Civil Engineering
Division of Structural Engineering
Research group of Lightweight Structures
Chalmers University of Technology
SE-412 96 Gothenburg
Telephone +46 31 772 1000

Cover: Visualisation of interactive buckling failure mode created in Abaqus of a circular hollow steel section loaded in axial compression.

Typeset in LaTeX
Printed by Chalmers Reproservice
Gothenburg, Sweden 2025

Interactive Buckling and Design Evaluation of Circular Hollow Sections
Assessment of Design Guidelines and Buckling Mode Interaction Through Numerical Analysis and Parametric Study of Buckling Resistance of Circular Hollow Steel Sections
Sebastian Knutsson
Hossein Nabavi
Department of Architecture and Civil Engineering
Chalmers University of Technology

Abstract

This master's thesis investigates the behaviour of circular hollow section (CHS) in steel under axial loading. Particular emphasis is placed on how the interaction between global and local buckling modes affects member strength. The objective was to complement and compare how current design guidelines assess these sections against the obtained results.

To fulfil the aim, the work began with a literature review to deepen understanding of the subject. This was followed by the development and validation of an FE-model capable of replicating buckling behaviour observed in previous studies. A subsequent parametric study was conducted, covering geometries and parameters relevant for a comprehensive perspective on CHS buckling behaviour.

The parametric study results, compared with design guidelines, show that current methods create issues for CHS classified as CSC 4. These are treated as shell structures, although their behaviour resembles columns, leading to unsafe and inefficient design. To improve accuracy, an effective area method and a local buckling reduction factor from the British steel design standard (BS5950-1) and a study by Toffolon and Taras (2017) were investigated. These methods aligned more closely with results and provided safer, more efficient CSC 4 designs.
In addition, the interaction between global and local buckling was studied. In columns showing interactive failure, ultimate load was reduced by 8 % compared to columns with only local modes, despite nearly identical geometry. Two parameters were identified for determining the transition from interactive to fully local buckling: L' which is defined as $L' = \sqrt{\frac{l^2 t}{r^3}}$ and $\frac{N_{cr,global}}{N_{cr,local}}$.

The major conclusions were: (i) current guidelines result in unsafe and inefficient design for CHS in CSC 4, and an effective area method, similar to the one established in the British standard, eliminate unsafe design but show conservative results for the reduction factor stated; and (ii) interactive buckling reduces buckling resistance of CHS of up to 8 % and thusly should be considered in design.

Keywords: Circular hollow section, interactive buckling, global buckling, local buckling, mode interaction, $\frac{D}{t}$-ratio, slenderness ratio, imperfections, parametric study.

Interaktiv knäckning och Designutvärdering av Cirkulära Ihåliga Ståltvärsnitt
Bedömning av Designriktlinjer och Knäckningsmodinteraktion Genom Numerisk Analys och Parametrisk Studie av Knäckningshållfasthet hos Cirkulärt Ihåliga Ståltvärsnitt
Sebastian Knutsson
Hossein Nabavi
Avdelningen för Arkitektur och Samhällsbyggnadsteknik
Chalmers Tekniska Högskola

Sammanfattning

Denna masteruppsats syftar till att ingående undersöka hur cirkulära ihåliga ståltvärsnitt (CHS) beter sig när dem blir belastade axiellt. Där emfas har lagts vid hur modinteraktionen mellan globala och lokala knäckningsmoder påverkar hållfastheten av dessa tvärsnitt. Ur detta var målet att komplettera och jämföra hur de nuvarande designriktlinjerna dimensionerar dessa tvärsnitt mot resultaten.
För att uppfylla syftet med denna masteruppsatsen började arbetet med en litteraturstudie för att fördjupa kunskapen i området. Detta efterföljdes av utvecklingen av en FE-modell som kunde efterlikna knäckningsbeteendet av andra studier följt av en parametrisk studie som täckte de geometrier och parametrar som var av relevans för att få ett helhetsperspektiv av knäckningsbeteendet för dessa stålrör.

Resultaten av den parametriska studien i jämförelse med designriktlinjerna visar att den nuvarande designmetoden skapar problem för stålrör i tvärsnittsklass 4 då dessa betraktas som en skalstruktur medan deras beteende liknas vid en pelare. Detta ledde till både över- och underdimensionering av stålrören. För att hitta en bättre metod undersöktes en effektiv area-metod och en lokal knäckningsreduktionsfaktor från Brittiska standarden för stålbyggnad (BS5950-1) och en studie av Toffolon and Taras (2017). Dessa två designmetoder överensstämde bättre med resultaten och gav både säkrare och mer effektiv dimensionering av stålrör i tvärsnittsklass 4.
Utöver detta lades fokus vid att undersöka modinteraktionen mellan global och lokal knäckning. Här påvisades det att i pelare med interaktiv brottmod sänktes den ultimata lasten med omkring 8 % jämfört med en pelare med enbart lokala moder även om geometrin för tvärsnittet var i princip likadan. Ur detta identifierades två parametrar som kan användas för att avgöra övergången från interaktivt till helt lokalt knäckningsbeteende - L' & $\frac{N_{cr,global}}{N_{cr,lokal}}$.

De viktigaste slutsaterna som kunde dras var: (i) De nuvarande designriktlinjerna tenderar att överskatta knäckhållfastheten av CHS i tvärsnittsklass 4 och en effektiv area-metod, likt den i brittiska standarden, eliminerar denna överskattning av knäckhållfastheten men ger konservativ design med reduktionsfaktorn som undersöktes, och (ii) interaktiv knäckning sänker knäckhållfastheten av CHS med upp till 8 % vilket gör att detta bör beaktas i design.

Nyckelord: Cirkulärt ihåligt tvärsnitt, interaktiv knäckning, global knäckning, lokal knäckning, modinteraktion, $\frac{D}{t}$-förhållande, slankhetstal, defekter, parametrisk studie.

Acknowledgements

This master's thesis represents the outcome of six months of work and marks the completion of a Master of Science degree in Structural Engineering. The project was carried out through a collaboration between the Department of Architecture and Civil Engineering at Chalmers University of Technology and the Bridge Department at WSP in Gothenburg. The work took place between January and June 2025 under the guidance of experienced structural engineer Jincheng Yang, doctoral student Fatima Hlal, and Professor Mohammad Al-Emrani.

We would like to express our sincere gratitude to our supervisor at WSP, Jincheng Yang, for his continuous guidance, support, and for generously sharing his extensive knowledge and experience throughout the project. It was truly a privilege to work under your supervision.

We are also deeply thankful to Fatima Hlal, whose support during Jincheng's absence and throughout the entire process specially programming which was invaluable.

A special thanks goes to our examiner, Professor Mohammad Al-Emrani, for his expert insights into steel structures and his helpful advice. It has been an honor to have your involvement in this work.

Finally, we would like to thank WSP for accepting and supporting this project, and for providing access to the necessary computer and software resources.

Sebastian Knutsson & Hossein Nabavi, Gothenburg, June 2025

List of Acronyms

BS5950-1	British standards: Structural use of steelwork in building. Part 1, Code of practice for design: rolled and welded sections.
CHS	Circular Hollow Section
CSC	Cross-section class
EC3	Eurocode 3
EN1993-1-1	Eurocode 3: Design of steel structures - Part 1-1: General rules and rules for buildings
EN1993-1-6	Eurocode 3: Design of steel structures - Part 1-6: Strength and stability of shell structures
EN1993-1-14	Eurocode 3: Design of steel structures - Part 1-14: Design assisted by finite element analysis
FE	Finite Element
FEM	Finite Element Method
GMNIA	Geometrical and Material Nonlinear Imperfection Analysis
LEA	Linear Elastic Analysis
OIC	Overall Interaction Concept
RHS	Rectangular Hollow Section

List of Symbols

Roman Upper-Case Letters

A	Cross-sectional area
A_{eff}	Effective cross-sectional area
C	Parameter in the formula for elastic critical meridional buckling stress
D	Diameter
E	Modulus of elasticity
I	Moment of inertia
L	Length
L_e	Effective length
L_{cr}	Critical buckling length
N	Load
N_{cr}	Critical buckling load
$N_{cr,G}$	Critical global buckling load
$N_{cr,L}$	Critical local buckling load
N_{Rd}	Design resistance
N_u	Ultimate load
P	Load
P_{cr}	Critical load
Q	Fabrication quality parameter

Roman Lower-Case Letters

b	Width
e_g	Global imperfection amplitude
e_l	Local imperfection amplitude

f_y	Yield strength
f_u	Ultimate tensile strength
r	Radius
t	Thickness

Greek Letters

ν	Poisson's ratio
ϕ	A parameter in the formula for the global buckling reduction factor
ψ	A parameter in the formula for the global buckling reduction factor
χ	Global buckling reduction factor
$\chi_{glob,gr}$	Global reduction factor including the effect of local buckling
$\chi_{x,loc}$	Local buckling reduction factor
ϵ	Strain
ϵ_y	Yield strain
ϵ_{true}	True strain
ϵ_u	Ultimate strain
ϵ_{sh}	Strain hardening strain
λ	Slenderness ratio
λ_m	Member slenderness ratio
λ_n	Non-dimensional slenderness ratio
λ_p	Plastic limit relative slenderness
λ_0	Meridional squash limit slenderness
σ	Stress
σ_{Rd}	Design buckling stress
σ_{Rk}	Characteristic buckling stress
σ_{cr}	Critical stress
σ_{true}	True stress
σ_{yield}	Yield stress
ω	Dimensionless length parameter

Contents

List of Figures

List of Tables

1
Introduction

Steel is widely used in various structural applications including buildings, towers, and bridges due to its high strength-to-weight ratio (Khalaf et al., 2022). Among the different steel profiles, circular hollow sections (CHS) are commonly employed in columns, trusses, and other load-bearing elements because of their geometric efficiency. However, the shape of this type of steel complicates the design, especially when local buckling occurs, requiring careful attention in the design process. This chapter will introduce the problem description regarding this and the approach used to deepen the knowledge regarding buckling in CHS members.

1.1 Background

The building industry moves towards reducing its carbon footprint in all aspects and particularly the use of steel as it has a energy demanding production phase. A crucial part of this is to optimise steel structures and that as little material is used as possible while maintaining the structural integrity of the finished building (Sizirici, Fseha, Cho, Yildiz, & Byon, 2021).
To implement an effective use of material in steel structures circular hollow sections (CHS) are widely used in civil engineering as trusses, beams, and columns due to its structural efficiency (Khalaf et al., 2022). However, a crucial gap in the design guidelines regarding CHS members have been identified. Steel members which are exposed to compressive stresses are divided into four different cross-section classes (CSC) depending on its slenderness ratio (ratio of diameter to wall thickness). Each class determines the risk of local buckling in a cross-section before it is loaded to its plastic rotation capacity (Al-Emrani, 2023). Each cross-section class can be predicted to have the following behaviour before local buckling is expected:

- CSC 1: Reaches full plastic behaviour and strain hardening.
- CSC 2: Reaches full plastic behaviour but no strain hardening.
- CSC 3: Reaches plastic limit but has no plastic behaviour.
- CSC 4: Local buckling before reaching the plastic capacity.

To account for the reduced buckling resistance of cross-sections in CSC 4 the usual design method uses a reduced effective area to accurately predict how these will behave. The design guidelines in EN1993-1-1 (CEN, 2005) cover how to design CHS members up to CSC 3 but for CSC 4 there is no design method fully adapted to CHS members established.
For cross-sections which are in the grey area between CSC 3 & 4 the lower limit of the global buckling resistance interacts with the local limit. This creates an overall

buckling resistance of the cross-section which is lower than each of the theoretical limits through mode interaction (Pignataro, 2005).
To enable the optimisation of steel structures and to further utilise the use of slender members a comprehensive design guide on CHS members in CSC 4 needs to be established as well as an insight into how mode interaction between local and global affect the buckling resistance of these members.

1.2 Aim and objectives

This thesis aims to thoroughly examine how CHS members with a large slenderness ratio behave when compressionally loaded. Emphasis will be put on how local buckling together with global buckling plays a crucial part in the overall buckling resistance of these members. Out of this it is expected that the current design guidelines will be complemented and allow for a comprehensive guide on how to dimension CHS members in the future.

To put this into a practical approach the following parts will be conducted:

- Create FE-models of axially loaded CHS members using Abaqus to simulate their buckling behaviour under critical load conditions.
- Conduct a parametric analysis to generate buckling resistances by varying cross-sectional parameters covering all different spectrums of buckling behaviour.
- Compare the FE-results with current design guidelines provided in relevant standards and alternative methods.
- Investigate impact of mode interaction between local and global buckling modes on buckling resistance and identify parameters which could be used for determining what behaviour is expected.
- Out of this, provide recommendations that can be incorporated into engineering design practices.

1.3 Methodology

To complement the current guidelines and create a design method valid for all CHS members the investigation will start with a state-of-the-art study which include:

- Thorough investigation of the current guidelines to identify the exact gaps that need to be covered in this thesis.
- Study similar investigations to not cover topics that have already been covered or complement studies that are investigating similar topics.
- Study material behaviour and geometrical imperfections to identify a relevant material model.
- Study the global and local mode interactions impact on the buckling resistance of CHS members.

After this a numerical analysis will be conducted which simulate the buckling behaviour of CHS members in critical load conditions and a parametric study which

generate resistance curves as a function of slenderness ratio. The numerical analysis consist of:

- Establish a FE-model in Abaqus which simulate the buckling behaviour of CHS members accurately.
- Validate FE-model against other experimental and numerical studies to check its accuracy.
- Develop a Python-script which makes the relevant parameters easy parametrise.
- Conduct a parametric study which cover the different buckling behaviours of CHS members.
- Compare the results of the parametric study with relevant design guidelines and investigate how mode interaction affect the buckling resistance of CHS members.

1.4 Limitations

The project is limited to considering only closed sections with a circular hollow shape, excluding other section types from the scope of interest. However, sections with a square and rectangular hollow shape will be used as a basis to set the expected behaviour since similar results can be expected in CHS members as well as there is more data and theoretical approaches are available for these.
Additionally, the project focuses on one specific material type, hot-rolled steel with a yield strength of $f_y = 355\ MPa$ and ultimate strength of $f_u = 510\ MPa$. This may limit the applicability of the results to only this material type but since the resources and time is limited the validation of other steel qualities and production types are out of the scope of this thesis.
Furthermore the study is considering only one specific loading type — axial compression — while excluding other conditions such as bending, torsion, or their combinations. This means that only global flexural and local buckling are the two types of buckling that can occur and the other types are out of the scope of this thesis.
Additionally, the effects of residual stresses will not be investigated individually but be included by a equivalent imperfection factor, this is presented more thoroughly in Section 3.5.
Lastly, the effects of temperature are not included in the analysis, assuming that temperature fluctuations are within the normal range giving no impact on the results.

1.5 Social, ethical and ecological aspects

The project primarily focuses on the buckling behaviour of CHS members, with social, ecological, and ethical aspects excluded from the main scope of the study. However, all of these are interconnected to the aim of the thesis in making the design of building members more efficient. A more efficient design reduce the material used in the construction process, lowering the climate impact and cost of a finished building which regard all of the aspects mentioned in the end.

2
Literature study

This chapter will present the relevant fundamental information regarding steel as a material together with the basic theory of buckling as a phenomena. Furthermore, the behaviour of real columns in general will be studied, narrowing in on the interaction between global and local buckling modes in CHS members in particular. Continuing on how the current design guidelines handle the problem of mode interaction in CHS members together with the current work that has been conducted on interactive buckling in box sections and CHS members in particular.

2.1 Hollow sections in civil engineering

Hollow structural steel sections is one of the most widely used elements in civil engineering (*Steel Tube Institute*, n.d.). They have a high radius of gyration around all axes which provide exceptional structural efficiency even with thin sections because of their high compressional resistance allowing for weight reduction and thus economical and environmental gains. Closed sections are not susceptible to torsional deformation meaning that they are favourable when resisting torsional loads (Al-Emrani, 2023). Because of hollow sections having closed sections and polished surfaces they are regarded as having an architecturally pleasing appeal and are often favoured to be used when the structural elements need to be exposed (*Steel Tube Institute*, n.d.).

Steel is an alloy which mainly consists of carbon and iron together with other alloying elements depending on the desired material properties which make it a versatile material (*NE.se*, n.d.-a). Its manufacturing cost is low and it has a very high tensile and compressional strength. Because of this structural steel has become one of the most important materials in the world. (*NE.se*, n.d.-b). Structural steel normally has a elastic modulus, E of 200 GPa, and normal strength steel has a yield strength, f_y, between $200 - 460$ MPa, while high strength steel can have a yield strength, f_y, of up to 1300 MPa according to EN1993-1-1 (CEN, 2005).

There are two common production types of steel - hot rolled and cold formed. Hot rolled steel means that the steel is heated up to a certain temperature to allow for easy forming of the steel into desired shape as well its material properties are improved (*NE.se*, n.d.-c). During the production of hot rolled steel the casting structure is changed and the material recrystallises and the grain size decreases. The outcome is a stronger material which is more ductile. Cold formed steel is hot rolled steel which have gone through an additional forming process (*NE.se*, n.d.-d). It is re-rolled at cold temperatures which allow for a much finer finished surface and more exact finished geometries. The cold forming process also makes the steel more brittle in the end.

2.2 Theory of buckling

The buckling instability phenomenon refers to significant deformation in a structural member due to a small increase in load (Vellaichamy, Kumarasamy, S K, & Veerasamy, 2019). In other words, failure can occur before the material reaches its ultimate compressive strength, classifying buckling as elastic instability. This phenomenon arises due to geometrical instability, primarily affecting compressed members, and the strength of such members depends on their slenderness ratio. According to Vellaichamy et al. (2019) buckling loads are proportioned with the modulus of elasticity, thickness, outer to inner radius ratio and all the column geometry parameters but not the column length.
When a structural element is subjected to compressive loading and undergoes buckling, it can deform into distinct patterns. These patterns are known as buckling modes (Timoshenko & Gere, 2012). The first buckling mode corresponds to the lowest critical load, meaning it requires the least amount of energy for the structure to become unstable. In contrast, higher-order buckling modes exhibit more complex geometries and are associated with higher critical loads. In finite element method (FEM) software, buckling modes are typically represented as eigenmodes derived from an eigenvalue problem (*ABAQUS User Manual*, n.d.-a).
Buckling failure can be categorized into local buckling, global buckling and interactive buckling (Pignataro, 2005). According to Gambhir (2004), the onset of structural instability depends on stiffness rather than material strength. Furthermore, he stated that instability can be prevented by maintaining equilibrium, which is defined as a structure's ability to remain in position and support the applied load even when slightly displaced from its original position. Figure 2.1 shows load versus deformation of axially loaded column where it can be seen that the deformation occurs before ultimate strength.

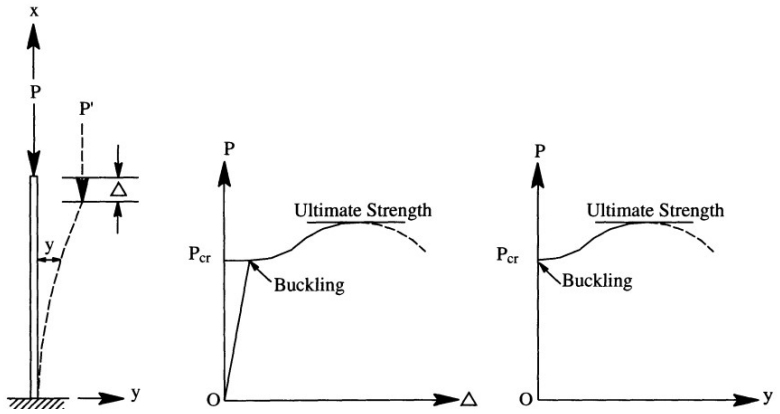

Figure 2.1: Load versus deformation curve in axially loaded column.

Source: (Gambhir, 2004)

In structural stability analysis, a member follows a primary equilibrium path until it reaches a critical load, P_{cr} (Jerath, 2020). Before this point the member returns to it's original shape. Beyond this point, the structure may either continue along the primary path or deviate to a secondary path due to small perturbations. The point

at which this transition occurs is known as the bifurcation point. Different types of bifurcation arise depending on the post-buckling response. In symmetric stable bifurcation, the structure remains stable and continues to carry additional load after buckling. In contrast, symmetric unstable bifurcation leads to a loss of stability as the load-carrying capacity decreases with increasing deflection. Additionally, asymmetric bifurcation occurs when the post-buckling behaviour varies depending on the buckling direction. Jerath (2020) also emphasized that in structural design, instability is primarily governed by the stiffness of the structure rather than the material strength. Figure 2.2 shows bifurcation equilibrium path and the critical load.

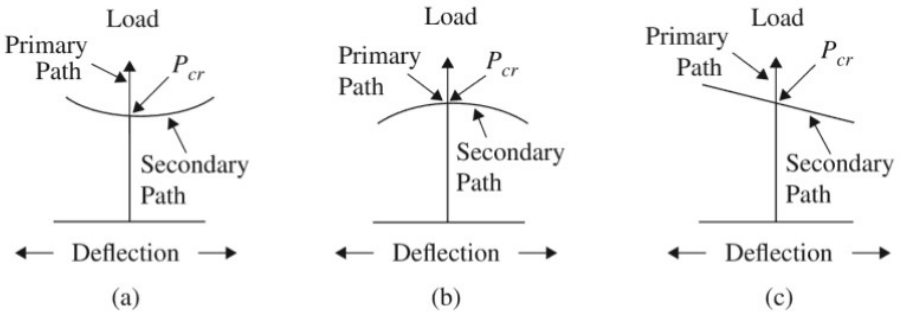

Figure 2.2: Bifurcation equilibrium paths: (a) Symmetric stable bifurcation; (b) Symmetric unstable bifurcation; (c) Asymmetric bifurcation.

Source: (Jerath, 2020)

2.2.1 Local buckling

Local buckling is a local displacement of a structure under load where the member exert lateral displacements locally with significant changes in cross-section geometry. The member as a whole does not necessarily exert any lateral displacement. In steel structures, local buckling occurs due to the instability of thin plate elements under compression (Davison & W. Owens, 2003). This phenomenon is more critical in cold-formed steel than in hot-rolled steel, as cold-formed sections tend to have thinner plates for material efficiency. The occurrence of local buckling depends on the section classification. Figure 2.3 shows local buckling of a CHS member.

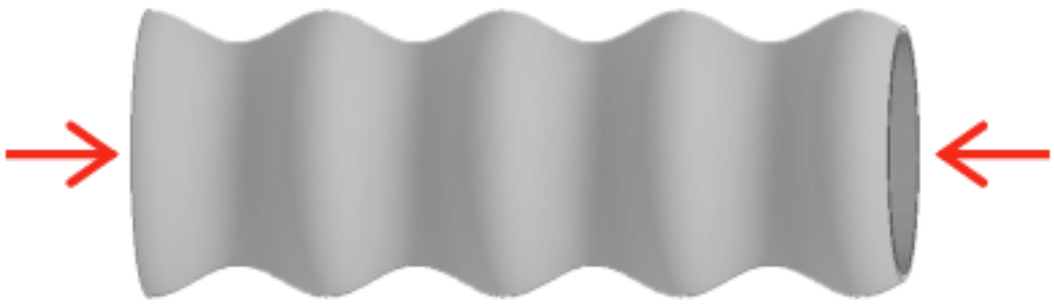

Figure 2.3: Local buckling failure mode of CHS member.

Source: (Bhaga & Steeves, 2018)

For compact sections, local buckling develops only after the section has reached its full cross-sectional capacity, meaning it does not significantly reduce strength. In contrast, for non-compact sections, local buckling occurs before the section reaches its full moment resistance, limiting its load-carrying capacity. Al-Emrani (2023) emphasizes that the width-to-thickness (b/t) ratio is a key factor in determining a section's susceptibility to local buckling. Furthermore, Gambhir (2004) states that built-up sections have lower capacity compared to plate sections. This is primarily due to two factors. First, the strength of built-up columns is highly dependent on the edge conditions along the length of their individual elements. Second, plates exhibit superior post-buckling performance, as they can redistribute stresses more effectively at the critical load, thereby maintaining greater load-carrying capacity after initial buckling.

2.2.2 Global buckling

Global buckling is the overall displacement of a structure under load where the whole member exert lateral displacement without any significant changes in cross-section geometry, as illustrated in Figure 2.4.

Figure 2.4: Global buckling failure mode of a CHS member.

Source: (Bhaga & Steeves, 2018)

According to Silva, Simões, and Gervásio (2014) global analysis must incorporate geometrical and material imperfections, such as residual stresses, lack of verticality, and member straightness deviations. These imperfections are represented using equivalent geometric imperfections which takes all the imperfections into account according to EN1993-1-1 (CEN, 2005). According to Al-Emrani (2023) global buckling is dependent on member slenderness ratio, which is the buckling length over the radius of gyration of a column. The member slenderness ratio is calculated according to Equation 2.1.

$$\lambda_m = \frac{L}{i} = \frac{L}{\sqrt{\frac{I}{A}}} \tag{2.1}$$

To determine whether second-order (global) effects should be considered, the elastic critical load factor (F_{cr}/F_{Ed}) is used. According to Silva et al. (2014), second-order effects must be included in the design if $F_{cr}/F_{Ed} < 10$ for elastic analysis or $F_{cr}/F_{Ed} < 15$ for plastic analysis.

Different types of global buckling are introduced by Galambos and Surovek (2008). For example, the first type, flexural buckling, refers to the overall bending deformation of a structure under compression. The second type, torsional buckling which refers to twisting of members. The third type is flexural-torsional buckling, which involves a combination of bending and twisting, which is particularly significant in thin-walled or asymmetric sections. Because of the geometry of CHS members torsional buckling cannot occur in these types of sections and will not be regarded in the final analysis. Figure 2.5 below shows different type of global buckling.

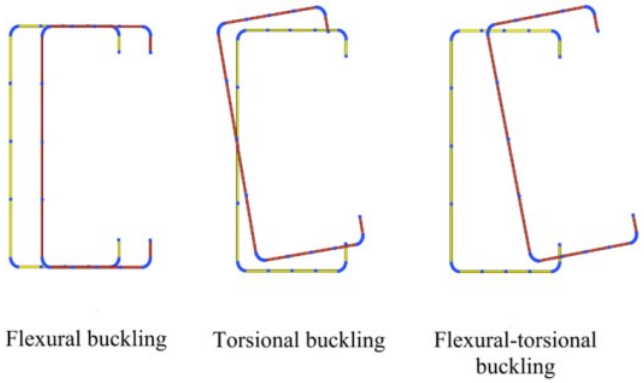

Figure 2.5: Different type of global buckling

Source: (Vuuren & Mahachi, 2021)

2.2.3 Interactive buckling

According to Pignataro (2005), interactive buckling occurs when two or more buckling modes interact, potentially resulting in unstable post-buckling behaviour, even if each individual mode remains stable. This interaction causes limit load erosion, meaning the ultimate strength of the structure is reduced. The erosion of limit loads is induced by non-linear buckling interactions, where at least two initially independent (linearly uncoupled) buckling modes combine. An interactive failure mode is visualised in Figure 2.6.

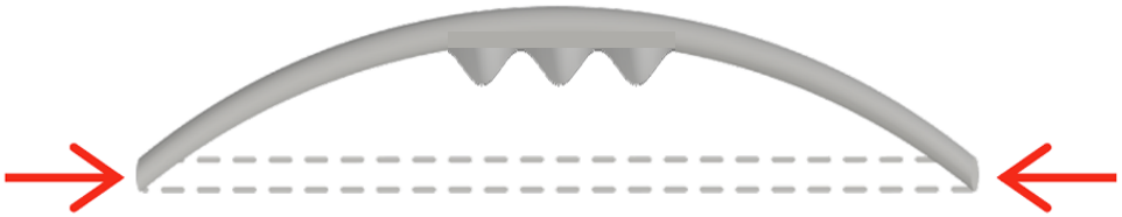

Figure 2.6: Interactive buckling of a CHS member in axial compression.

Pignataro (2005) emphasize that thin-walled members are particularly susceptible to interactive buckling, especially when involving Euler/flexural-torsional buckling coupled with local buckling. In circular hollow sections, global-local interaction buckling is the predominant form of interactive buckling that can occur (Huang & Zhang, 2022). Moreover, Cai (2016) highlight that for thin-walled members when

the walls become very thin a member which exert purely global buckling behaviour can be influenced by local buckling. When the lowest elastic buckling modes is highly mixed between different buckling types it is likely that the failure mode becomes interactive as well.

According to Pignataro (2005), post-buckling strength in interactive buckling refers to the structural behaviour beyond the critical buckling load, often characterized by a non-linear response. They categorize post-buckling into stable and unstable regimes: the former allows continued load-carrying with limited stiffness degradation, while the latter leads to sudden collapse. Importantly, interactive buckling typically results in unstable post-critical behaviour, which exacerbates the reduction in limit load. While individual buckling modes might permit further load-bearing after buckling, their interaction significantly lowers the load-carrying capacity. In the case of Eulerian/local interaction, antisymmetric post-buckling behaviour dominates, leading to progressive deformation influenced strongly by initial imperfections. These imperfections are a key factor in the erosion of limit loads. In contrast, the post-buckling behaviour of flexural-torsional/local interaction varies depending on whether the local buckling mode is symmetric or antisymmetric. Figure 2.7 illustrates how a more unstable post-critical path leads to greater strength reduction, while a less unstable path results in milder load loss.

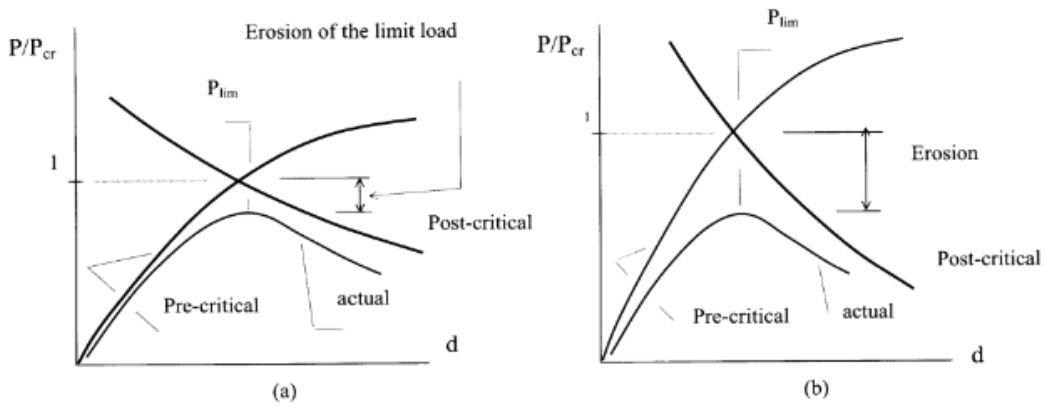

Figure 2.7: Illustration of how interactive buckling can influence the actual resistance of a cross-section.

Source: (Pignataro, 2005)

2.3 Behaviour of real columns

The behaviour of a real column does not exactly match theoretical predictions due to several idealizations in modelling (Davison & W. Owens, 2003). This includes assumptions of perfect straightness, where deviations in column geometry are either ignored or overly simplified. These geometrical deviations are called initial imperfections. Additionally, material behaviour is idealized, neglecting variations in yield stress along the column and the effects of residual stresses induced by thermal processes, cold working, and roller straightening. According to Pignataro (2005), as

the axially applied load eccentricity increases, initial imperfections in the column cause lateral displacements to develop, leading to non-linear behaviour compared to a perfect column, which would remain linear until sudden buckling. Additionally, post-buckling behaviour is often neglected in simplified analyses. However, in inelastic buckling, material effects such as strain hardening can influence the post-buckling response, particularly in slender members. According to Al-Emrani (2023) very stocky columns (very low slenderness) have a higher capacity than the yield strength, while very slender columns (high slenderness) almost follow Euler's buckling theory. For intermediate slenderness columns the capacity are much lower due to imperfections and non-linear effects. Figure 2.8 illustrate how predicted buckling by Euler differ from the real buckling behaviour of a member. According to Farkas and Jármai (2013) including the effect of imperfections is essential where ignoring these effect can lead to unsafe design due to loss of strength.

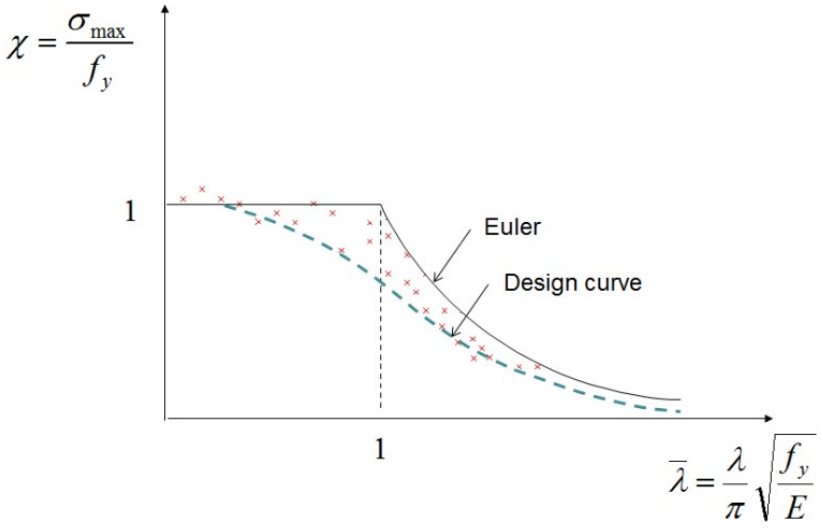

Figure 2.8: Test results on steel columns in relation to the buckling curve derived according to classical buckling theory.

Source: (Al-Emrani, 2023)

2.3.1 Effects of imperfections

This chapter explains different types of imperfection in more detail, as the impact of them is crucial to take into account for a safe design of structures. Bernuzzi and Cordova (2016) emphasise that imperfections are divided into two types: mechanical imperfections, which consider residual stresses caused from production, and geometric imperfections, which consider the deviation from exact geometry.

2.3.1.1 Geometric imperfections

According to Bernuzzi and Cordova (2016) geometric imperfections refer to deviation in theoretical shape and real size of the structure or system as a whole or as-built structures can be described as:

- Cross-sectional imperfections: Refers to cross sectional variation due to production but also different values of area, moments of inertia and section moduli which can lead to loss of capacity or worse bending moment performance.
- Member imperfections: Longitudinal bow imperfection is the most important among the member imperfections. Here the axis of the a structural member is not straight line due to manufacturing.
- Structural system imperfections: Refers to variations in member lengths, lack of verticality in columns, or misalignment of beams and foundations. These type of imperfections must be considered in global analysis.

These type of geometric imperfections can be taken into account by two parameters, load eccentricity at the end of the columns and mid-span deflection due to initial curvature (Ballio & Mazzolani, 1989). For an illustration of the differences between gobal and local geometric imperfections, see figure 2.9.

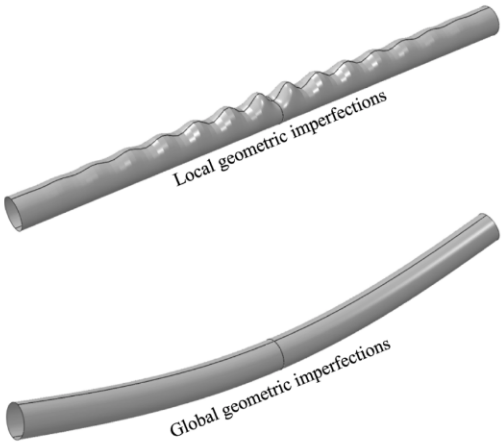

Figure 2.9: Illustration of global imperfection and local imperfection of a circular hollow section.

Source: (Meng & Gardner, 2022)

2.3.1.2 Initial imperfections and 2nd order effects

According to Al-Emrani (2023) initial imperfections lead to second order moment on the overall behaviour of columns. However, EN1993-1-1 (CEN, 2005) consider these type of imperfections and are not needed to be taken into account. Al-Emrani (2023) means that initial bow in columns generate an additional moment due to eccentricity of loading which increase lateral deflection. The formula for second order moment is described in Equation2.2:

$$M_{II} = \frac{1}{1 - \frac{N}{N_{cr}}} \cdot M_{Max} = \frac{N}{N_{cr} - N} \cdot e_0 \tag{2.2}$$

The influence of initial imperfections on lateral deflection and bending moment has been analysed by Al-Emrani (2023). As illustrated in Figure 2.10, a larger initial bow (L/250) leads to a significant increase in second-order moments and deflections. Additionally, when the initial eccentricity is zero, the column behaves according to

bifurcation theory. It is also observed that prior to reaching the critical load, N_{cr}, both lateral deflection and bending moment remain zero; however, beyond this point, they increase indefinitely.

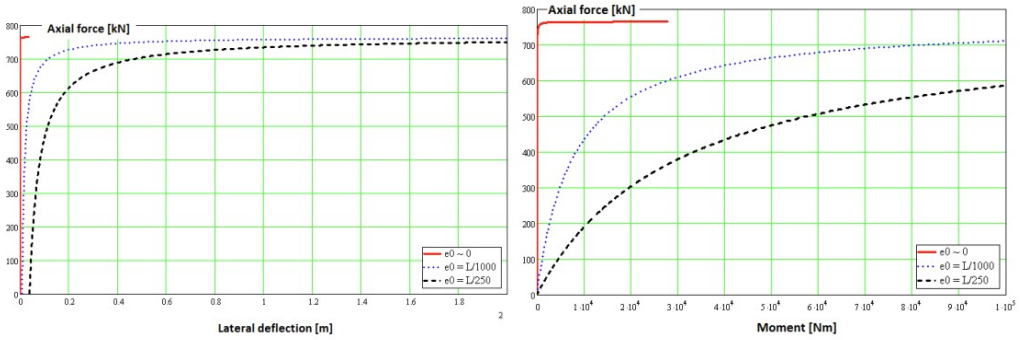

Figure 2.10: The response of a 10 m HEA 200 column having different initial imperfection magnitudes.

Source: (Al-Emrani, 2023)

2.3.2 Effect of residual stresses

The residual stresses from welding are significantly more severe than those generated during the steel manufacturing process (Davison & W. Owens, 2003). This is due to fusion welding creating intense temperature gradients and high thermal stresses. Residual stresses play a crucial role in brittle fracture, fatigue, and distortion. In materials with low fracture toughness operating below their transition temperature, brittle fracture can occur at relatively low applied stresses. However, if a material undergoes yielding before failure, residual stresses have little impact on its overall structural strength. The residual stress pattern according to the Wagner model along the circumference of a CHS member is shown in Figure 2.11.

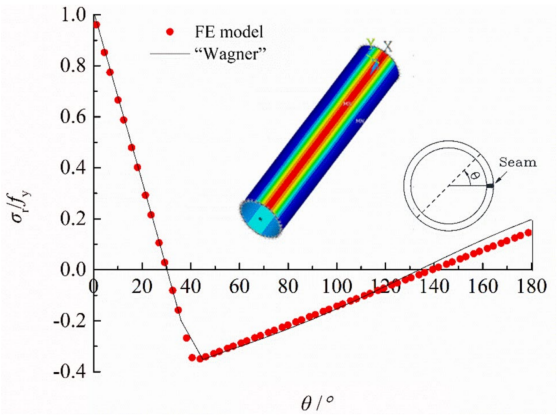

Figure 2.11: Wagner model of how residual stress is distributed along circumference of a CHS member

Source: (Huang & Zhang, 2022)

Davison and W. Owens (2003) also highlighted that welding-induced residual stresses can lead to shrinkage, bending, and buckling deformations, which should be managed by pre-setting components or allowing for shrinkage during fabrication. Additionally, he noted that certain design codes, such as BS 5950, account for manufacturing-induced residual stresses by applying varying factors to the permissible stresses, depending on the section shape. According to Pignataro (2005) residual stresses for cold form thin members are relatively low and does not count as the most important factor when it comes to stability issues of the structure. The author also mentioned that residual stresses together with geometric imperfections play a crucial role in interactive buckling. According to Pignataro (2005) more imperfections in the structure leads to more loss of capacity in interactive buckling.

2.4 Design methodologies of CHS columns

In this chapter the design method of columns under axial compression according to EN1993-1-1 (CEN, 2005) and EN1993-1-6 (CEN, 2007) together with alternative methods outside of these are described.

2.4.1 Cross-section classification

According to EN1993-1-1 (CEN, 2005) four different classes of cross-sections are defined. The aim of this classification is to determine whether the cross sections' ability to reach its full plastic rotation capacity. The definitions of these four classifications are as follows:

- Class 1: Cross-section develop plastic hinges and utilise full plastic rotation capacity. They are used in plastic design without reduction of resistance.
- Class 2: Cross-section can develop full plastic moment resistance but plastic rotation capacity is limited when yield limit is reached due to local buckling.
- Class 3: Stress in the extreme compression fibre of the steel member reach yield limit but development of full plastic moment resistance is prevented due to local buckling.
- Class 4: Local buckling occur before yielding.

According to McKenzie (2004), the classifications for Class 1 to Class 4 are as follows: plastic sections, compact sections, semi-compact sections, and slender sections, respectively. The author illustrate the moment as a function of rotation characteristics of a section in Figure 2.12.

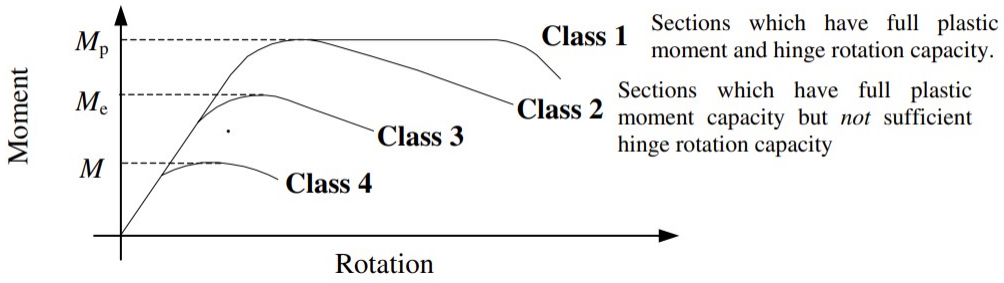

Figure 2.12: Moment of a section with regard to rotation.

Source: (McKenzie, 2004)

Based on these characteristics, it can be determined whether a fully plastic moment capacity can develop or if sufficient rotational capacity exists to allow for the redistribution of moments in structures (McKenzie, 2004). Observing the stress diagram in Figure 2.13, it is evident that the bending stress distribution initially follows a linear elastic pattern, with extreme fibre stresses below the design strength p_y. As the loading increases, the section can transition to a state where all fibres are considered to have reached the design strength.

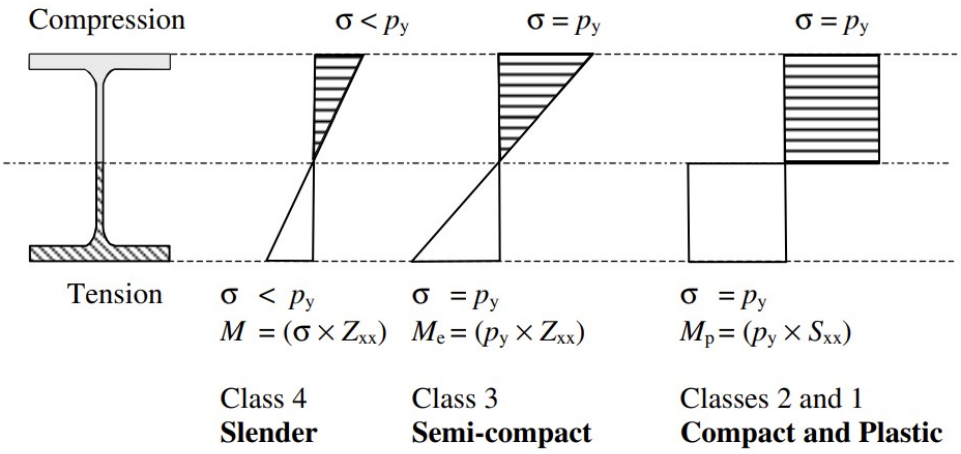

Figure 2.13: Stress diagram of a beam under bending.

Source: (McKenzie, 2004)

where:

- Z_{xx} : Elastic section modulus
- S_{xx} : Plastic section modulus
- σ : Plastic stress
- P_y : Design strength

The different cross-section class limits for CHS members according to EN1993-1-1

(CEN, 2005) are calculated with equation 2.3:

$$\frac{d}{t} \leq \begin{cases} 50\varepsilon^2, \text{Class 1} \\ 70\varepsilon^2, \text{Class 2} \\ 90\varepsilon^2, \text{Class 3} \end{cases} \tag{2.3}$$

$$\text{Where} \qquad \varepsilon = \sqrt{\frac{235}{f_y}}$$

The Figure 2.14 by Trahair (2008) illustrate a flow chart for designing member under compression according to EC3.

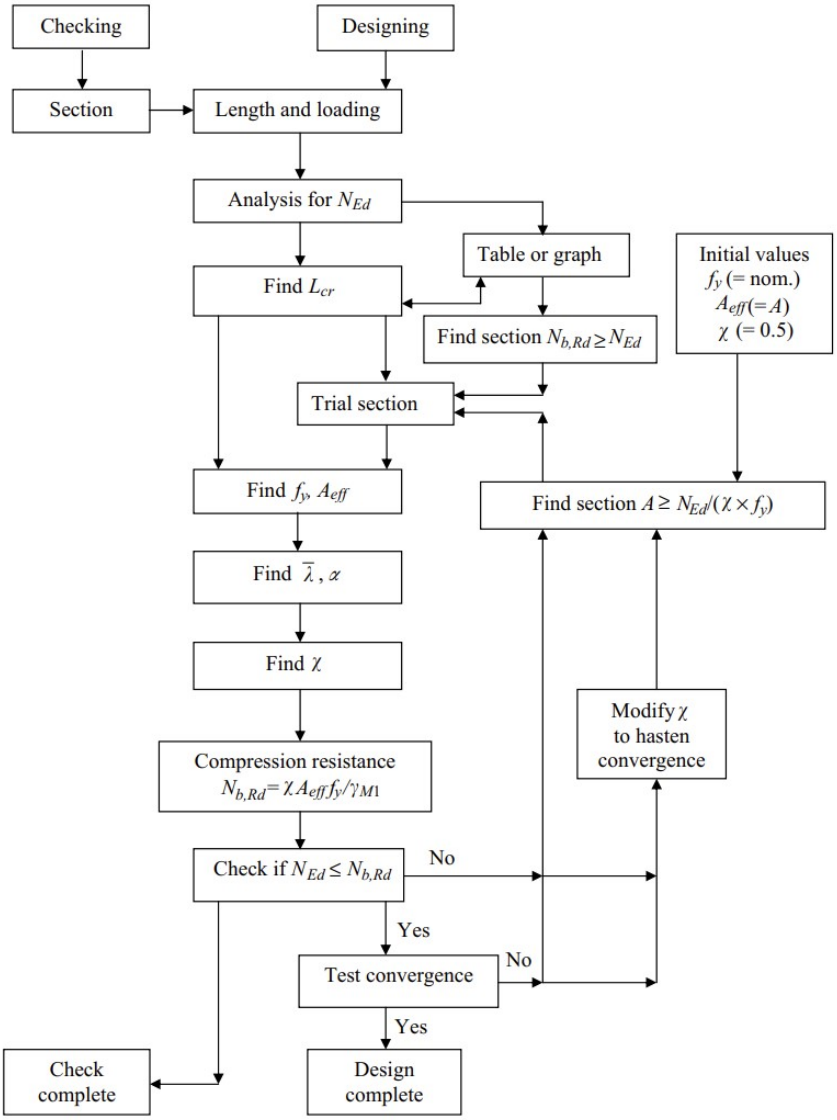

Figure 2.14: Flow chart for the design of compression members

Source: (Trahair, 2008)

2.4.2 Design of CHS members according to EC3, EN1993-1-1: General rules and rules for buildings

According to EN1993-1-1 (CEN, 2005) the global buckling resistance for CHS members in compression, depending on the cross-section class, is calculated using equation 2.4:

$$\begin{aligned} N_{\mathrm{Rd}} &= \frac{\chi\, A\, f_y}{\gamma_{\mathrm{M1}}} \qquad \text{for Cross-section class 1, 2, and 3} \\ N_{\mathrm{Rd}} &= \frac{\chi\, A_{\mathrm{eff}}\, f_y}{\gamma_{\mathrm{M1}}} \qquad \text{for Cross-section class 4} \end{aligned} \tag{2.4}$$

Where f_y is the yield strength, A is the gross cross-section area, A_{eff} is the effective area of the cross-section, $\gamma_{\mathrm{M1}} = 1.0$, and χ is the global buckling reduction factor. Since there is no established method for determining A_{eff} in EC3 for CHS members, alternative methods for calculation of this will be explained further in Section 2.4.4. χ is dependent on the non-dimensional slenderness, $\bar{\lambda}_n$, and the relevant buckling curve and is calculated according to equation 2.5

$$\chi = \frac{1}{\Phi + \sqrt{\Phi^2 - \bar{\lambda}_n^{\,2}}} \qquad \text{where} \qquad \Phi = 0.5\left[1 + \alpha\left(\bar{\lambda}_n - 0.2\right) + \bar{\lambda}_n^{\,2}\right] \tag{2.5}$$

The non-dimensional slenderness, $\bar{\lambda}_n$, is calculated using equation 2.6 and 2.7

$$\bar{\lambda}_n = \sqrt{\frac{A\, f_y}{N_{cr}}} = \frac{L_{\mathrm{cr}}}{i} \cdot \frac{1}{\lambda_1} \qquad \text{for Class 1, 2 and 3 cross-sections} \tag{2.6}$$

$$\bar{\lambda}_n = \sqrt{\frac{A_{\mathrm{eff}}\, f_y}{N_{cr}}} = \frac{L_{\mathrm{cr}}}{i} \frac{\sqrt{\frac{A_{\mathrm{eff}}}{A}}}{\lambda_1} \qquad \text{for Class 4 cross-sections} \tag{2.7}$$

Where L_{cr} is the critical buckling length, i is the radius of gyration of the gross cross-section, and λ_1 is determined by equation 2.8:

$$\lambda_1 = \pi\sqrt{\frac{E}{f_y}} = 93.9\varepsilon \qquad \text{where} \qquad \varepsilon = \sqrt{\frac{235}{f_y}} \tag{2.8}$$

α is an imperfection factor depending on the relevant buckling curve. The imperfection factor for each buckling curve is shown in table 2.1.

Buckling curve	a_0	a	b	c	d
Imperfection factor, α	0.13	0.21	0.34	0.49	0.76

Table 2.1: Imperfection factor for each buckling curve.

For CHS members the buckling curve depend on the production method of the steel and the steel strength and the relevant buckling curves are shown in table 2.2.

Type	S235, S275, S355, S420	S460
Hot rolled	a	a_0
Cold formed	c	c

Table 2.2: Relevant buckling curve for different steel strengths and production type.

The reduction factor as a function of non-dimensional slenderness with the different buckling curves is shown in figure 2.15 below. For $\bar{\lambda} < 0.2$ the buckling of the member is negligible i.e. $\chi = 1$.

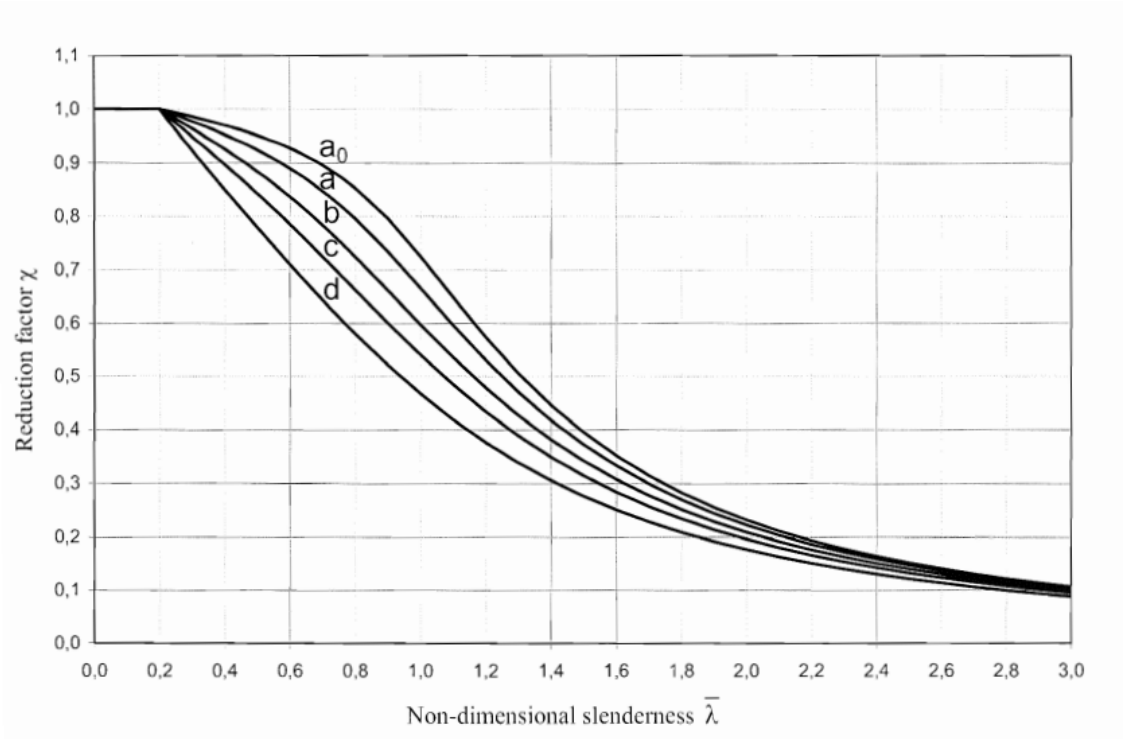

Figure 2.15: The different buckling curves for CHS members susceptible to buckling.

Source: (CEN, 2005)

2.4.3 Design of CHS members according to EC3, EN 1993-1-6: Strength and Stability of Shell Structures

As mentioned in previous section there is no explicit method to determine the effective area, A_{eff}, in EN1993-1-1 (CEN, 2005) and for dimensioning of CHS members in CSC 4 it refers to EN1993-1-6 (CEN, 2007). Since this thesis only considers uniformly axially compressed CHS members, only the relevant and in some cases simplified approaches from EN1993-1-6 (CEN, 2007) are included to act as a comparison with the FE-analysis. EN1993-1-6 (CEN, 2007) consider design of shell structures with a $\frac{r}{t}$-ratio within the range $20 \leq \frac{r}{t} \leq 5000$. Since EN1993-1-6 consider design of shell structures and this thesis handle columns, emphasis will be put on how this design guideline regard the dimensioning process of these. The geometry and cross-sectional parameters, together with the loading case mentioned above, are illustrated in 2.16 below.

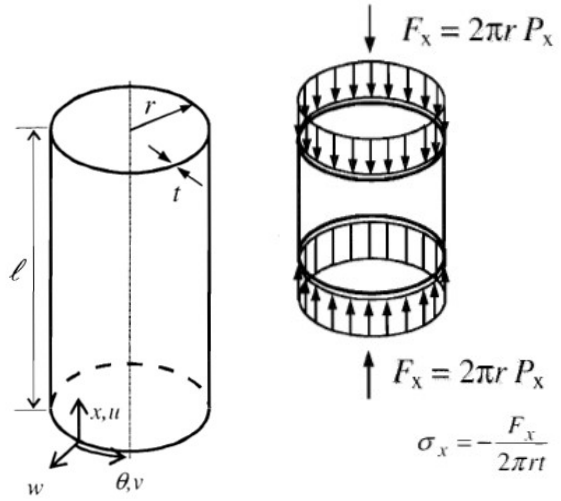

Figure 2.16: Geometry and loading conditions of CHS members.

Source: (CEN, 2007)

The dimensioning buckling stress of a shell element is calculated according to equation 2.9:

$$\sigma_{\mathrm{Rd}} = \frac{\sigma_{\mathrm{Rk}}}{\gamma_{\mathrm{M1}}} \tag{2.9}$$

Where $\gamma_{\mathrm{M1}} = 1.1$
The characteristic buckling stress is calculated as the yield strength f_{yk}, multiplied by the relevant buckling reduction factor, χ_x. this is shown in equation 2.10

$$\sigma_{\mathrm{Rk}} = \chi\ f_{\mathrm{yk}} \tag{2.10}$$

Where the buckling factor depends on the slenderness ratio of the cross-section.

$$\begin{array}{lll} \chi = 1 & \text{when} & \bar{\lambda} \leq \bar{\lambda}_0 \\ \chi = 1 - \beta \left(\frac{\bar{\lambda} - \bar{\lambda}_0}{\bar{\lambda}_p - \bar{\lambda}_0} \right)^{\eta} & \text{when} & \bar{\lambda}_0 < \bar{\lambda} < \bar{\lambda}_p \\ \chi = \frac{\alpha}{\bar{\lambda}^2} & \text{when} & \bar{\lambda}_p \leq \bar{\lambda} \end{array} \tag{2.11}$$

The plastic range factor, β, and the interaction factor, η should be set as:

$$\beta = 0.60 \qquad \eta = 1.0$$

The different slenderness limits and relative slenderness for shell elements are determined by 2.12 where the first parameter is the meridional squash limit slenderness, the second is the actual relative slenderness of the member, and the third is the plastic limit relative slenderness.

$$\bar{\lambda}_0 = 0.2 \qquad \bar{\lambda} = \sqrt{\frac{f_{\mathrm{yk}}}{\sigma_{\mathrm{Rcr}}}} \qquad \bar{\lambda}_p = \sqrt{\frac{\alpha}{1-\beta}} \tag{2.12}$$

The elastic critical meridional buckling stress, σ_{Rcr}, is determined by equation 2.13:

$$\sigma_{\mathrm{Rcr}} = 0.605 E\, C\, \frac{t}{r} \tag{2.13}$$

The parameter C is varying depending on the dimensionless length parameter, ω, and is determined using equation 2.14:

$$\begin{array}{lll} C = 1 & \text{when} & 1.7 \leq \omega \leq 0.5\,\frac{r}{t} \\ C = 1.36 - \frac{1.83}{\omega} + \frac{2.07}{\omega^2} & \text{when} & \omega \leq 1.7 \\ C = \max\left(1 + \frac{0.2}{C_{xb}}\left[1 - 2\,\omega\,\frac{t}{r}\right],\ 0.6\right) & \text{when} & 0.5\,\frac{r}{t} \leq \omega \end{array} \tag{2.14}$$

The length of the shell segment is determined by a dimensionless parameter, ω, which is determined by equation 2.15:

$$\omega = \frac{l}{\sqrt{r\,t}} \tag{2.15}$$

The meridional elastic imperfection reduction factor, α, is determined using equation 2.16 together with the characteristic imperfection amplitude, Δw_k:

$$\alpha = \frac{0.62}{1+1.91(\Delta w_k/t)^{1.44}} \qquad \text{where} \qquad \Delta w_k = \frac{1}{Q}\sqrt{\frac{r}{t}} \cdot t \tag{2.16}$$

Q is the fabrication quality parameter varying depending on the tolerance quality class and is determined by table 2.3:

Table 2.3: Values of fabrication quality parameter Q

Fabrication tolerance quality class	**Description**	**Q**
Class A	Excellent	40
Class B	High	25
Class C	Normal	16

2.4.4 Design of CHS members in CSC 4 according to British standards

In BS5950-1 (British Standards Institution, 2008) guidelines for rolled and welded steel sections an additional method for determining the buckling resistance of CHS members using the effective area method which are valid for section CSC 4 have been established. The method follow the one presented in section 2.4.2 with the addition of having an expression for determining the effective area, A_{eff}, and the non-dimensional slenderness, $\bar{\lambda}$ of CHS members in CSC 4. This method cover a key area that is missing in the current EN1993-1-1 (CEN, 2005) in the design of CHS members.

The effective area , A_{eff}, is determined by equation 2.17:

$$A_{eff} = A\sqrt{\frac{90\ \varepsilon^2}{d/t}} \qquad \text{valid for} \qquad 90\ \varepsilon^2 < \frac{d}{t} < 240\ \varepsilon^2 \tag{2.17}$$

The non-dimensional slenderness, $\bar{\lambda}$, for pinned columns is then determined by equation 2.18:

$$\bar{\lambda} = \sqrt{\frac{A_{eff}\ f_y}{N_{cr}}} = \sqrt{\frac{A_{eff}\ f_y\ L_{cr}^2}{\pi^2\ E\ I}} \tag{2.18}$$

2.4.5 Design of CHS members according to Toffolon and Taras (2017)

Another study by Toffolon and Taras (2017) investigates the current design guidelines and performs a numerical analysis to better adapt them to the mode interaction behaviour of CHS members. The report proposes more efficient design rules by studying global and local buckling, based on findings from another project called the HOLLOSSTAB project. The study has focused on thin walled circular sections with yield strength up to S770. During this study a numerical analysis called GMNIA (Geometrically and Materially Nonlinear and account for Imperfections) has been done to analyze the effect of local buckling in slender elements under compression. The result from the numerical analysis has been used in order to refine the analytical formulas. As long as the reduction factor in EN1993-1-1 (CEN, 2007) are not directly usable in OIC (overall interaction concept), therefore Ayrton-Perry formula is used to to convert them into a more compatible form for use within the OIC framework. Finally a refined reduction factor for local buckling has been derived as below:

$$\chi_{x,\mathrm{loc}} = \frac{1}{\Phi_{\mathrm{loc}} + \sqrt{\Phi_{\mathrm{loc}}^2 - \frac{\bar{\lambda}_{\mathrm{loc}}^2}{\alpha_1}}} \leq 1.0 \tag{2.19}$$

$$\Phi_{\mathrm{loc}} = 0.5 \cdot \left(1 + \alpha_0 \left(\bar{\lambda}_{\mathrm{loc}} - \bar{\lambda}_{\mathrm{loc},0}\right) + \frac{\bar{\lambda}_{\mathrm{loc}}^2}{\alpha_1}\right) \tag{2.20}$$

$$\alpha_0 = 0.5, \quad \alpha_1 = 0.8 \cdot \left(1 + 2\left(\frac{w_k}{t}\right)^{1.5}\right), \quad \Delta_{w_k}/t = \frac{1}{Q}\sqrt{\frac{r}{t}} \tag{2.21}$$

The plateau value $\bar{\lambda}_{\text{loc},0}$ will typically take values between 0.2 and 0.4, and $\bar{\lambda}_{\text{loc}}$ is defined as $\bar{\lambda}_{\text{loc}} = \sqrt{\frac{f_y}{\sigma_{cr}}}$. The parameter Q is imperfection quality factor, which can be taken from 2.4.3 and w_k is initial out-of-plane imperfection amplitude.
The approximation of the reduction factor was initially evaluated and compared with EN 1993-1-6 and the results from GMNIA. The findings showed a good alignment of the approximation with the Eurocode but significant deviations from GMNIA as the $\frac{D}{t}$-ratio increased. To improve the alignment of the reduction factor approximation with GMNIA, the value of $\bar{\lambda}_{\text{loc},0}$ was increased to 0.4, resulting in a better match with GMNIA results.
In the numerical analysis, a diameter $D = 300\,\text{mm}$ was used while varying the thickness t from 1.5 mm to 10 mm. The results showed that the reduction factor was approximately 1 for stocky sections ($D/t \approx 88.1$) but gradually decreased to 0.813 for slender sections ($D/t \approx 587.2$) due to local buckling. Figure 2.17 below shows the results of the study.

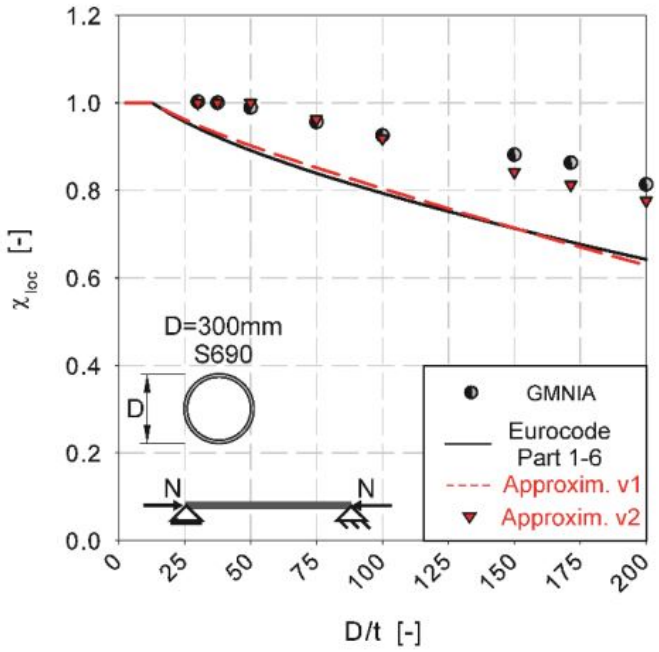

Figure 2.17: Reduction factor as a function of D/t.

Source: (Toffolon & Taras, 2017)

According to Taras, Nseir, and Boissonnade (n.d.) the main strength issue in circular hollow sections are in interaction between local and global buckling. For this the authors proposed formula which shown in Equation2.22 to2.24.

$$\chi_{\text{glob,gr}} = \chi_{x,\text{loc}} \cdot \min\left[\frac{1}{\Phi_{\text{glob}} + \sqrt{\Phi^2_{\text{glob}} - \bar{\lambda}^2_{\text{glob}}}}; 1.0\right] \tag{2.22}$$

$$\Phi_{\text{glob}} = 0.5 \cdot \left(1 + \alpha_{\text{glob}} \left(\bar{\lambda}_{\text{glob+loc}} - 0.2\right) + \bar{\lambda}^2_{\text{glob+loc}}\right) \tag{2.23}$$

$$\bar{\lambda}_{\text{glob+loc}} = \sqrt{\frac{\chi_{x,\text{loc}} \cdot A \cdot f_y}{\pi^2 EI / L^2_{\text{cr}}}} = \bar{\lambda}_{\text{glob,gr}} \cdot \sqrt{\chi_{x,\text{loc}}} \tag{2.24}$$

Where $\chi_{\text{glob,gr}}$ is the global reduction factor and include the effect of local buckling where $A \cdot f_y$. $\chi_{x,\text{loc}}$ is the purely local reduction factor. Figure 2.18 below shows global reduction factor with regard to global slenderness ratio for locally and globally slender columns based on Equation2.24.

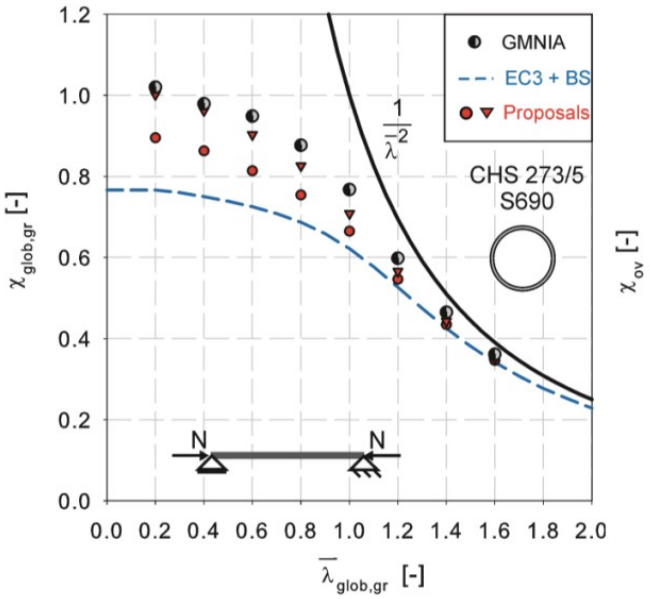

Figure 2.18: Buckling strength of beam-columns using the "Overall Interaction Concept"; locally and globally slender column

Source: (Toffolon & Taras, 2017)

2.5 Interactive buckling of steel sections

In columns with a cross-sectional slenderness ratio close to the limit of CSC 4, the global and local buckling modes can interact. As previously discussed this forms an interactive buckling buckling mode, which arises a series of problems in the design of CHS members with this slenderness ratio. In this chapter a closer look into theoretical, numerical, and experimental studies which handle interactive buckling in RHS members as a basis for the problem and then CHS members will be presented.

2.5.1 Interactive buckling of steel box sections

In a two-part study produced by Goltermann and Møllmann they investigated the post-buckling behaviour of two different types of thin-walled steel structures (I-beam and square steel box section) exposed to a combination of bending and axial force (Goltermann & Møllmann, 1989a), (Goltermann & Møllmann, 1989b). They analysed this by employing a non-linear plate theory and through this a theoretical combination of the finite strip method and Koiter's asymptote theory of stability.
The authors found that the interaction between local and global buckling modes, combined with the imperfection sensitivity of the member, significantly reduced the buckling resistance by up to 50 %. In theory, however, each buckling mode considered in isolation would correspond to a stable-symmetric bifurcation and yield a higher buckling resistance. Goltermann and Møllmann (1989b) reinforced the impact of small imperfections which controls the buckling load and post buckling behaviour.
The findings in this study show that in the analysis of steel sections with an intermediate slenderness ratio is an extremely important subject and shows that the design guidelines need to be further complemented.

More recent studies have investigated interactive buckling of rectangular box sections with different material properties and production methods using both experimental and numerical analysis to compare how this affect the predicted buckling resistance given in the design guidelines. Two particularly interesting studies in this area have been conducted analysing welded steel box-sections.

Yang, Shi, Zhao, and Zhou (2017) analysed the interactive buckling behaviour both experimentally, through 12 different sections with two different steel strengths and slenderness ratios, and numerically, through FE-analysis conducting a parametric study of different geometries, slenderness ratios, and steel strengths. The study aimed to cover a wide variety of parameters to see their individual impact and load the members until failure by interactive buckling. Through their analysis they compared the experimentally gathered results with the current American (AISC) and European (EC3) codes and found that the members generally failed by interactive buckling before they reached their predicted resistance. Their test results are illustrated in Figure 2.19.

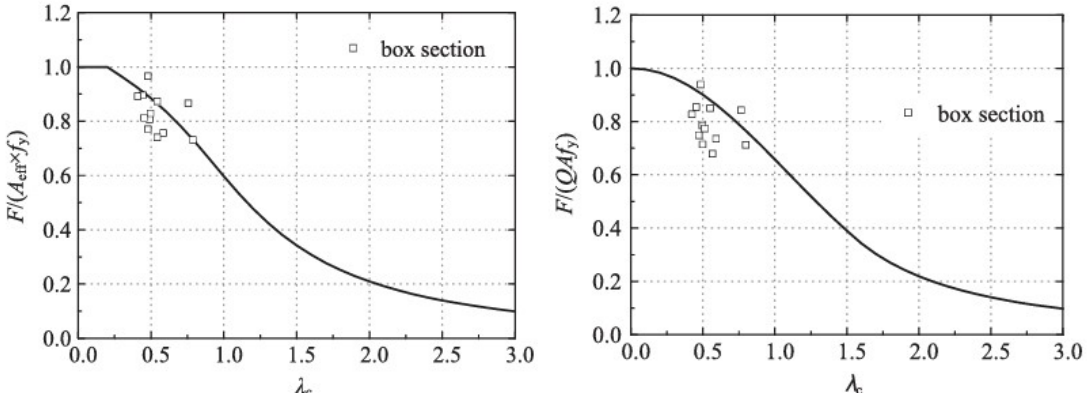

Figure 2.19: Test results compared to the design buckling curves in EC3 (left) and AISC (right).

Source: (Yang et al., 2017)

In their FEA and parametric study they could produce a large number of data points showing the interactive buckling resistances and found that all of the codes over predict the resistances. The comparison with relevant buckling curves according to the European and American guidelines and FE-results are shown in figure 2.20 and figure 2.21 respectively.

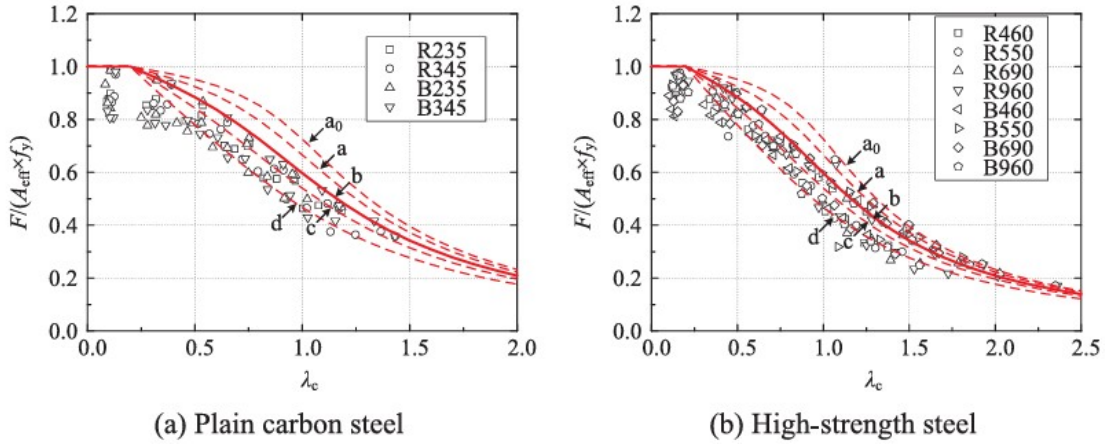

Figure 2.20: Comparison of buckling curves between EC3 and FEA for plain carbon and high strength steel.

Source: (Yang et al., 2017)

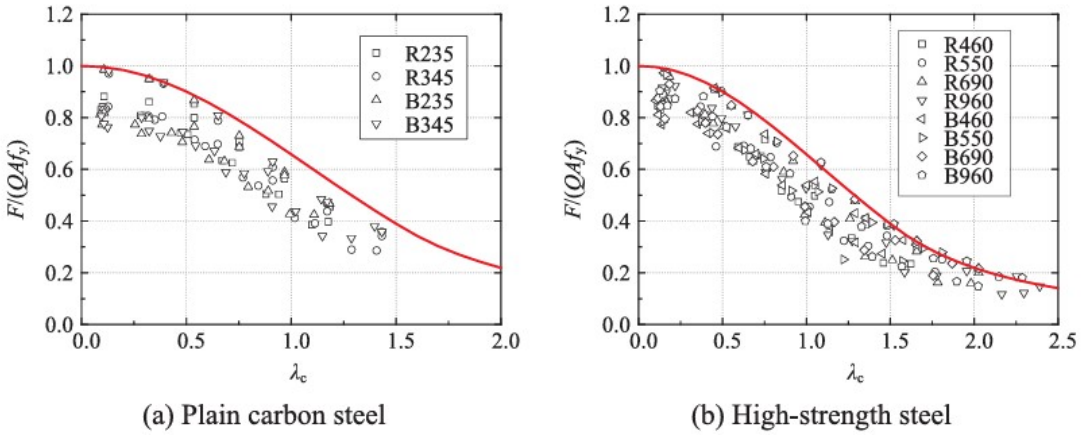

Figure 2.21: Comparison of buckling curves between AISC and FEA for plain carbon and high strength steel.

Source: (Yang et al., 2017)

Another similar study, produced by Yuan, Wang, Gardner, and Shi (2014), analysed interactive buckling of stainless steel box sections and found contradicting results when comparing with the design codes. For stainless steel the buckling curve does not differ depending on steel grade. In the study it was found that for austenitic steel sections the resistance was over predicted while for duplex the resistance was under predicted. This led to a new proposal where the design guidelines would use two different buckling curves instead.

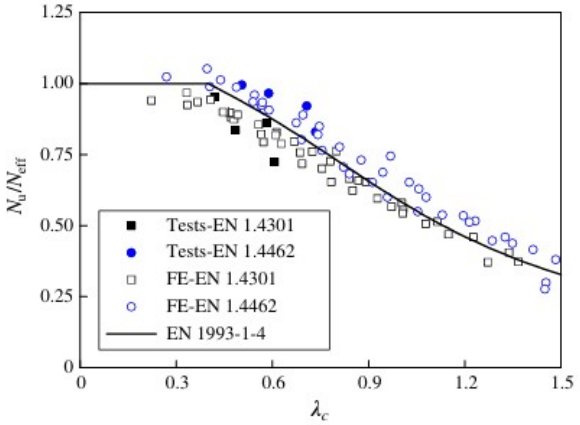

Figure 2.22: Comparison of buckling curves in EC3 and FE-results normalised against yield strength.

Source: (Yuan et al., 2014)

The main conclusion to be taken out of these studies is that interactive buckling is a phenomenon that leads to a lowering of the predicted resistance of steel box sections that is yet to be handled in the design guidelines.
In the study by Yuan et al. (2014) five different combination of local and global imperfections has been used as follow:

- $b/200 - L_e/500$ (most severe combination)
- $b/200 - L_e/1000$ (standard combination)
- $b/300 - L_e/1000$
- $b/500 - L_e/1000$
- $b/500 - L_e/2000$ (least severe combination)

Where the effective length of the columns is denoted as L_e. Yuan et al. (2014) found that columns with intermediate overall slenderness exhibited the greatest variation in buckling resistance, indicating a higher sensitivity to initial geometric imperfections. Consequently, the standard combination $b/200 - L_e/1000$ was adopted for numerical analysis.

Additionally, the authors reported that neglecting residual stresses led to an overestimation of the buckling resistance by approximately 5%, while test results showed better agreement when residual stresses were included. These residual stresses contributed to the earlier onset of local buckling. According to Yuan et al. (2014), welded stainless steel box sections are more sensitive than cold-formed sections due to their predominantly axial residual stress nature and specific distribution pattern.

In a numerical study by Shen, Wadee, and Sadowski (2015), the buckling behaviour of box sections under compression was analysed across varying slenderness ratios. Using a consistent cross-section with three different column lengths, the results indicated that interactive buckling is most pronounced in columns with intermediate slenderness. This finding aligns with previous experimental observations by Goltermann and Møllmann (1989a) and Goltermann and Møllmann (1989b). For short columns ($L = 2400$ mm), local buckling was the dominant failure mode, with the largest deformation occurring near the loaded end. In intermediate columns ($L = 5247$ mm), local and global buckling occurred simultaneously, with their buckling loads differing by only 0.04%, leading to strong interactive buckling. For long columns ($L = 7200$ mm), global buckling was the dominant mode, with no significant post-buckling strength, in contrast to short columns, where post-buckling strength was high.
Thusly the conclusion could be drawn that when the magnitude of the critical local buckling load and the critical global buckling load are in the vicinity of each other, the unstable interactive buckling failure governs the capacity.

2.5.2 Interactive buckling of circular hollow sections

The length-to-radius ratio (l/r) and radius-to-thickness ratio (r/t) play a crucial role in determining the buckling response (Wong & Weaver, 2006). Depending on the interaction between these parameters, local buckling, global buckling, or an interaction of both may occur.
To investigate this, the authors analysed the mode interaction between local and global buckling through five analytical shell models, a wide range of geometries, and two different materials (stainless steel and aluminium) and compared them with results from a FEA to determine the conditions under which different types of buckling occur.

Interactive buckling refers to a transitional phase where both local and global buckling contribute to structural stability, creating a distinct gap between the two failure modes. The study was able to identify different ranges where different types of buckling occur through a parameter, L', which is calculated with equation 2.25.

$$L' = \sqrt{\frac{(l/r)^2}{(r/t)}} = \sqrt{\frac{l^2 t}{r^3}} \tag{2.25}$$

The different buckling ranges were as follows:

- **For** $L' < 1$, local buckling dominates
- **For** $L' > 3$, global buckling governs
- **For** $1 < L' < 3$, Interactive buckling

Since this study investigated the interactive range of stainless steel and aluminium its applicability is not exactly transferable to hot-rolled steel as this thesis will handle. It is however of interest to see if L' is transferable and can yield consistent results for hot-rolled steel as well.

Another study by Huang and Zhang (2022) investigated the interactive buckling of hot-rolled high strength steel (Q460, Q690, and Q960) CHS members caused by individual parameters focusing on local and global geometric imperfections, and residual stresses. Out of a combination of the global and local buckling resistance of the members the interactive buckling resistance was then evaluated against EC3. Looking at the individual parameters all reduced the resistance of the members with varying magnitude:

- Global geometric imperfections had a significant reduction on members with intermediate slenderness where its influence was lowered with increasing steel strength. Three different imperfection amplitudes of:

  $$\frac{L}{2000}, \ \frac{L}{1000}, \text{ and } \frac{L}{1000} + \frac{t\sqrt{\frac{D}{2t}}}{16.5}$$

  Since $L/2000$ is such a small amplitude it was used as a basis in the evaluation because it is assumed to act as a near perfect column. The average reduction when analysing $L/1000$ was then 5.05 %, 5.35 %, and 3.23 % for the different steel strengths. When also considering the local imperfection amplitude an additional reduction of 1.50 %, 1.73 %, and 2.37 % was calculated for the different steel strengths. As expected with a higher steel strength the imperfection sensitivity in global buckling is decreased while for local buckling it is increased.
- Residual stresses had the highest impact on the reduction of buckling resistance and the reduction was the largest among the lower steel strengths. The residual stresses were applied with a maximum along the weld seam with an self-balancing stress field along the circumference of the CHS members. Two different magnitudes of the residual stresses was analysed with a factor of 0.5 and 1.0. Their impact on the resistance was then analysed together with a global geometric imperfection amplitude of $L/1000$ together with a local imperfection amplitude of $t\sqrt{D/2t}/16.5$. The average decrease in resistance

compared to the firstly analysed case when only half of the residual stress magnitude was applied was 2.15 %, 3.45 %, and 1.13 % for the different steel strengths. When the whole residual stress magnitude was applied an average decrease in resistance was 5.45 %, 4.84 %, and 3.53 %. At certain data points an decrease of up to 11.39 %, 8.93 %, and 6.54 % was calculated showing the impact of residual stresses.

When evaluating the interactive buckling resistance of the members against the design codes they were able to match the different steel grades against the global buckling curves prescribed. According to the results of the FEA the different steel grades Q460, Q690, and Q960 were matched with the corresponding global buckling curves *b*, *a*, and *a*, respectively. Their FEA together with the buckling curves are shown in figure 2.23 below.

When looking at EN1993-1-1 CEN (2005), which only cover steel grades up to S460, a hollow section of this grade should be dimensioned according to buckling curve a_0 which is not included in Figure 2.23. This is a significant reduction in buckling resistance meaning that their results match lower buckling curves than expected and shows the importance of further investigating the impact on interactive buckling of CHS members.

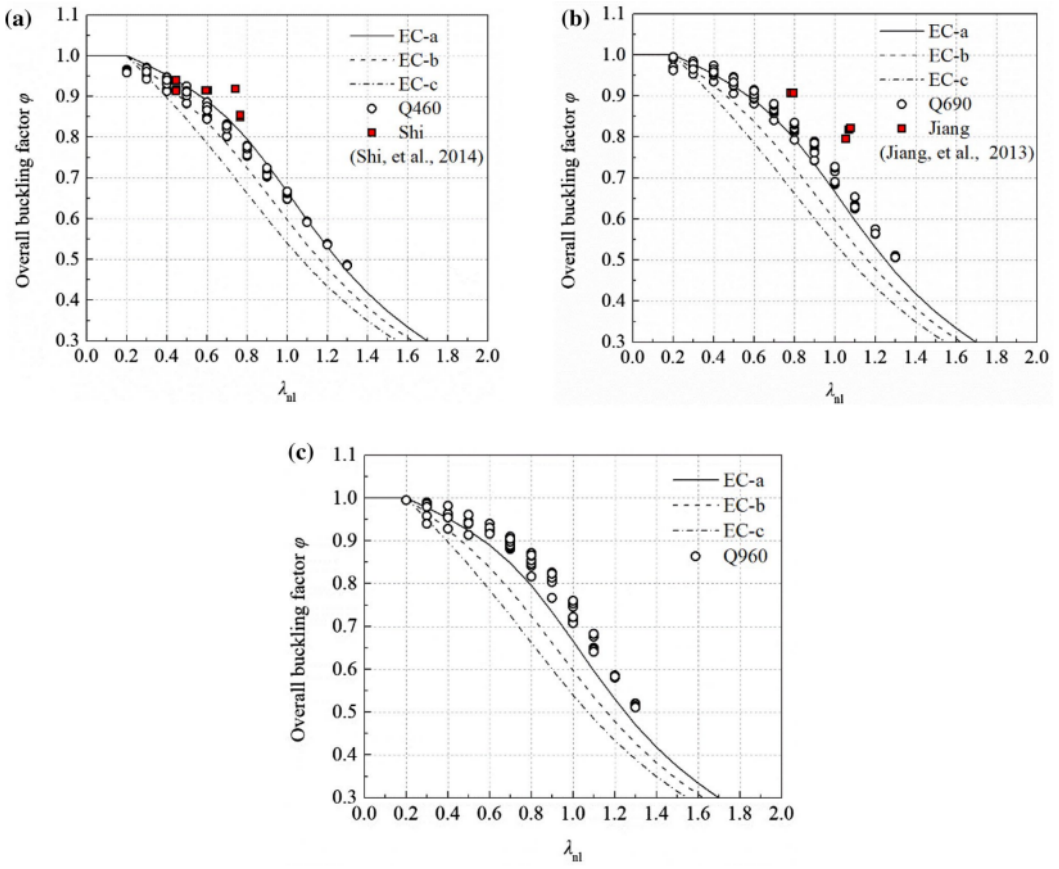

Figure 2.23: FE-results normalised against yield strength for (a) Q460, (b) Q690, and (c) Q960 together with the relevant buckling curves from EN 1993-1-1.

Source: (Huang & Zhang, 2022)

Another similar study by Huang and Hong (2020) examined the interactive buckling of hot-rolled high strength steel CHS members with quality S420. Similar conclusions can be drawn as in the study presented previously regarding imperfections where the most interesting results were:

- The impact on the resistance of residual stresses on columns with intermediate slenderness was a reduction of up to 11.8 %.
- On columns with an global slenderness ratio, λ_m, over 25 overall geometric imperfections had a much larger impact on reducing the resistance compared to local geometric imperfections. The resistance was reduced by up to 11.5 % when considering global imperfections and the local imperfections had reduction of 3.7 % smaller than this.

Furthermore, they introduced new proposals to the design values regarding the local buckling limits. As presented in section 2.4.1 the $\frac{d}{t}$-ratio is used to determine the sections' ability to develop full plastic rotation before yielding where the current limit for local buckling before the yield limit is $\frac{d}{t} > 90\,\varepsilon^2$ which for $f_y = 420$ MPa gives $\frac{d}{t} = 50.36$, according to EN1993-1-1 (CEN, 2005). The authors propose a significant reduction to this limit where the new suggested limit is $\frac{d}{t} = 27$ which for $f_y = 420$ MPa gives new limit of $\frac{d}{t} > 48.26\,\varepsilon^2$ (Huang & Hong, 2020). For perspective the limit for CSC 1 (can utilise the full plastic rotational capacity before local buckling) in EC3 is $\frac{d}{t} \leq 50\,\varepsilon^2$, according to EN1993-1-1 (CEN, 2005). This means that according to Huang and Hong (2020) a cross-section that is in CSC 1 according to EC3 can still be expected to have local buckling before reaching the yield limit. The authors have commented that their results can originate from (i) the inconsistencies of the applied modes of residual stresses and geometric imperfections due to differences between the research on the subject, and (ii) significant weakening of the section area due to when the yield limit is reached the FE-model changes the Young's modulus to 0 (Huang & Hong, 2020). The FE-results compared with $\frac{D}{t}$-limit for reduction of local buckling between FE-results and different design guidelines is illustrated in Figure 2.24.

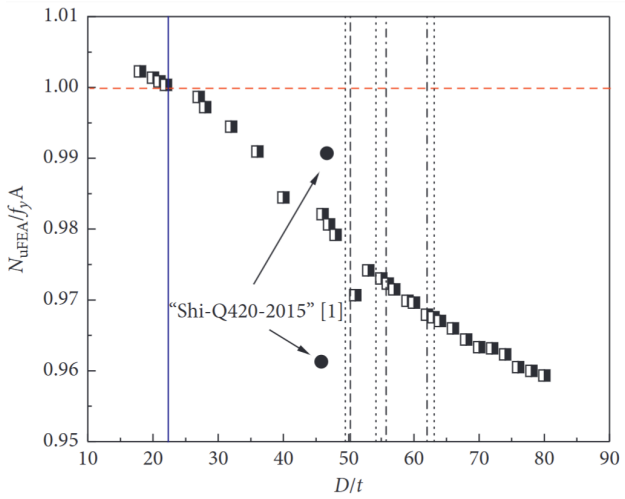

Figure 2.24: Comparison of $\frac{D}{t}$-limit for reduction of local buckling between FE-results and different design guidelines.

Source: (Huang & Hong, 2020)

When assessing the interactive buckling resistance of the members Huang and Hong (2020) neglect the impact of the local buckling effects on the design buckling curves. Out of the FEM-results they found that, according to the global buckling curves provided in EN1993-1-1 (CEN, 2005), buckling curve a should act as design curve. Their FEM-results together with the buckling curves are shown in figure 2.25 below.

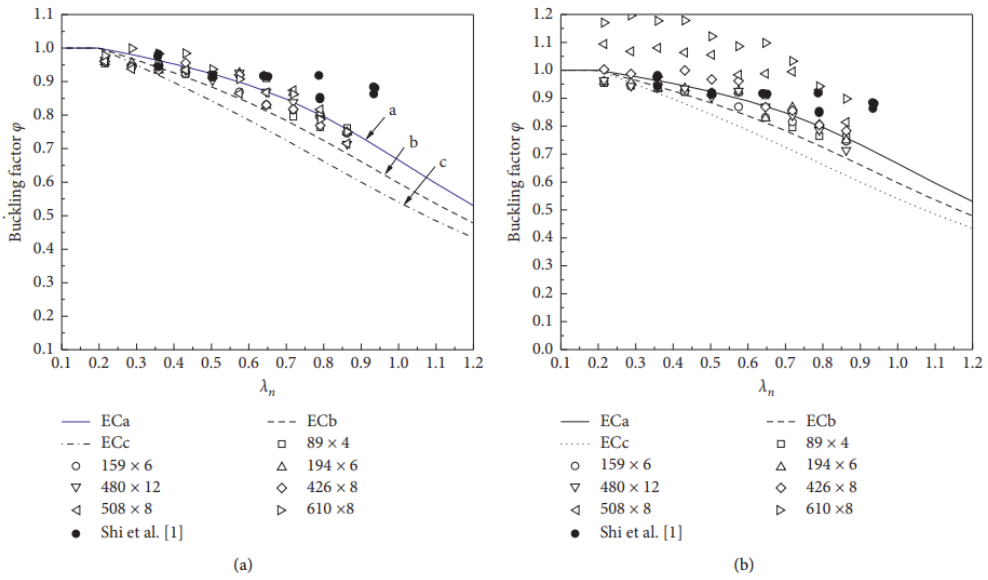

Figure 2.25: Reduction factor as a function of global slenderness together with FE-results and buckling curves according to EC3.

Source: (Huang & Hong, 2020), (CEN, 2005)

3
Finite Element Analysis

For the parametric study, ABAQUS will be used to model the buckling behaviour of CHS members under compression. The focus will be on the effects of both the local and global buckling behaviour. In this chapter the process of building an FE-model which simulates the buckling behaviour will be presented together with all modelling choices and validation of this that have been done.

3.1 The software

In this study, ABAQUS-2024 will be employed to account for both geometric and material nonlinearities, following the approach in EN1993-1-14 (CEN, 2022), which uses an equivalent imperfection amplitude that incorporates the effects of both geometric and material imperfections.

3.2 Element type

Because of the geometry of CHS members three-dimensional, quadrilateral, conventional stress-displacement shell element was chosen as the most appropriate for the parametric analysis. The outer surface of the shell was chosen as the reference surface, meaning that the thickness is integrated in from this.

The CHS member was modelled using first-order structural elements (S4R & S4) and second-order structural elements (S8R), which include additional degrees of freedom. The S8R elements are capable of accurately modelling finite strains and are particularly useful for describing complex behaviour with a coarser mesh (*ABAQUS User Manual*, n.d.-b). This approach allows for quicker simulations, making it ideal for parametric studies where reducing computational time is crucial.

3.3 Material model for hot-rolled steel

The FE-model will primarily be used for comparison against Eurocode and thusly the material model will aim to use the nominal values presented in these to create a model with a fair comparison. To narrow down the computational time of the analysis only one commonly used steel quality will be analysed. The steel quality in question is normal strength steel, S355.

3.3.1 Modulus of elasticity

The modulus of elasticity, E, should be assumed according to EN1993-1-1 (CEN, 2005) which means that for carbon steel it is set to 210 GPa. In case of a GMNIA where elastic instability is dominant a reduced modulus of elasticity should be used according to EN1993-1-14 (CEN, 2022). For this case E should be set to 200 GPa for carbon steel and 191 GPa for stainless steel.

3.3.2 Stress-strain curve for hot-rolled normal strength steel

As this thesis main focus is the parametric study representative stress-strain curves will be used which is adoptable to different steel qualities and production methods. A quad-linear material model for hot-rolled steel is deemed to be of sufficient accuracy while still offering a simplicity in FE-modelling. An illustration of a quad-linear material model is shown in Figure 3.1 below.

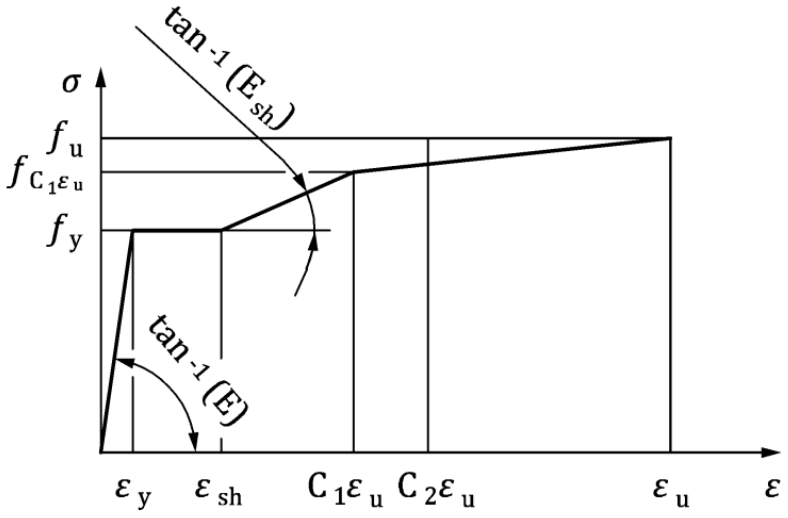

Figure 3.1: Illustration of a quad-linear material model stress-strain curve.
Source:EN1993-1-14 (CEN, 2022)

The stress-strain curve can be described by a series of equations which define the different linear relationships using equation 3.1.

$$\sigma(\varepsilon) = \begin{cases} E\varepsilon & \text{for } \varepsilon \leq \varepsilon_y \\ f_y & \text{for } \varepsilon_y < \varepsilon \leq \varepsilon_{sh} \\ f_y + E_{sh}(\varepsilon - \varepsilon_{sh}) & \text{for } \varepsilon_{sh} < \varepsilon \leq C_1\varepsilon_u \\ f_{c_1\varepsilon_u} + \frac{f_u - f_{c_1\varepsilon_u}}{\varepsilon_u - C_1\varepsilon_u}(\varepsilon - C_1\varepsilon_u) & \text{for } C_1\varepsilon_u < \varepsilon \leq \varepsilon_u \end{cases} \tag{3.1}$$

where:

- f_y is the yield stress
- $\varepsilon_y = \frac{f_y}{E}$ is the yield strain
- f_u is the ultimate tensile strength
- ε_{sh} is the strain hardening strain which is given by:

$$\varepsilon_{sh} = 0.1\frac{f_y}{f_u} - 0.055 \quad \text{but} \quad 0.015 \leq \varepsilon_{sh} \leq 0.03 \tag{3.2}$$

- ε_u is the ultimate strain which is given by:

$$\varepsilon_u = 0.6\left(1 - \frac{f_y}{f_u}\right) \quad \text{but} \quad 0.06 \leq \varepsilon_u \leq A \tag{3.3}$$

- A is the elongation after fracture defined in the relevant material specification
- C_1 is a material coefficient which is given by:

$$C_1 = \frac{\varepsilon_{sh} + 0.25(\varepsilon_u - \varepsilon_{sh})}{\varepsilon_u} \tag{3.4}$$

- E_{sh} is a strain hardening modulus which is given by:

$$E_{sh} = \frac{f_u - f_y}{C_2\varepsilon_u - \varepsilon_{sh}} \tag{3.5}$$

- C_2 is a material coefficient which is given by:

$$C_2 = \frac{\varepsilon_{sh} + 0.4(\varepsilon_u - \varepsilon_{sh})}{\varepsilon_u} \tag{3.6}$$

3.3.3 Material input data

S355H have been chosen as an appropriate steel quality for this analysis and has a yield strength, f_y, of 355 MPa, an ultimate strength, f_u, of 510 MPa according to EN1993-1-14 (CEN, 2005), and an A-value of 22 % (*SS-EN 10219-1:2006*, 2006). Out of these values together with equations 3.1-3.6 the plastic material model that were to be inputted into Abaqus could be calculated. The calculated elastic and plastic material parameters to create a quad-linear material model as figure 3.1 are shown in table 3.1 below.

FEM material parameters	
Yield stress [MPa]	**Plastic strain [-]**
355	0
355	0.0150
452	0.0568
510	0.1824

Table 3.1: Material parameters for the FE-model

To account for volumetric change after yielding true stress and true strain of the material is used. The material properties implemented in FEM were modelled using the true plastic stress-strain values from Equations 3.7 and 3.8 according to EN1993-1-14 (CEN, 2022). The implemented values in ABAQUS is shown in 3.2

$$\sigma_{\text{true}} = \sigma(1 + \varepsilon) \tag{3.7}$$

$$\varepsilon_{\text{true,pl}} = \ln(1 + \varepsilon) - \frac{\sigma_{\text{true}}}{E_0} \tag{3.8}$$

FEM material parameters	
True stress [MPa]	**True plastic strain [-]**
355	0
360.33	0.0132
477.56	0.0530
603	0.1646

Table 3.2: True stress and true plastic strain implemented in FE-model

3.4 Boundary conditions and loads

To simulate the buckling behaviour a concentrated load was placed at one end of the specimen.
The specimens were hinged at both ends as shown in 3.2. At the end where the load is applied, displacements are allowed only in the direction of loading, while at the opposite end, all displacements are restrained. The rotational degrees of freedom at both ends are allowed to rotate in a single direction, ensuring that buckling occurs only in that direction.
To implement the boundary conditions, two reference points were created and coupled to the corresponding end surfaces, ensuring that the entire end surface and the reference point move together as a single unit.

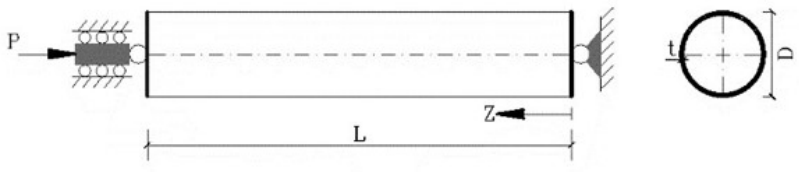

Figure 3.2: Specimen boundary condition

Source: (Huang & Zhang, 2022)

3.5 Initial geometric imperfections

In order to improve the accuracy of the FE analysis, the specimens in the model include both global and local imperfections, which better represent the real geometry of actual columns. Initially, an elastic analysis was conducted, followed by the evaluation of the first global and first local mode shapes. In other words, the imperfection shapes were derived from an initial eigenvalue buckling analysis, using the lowest global and local buckling modes to represent the global and local imperfections, respectively (*ABAQUS User Manual*, n.d.-c). The amplitudes of these imperfections, described below, were implemented using the IMPERFECTION command, with the local and global imperfections linearly superimposed.
According to Eurocode the global initial imperfection, e_0, depend on the buckling curve and the imperfection magnitude is calculated according to equation 3.9 below according to EN1993-1-14 (CEN, 2022). This is an equivalent imperfection magnitude incorporates the imperfection caused by residual stresses as well.

$$e_g = \frac{\alpha\ L}{150} \geq \frac{L}{1000} \tag{3.9}$$

Where α is the imperfection factor depending on the buckling curve previously introduced. With steel quality 355J2H the imperfection factor is $\alpha = 0.21$. This gives e_g the following value:

$$e_g = \frac{1.4\ L}{1000}$$

The local imperfection amplitude is determined by equation 3.10 according to EN1993-1-6 (CEN, 2007).

$$e_l = \frac{1}{Q}\sqrt{\frac{r}{t}} \cdot t \tag{3.10}$$

Where Q is the fabrication quality parameter varying depending on the tolerance quality class and is presented in chapter 2.4.3.

According to EN1993-1-6 (CEN, 2007), when identifying the leading imperfection, the accompanying imperfections should be included with their amplitudes reduced to 70% of their specified values. Each imperfection type should then be considered individually as the leading imperfection, with the others treated as accompanying imperfections.

3.6 Mesh sensitivity analysis

A convergence study has been performed to determine which element type is the most suitable for the parametric analysis, and the results of these are summarised in Table 3.3-3.5. As shown in the results of the convergence study the S8R elements demonstrate greater stability where the ultimate load has already converged for a coarse mesh. The S4R and S4 elements are more sensitive to mesh size requiring a small mesh and thus a long computational time for the ultimate load to converge. The ultimate load with a S8R mesh also matches the ultimate load of the test results more accurately than the other mesh types and was thusly chosen as an appropriate choice.

S8R			
Mesh size	**Mesh size [mm]**	**Ultimate load [MN]**	$N_{\mathbf{u,FEM}}/N_{\mathbf{test}}$
$0.092\sqrt{DL}$	100	2.10499	1.0024
$0.046\sqrt{DL}$	50	2.10152	1.0007
$0.026\sqrt{DL}$	25	2.10345	1.0016
$0.012\sqrt{DL}$	12.5	2.10113	1.0005

Table 3.3: Mesh sensitivity analysis results for S8R elements.

S4R			
Mesh size	**Mesh size [mm]**	**Ultimate load [MN]**	$N_{\mathbf{u,FEM}}/N_{\mathbf{test}}$
$0.092\sqrt{DL}$	100	2.05192	0.9771
$0.046\sqrt{DL}$	50	2.09938	0.9997
$0.026\sqrt{DL}$	25	2.11227	1.0058
$0.012\sqrt{DL}$	12.5	2.11514	1.0072

Table 3.4: Mesh sensitivity analysis results for S4R elements.

S4			
Mesh size	**Mesh size [mm]**	**Ultimate load [MN]**	$N_{\mathbf{u,FEM}}/N_{\mathbf{test}}$
$0.092\sqrt{DL}$	100	2.06557	0.9836
$0.046\sqrt{DL}$	50	2.10258	1.0012
$0.026\sqrt{DL}$	25	2.11313	1.0063
$0.012\sqrt{DL}$	12.5	2.11546	1.0074

Table 3.5: Mesh sensitivity analysis results for S4 elements.

To ensure the accuracy of the FE analysis, a mesh sensitivity analysis was performed on specimen D420-40-2 from the validation of the FE-model, see section 3.8. The analysis was conducted with four different mesh sizes, considering S4, S4R, and S8R elements. The ultimate load from the FE-results was studied for each mesh size, and the corresponding values are presented previously in Table 3.3-3.5. The mesh size

sensitivity analysis is visualised in Figure 3.3 where the FE-results are normalised against the test results of D420-40-2.

Since the diameter and length of the specimens in the parametric study vary greatly, achieving mesh which yield consistent results and reasonable computational time for all specimens becomes challenging. To address this issue, a mesh size approach based on the length and diameter of the specimen was chosen. The proposed mesh size is give in equation 3.11. With this approach computational time will be reduced while accounting for variations in specimen dimensions, thereby avoiding excessively fine or overly coarse meshes.

$$\text{mesh size} = \alpha\sqrt{DL} \tag{3.11}$$

As seen in the results from the convergence and mesh sensitivity analysis, the S8R element demonstrated greater stability, as previously discussed the results converge at a very coarse mesh. Thusly, a mesh size of $0.05\sqrt{DL}$ was deemed as the most suitable size for the parametric analysis. The final mesh configuration of an FE-model with a mesh size $0.05\sqrt{DL}$ is visualised in Figure 3.4

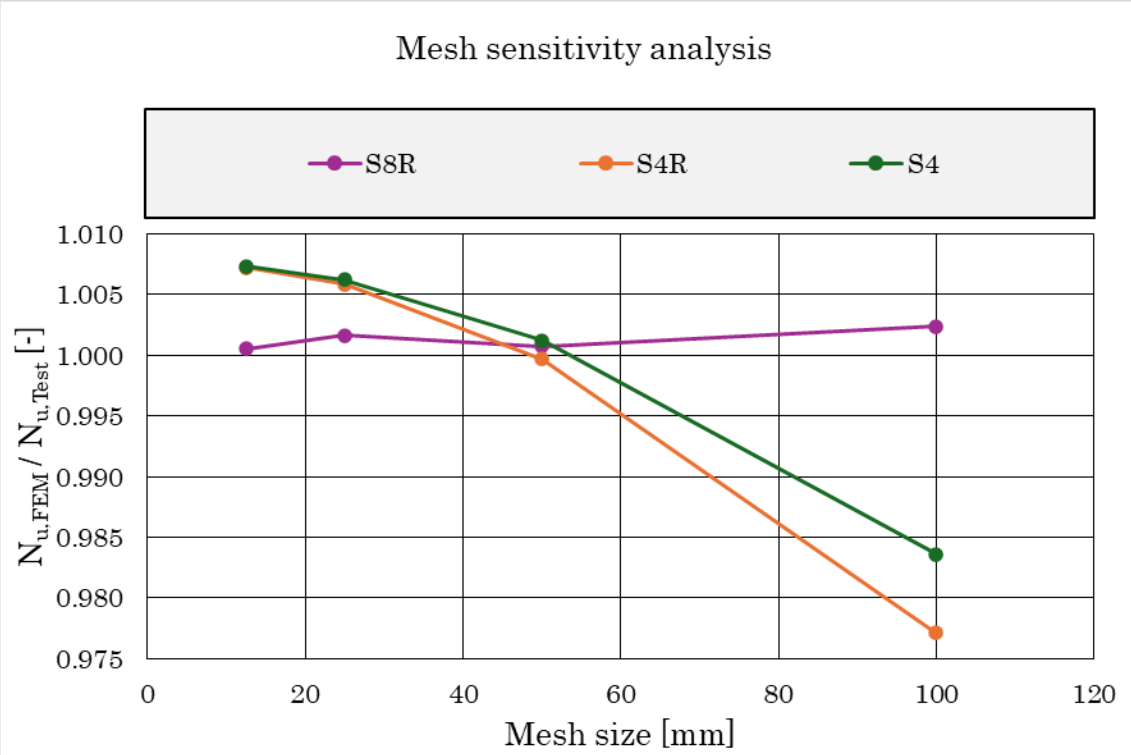

Figure 3.3: Convergence study of mesh size

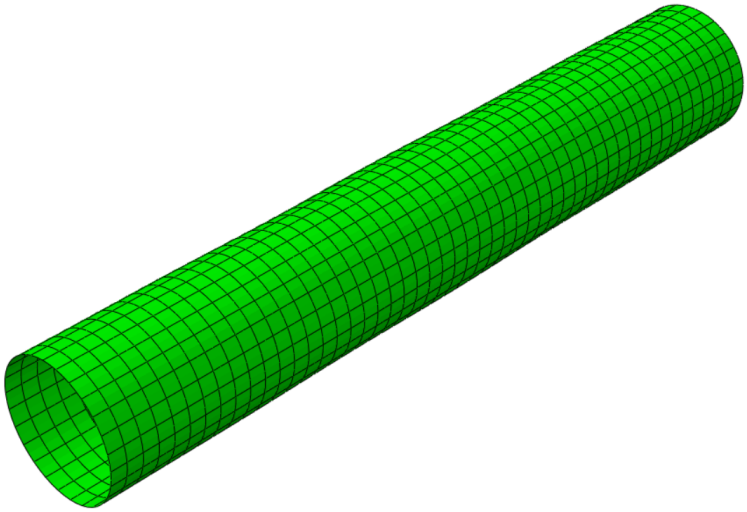

Figure 3.4: Mesh configuration of specimen with $L = 3000\ mm, D = 500\ mm, t = 6\ mm$

3.7 Linear elastic and non-linear analysis

To extract the buckling modes for each member in the parametric analysis, an linear eigenvalue buckling analysis was conducted. For the linear analysis the BUCKLE step was used with the subspace iteration eigenvalue extraction method in ABAQUS, with the load and boundary conditions applied as previously mentioned. Using this, the desired number of eigenvalues is stated and a suitable number of vectors is created to the subspace iteration procedure which generate the buckling mode shapes as a normalised vector with a maximum displacement of 1.0 (*ABAQUS User Manual*, n.d.-a). The generated local and global buckling modes as well as the critical (bifurcation) load of the CHS members were then used as the imperfection shapes where the imperfection amplitudes was applied in the GMNIA.

In order to capture the post buckling behaviour of the specimens a GMNIA was conducted. The modified RIKS method in ABAQUS has been used which apply the load in incremental steps to capture this behaviour (*ABAQUS Theory Manual*, n.d.). The lowest local and global buckling modes are used to represent the imperfect shape of the member and the imperfection amplitude is applied as presented above. Furthermore, the nonlinear geometric parameter (*NLGEOM) was used in order to consider large displacement analysis. By this the non-linear behaviour of each specimen is captured and also post-buckling response where it moves beyond the ultimate load point.

3.8 Validation of FE-model

The validation was carried out replicating test and FEA results from Huang and Zhang (2022), which is described later in this chapter. The validation was conducted by comparing the experimental tests and FEA results by Huang and Zhang (2022) with the created FE-model, considering both global and local imperfections. The buckling resistance from the FE analysis was compared with the test results for the non-linear analysis. The FE-model validation was conducted using 10 specimens. The process began with a single specimen from the study by Huang and Zhang (2022), which involved a mesh sensitivity analysis. Once the model's accuracy was confirmed, additional models were run and their results compared with those from the referenced study to further validate the accuracy of the developed FE model.

3.8.1 Description of test specimens

The failure mode of the test specimens is a variation of local buckling and interactive buckling failure with CSC varying between Class 3 and Class 4 according to EN1993-1-1 CEN (2005). The specimen's diameter-to-thickness ratio (D/t) is close the limit of Class 4 meaning that interactive buckling behaviour is expected since this range of D/t-ratio has a high susceptibility to this failure mode under axial compression. It is important to note that residual stresses were neglected in this study, whereas they were considered in the referenced report, which may result in a higher deviation compared to the findings presented here.

3.8.2 Material model, initial imperfections & boundary conditions

In the FE study conducted by Huang and Zhang (2022), the mechanical properties are modelled using a multi-point follow-up hardening approach. The specimen's stress-strain curve shows a yield plateau, which is represented by a trilinear model where the material parameters are shown in table 3.6 and the stress-strain curve in figure 3.5. The boundary conditions of the test results are as presented above where one end has its displacements fixed and can rotate around on axis and the other end has the same but can move in the direction of the applied load. The magnitude of the global buckling imperfection is set to $L/1000$, while for local buckling, the magnitude is defined as $t\sqrt{D/2t}/16.5$.

Material model					
E **[MPa]**	f_y **[MPa]**	f_u [MPa]	ε_1 [%]	ε_2 [%]	ε_3 [%]
206000	460	550	$\frac{f_y}{E}$	2.0	14

Table 3.6: Material parameters for the stress-strain curve

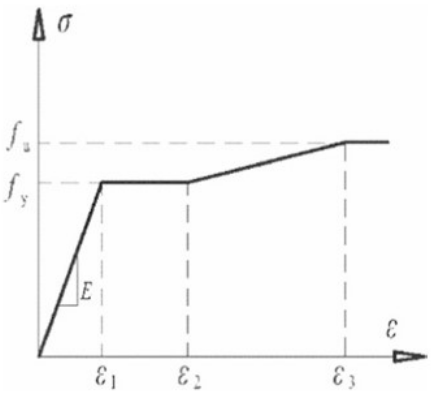

Figure 3.5: Stress–strain curve (trilinear isotropic hardening material model)
Source: (Huang & Zhang, 2022)

3.8.3 Results of validation

The FE-model was assessed on its ability to accurately predict the ultimate load on a set of experiments conducted by Huang and Zhang (2022) focusing on columns that failed by interactive buckling. Huang and Zhang (2022) validated their FE-model against these tests and found that their FE-model under predicted the ultimate load by a mean of 1.97 %.
When validating the FE-model to these experiments with the chosen mesh presented above the FE-model over predicted the ultimate load by a mean of 2.06 %. The reason for Huang and Zhang (2022) model under predicting and our model over predicting probably originate from their model incorporating residual stresses. Hence, this deviation is deemed acceptable since residual stresses is incorporated into the geometric imperfections in the parametric study later on but not in the validation process. The results from the validation is shown in table 3.7 below.

Specimen	**D**	**t**	**L**	**D/t**	**CSC**	**Failure mode**	$\mathbf{N_{test}}$	$\mathbf{N_{FEM}}$	**Difference %**
D420-20-1	274	6.01	2362	45.59	3	L	2095	2277	8.01
D420-30-1	273	5.85	3305	46.67	4	I	2075	2152	3.56
D420-30-2	273	5.95	3307	45.88	3	I	2094	2189	4.34
D420-30-3	273	5.91	3306	46.19	4	I	2042	2174	6.08
D420-40-1	275	5.89	4248	46.69	4	I	2027	2114	4.11
D420-40-2	276	5.83	4249	47.34	4	I	2100	2103	0.16
D420-40-3	271	5.91	4248	45.85	3	I	2026	2086	2.87
D420-50-1	274	5.87	5193	46.68	4	I	2038	1974	-3.25
D420-50-2	273	5.88	5192	46.43	4	I	1997	1953	-2.28
D420-50-3	273	5.88	5193	46.43	4	I	2012	1952	-3.05
Mean									**2.06**

Table 3.7: Comparison of Test and FEM Results

Out of the results presented above the developed FE-model is deemed to be able to predict the ultimate load and buckling behaviour of CHS members accurately. This means that the FE-model can be used as basis for a larger parametric study to generate a large amount of data to be used to investigate how the interactive buckling behaviour impact the ultimate load of CHS members.

4

Parametric Study

In this chapter the parametric study which is designed to investigate the buckling behaviour of CHS members under axial compression is presented. The main goal of this study is to generate a lot of data to explore how different geometry such as length, diameter and slenderness ratio influence the ultimate capacity of the members when transitioning between pure local and global and interactive buckling.
The validated FE-model developed in Chapter 3 served as the foundation for this analysis. Furthermore, a Python script was employed to parametrise models, apply loads, and extract the ultimate load for each specific geometry from ABAQUS, enabling high-efficiency simulation over a wide range of geometric data. The python script in its entirety in shown in Appendix A.

The script is designed in order to automate the steps in ABAQUS which significantly reduces the time and ensure accuracy of the result for each simulation. Through a simple CSV file as input an output CSV file with relevant results are is created after the FEA is conducted. The key functionalities of this script include:

- Automated data input: The script reads input values for diameter (D), length (L), and thickness (t) from a predefined CSV file.
- Dynamic mesh size Calculation: For each specimen, the script calculates the mesh size based on $0.05\sqrt{DL}$.
- Model creation and configuration: It creates a new 3D model for each unique combination of D, L, and t, and configures the geometry of the CHS member according to the specified dimensions.
- Material property assignment: The script assigns the material properties, including Young's modulus and plastic behaviour, to the model.
- Boundary conditions and load: It applies a pinned-pinned boundary conditions and also axial loads to simulate axial compression.
- Linear buckling analysis: The script performs a linear buckling analysis to identify the first 20 buckling modes of each specimen. The script then analyses the shape of the buckling mode and identifies if it is a global or local buckling mode and labels them accordingly. Typical local and global failure modes are visualised in Figure 5.1 below.
- Initial imperfection application: Out of the LEA, the script applies initial imperfections to the model on the first local and global buckling modes. If no global buckling modes are present the imperfections are only applied on the first local buckling mode and vice versa.
- Post-Buckling behaviour simulation: Using the Riks method in a GMNIA, the script applies the axial load incrementally to capture the post-buckling

behaviour of the columns. Three of the typical failure modes are visualised in Figure 5.2 below.
- Result extraction and documentation: The ultimate load capacity ($N_{u,\mathrm{FEM}}$) for each simulation is extracted and saved to a CSV file.
- Error handling: The script capture and record any issues occurred during the simulation.

For the first part of the parametric study the geometries was chosen iteratively in order to set the outer thresholds of the dataset i.e. extremely stocky columns which only have local buckling modes to extremely slender columns which only have global buckling modes. A reasonable step size in length and diameter was chosen to include the transition from only local or global buckling modes to the interactive buckling modes with both local and global buckling occurring at the same time. Consideration was also put on having a reasonable step size so that possible flaws in the design guidelines could be identified. Out of this the first dataset of geometries was created. The lengths and diameters that were chosen ranged from $2000 - 10000\ mm$ and $100 - 1000\ mm$ respectively while the thickness of the members was kept constant at 6 mm. With this the parametric study included $\frac{D}{t}$-ratio which ranges from $16.7 - 166.7$ and non-dimensional slenderness ratio, λ_n, which ranges from $0.07 - 3.93$. This meant that the parametric study would be able to contain the transition phase from either exclusively global or local buckling modes to interactive buckling modes across a large variety of specimens.

After the first part of the parametric study was conducted the points of interest was refined, to produce more data points in these parts to fully capture the behaviour there. These include the transition from CSC 3 to 4 to fully depict how the transition phase of the design guidelines from seeing the column as a column (EN1993-1-1) to a shell structure (EN1993-1-6) and the transition from exclusively local or global buckling modes to interactive buckling modes to fully capture the columns behaviour in these type of columns. As mentioned above, the parametric study only analyse one steel quality and a constant thickness which means that the CSC limit for class 4 members is constant in the whole study. The limit is calculated according to equation 4.1 which means that all members with a diameter over 357.5 mm is in CSC 4. Out of this additional members with diameters close to this is examined for all lengths.

$$\frac{D}{t} \leq 90\varepsilon^2 \Rightarrow D \leq 90t\varepsilon^2 = 357.5\ mm \tag{4.1}$$

The additional members that were examined through mode interaction is further explained in 5.5. The parameters and ranges used in the study are summarized in Table 4.1 below.

Table 4.1: Summary of parameters used in the parametric study

Parameter	**Variable**	**Range / Value**	**Units**
Cross-section type	–	Circular Hollow Section (CHS)	–
Steel grade	–	S355H	–
Yield strength	f_y	355	MPa
Ultimate strength	f_u	510	MPa
Length	L	2000–10000	mm
Diameter	D	100–1000	mm
Wall thickness	t	6	mm
Diameter-to-thickness ratio	D/t	16.7–166.7	–
Length to radius ratio	L/r	4–200	–
Non-dimensional slenderness	λ_n	0.07–3.93	–
Mesh size	–	$0.05\sqrt{DL}$	mm
Global imperfection	e_g	$1.4L/1000$	mm
Local imperfection	e_l	$t\sqrt{D/2t}/16$	mm

5
Results

In this chapter the results of the parametric study are presented. Since the focus is on evaluating the design standards, the results are compared with design resistances from current and alternative design methods to assess their accuracy in estimating the capacity of CHS steel members and to determine whether their predictions are reliable. Out of this the mode interaction impact on the buckling resistance of CHS members is evaluated, together with imperfection and buckling mode sensitivity impact on mode interaction behaviour.

5.1 Results of parametric study

The results from the linear elastic analysis (LEA) rendered buckling modes for each column where the global and local buckling modes was used as imperfection shapes where the imperfection amplitude was applied on in the GMNIA. Typical local and global buckling modes which were used from the LEA are illustrated in Figure 5.1.

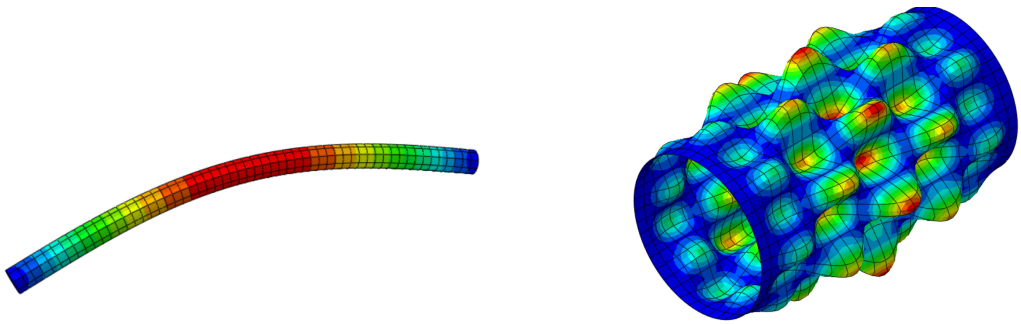

(a) Global buckling mode of column with $L = 2000\ mm,\ D = 100\ mm$

(b) Local buckling mode of column with $L = 2000\ mm,\ D = 1000\ mm$

Figure 5.1: Illustration of typical local and global buckling modes from LEA.

The results from the GMNIA where then used as final results where the ultimate loads was extracted. Three different buckling failure modes was observed - global, interactive, and local. Each different buckling failure modes are illustrated in Figure 5.2.

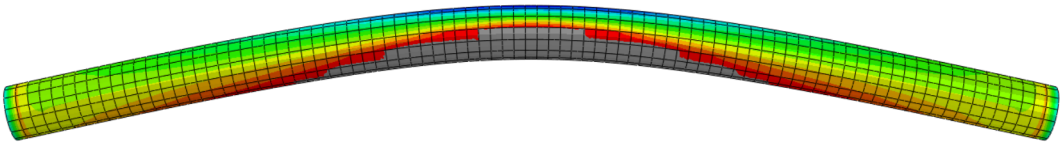

(a) Global buckling failure mode of column with $L = 2000\ mm,\ D = 100\ mm$

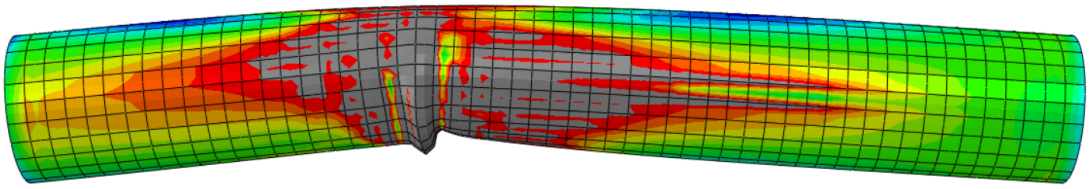

(b) Interactive buckling failure of column with $L = 2000\ mm,\ D = 280\ mm$

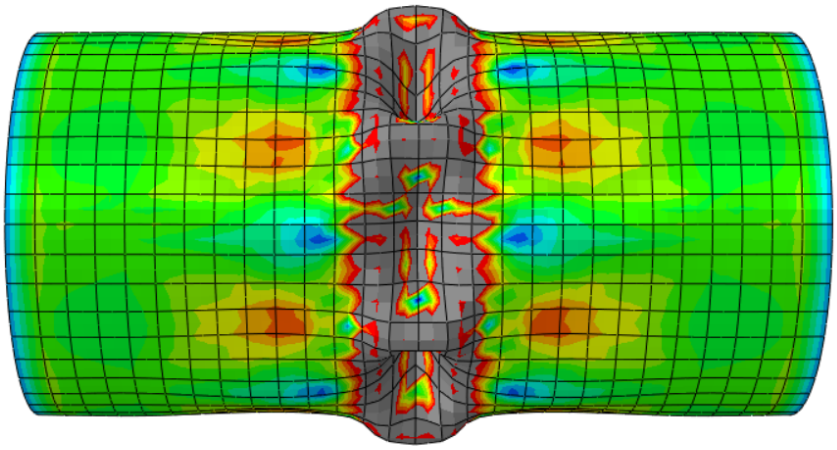

(c) Local buckling failure mode of column with $L = 2000\ mm,\ D = 1000\ mm$

Figure 5.2: Illustration of typical global, interactive, and local failure modes from GMNIA of three different columns with $L = 2000\ mm,\ D = 100, 280, 1000\ mm$ where the gray part shows yielding limit of each specimen.

The three failure modes exhibited distinct behaviours under incremental loading, with cross-sectional deformations aligning with expectations.
The slender column (L = 2000 mm, D = 100 mm) showed no local deformation but significant lateral midspan deflection, indicating global buckling. The stocky column (L = 2000 mm, D = 1000 mm) exhibited large local deformation with negligible lateral deflection, characteristic of local buckling. The intermediate column (L = 2000 mm, D = 280 mm) displayed a mix of both: the compressed side of the cross-section experienced local deformation, while the tensioned side did not, and the member showed global deflection—typical of interactive buckling. Cross-sectional deformation compared to the undeformed shape is shown in Figure 5.3.
Stiffness differences were also evident. The locally buckling column remained stiff until failure, the globally buckling column deflected significantly before peak load, and the interactive case showed intermediate stiffness. Load–displacement curves are illustrated in Figure 5.4.

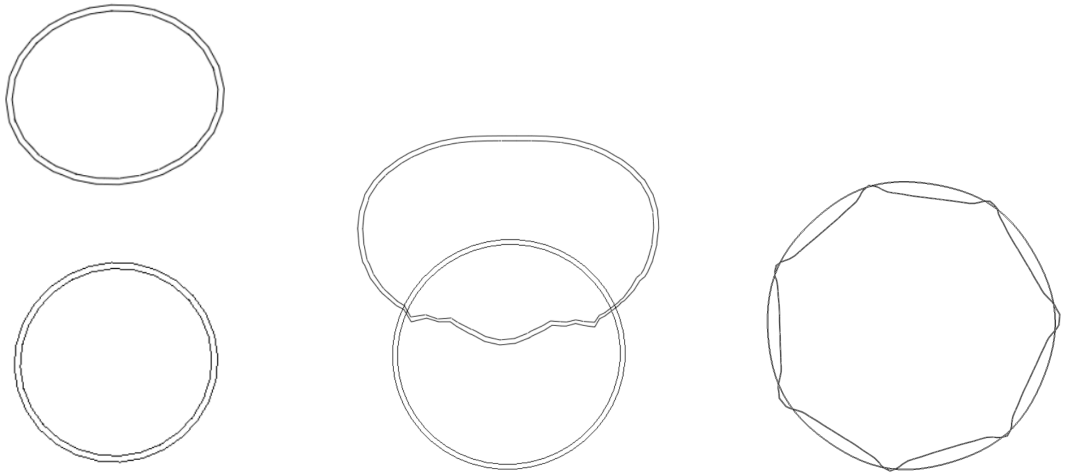

(a) $L = 2000$ mm
$D = 100$ mm

(b) $L = 2000$ mm
$D = 280$ mm

(c) $L = 2000$ mm
$D = 1000$ mm

Figure 5.3: Cross-sectional views of the deformed and undeformed shapes corresponding to (a) global buckling ,(b) interactive buckling and (c) local buckling.

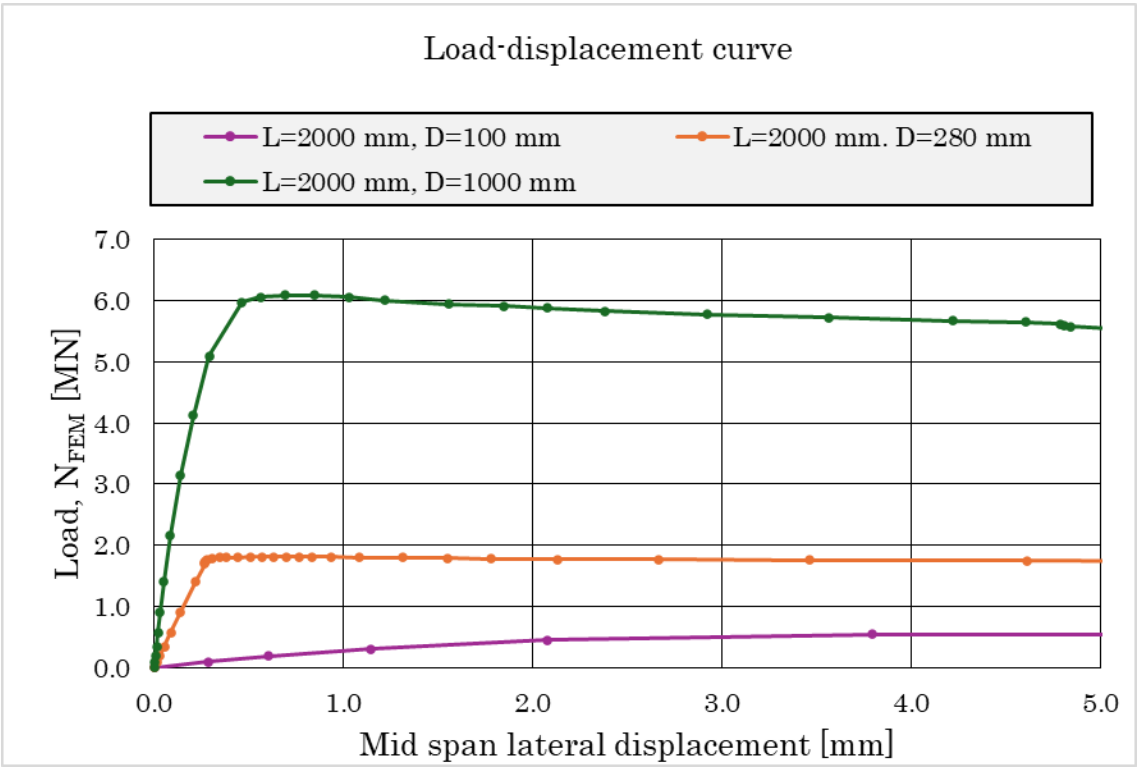

Figure 5.4: Load-displacement curve showing the different stiffnesses of each behaviour for three different columns exerting purely local (D=1000 mm), interactive (D=280 mm), and purely global buckling behaviour (D=100 mm).

Through the parametric study 223 CHS members was analysed. The final results of the 223 specimens in the parametric study are visualised in Figure 5.5 where the ultimate load, $N_{u,FEM}$, is normalised against the yield strength, f_y and plotted against non-dimensional slenderness, λ_n. For the geometry, $\frac{D}{t}$-ratio, λ_n, and ultimate loads from each specimen, see Appendix B.

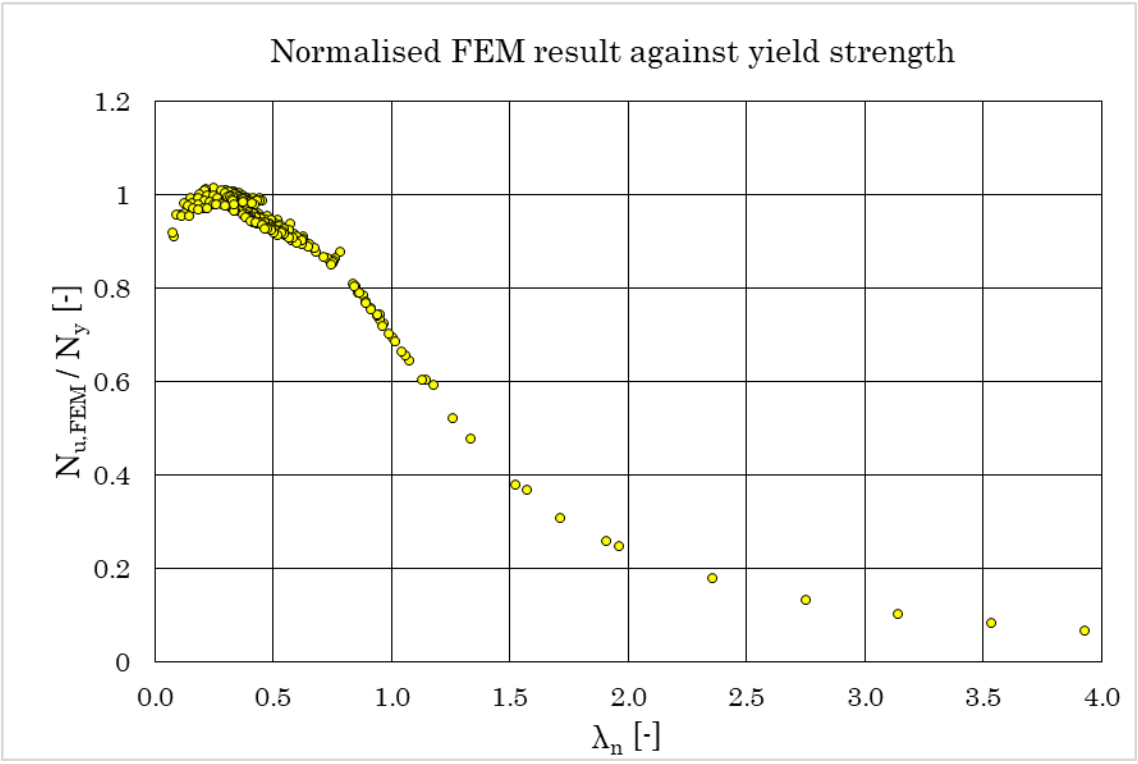

Figure 5.5: Results of the parametric study normalised against the yield strength.

5.2 Comparison with Eurocode

Figure 5.6 shows buckling curves a, b, and c from EN1993-1-1 (CEN, 2005), while the points represent the FE results normalized by the yield strength, forming an FE-based buckling curve. In this comparison the FE result should be compared to buckling curve a which is for hot-rolled CHS members. It can be seen that the result follow buckling curve a for for slender CHS members, i.e. when λ_n is large, and that for stocky and intermediate slender CHS members the results deviate from the buckling curve. It can also be observed in Figure 5.7 some unsafe result for a specific range when λ_n is less than 0.6. In this area the interactive buckling appears where local and global buckling modes occur simultaneously which leads to overestimation of the capacity where the resistance of the results are lower than the reduction factor given in EN1993-1-1, this is further described in Section 5.5. For a clearer visualization of the results, Figure 5.8 shows the FE results normalised against buckling curve a. It can be observed that the capacity may be underestimated by up to 10% where the results exceed 1, and overestimated due to interactive buckling by up to 2% where the results fall below 1. Comparison of Eurocode buckling curves with normalised FE results for each length is plotted and shown in Appendix C.

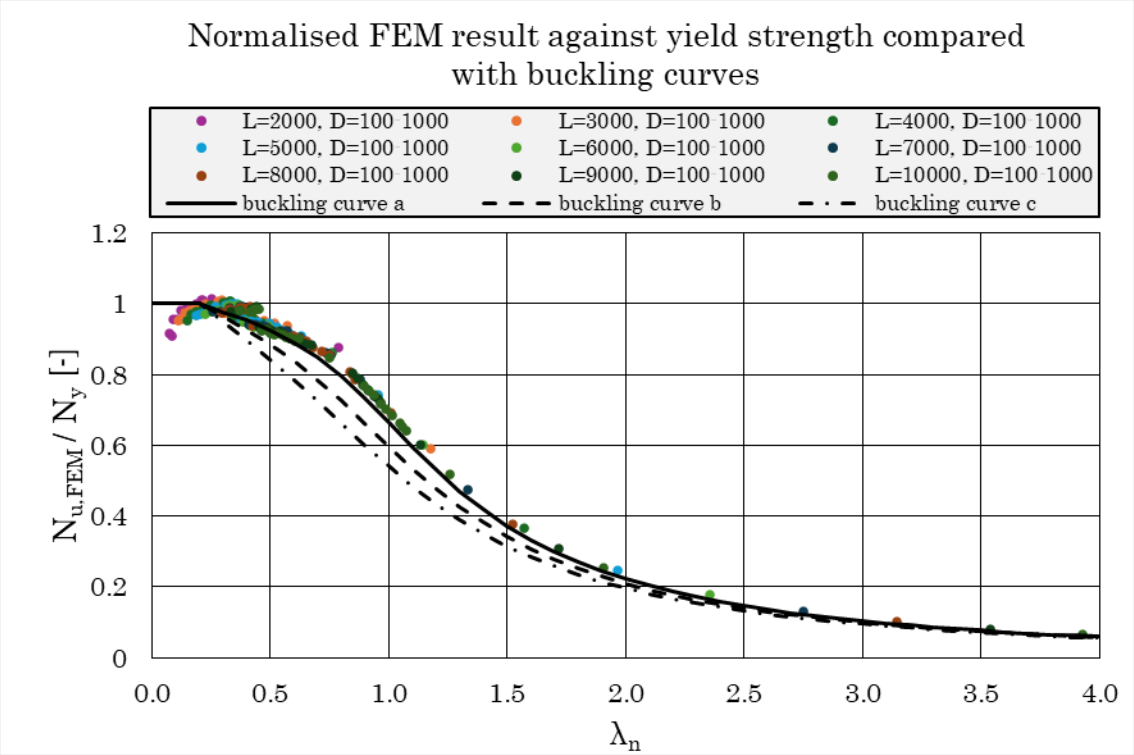

Figure 5.6: Comparison of Eurocode buckling curves with normalized FE results.

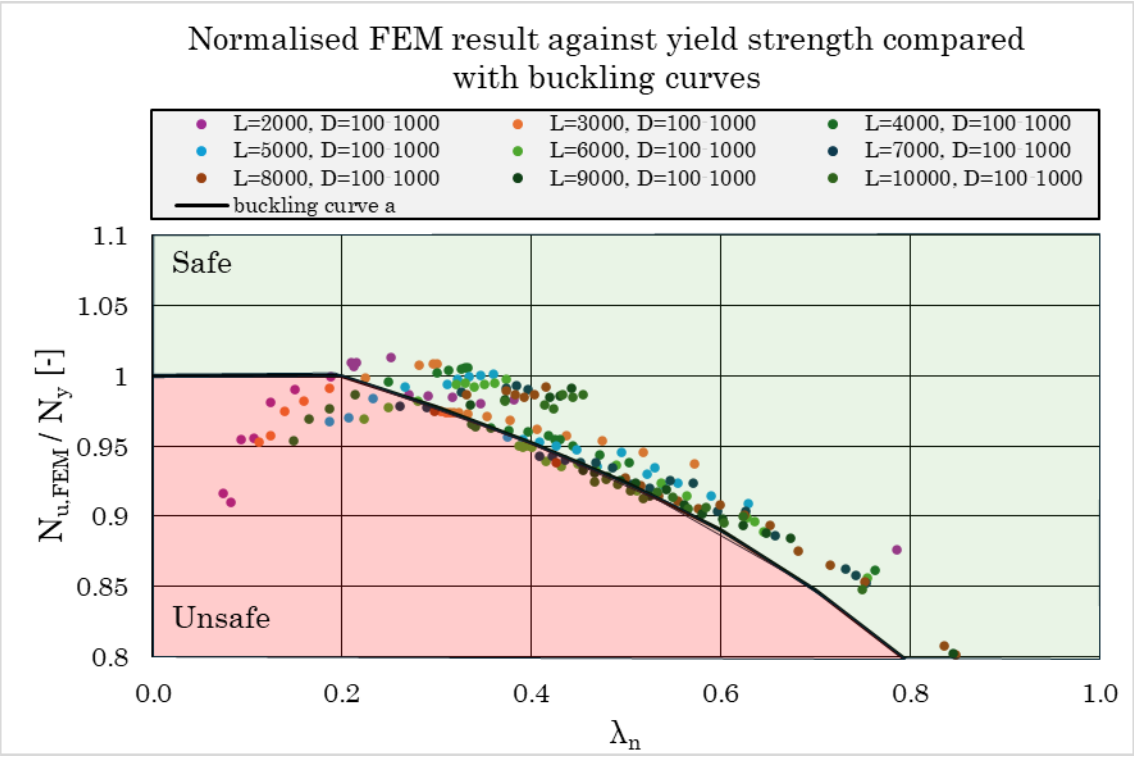

Figure 5.7: Zoomed-in comparison of Eurocode buckling curve a with normalized FE results in the unsafe region.

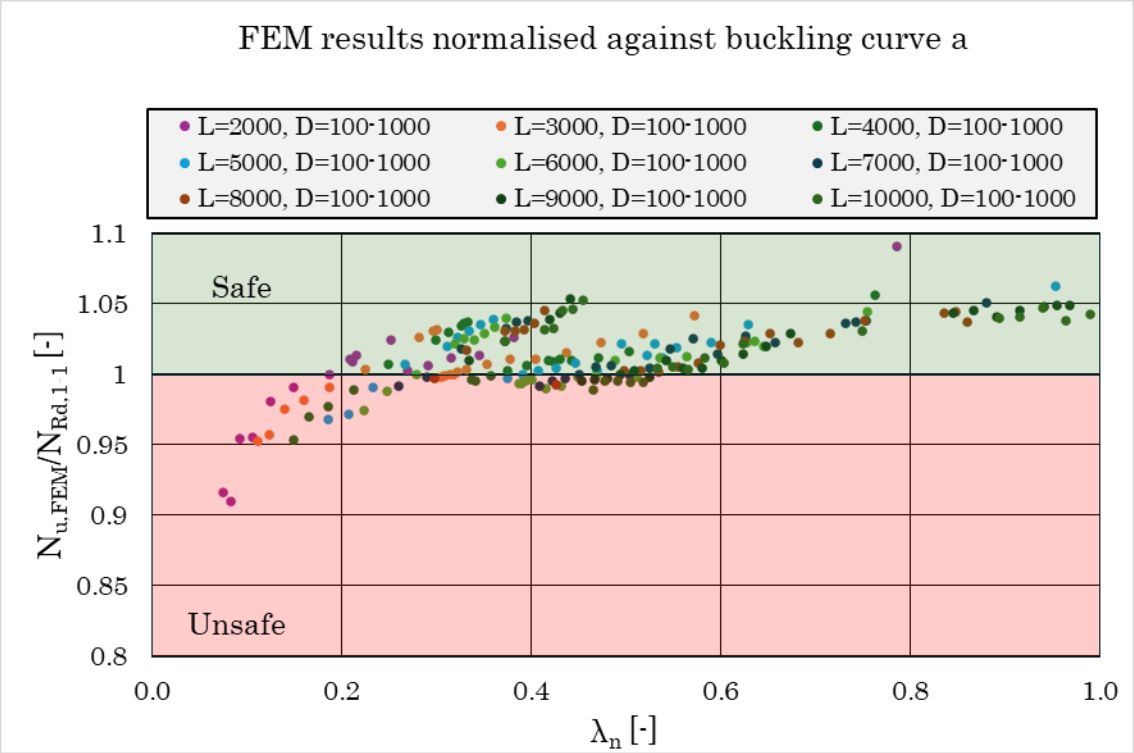

Figure 5.8: Normalised FE-results against curve a

The FEM-results have been compared against the design guidelines presented in 2.4.2 and 2.4.3. As of now the guidelines state that CHS members in CSC 1-3 should be designed as a column while CHS members in CSC 4 should be designed as a shell structure. The FEM-results normalised against N_{Rd} in EN1993-1-1 (CEN, 2005) for CSC 1-3 and EN1993-1-6 (CEN, 2007) for CSC 4 plotted against λ_n and against $\frac{D}{t}-$ratio are visualised in figure 5.9 and 5.10. For an easier overview of each series the individual series are visualised in Appendix D
The results show that the current design method could overestimate the buckling resistance of CHS members. In the transition from CSC 3 to 4 (from designing according to EN1993-1-1 to EN 1993-1-6) the columns that are in CSC 4 but close to the limit show a over prediction of up to 17 % in the worst case. This problem is exclusively present in the longest members ($L = 9000 - 10000\ mm$) where column-like global buckling behaviour is more present than shell-like local buckling behaviour. In the shorter sections ($L = 2000 - 5000\ mm$) no unsafe prediction of the buckling resistance is present but the design guidelines tend to be quite conservative instead having a sudden increase of resistance of up to 25 % in the transition from CSC 3 to 4. To summarise there seems arise a problem with the current design guidelines which leads to both unsafe and inefficient design for CHS members in CSC 4.

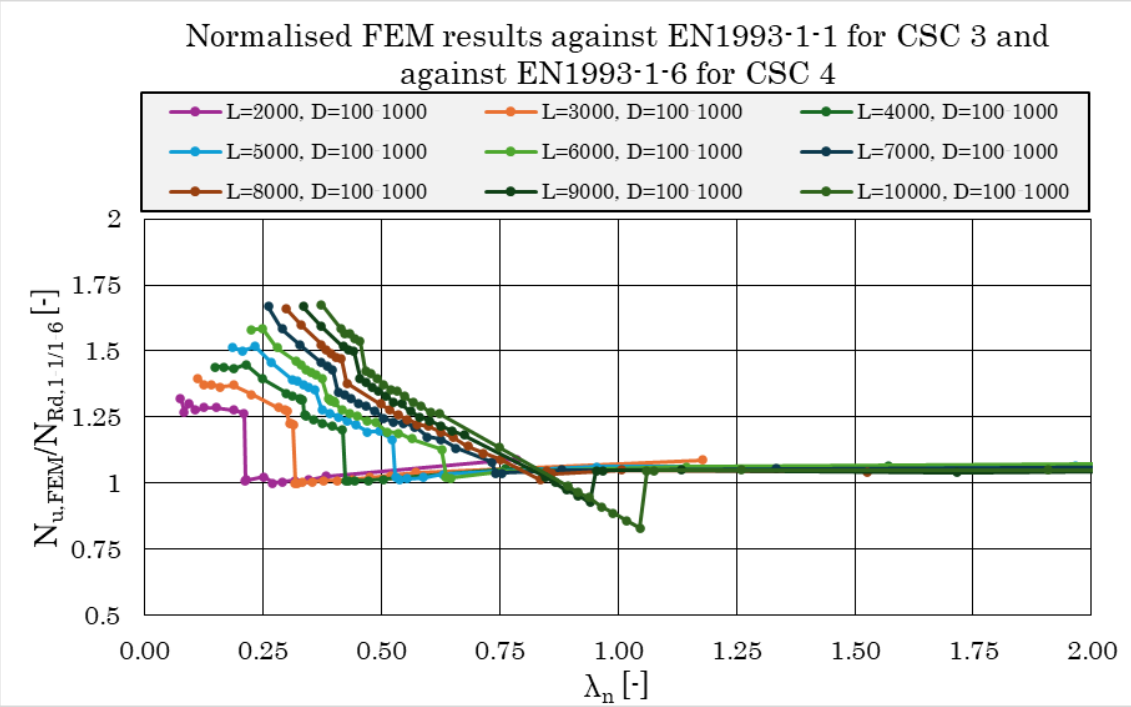

Figure 5.9: FEM-results normalised against N_{Rd} in EN1993-1-1 for CSC 1-3 and EN1993-1-6 for CSC 4 plotted against λ_n

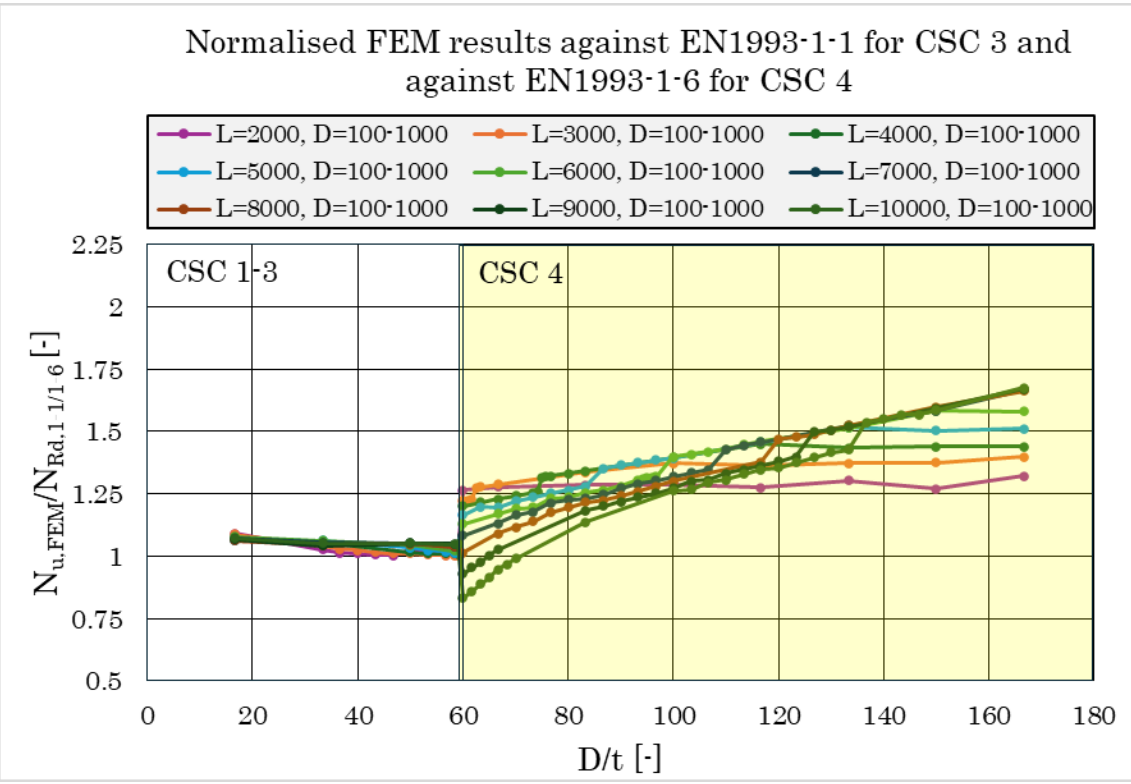

Figure 5.10: FEM-results normalised against N_{Rd} in EN1993-1-1 for CSC 1-3 and EN1993-1-6 for CSC 4 plotted against $\frac{D}{t}$ – ratio

5.3 Comparison with British standard (BS5950)

As presented in the previous section, the current European design guidelines lead to both unsafe and inefficient design for CHS members in CSC 4. Therefore alternative design methods have been analysed to compare if these can achieve a more satisfactory design. The first method that have been analysed was the BS5950-1 (British Standards Institution, 2008) which have developed an effective area method which is valid for CHS members in CSC 4, presented in chapter 2.4.4. The FEM-results normalised against N_{Rd} in EN1993-1-1 (CEN, 2005) for CSC 1-3 and BS5950-1 (British Standards Institution, 2008) for CSC 4 plotted against λ_n and against $\frac{D}{t}-$ ratio are visualised in figures 5.11 and 5.12. For an easier overview of each series, the individual series are visualised in Appendix E

The results show that the problem of overestimating the buckling resistance of CHS members in CSC 4 close to the CSC limit is eliminated with the effective area method for CSC 4. Contrary to Eurocode, the effective area method shows a transition from CSC 3 to 4 where the expected buckling resistance of the columns decreases with increasing $\frac{D}{t}-$ratio. However, even though unsafe design is avoided using BS5950-1 (British Standards Institution, 2008) the results still show an inefficient design when the $\frac{D}{t}-$ ratio increases beyond the limit of CSC 4. The results show that for the columns with the largest $\frac{D}{t}-$ ratio only half of the ultimate load is reached, leading to a large portion of the resistance not being fully utilised. This shows that the conservativity of the reduction of area due to local buckling could be further adapted to use more of the unused resistance of the cross-section.

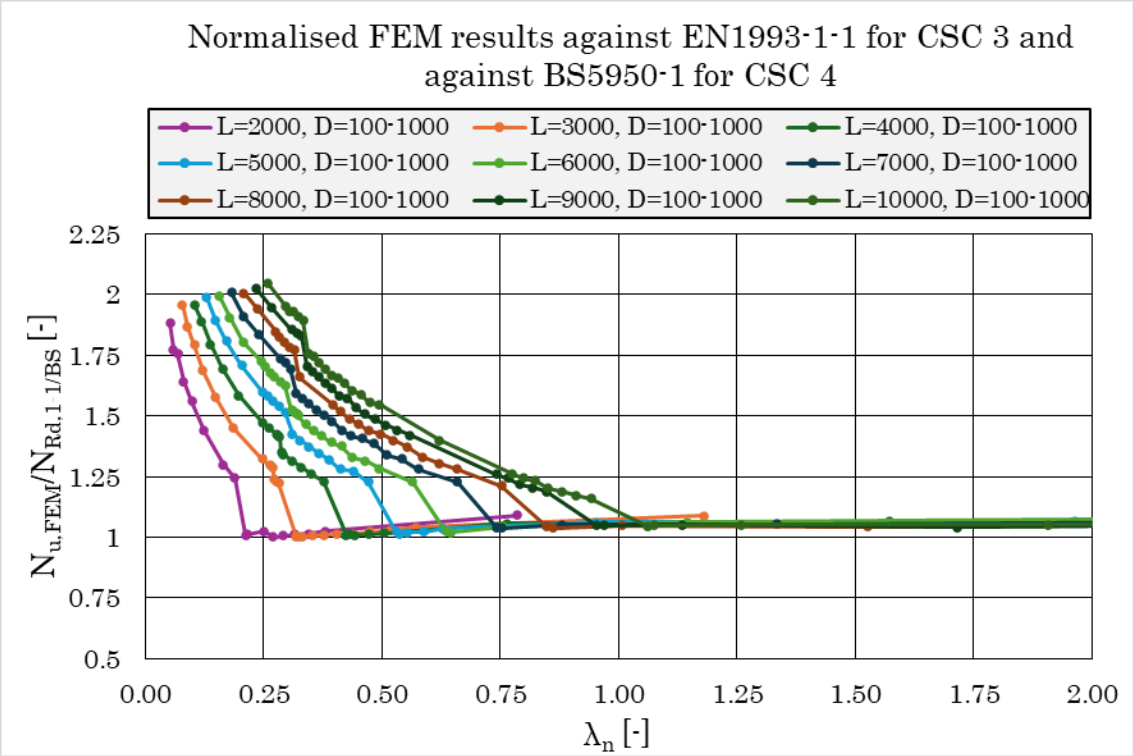

Figure 5.11: FEM-results normalised against N_{Rd} in EN1993-1-1 for CSC 1-3 and BS5950-1 for CSC 4 plotted against λ_n

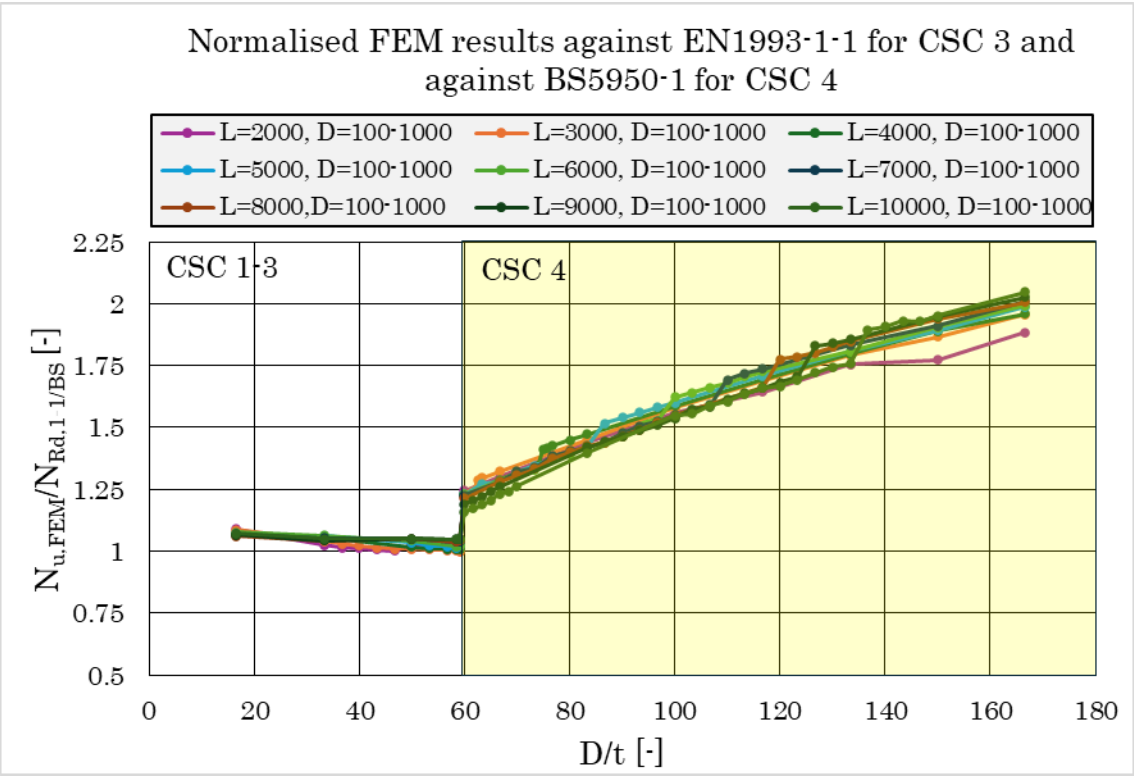

Figure 5.12: FEM-results normalised against N_{Rd} in EN1993-1-1 for CSC 1-3 and BS5950-1 for CSC 4 plotted against $\frac{D}{t}$ – ratio

5.4 Comparison with a local reduction factor

Another method produced by Toffolon and Taras (2017), presented in 2.5.2, introduced a local buckling reduction factor that is multiplied with the global buckling reduction factor. The additional factor in the local behaviour of the column depends on its geometry, thus offering a design which takes both the local and global buckling modes into account. The effect on buckling curve a while introducing a local reduction factor for the columns considered in the parametric study is visualised in Figure 5.13.

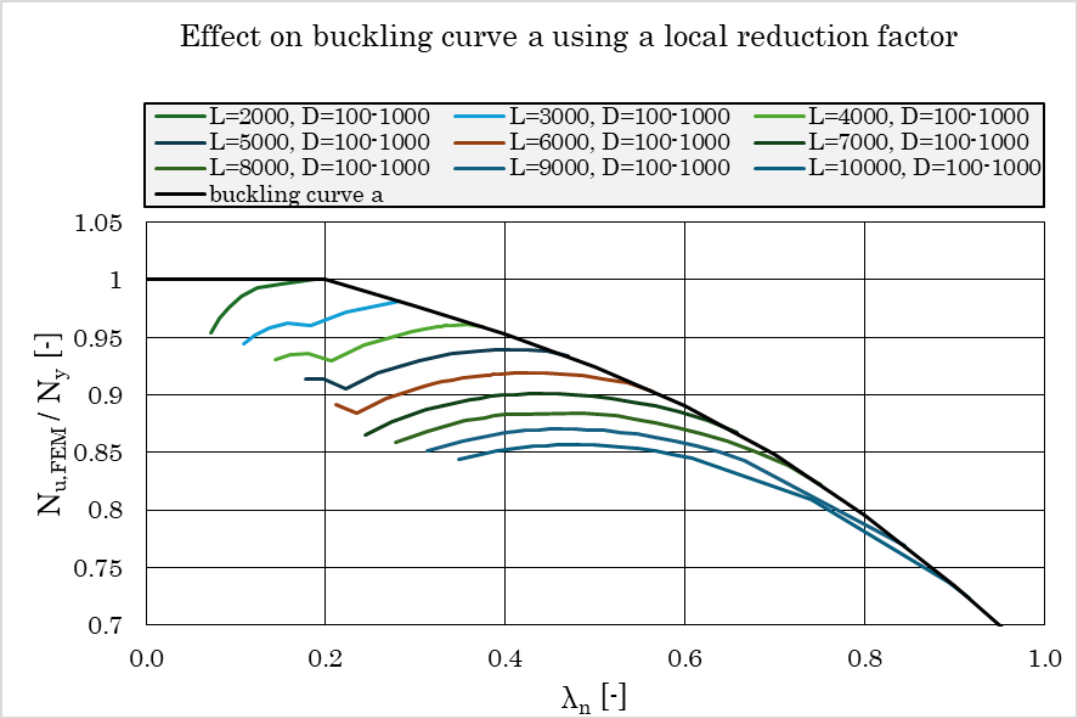

Figure 5.13: Effect on buckling curve a introducing a local reduction factor for the columns considered in the parametric study

The addition of the local buckling reduction factor disregards the CSC of the section and reduces its buckling resistance based on the geometry when local buckling is expected to reduce the capacity. The FEM-results normalised against N_{Rd} in EN1993-1-1 (CEN, 2005) with the addition of a local buckling reduction factor plotted against λ_n and against $\frac{D}{t}$ – ratio are visualised in figures 5.14 and 5.15. For an easier overview of each series, the individual series are visualised in Appendix F.
The results show that the problem of overestimating the buckling resistance of CHS members in CSC 4 close to the CSC limit is eliminated by using a local buckling reduction factor. The design of the columns with a local buckling reduction factor offers a safe design with the exception of the columns with 2000 *mm* lengths. This indicates that the local reduction factor is unconservative in the design of the extremely stocky columns. The advantage of the local buckling reduction factor is that it offers an efficient design compared to the other design methods. It utilises the material most efficiently resulting in the least conservative design method - reaching 14.1 % underprediction of the ultimate load compared to 40.3 % for EN1993-1-1 (CEN, 2005) and EN1993-1-6 (CEN, 2007) and 51.1 % for EN1993-1-1 (CEN, 2005)

and BS5950-1 (British Standards Institution, 2008).

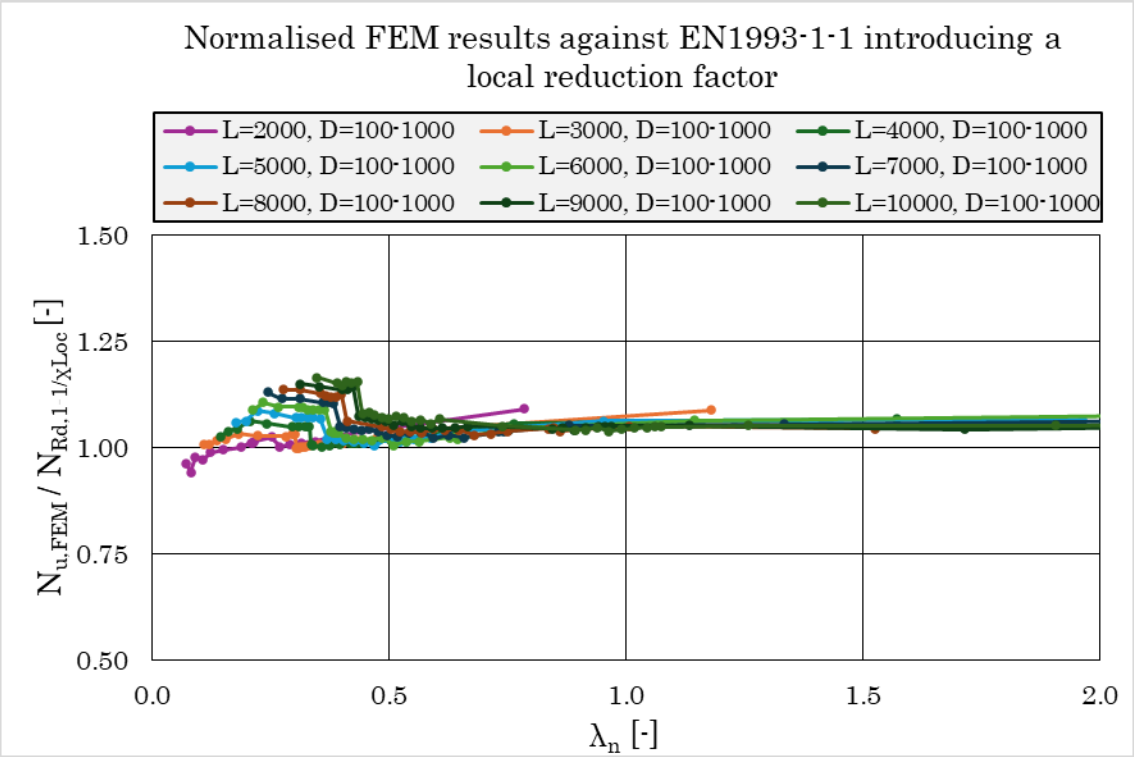

Figure 5.14: FEM-results normalised against N_{Rd} in EN1993-1-1 with the addition of a local reduction factor plotted against λ_n

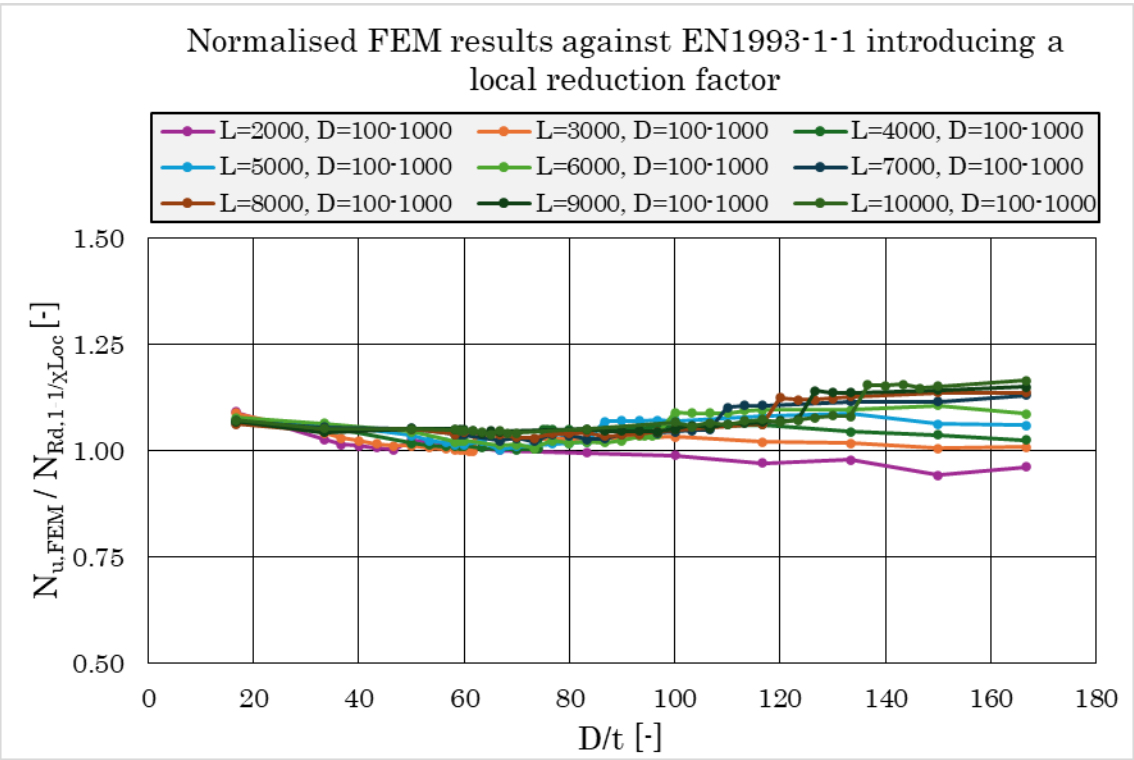

Figure 5.15: FEM-results normalised against N_{Rd} in EN1993-1-1 with the addition of a local reduction factor plotted against $\frac{D}{t}$ – ratio

5.5 Mode interaction analysis

In the results of the parametric study an interesting phenomena is observed. A sudden increase in capacity of up to 8 % is seen at different slenderness ratios, λ_n, for each length. Two of the FEM results, normalised against buckling curve a, plotted with regard to λ_n are visualised in Figure 5.16 to show the increase in capacity. When looking closer at the FEA it can be concluded that this increase occurs because the specimen transitions from having interactive buckling to experiencing purely local buckling.

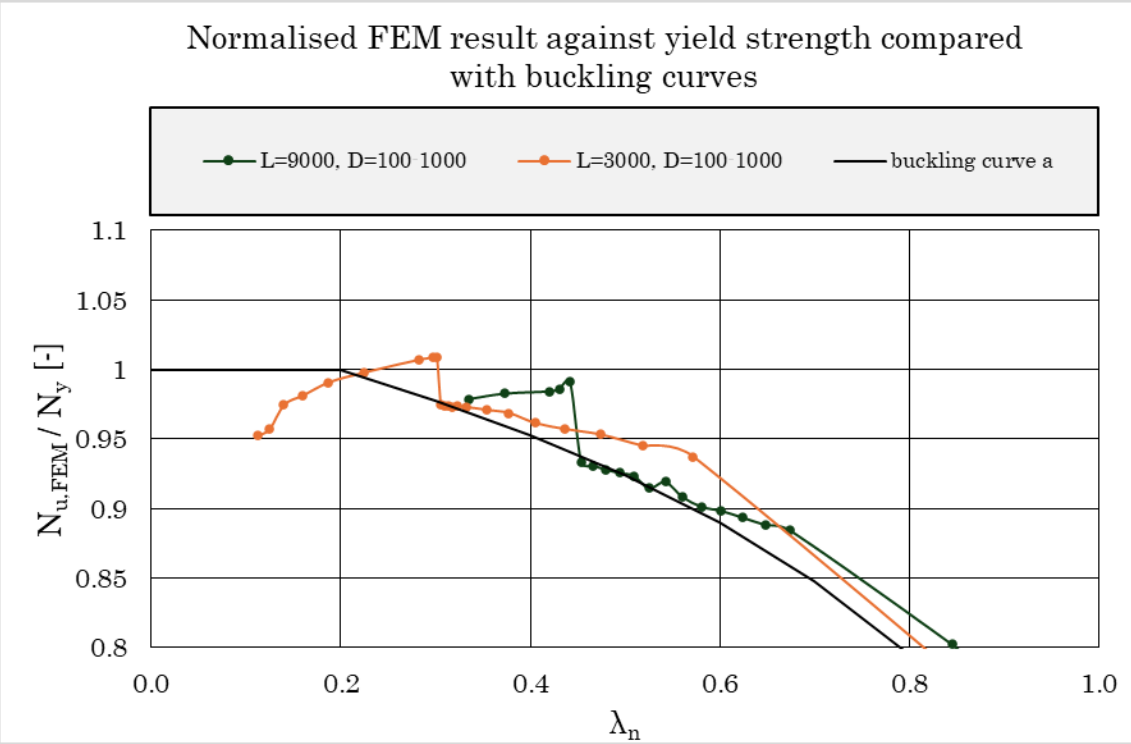

Figure 5.16: Visualization of sudden increase in buckling resistance for columns with $L = 3000, 9000\ mm, D = 100 - 1000\,\text{mm}$

During interactive buckling, the buckling modes in the linear elastic analysis are a combination of global and local buckling modes, where global buckling governs and initiates before local buckling. As a result, the structure carries less load compared to the case of pure local buckling, where the absence of global buckling influence allows the specimen to sustain higher loads. It can be seen that just before the columns transition to purely local buckling modes, the buckling resistance of the columns is at their minimum, indicating that this is the point where the interactive buckling behaviour has its strongest impact. An increase in buckling resistance of up to 8 % is observed between columns that in principle are nearly identical members but one has a slightly larger diameter, making it exert purely local buckling behaviour.

As seen, in Table 5.1 the transition from interactive buckling to pure local buckling in terms of $\frac{D}{t}$-ratio and λ_n is shown. The table indicates that the more slender the columns are, the transition occurs at a higher $\frac{D}{t}$-ratio. This means that the local buckling failure is strongly dependent on the length of the members.

Comparison of where transition from interactive to purely local occur			
$\boldsymbol{L}$ **[mm]**	$\boldsymbol{D}$ **[mm]**	$\frac{\boldsymbol{D}}{\boldsymbol{t}}$ **[−]**	$\boldsymbol{\lambda_n}$
2000	280–300	46.7–50	0.25–0.27
3000	370–375	61.7–62.5	0.30–0.31
4000	445–450	74.2–75	0.33–0.34
5000	500–520	83.3–86.7	0.36–0.37
6000	580–600	96.7–100	0.37–0.39
7000	640–660	106.7–110	0.40–0.41
8000	700–720	116.7–120	0.41–0.43
9000	740–760	123.3–126.7	0.44–0.45
10000	800–820	133.3–136.7	0.45–0.47

Table 5.1: Comparison of where transition from interactive to purely local occur for different lengths.

Since the transition from interactive buckling to purely local buckling vary with λ_n other parameters have been investigated to find a parameter which yield consistent results for all specimens. Two parameters have been identified which give consistent results for all specimens - ratio between global to local critical buckling forces and L'.

The ratio of global to local critical buckling forces is calculated using the ratio between Euler formula for critical buckling force for global buckling and EN1993-1-6 (CEN, 2007) formula for critical buckling force for shell elements for local buckling (presented in 2.4.3). The ratio between the critical global and local buckling force, $N_{cr,GL-ratio}$, is calculated using equation 5.1. The trend of this ratio shows that for very slender columns the ratio is very small, i.e. the global critical buckling force is small while the local buckling force is large, and vice versa for stocky columns.

$$N_{cr,GL-ratio} = \frac{N_{cr,G}}{N_{cr,L}} = \frac{\frac{\pi^2 EI}{L^2}}{\frac{0.605Ct/R}{A}} = \frac{\pi^2 IAR}{0.605CtL^2} \tag{5.1}$$

The FEM results, normalized against N_{Rd} and N_y according to EN1993-1-1 (CEN, 2005) against the ratio of global to local critical buckling forces are visualised in Figure 5.17 and Figure 5.18. Figure 5.17 & 5.18 indicates that when the ratio between global and local critical buckling force is greater than 1.5 only local buckling modes occur in all columns. When the ratio between global and local critical buckling force is between $0.8 - 1.5$ the interactive buckling behaviour has its strongest impact resulting in buckling capacities lower than the design value.

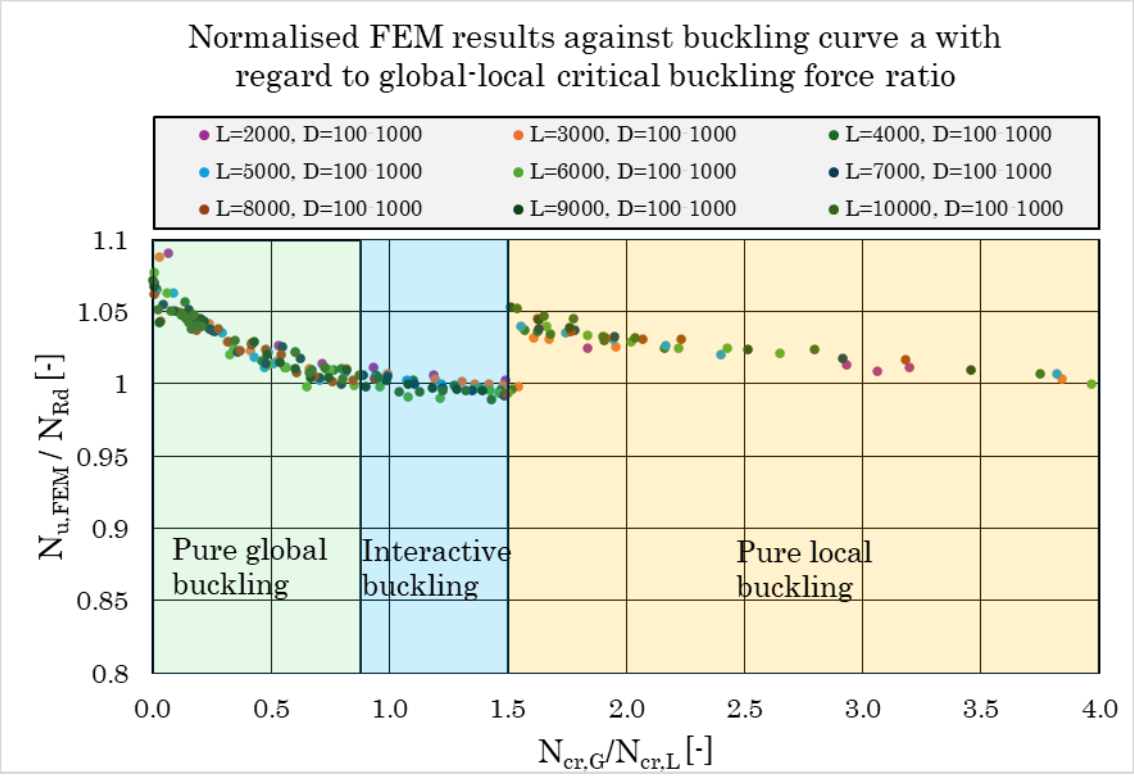

Figure 5.17: FEM results normalised against N_{Rd} in EN1993-1-1 plotted against the ratio between global and local critical buckling force, N_{cr}.

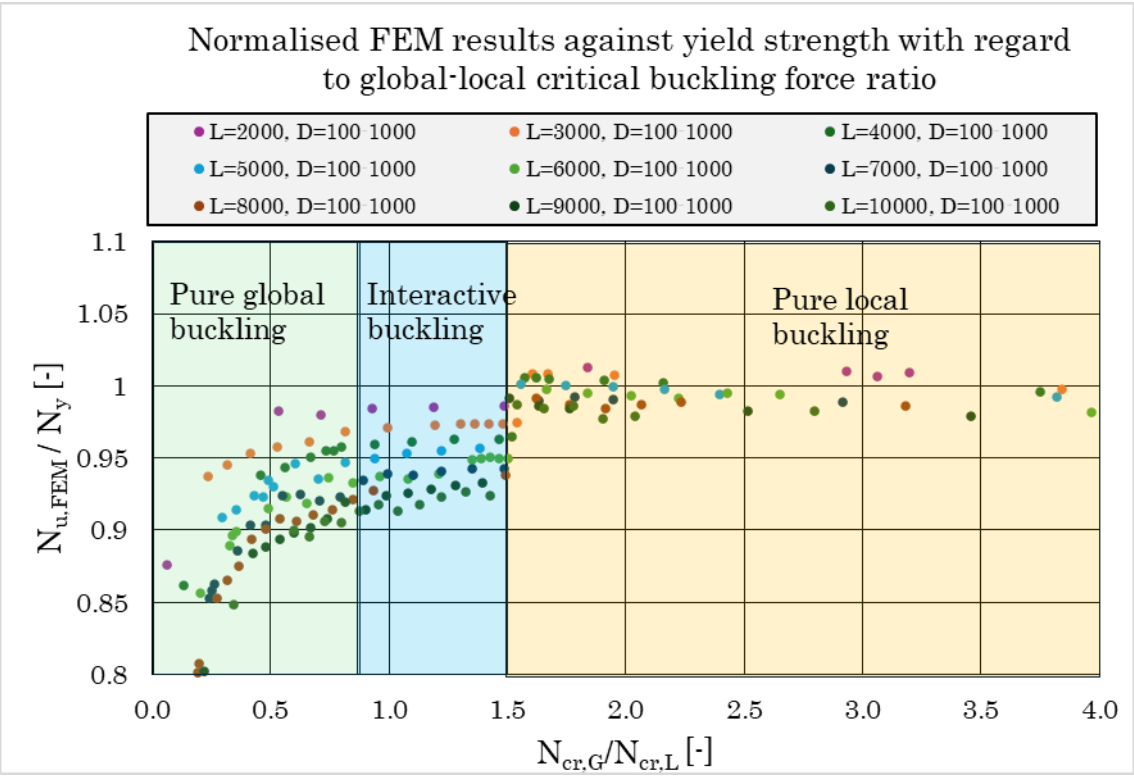

Figure 5.18: FEM results normalised against the yield strength, f_y, plotted against the ratio between global and local critical buckling force, N_{cr}.

The other parameter, L' (presented in 2.5.2), is used to determine the range in which different buckling behaviour occur. It is a geometrical parameter taking the shape of the member into account and for very slender members L' is very large while for very stocky members L' is very small. L' is calculated using equation 2.25 and is shown again below.

$$L' = \sqrt{\frac{l^2 t}{r^3}}$$

The FEM results, normalised against N_{Rd} and N_y according to EN1993-1-1 (CEN, 2005), against L' are visualised in Figure 5.19 and 5.20. Figure 5.19 & 5.20 indicate that when L' is smaller than 3 only local buckling modes occur in the columns. When L' is between $3-4.25$ interactive buckling behaviour has its strongest impact resulting in buckling capacities lower than the design value.

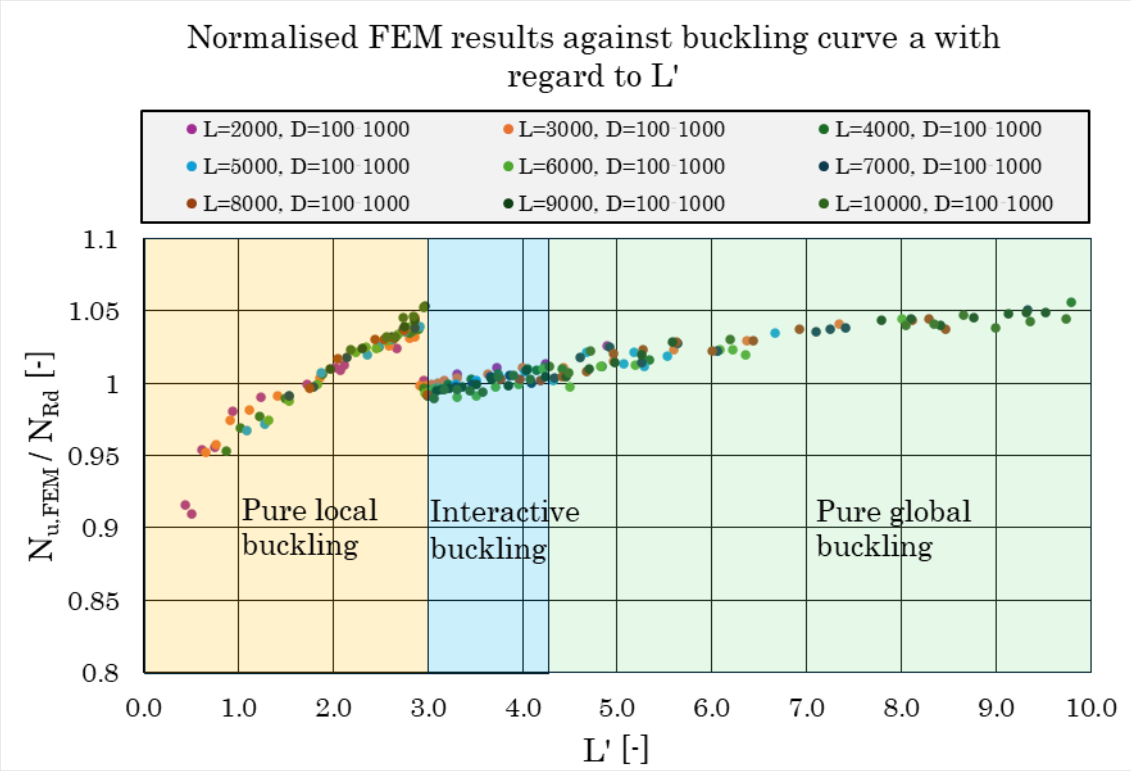

Figure 5.19: FEM results normalised against N_{Rd} in EN1993-1-1 plotted against L'

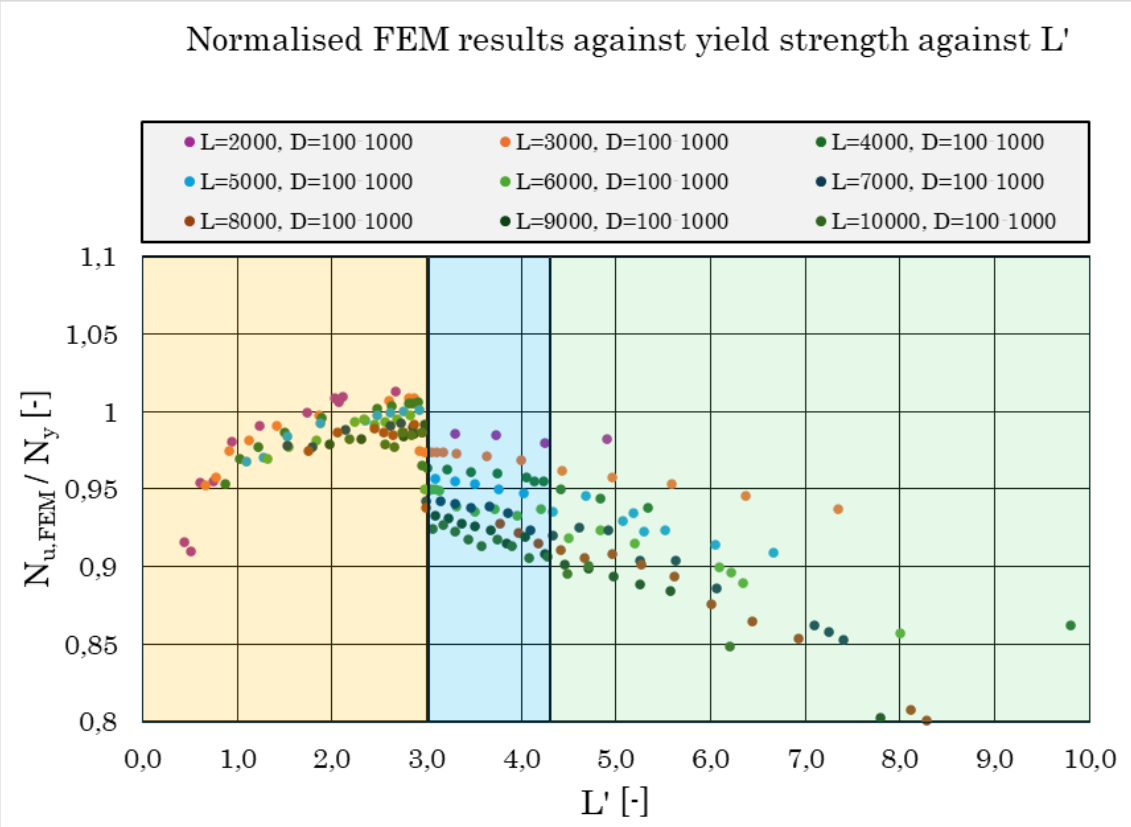

Figure 5.20: FEM results normalised against the yield strength, f_y, plotted against L'

5.6 Imperfection and buckling mode sensitivity

This section presents the effects of various imperfections and buckling modes on the ultimate capacity of the members in nonlinear analysis. For instance, Eurocode-based imperfection as specified in EN1993-1-14 (CEN, 2022) is compared with other imperfection magnitudes. Additionally, the influence of different buckling modes is examined, focusing on how variations in the shape of these modes affect the results.

5.6.1 Imperfection sensitivity

In the parametric study, two types of geometric imperfections were considered: local and global. The imperfection magnitudes and how they should be applied are presented in detail in 3.5. To investigate the impact of imperfection on the buckling behaviour, both types of imperfection were analysed separately and combined. All specimens had a length of 4000 mm while the diameter varied between 200-445 mm and exhibited interactive buckling modes (local and global buckling occur at the same time) in linear elastic analysis. For these specimens, the slenderness ratio λ_n ranged between 0.337 and 0.763.

Six imperfection sensitivity cases were examined:

- Case 1: Only global imperfection was applied, based on EN1993-1-14 (CEN, 2022), with an amplitude of 1.4L/1000.
- Case 2: Only global imperfection was applied, based on EN1993-1-14 (CEN, 2022), with the amplitude reduced by half.
- Case 3: Only global imperfection was applied, based on EN1993-1-14 (CEN, 2022), with the amplitude reduced to one-sixth.
- Case 4: Global and local imperfections were applied, both according to EN1993-1-14 (CEN, 2022).
- Case 5: Global and local imperfection was applied according to EN1993-1-14 (CEN, 2022), while the local imperfection amplitude was doubled.
- Case 6: Global and local imperfection was applied according to EN1993-1-14 (CEN, 2022), while the local imperfection amplitude was multiplied by eight.
- Case 7: Only local imperfection was applied according to EN1993-1-6 (CEN, 2007), while the amplitude is multiplied by 0.7.
- Case 8: Only local imperfection was applied according to EN1993-1-6 (CEN, 2007), while the amplitude is multiplied by 1.4.
- Case 9: Only local imperfection was applied according to EN1993-1-6 (CEN, 2007), while the amplitude is multiplied by 5.6.

The results of the imperfection sensitivity analysis are visualised in Figure 5.21. The impact of imperfections on the ultimate loads of the columns is summarised in Appendix G. It can be observed that the global and local imperfection amplitude significantly affects the ultimate capacity.

When only applying global imperfections the more slender the column (higher λ_n) the larger the reduction in ultimate load is. The largest decrease in ultimate load when only considering global imperfections occurs when the local and global modes

in the linear elastic analysis are not close to each other, specifically when $\lambda_n = 0.763$. In this case the critical buckling force for global buckling modes is far less than that of the local buckling modes meaning that the global imperfection has a larger impact in slender columns.
When only applying local imperfections the more stocky the column (lower λ_n) the larger the reduction in ultimate load is. The largest decrease in ultimate load when only considering local imperfections occurs when the local and global modes in the linear elastic analysis are close to each other, specifically when $\lambda_n = 0.337$. In this case the critical buckling force for local buckling modes is far less than that of the global buckling modes meaning that the local imperfection has a larger impact in stocky columns.
When combining local and global imperfections the largest decrease in ultimate load is observed. When λ_n is between 0.337-0.504 the global imperfection is applied at mode 1 while the local imperfection is applied at mode 2. It can be seen that for the most stocky column the influence of the local imperfection on the reduction of ultimate load is increasing. For the most slender columns the first global buckling mode is at mode 1 and the first local buckling mode is at mode 5. At this point, the global imperfection is applied at mode 1 while the local imperfection is applied at mode 5. Since these are far from each other the local critical buckling force is much larger than the global meaning that the influence from this is lowered but the influence from the global imperfection is large. Through combination of local and global imperfections it can be seen that for columns that exert interactive buckling are sensitive for large imperfection amplitudes.

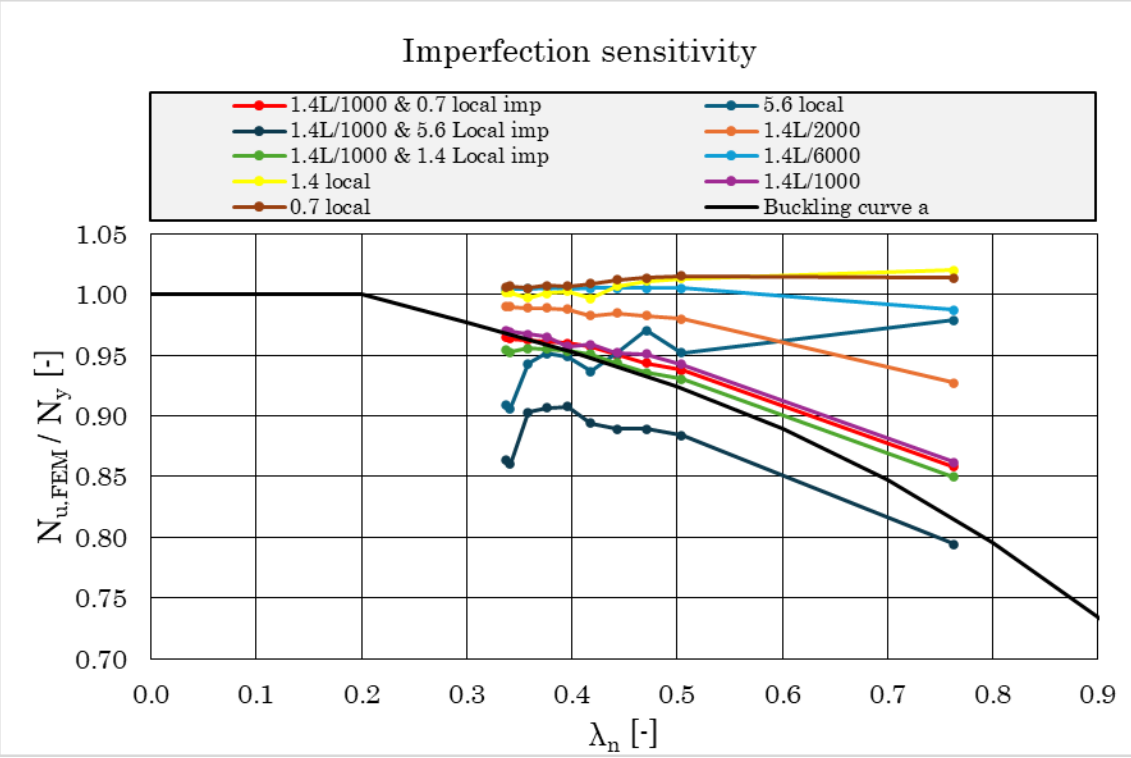

Figure 5.21: Impact of applying different imperfection amplitudes and combinations on the ultimate loads for L=4000 mm and D=200-445 mm.

5.6.2 Buckling mode sensitivity

For the combination of local and global imperfections in the non-linear analysis, the first global and first local buckling modes, assuming to be corresponding to the most critical eigenvalues from the linear elastic analysis, have been used. While the first global mode is consistently the most critical (in interactive and purely global buckling), the local buckling mode shapes also play an important role, as they influence the non-linear response.
Because of the geometry of CHS members the member is free to buckle in all directions. For global buckling the members can be manipulated to buckle in desired direction through the boundary conditions. The same does not apply to local buckling where the local mode shapes are not identical and can have asymmetry which results in buckling in different directions which can cause higher buckling resistance. Because of this it is important to perform a buckling mode sensitivity analysis to assess whether the ultimate load capacity depends on the selected buckling mode. To investigate this the specimen as in the imperfection sensitivity analysis (L=4000mm & D=200-445mm) has been studied to see the impact of different local buckling modes impact the buckling resistance.
The imperfection used for this analysis are according to EN1993-1-14 (CEN, 2022). The results of choosing different local buckling modes normalised against the ultimate load when choosing local buckling mode 2 plotted against λ_n is visualised in Figure 5.22. The results show that the choice of different local buckling modes does not significantly affect the buckling resistance of the members, having a maximum increase in resistance of 1.2 % and a maximum decrease of 0.5 %.

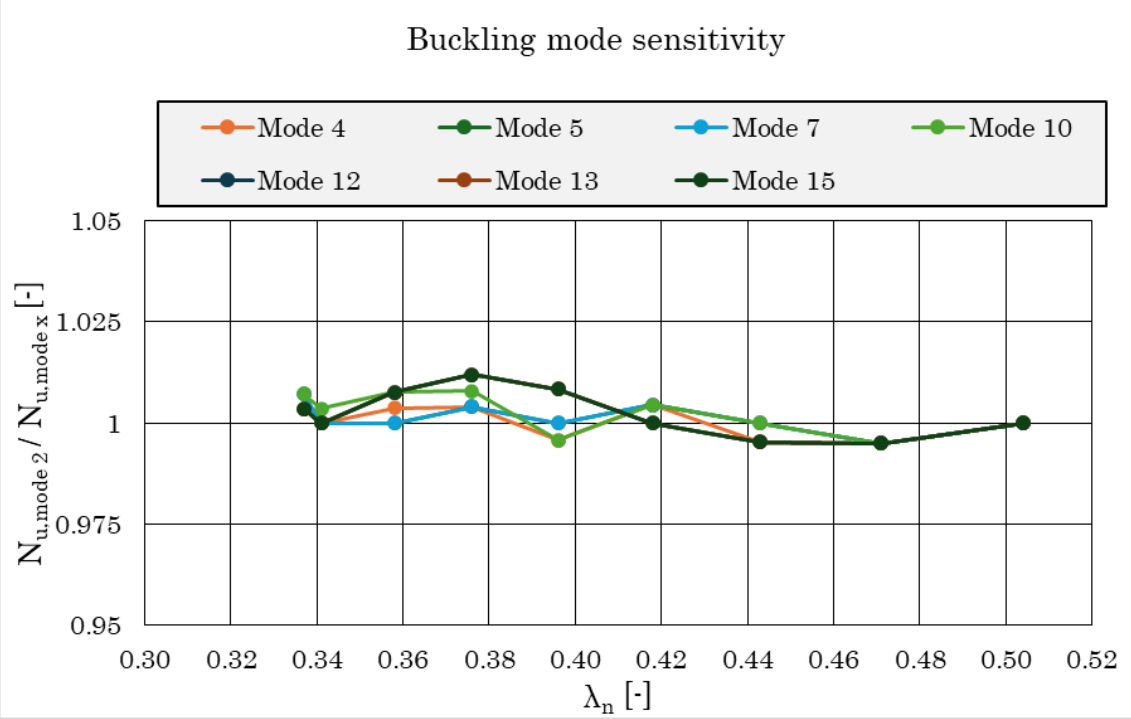

Figure 5.22: Impact of different local buckling modes on the ultimate load.

The results show that when $\lambda_n = 0.376$ (with $D = 400$ mm), the second mode out

of 20 is the first mode to exhibit local buckling. In this case, modes 4, 7, 10, and 12 were also analysed to assess their impact. The shapes of the different local buckling modes at $\lambda_n = 0.376$ can be seen in Figure 5.23 - 5.27. As shown, the shapes vary, and the magnitudes of the eigenvalues change as well. Table 5.2 demonstrates that the ultimate load is not significantly affected by the choice of buckling mode for the non-linear analysis, as the ultimate loads remain almost identical. The reason behind this may be that local buckling modes primarily affect localised regions rather than the whole structure. In contrast, the global buckling mode, being the first mode, governs the overall behaviour, and the failure of the structure is more influenced by this mode. Figure 5.23 - 5.27 shows how each buckling shape from linear elastic analysis affect the failure mode in non-linear analysis. As it can be seen the more symmetric the buckling shape in linear elastic analysis is the more buckling occur in the middle in non-linear analysis.

Buckling mode sensitivity								
λ_n	Mode 2	Mode 4	Mode 5	Mode 7	Mode 10	Mode 12	Mode 13	Mode 15
0.763	-	-	1.110	1.110	1.120	1.120	1.120	1.120
0.504	1.850	1.850	1.850	1.850	1.850	1.850	1.850	1.850
0.471	1.980	1.990	1.990	1.990	1.990	1.990	1.990	1.990
0.443	2.120	2.130	2.120	2.120	2.120	2.130	2.130	2.130
0.418	2.270	2.260	2.260	2.260	2.260	2.270	2.270	2.270
0.396	2.400	2.410	2.400	2.400	2.410	2.380	2.380	2.380
0.376	2.540	2.530	2.530	2.530	2.520	2.510	2.510	2.510
0.358	2.670	2.660	2.670	2.670	2.650	2.650	2.650	2.650
0.341	2.800	2.800	2.800	2.800	2.790	2.800	2.800	2.800
0.337	2.840	2.830	2.820	2.820	2.820	2.830	2.830	2.830

Table 5.2: Impact of choosing different local buckling modes on the ultimate load.

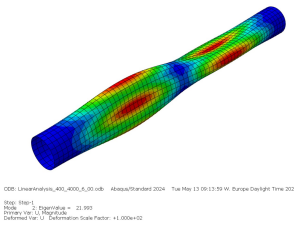

(a) Mode shape of buckling mode 2 of column with $L = 4000\ mm$, $D = 400\ mm$

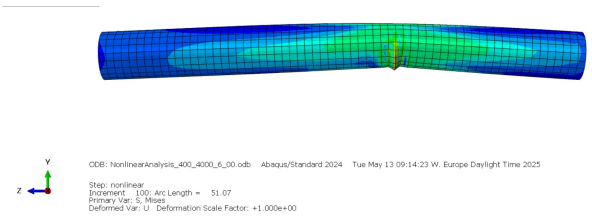

(b) Nonlinear behaviour of column with $L = 4000\ mm$, $D = 400\ mm$

Figure 5.23: Illustration of buckling shape of LEA and GMNIA while mode 2 is chosen for GMNIA

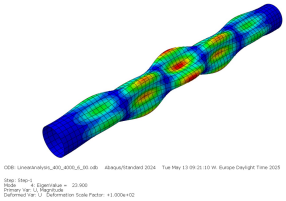

(a) Mode shape of buckling mode 4 of column with $L = 4000\,mm$, $D = 400\,mm$

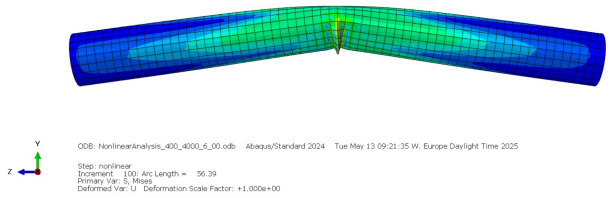

(b) Nonlinear behaviour of column with $L = 4000\,mm$, $D = 400\,mm$

Figure 5.24: Illustration of buckling shape of LEA and GMNIA while mode 4 is chosen for GMNIA

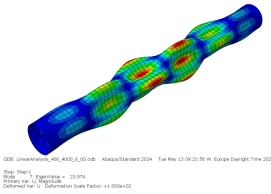

(a) Mode shape of buckling mode 7 of column with $L = 4000\,mm$, $D = 400\,mm$

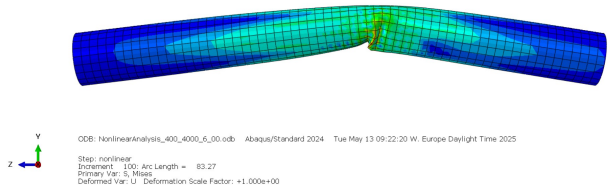

(b) Nonlinear behaviour of column with $L = 4000\,mm$, $D = 400\,mm$

Figure 5.25: Illustration of buckling shape of LEA and GMNIA while mode 7 is chosen for GMNIA

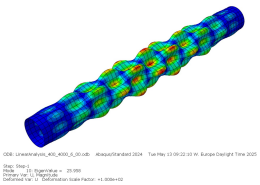

(a) Mode shape of buckling mode 10 of column with $L = 4000\,mm$, $D = 400\,mm$

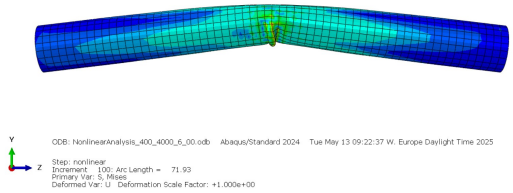

(b) Nonlinear behaviour of column with $L = 4000\,mm$, $D = 400\,mm$

Figure 5.26: Illustration of buckling shape of LEA and GMNIA while mode 10 is chosen for GMNIA

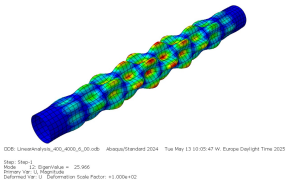

(a) Mode shape of buckling mode 12 of column with $L = 4000\,mm,\ D = 400\,mm$

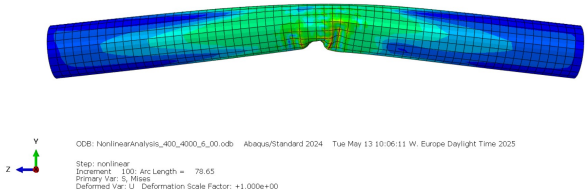

(b) Nonlinear behaviour of column with $L = 4000\,mm,\ D = 400\,mm$

Figure 5.27: Illustration of buckling shape of LEA and GMNIA while mode 12 is chosen for GMNIA

6
Discussion

In this chapter the results from the parametric study will be discussed. This include two parts: (I) review of the current design guidelines and how alternative design methods treat the same problem for the design of CHS members and (II) how mode interaction is treated in the current design guidelines and what impact this has on the resistance of CHS members together with an insight into what indicators can be implemented to identify which members are susceptible to interactive buckling.

6.1 Design guidelines

As presented in section 5.2, the major finding when comparing the results with the current design guidelines in EN1993-1-1 (CEN, 2005) and EN1993-1-6 (CEN, 2007) is that problems arise when designing CHS members in CSC 4.
It is stated in EN1993-1-1 (CEN, 2005) that CHS members in CSC 4 should be dimensioned according to EN1993-1-6 (CEN, 2007). The definition, scope, and application of EN1993-1-6 (CEN, 2007) are presented in section 2.4.3, and it can be concluded that all of the columns that are in CSC 4 and modelled in the parametric study are covered by this standard. Why are these problems arising in the determination of the buckling resistance of these members then? When designing shell structures a significant part of the resistance is based on imperfections since these are correlated to the local buckling. This results in a design approach which is focusing heavily on the local buckling of the cross-section and is almost independently basing the whole resistance of the cross-section on this neglecting the global behaviour. The effect of this is shown in Table 6.1 where EN1993-1-6 (CEN, 2007) designs a CHS member in CSC 4 with a constant cross-section but increasing length with the same resistance where the numerical analysis shows that the length has significant impact on the ultimate load. This results in over prediction of the buckling resistance of member with a slender section while being conservative for stocky sections.

Comparison of ultimate loads and resistances from design guidelines						
D $[mm]$	L $[mm]$	$N_{u,FEM}$ $[kN]$	$N_{Rd,1-1}$ $[kN]$	$N_{u,FEM}/N_{Rd,1-1}$	$N_{Rd,1-6}$ $[kN]$	$N_{u,FEM}/N_{Rd,1-6}$
360	2000	2390	2364	1.01	1889	1.27
360	6000	2130	2083	1.02	1889	1.13
360	10000	1571	1501	1.05	1889	0.83

Table 6.1: Comparison of ultimate loads from FEM and resistances from EN 1993-1-1 and EN 1993-1-6.

Even though length as parameter is included in the length parameter ω according to EN1993-1-6 (CEN, 2007), which affect the buckling parameter C, its weight in determining the buckling resistance of the member is miniscule compared to the local cross-section parameters. This results in both over- and under dimensioning CHS members which are in CSC 4. The overall conclusion when assessing the current design guidelines is that regarding members which exert column-like behaviour as shell structures is not ideal when trying to achieve a safe and efficient design even though they are exposed to local buckling. As the design approach of CHS members in CSC 4 in the current design guidelines are deemed to be inefficient and unsafe two alternative methods were investigated.

The design method provided in BS5950-1 (British Standards Institution, 2008), presented in section 2.4.4, reduces the area based on the area of the cross-section which is expected to exert local buckling. This is the same method that is currently adopted in Eurocode for other cross-section geometries but not yet for CHS members. Therefore, this was beforehand deemed as the most promising method to use because of the similarity to already widely adopted design methods in Eurocode as well as its simplicity in use. The applicability is limited to CHS members within the range $90\epsilon^2 \leq \frac{D}{t} \leq 240\epsilon^2 \Rightarrow 357.5\ mm \leq D \leq 953.2\ mm$. Since the parametric study includes CHS members with diameters of up to 1000 mm some of the members have been disregarded with this method but it does not affect the overall results when assessing its applicability in design.
The design approach of using an effective area for CSC 4 eliminates the unsafe design for the CHS members in the transition from CSC 3 to 4 which was the major drawback of the current design approach. Striving for a design approach which renders in a safe structure is the first and most important demand, secondly is striving for a material efficient design. When looking closer at the results when using the effective area method is that it seems to be very conservative when designing for CHS members with a very large $\frac{D}{t}$-ratio. The effective area method greatly under predicts the buckling resistance of these members only designing for half of the ultimate load that was achieved in the numerical analysis. This indicate that the reduction of the area could be lowered to further use more of the resistance of the cross-section.
A less conservative reduction of area due to local buckling would yield more efficient use of the material resulting in a design method which is easy to use and is alike to the method already used for other cross-section geometries while eliminating the

possibility of unsafe design.

The second alternative design methods was introducing a local reduction factor introduced by Toffolon and Taras (2017), presented in section 2.5.2. This method was firstly produced by a numerical and experimental approach for stainless steel CHS members and its applicability was verified against hot-rolled steel.
This method disregarded the current use of CSC and does not compartmentalise cross-sections into different classes. Instead it introduces a local buckling reduction factor which is based on the geometry of the section and reduces the buckling resistance accordingly. This local reduction factor is then implemented into the global buckling reduction factor creating a buckling reduction factor which takes the global and local behaviour of the cross-section into account.
The results show that the design method of using a local buckling reduction factor eliminates unsafe design for all columns with the exception of some of the extremely stocky columns with $L = 2000\ mm$ where the buckling resistance is over predicted by a small margin. Overall this design method produce the most efficient design under predicting the resistance by a maximum of 16 % compared to 40.3 % and 51.1 % in EN1993-1-6 (CEN, 2007) and BS5950-1 (British Standards Institution, 2008) . However, the design method with a local buckling reduction factor seem be conservative in columns that are slender and are the least prone to experience local buckling and in contrary show unconservative design in columns that are extremely stocky which are more susceptible to this. This seem counter-intuitive and show that this method would need a slight adjustment in its how the local buckling reduction factor is applied to further increase validity in hot-rolled CHS members as well.

6.2 Mode interaction analysis

The overall result of the parametric analysis indicates that the Eurocode design guidelines are overly conservative with respect to local buckling. A comparison between the buckling curve provided in EN1993-1-1 (CEN, 2005) and the FE results shows that the buckling resistance is overpredicted when local and global buckling modes interact, see Figure 6.1.

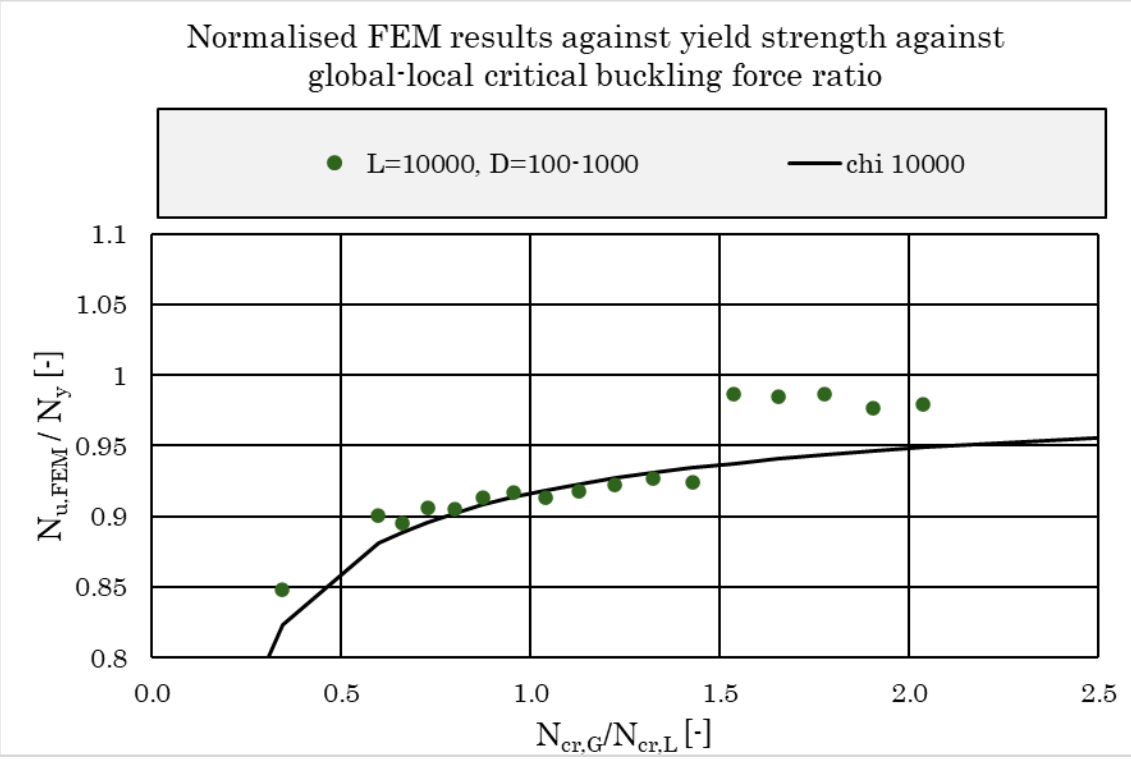

Figure 6.1: Comparison between obtained FE-curve and buckling curve from EN1993-1-1

Mode interaction between global and local buckling modes is shown to have an impact on the buckling resistance of CHS members. When comparing this impact with the current design guidelines it is shown that the interactive buckling reduction does not render in any unsafe design. However, in order for a column to have an interactive failure mode the presence of a global and local buckling mode need to be present at the same time, i.e. the column needs to have an intermediate to stocky slenderness to allow for a local buckling mode to be present. As seen in Table 5.1, the transition from interactive to purely local buckling occurs mainly in columns which are in CSC 4 where the design guidelines are extremely conservative and treats the columns as a shell structure, as presented earlier in Section 5.2. Therefore, it was deemed more appropriate to compare the results to the global buckling curve which aligned better with the column-like behaviour even though the results may not be deemed as a design curve.
A closer look at the results presented in section 5.5 are visualised in Figure 6.2

where the gain in buckling resistance when the columns transition from interactive to purely local buckling is shown. When comparing with the global buckling curve the results show that in the interactive buckling zone the resistance is over predicted by 2 % which is not deemed enough to be considered unsafe since this is within the error of the numerical analysis. However, the results show that the gain from the transition from interactive to purely local buckling behaviour can be up to 8 % showing that columns that have an interactive buckling failure mode have a significant loss in resistance. This together with the uncertainties in the design method of CHS members in CSC 4 show that there are a lot still to study in how the interactive buckling affect CHS members.

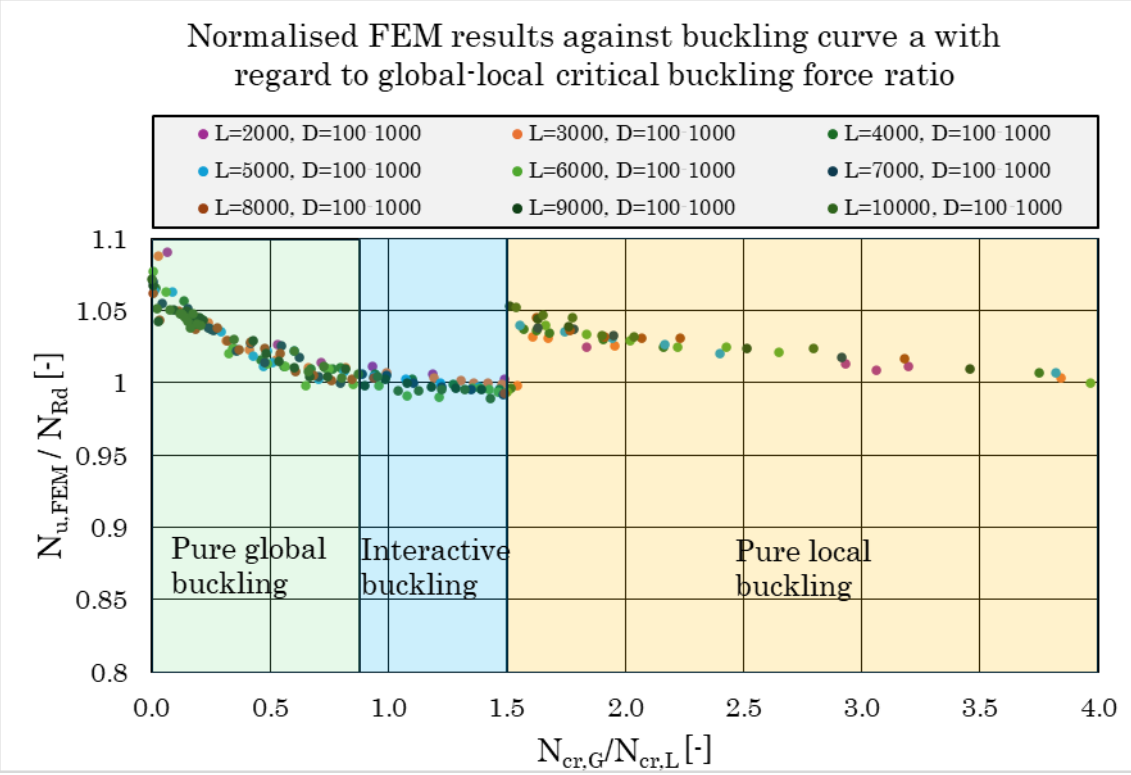

Figure 6.2: Transition zone from interactive to purely local buckling behaviour.

As discussed in Section 5.6.2, the influence of local imperfections on interactive buckling is minimal, primarily because global buckling governs the failure mode. Consequently, the member's capacity is more sensitive to global imperfections than to local ones. The analysis also shows that applying larger imperfections in both local and global modes results in a noticeable reduction in capacity. However, the magnitude of this reduction is not entirely reliable. This suggests that while local imperfections do have an effect, their amplitude—as defined in EN1993-1-6 (CEN, 2007)—has a limited influence on the ultimate capacity of members. Determining the suitability of the global imperfection defined in EN1993-1-14(CEN, 2022) is challenging because it represents an equivalent imperfection which not only accounts for geometric imperfections but also consider the effects of residual stresses. This makes direct comparison with experimental imperfections difficult. Experimental results indicate that the global imperfection magnitude providing the best agreement with

FE simulations is L/1000 while it is 1.4L/1000 according to EN1993-1-14 (CEN, 2022) including residual stresses, highlighting the complexity of evaluating its accuracy.

As long as the impact of local imperfection is low, the choice of local buckling mode does not significantly influence the ultimate capacity of the members. The local imperfection does serve to localise the failure zone in the non-linear analysis during interactive buckling. It can be seen in Figure 5.23 to 5.27 that the region that has higher stress in linear elastic analysis correspond to the locations where local failure occurs in the nonlinear analysis.

To identify the range in which interactive buckling is likely to occur, two plots have been proposed, each providing an indication of interactive buckling behavior. According to Figure 5.17, where the FE results are normalized against buckling curve a and plotted with respect to the ratio of global to local critical buckling forces, interactive buckling tends to occur when this ratio lies between 1.0 and 1.5. Within this range, Class 3 and Class 4 sections are observed, which involve both global and local imperfections.

However, determining this ratio can be challenging in practice, as calculating the local critical buckling force, $N_{cr,L}$, requires several parameters in according to EN1993-1-6 (CEN, 2007). To address this, an alternative indicator has been proposed by comparing the normalized FE results against buckling curve a, this time in terms of the non-dimensional slenderness parameter L', defined by equation (2.25). Based on this approach, interactive buckling is more likely to occur when L' falls within the range of 3.0 to 3.5, see Figure 5.19.

7
Conclusion

An FE-model was created that could satisfactorily simulate the buckling behaviour of CHS members loaded in axial compression with accurate results and low computational cost. It was successfully validated against another pre-existing FE-model and test results.

A Python script was developed which enabled the analysis of 223 CHS members to be parametrised. Through a simple input file the desired results could be easily obtained in an output file at low computational cost which contained all parameters specified beforehand. This enabled a large dataset of buckling resistances across different parameters of CHS members to be created. Together with the analytical calculations of the same CHS members important findings in the buckling behaviour of CHS was highlighted.

The results from the parametric study was compared to existing and alternative design guidelines and methods for CHS members. The final and overall concluding remarks regarding these show that:

- The current design guidelines need to be reconsidered since problems arise when designing a CHS member as a shell structure when it primarily exert column-like behaviour. For members in CSC 4 with a $\frac{D}{t}$-ratio close to the CSC limit the current design guidelines could produce unsafe design. For CHS members with a large $\frac{D}{t}$-ratio the current design guidelines produce inefficient design.
- The effective area method, presented in BS5950-1, show promising results. Its similarity to how the current design guidelines design other cross-section geometries in CSC 4 would make it easily transferable. However, a less conservative area reduction would need to be implemented to fully make it applicable and efficient.
- The Toffolon method has an promising applicability and easy design method eliminating the use of CSC, replacing this with a local buckling reduction factor. With an adjustment in how the local buckling reduction factor is applied, increasing conservativity in extremely stocky sections and decreasing in slender sections, this method seem to be a good alternative to implement in the design of CHS members. However, since its applicability is exclusively for CHS members the effective area method is deemed more applicable to use together with the current guidelines.

The impact of mode interaction between local and global buckling modes on buckling resistance of CHS members was investigated. The final and overall concluding remarks regarding these show that:

- Mode interaction has impact on the buckling resistance of CHS members. An decrease of up to 8 % is observed when transitioning from pure local buckling behaviour to interactive buckling behaviour even though the members have very similar cross-sections.
- Two parameters were investigated which can be used to predict the buckling behaviour - L' and $\frac{N_{cr,G}}{N_{cr,L}}$-ratio. L' was already established for stainless steel and its validity was investigated for hot-rolled steel, which show similar results in determining buckling behaviour but for different ranges. $\frac{N_{cr,G}}{N_{cr,L}}$-ratio was also investigated and similar results as for L' was observed. L' showed very promising results which yielded consistent results across all members with only geometrical parameters needed where as $\frac{N_{cr,G}}{N_{cr,L}}$-ratio required more calculations to achieve the same results. The following ranges were observed to yield consistent results for all specimens in determining buckling behaviour:

Local buckling:	$L' < 3.0$	$\frac{N_{cr,G}}{N_{cr,L}} > 1.5$
Interactive buckling:	$3 < L' < 4.25$	$0.8 < \frac{N_{cr,G}}{N_{cr,L}} < 1.5$
Global buckling:	$L' > 4.25$	$\frac{N_{cr,G}}{N_{cr,L}} < 0.8$

- When failure occurs due to mode interaction, the buckling resistance is primarily influenced by the global imperfection magnitude, which dominate the overall buckling behaviour of the member.
- Local imperfections tend to dictate the location and development of the final failure in a structural member, acting as initiation points for local buckling but does not influence the buckling resistance as severely as global imperfection magnitude.
- The selection of different local buckling modes has a minimal effect on the ultimate load-carrying capacity of CHS members, indicating a relatively low sensitivity to mode shape variations.

To summarise, after the parametric FEA was conducted design recommendations regarding the buckling behaviour of CHS members were provided that can be incorporated into engineering design practices.

8

Suggestion for further study

1. To further deepen the understanding of exactly how interactive buckling affects the buckling resistance of CHS members, a more extensive experimental study would have to be conducted. This thesis provides different approaches to identify a range where the geometry and ratio between global and local critical buckling forces can be used to determine whether interactive buckling will be the failure mode in CHS members through a numerical approach. To verify this, experiments which handle CHS members in this range would need to be tested to find that the numerical results align with how real columns behave.

2. As established the current design guidelines can cause problems when designing CHS members in CSC 4. To allow for a consistent design method an effective area method valid for these members need to be adopted. A method is already developed in BS5950-1 (British Standards Institution, 2008) but this result in conservative design of these. Therefore, a comprehensive experimental and numerical study on the exact impact of local buckling of CHS members need to be conducted to modify the area reduction factor to allow for an effective design of these utilising the full capacity of CHS members in CSC 4.

3. Since different steel grades have varying structural properties, and the manufacturing process also affects the structural capacity of members, it is worthwhile to investigate steel grades other than S355H, as well as alternative types such as cold-formed steel.

References

ABAQUS Theory Manual. (n.d.). Retrieved 2025-05-23, from https://classes.engineering.wustl.edu/2009/spring/mase5513/abaqus/docs/v6.6/books/stm/default.htm?startat=ch02s03ath18.html

ABAQUS User Manual. (n.d.-a). Retrieved 2025-05-23, from https://classes.engineering.wustl.edu/2009/spring/mase5513/abaqus/docs/v6.6/books/usb/default.htm?startat=pt03ch06s02at02.html

ABAQUS User Manual. (n.d.-b). Retrieved 2025-05-26, from https://classes.engineering.wustl.edu/2009/spring/mase5513/abaqus/docs/v6.6/books/usb/default.htm?startat=pt06ch23s06alm15.html

ABAQUS User Manual. (n.d.-c). Retrieved 2025-05-23, from https://classes.engineering.wustl.edu/2009/spring/mase5513/abaqus/docs/v6.6/books/usb/default.htm?startat=pt04ch11s03aus55.html

Al-Emrani, M. (2023). *Steel Structures*.

Ballio, G., & Mazzolani, F. M. (1989, January). *(PDF) Theory and Design of Steel Structures.* Retrieved 2025-02-10, from https://www.researchgate.net/publication/274217708_Theory_and_Design_of_Steel_Structures

Bernuzzi, C., & Cordova, B. (2016). *Structural Steel Design to Eurocode 3 and AISC Specifications*. John Wiley & Sons.

Bhaga, B., & Steeves, C. (2018, May). Compressive Instabilities In Metal-Coated Polymer Microtrusses. In *Progress in Canadian Mechanical Engineering.* York University Libraries. Retrieved 2025-05-27, from http://hdl.handle.net/10315/35230 doi: 10.25071/10315/35230

British Standards Institution. (2008). *Structural use of steelwork in building. Part 1, Code of practice for design: rolled and welded sections.* BS5950-1.

Cai, J. (2016). *Interactive Buckling and Post-Buckling Studies of Thin-Walled Structural Members with Generalized Beam Theory*.

CEN. (2005). *Eurocode 3: Design of steel structures - Part 1-1: General rules and rules for buildings.* EN 1993-1-1.

CEN. (2007). *Eurocode 3: Design of Steel Structures - Part 1-6: Strength and Stability of Shell Structures.* EN 1993-1-6.

CEN. (2022). *Eurocode 3: Design of steel structures - Part 1-14: Design assisted by finite element analysis.* EN 1993-1-14.

Davison, B., & W. Owens, G. (2003). *STEEL DESIGNERS'MANUAL* (6th ed.).

Farkas, J., & Jármai, K. (2013). *Optimum design of steel structures*. Berlin: Springer.

Galambos, T. V., & Surovek, A. E. (2008). *Structural Stability of Steel: Concepts and Applications for Structural Engineers* (1st ed.). Wiley. Retrieved

2025-02-08, from https://onlinelibrary.wiley.com/doi/book/10.1002/9780470261316

Gambhir, M. L. (2004). *Stability Analysis and Design of Structures*.

Goltermann, P., & Møllmann, H. (1989a). Interactive buckling in thin-walled beams—II. Applications. *International Journal of Solids and Structures*, *25*(7), 729–749. Retrieved 2025-02-05, from https://linkinghub.elsevier.com/retrieve/pii/0020768389900103 doi: 10.1016/0020-7683(89)90010-3

Goltermann, P., & Møllmann, H. (1989b). Interactive buckling in thin-walled beams—I. Theory. *International Journal of Solids and Structures*, *25*(7), 715–728. Retrieved 2025-02-05, from https://linkinghub.elsevier.com/retrieve/pii/0020768389900097 doi: 10.1016/0020-7683(89)90009-7

Huang, B., & Hong, Z. C. (2020, January). Interactive Buckling of Q420 Welded Circular Tubes under Axial Compression. *Advances in Materials Science and Engineering*, *2020*(1), 4028907. Retrieved 2025-02-12, from https://onlinelibrary.wiley.com/doi/10.1155/2020/4028907 doi: 10.1155/2020/4028907

Huang, B., & Zhang, W. F. (2022, April). Local-Overall Interactive Buckling of High Strength Steel Welded Circular Tubes under Axial Compression. *International Journal of Steel Structures*, *22*(2), 632–647. Retrieved 2025-02-07, from https://link.springer.com/10.1007/s13296-022-00596-0 doi: 10.1007/s13296-022-00596-0

Jerath, S. (2020). *Structural Stability Theory and Practice: Buckling of Columns, Beams, Plates, and Shells*. John Wiley & Sons.

Khalaf, M. S., Ibrahim, A. M., Najm, H. M., Sabri, M. M. S., Morkhade, S., Agarwal, A., … Alarifi, I. M. (2022, June). Experimental Analysis of Steel Circular Hollow Section under Bending Loads: Comprehensive Study of Mechanical Performance. *Materials*, *15*(12), 4350. Retrieved 2025-05-16, from https://www.ncbi.nlm.nih.gov/pmc/articles/PMC9230980/ doi: 10.3390/ma15124350

McKenzie, W. M. C. (2004). *Design of structural elements*. Basingstoke: Palgrave Macmillan.

Meng, X., & Gardner, L. (2022, January). Stability and design of normal and high strength steel CHS beam-columns. *Engineering Structures*, *251*, 113361. Retrieved 2025-05-16, from https://linkinghub.elsevier.com/retrieve/pii/S0141029621014747 doi: 10.1016/j.engstruct.2021.113361

NE.se. (n.d.-a). Retrieved 2025-05-16, from https://www.ne.se/uppslagsverk/encyklopedi/l%C3%A5ng/st%C3%A5l

NE.se. (n.d.-b). Retrieved 2025-05-16, from https://www.ne.se/uppslagsverk/encyklopedi/l%C3%A5ng/konstruktionsst%C3%A5l

NE.se. (n.d.-c). Retrieved 2025-05-16, from https://www.ne.se/uppslagsverk/encyklopedi/l%C3%A5ng/varmbearbetning

NE.se. (n.d.-d). Retrieved 2025-05-16, from https://www.ne.se/uppslagsverk/encyklopedi/l%C3%A5ng/valsning

Pignataro, M. (2005). *Phenomenological and Mathematical Modelling of Structural Instabilities* (1st ed ed.) (No. v.470). Vienna: Springer Wien.

Shen, J., Wadee, M. A., & Sadowski, A. J. (2015). NUMERICAL STUDY OF INTERACTIVE BUCKLING IN THIN- WALLED SECTION BOX COLUMNS UNDER PURE COMPRESSION.

Silva, L. S. d., Simões, R., & Gervásio, H. (2014). *Design of steel structures: Eurocode 3; part 1-1- general rules and rules for buildings* (Rev. second impression 2013 ed.). Berlin s.l: ECCS.

Sizirici, B., Fseha, Y., Cho, C.-S., Yildiz, I., & Byon, Y.-J. (2021, October). A Review of Carbon Footprint Reduction in Construction Industry, from Design to Operation. *Materials*, *14*(20), 6094. Retrieved 2025-05-16, from https://www.ncbi.nlm.nih.gov/pmc/articles/PMC8540435/ doi: 10.3390/ma14206094

SS-EN 10219-1:2006. (2006).

Steel Tube Institute. (n.d.). Retrieved 2025-05-22, from https://steeltubeinstitute.org/hollow-structural-sections/hss-product-overview-benefits/

Taras, A., Nseir, J., & Boissonnade, N. (n.d.). Cylindrical Shell Buckling Strength according to the "Overall Method" of Eurocode 3 - Background and Applicability to the Design of High Strength Steel Circular Hollow Sections.

Timoshenko, S. P., & Gere, J. M. (2012). *Theory of Elastic Stability*. Courier Corporation.

Toffolon, A., & Taras, A. (2017, September). 12.16: Numerical investigation of the local buckling behaviour of high strength steel circular hollow sections. *ce/papers*, *1*(2-3), 3603–3612. Retrieved 2025-01-31, from https://onlinelibrary.wiley.com/doi/10.1002/cepa.416 doi: 10.1002/cepa.416

Trahair, N. S. (Ed.). (2008). *The behaviour and design of steel structures to EC3* (4. ed ed.). London New York: Taylor & Francis.

Vellaichamy, P., Kumarasamy, K., S K, N., & Veerasamy, S. k. (2019, April). Buckling Analysis of columns. *IOSR Journal of Engineering*.

Vuuren, J. V., & Mahachi, J. (2021, May). A Comparison Investigation into Analysis Methods to Determine theBuckling Capacity of South African Cold-Formed Steel Lipped ChannelSections.. Retrieved 2025-02-08, from https://avestia.com/ICCSTE2021_Proceedings/files/paper/ICCSTE_133.pdf doi: 10.11159/iccste21.133

Wong, K. F. W., & Weaver, P. (2006, May). Prediction of Local, Global Buckling and Their Interactions on Thin Circular Cylindrical Shells. In *47th AIAA/ASME/ASCE/AHS/ASC Structures, Structural Dynamics, and Materials Conference
 14th AIAA/ASME/AHS Adaptive Structures Conference
 7th.* Newport, Rhode Island: American Institute of Aeronautics and Astronautics. Retrieved 2025-02-06, from http://arc.aiaa.org/doi/abs/10.2514/6.2006-1788 doi: 10.2514/6.2006-1788

Yang, L., Shi, G., Zhao, M., & Zhou, W. (2017, June). Research on interactive buckling behavior of welded steel box-section columns. *Thin-Walled Structures*, *115*, 34–47. Retrieved 2025-02-03, from https://linkinghub.elsevier.com/retrieve/pii/S0263823117301052 doi: 10.1016/j.tws.2017.01.030

Yuan, H., Wang, Y., Gardner, L., & Shi, Y. (2014, May). Local–overall interactive buckling of welded stainless steel box section compression members.

Engineering Structures, *67*, 62–76. Retrieved 2025-02-05, from https://linkinghub.elsevier.com/retrieve/pii/S0141029614001059 doi: 10.1016/j.engstruct.2014.02.012

A

Python script

```python
# =====================
# Input Data
# =====================
E = 210000
yield_stress_1 = 355
plastic_strain_1 = 0.0
yield_stress_2 = 360.33
plastic_strain_2 = 0.0132
yield_stress_3 = 477.56
plastic_strain_3 = 0.0530
yield_stress_4 = 603
plastic_strain_4 = 0.1646
increment = 100
initialArcInc = 0.1
maxArcInc = 1

# =====================
# Imports
# =====================
from part import *
from material import *
from section import *
from assembly import *
from step import *
from interaction import *
from load import *
from mesh import *
from optimization import *
from job import *
from sketch import *
from visualization import *
from connectorBehavior import *
import math
import csv
import os

# =====================
# Working Directory and Results CSV Setup
# =====================
cwd = os.getcwd()
os.chdir(cwd)
results_csv_path = 'all_results_LPF.csv'
if not os.path.exists(results_csv_path):
    with open(results_csv_path, mode='w') as results_file:
        writer = csv.writer(results_file, delimiter=';')
        writer.writerow(['D (mm)', 'L (mm)', 't (mm)', 'Mode Number', 'Max LPF'])

# =====================
# Read Input CSV Data
# =====================
D_values = []
L_values = []
t_values = []
csv_name = "loop.csv"
with open(csv_name, 'r') as f:
    reader = csv.reader(f, delimiter=';')
```

```
    next(reader)
    for row in reader:
        D_values.append(float(row[0]))
        L_values.append(float(row[1]))
        t_values.append(float(row[2]))

# =====================
# Main Analysis Loop
# =====================
with open(results_csv_path, mode='a') as results_file:
    writer = csv.writer(results_file, delimiter=';')
    for i, (D, t, L) in enumerate(zip(D_values, t_values, L_values)):
        try:
            t_formatted = "{:.2f}".format(t).replace('.', '_')
            linear_model_name = 'Linear_{}_{}_{}'.format(int(D), int(L),
                ↪ t_formatted)
            nonlinear_model_name = 'Nonlinear_{}_{}_{}'.format(int(D), int(L),
                ↪ t_formatted)
            linear_job_name = 'LinearAnalysis_{}_{}_{}'.format(int(D), int(L),
                ↪ t_formatted)
            nonlinear_job_name = 'NonlinearAnalysis_{}_{}_{}'.format(int(D), int(L)
                ↪ , t_formatted)
            if i > 0:
                mdb.close()

            # =====================
            # Linear Buckling Model Creation
            # =====================
            mdb.Model(name=linear_model_name)
            mdb.models[linear_model_name].ConstrainedSketch(name='__profile__',
                ↪ sheetSize=5000.0)
            mdb.models[linear_model_name].sketches['__profile__'].
                ↪ CircleByCenterPerimeter(center=(0.0, 0.0), point1=(D/2, D
                ↪ /2*175/200))
            mdb.models[linear_model_name].sketches['__profile__'].ObliqueDimension(
                ↪ textPoint=(-654.515258789062, 557.407409667969),
            value=D/2, vertex1=mdb.models[linear_model_name].sketches['__profile__'
                ↪ ].vertices[0], vertex2=mdb.models[linear_model_name].sketches['
                ↪ __profile__'].vertices[1])
            mdb.models[linear_model_name].Part(dimensionality=THREE_D, name='Column
                ↪ ', type=DEFORMABLE_BODY)
            mdb.models[linear_model_name].parts['Column'].BaseShellExtrude(depth=L,
                ↪  sketch=mdb.models[linear_model_name].sketches['__profile__'])
            del mdb.models[linear_model_name].sketches['__profile__']
            mdb.models[linear_model_name].Material(name='Material-1')
            mdb.models[linear_model_name].materials['Material-1'].Elastic(table=((E
                ↪ , 0.3),))
            mdb.models[linear_model_name].HomogeneousShellSection(idealization=
                ↪ NO_IDEALIZATION, integrationRule=SIMPSON, material='Material-1',
            name='ColumnSection', nodalThicknessField='', numIntPts=5,
                ↪ poissonDefinition=DEFAULT, preIntegrate=OFF,
            temperature=GRADIENT, thickness=t, thicknessField='', thicknessModulus=
                ↪ None, thicknessType=UNIFORM, useDensity=OFF)
            mdb.models[linear_model_name].parts['Column'].SectionAssignment(offset
                ↪ =0.0, offsetField='', offsetType=TOP_SURFACE, region=Region(
                ↪ faces=mdb.models[linear_model_name].parts['Column'].faces.
                ↪ getSequenceFromMask(mask=('[#1 ]', ), )),
            sectionName='ColumnSection', thicknessAssignment=FROM_SECTION)
            mdb.models[linear_model_name].BuckleStep(name='Step-1', numEigen=20,
                ↪ previous='Initial', vectors=50, maxIterations=350)
            mdb.models[linear_model_name].rootAssembly.DatumCsysByDefault(CARTESIAN
                ↪ )
            mdb.models[linear_model_name].rootAssembly.Instance(dependent=ON, name=
                ↪ 'Column-1', part=mdb.models[linear_model_name].parts['Column'])
            mdb.models[linear_model_name].rootAssembly.DatumPointByMidPoint(point1=
                ↪ mdb.models[linear_model_name].rootAssembly.instances['Column-1'
                ↪ ].InterestingPoint(
                mdb.models[linear_model_name].rootAssembly.instances['Column-1'].
                    ↪ edges[0], MIDDLE),
```

```
101                 point2=mdb.models[linear_model_name].rootAssembly.instances['Column
                        ↪ -1'].vertices[0])
102             mdb.models[linear_model_name].rootAssembly.ReferencePoint(point=mdb.
                    ↪ models[linear_model_name].rootAssembly.datums[4])
103             mdb.models[linear_model_name].rootAssembly.DatumPointByMidPoint(point1=
                    ↪ mdb.models[linear_model_name].rootAssembly.instances['Column-1'
                    ↪ ].vertices[1],
104                 point2=mdb.models[linear_model_name].rootAssembly.instances['Column
                        ↪ -1'].InterestingPoint(
105                 mdb.models[linear_model_name].rootAssembly.instances['Column-1'].
                        ↪ edges[1], MIDDLE))
106             mdb.models[linear_model_name].rootAssembly.ReferencePoint(point=mdb.
                    ↪ models[linear_model_name].rootAssembly.datums[6])
107
108             # ======================
109             # Load Application
110             # ======================
111             mdb.models[linear_model_name].ConcentratedForce(cf3=-1000000.0,
                    ↪ createStepName='Step-1', distributionType=UNIFORM,
112                 field='', localCsys=None, name='ConcentratedLoad', region=Region(
                        ↪ referencePoints=(mdb.models[linear_model_name].rootAssembly.
                        ↪ referencePoints[5], )))
113
114             # ======================
115             # Boundary Conditions
116             # ======================
117             mdb.models[linear_model_name].Coupling(alpha=0.0, controlPoint=Region(
                    ↪ referencePoints=(mdb.models[linear_model_name].rootAssembly.
                    ↪ referencePoints[5], )),
118                 couplingType=KINEMATIC, influenceRadius=WHOLE_SURFACE, localCsys=
                        ↪ None, name='RollerEnd', surface=Region(
119                 side1Edges=mdb.models[linear_model_name].rootAssembly.instances['
                        ↪ Column-1'].edges.getSequenceFromMask(mask=('[#1␣]', ), )),
120                 u1=ON, u2=ON, u3=ON, ur1=ON, ur2=ON, ur3=ON)
121             mdb.models[linear_model_name].Coupling(alpha=0.0, controlPoint=Region(
                    ↪ referencePoints=(mdb.models[linear_model_name].rootAssembly.
                    ↪ referencePoints[7], )),
122                 couplingType=KINEMATIC, influenceRadius=WHOLE_SURFACE, localCsys=
                        ↪ None, name='PinnedEnd', surface=Region(
123                 side1Edges=mdb.models[linear_model_name].rootAssembly.instances['
                        ↪ Column-1'].edges.getSequenceFromMask(mask=('[#2␣]', ), )),
124                 u1=ON, u2=ON, u3=ON, ur1=ON, ur2=ON, ur3=ON)
125             mdb.models[linear_model_name].DisplacementBC(amplitude=UNSET,
                    ↪ buckleCase=PERTURBATION_AND_BUCKLING, createStepName='Step-1',
126                 distributionType=UNIFORM, fieldName='', fixed=OFF, localCsys=None,
                        ↪ name='RollerEnd', region=Region(referencePoints=(
127                 mdb.models[linear_model_name].rootAssembly.referencePoints[5], )),
                        ↪ u1=0.0, u2=0.0, u3=UNSET, ur1=UNSET, ur2=0.0, ur3=0.0)
128             mdb.models[linear_model_name].DisplacementBC(amplitude=UNSET,
                    ↪ buckleCase=PERTURBATION_AND_BUCKLING, createStepName='Step-1',
129                 distributionType=UNIFORM, fieldName='', fixed=OFF, localCsys=None,
                        ↪ name='PinnedEnd', region=Region(referencePoints=(
130                 mdb.models[linear_model_name].rootAssembly.referencePoints[7], )),
                        ↪ u1=0.0, u2=0.0, u3=0.0, ur1=UNSET, ur2=0.0, ur3=0.0)
131
132             # ======================
133             # Mesh
134             # ======================
135             mesh_size = 0.05 * math.sqrt(D*L)
136             mdb.models[linear_model_name].parts['Column'].seedPart(deviationFactor
                    ↪ =0.1, minSizeFactor=0.1, size=mesh_size)
137             mdb.models[linear_model_name].parts['Column'].seedEdgeBySize(constraint
                    ↪ =FINER, deviationFactor=0.1,
138                 edges=mdb.models[linear_model_name].parts['Column'].edges.
                        ↪ getSequenceFromMask(('[#3␣]', ), ),
139                 minSizeFactor=0.1, size=mesh_size)
140             mdb.models[linear_model_name].parts['Column'].generateMesh()
141             mdb.models[linear_model_name].parts['Column'].setElementType(elemTypes
                    ↪ =(ElemType(
142                 elemCode=S8R, elemLibrary=STANDARD, secondOrderAccuracy=OFF,
```

```
143                 hourglassControl=DEFAULT), ElemType(elemCode=STRI65, elemLibrary=
                        ↪ STANDARD)),
144                 regions=(mdb.models[linear_model_name].parts['Column'].faces.
                        ↪ getSequenceFromMask((
145                 '[#1 ]', ), ), ))
146             mdb.models[linear_model_name].rootAssembly.regenerate()
147             mdb.saveAs(linear_model_name + '.cae')
148             mdb.Job(atTime=None, contactPrint=OFF, description='', echoPrint=OFF,
                    ↪ explicitPrecision=SINGLE,
149                     getMemoryFromAnalysis=True, historyPrint=OFF, memory=90,
                            ↪ memoryUnits=PERCENTAGE, model=linear_model_name,
150                     modelPrint=OFF, multiprocessingMode=DEFAULT, name=
                            ↪ linear_job_name, nodalOutputPrecision=SINGLE, numCpus=1,
151                     numGPUs=0, numThreadsPerMpiProcess=1, queue=None, resultsFormat
                            ↪ =ODB, scratch='', type=ANALYSIS, userSubroutine='',
152                     waitHours=0, waitMinutes=0)
153             mdb.models[linear_model_name].steps['Step-1'].setValues(maxIterations
                    ↪ =350, vectors=35)
154             mdb.models[linear_model_name].keywordBlock.synchVersions(
                    ↪ storeNodesAndElements=False)
155             mdb.models[linear_model_name].keywordBlock.insert(49,
156                 '\n*NODE FILE, GLOBAL=YES, LAST MODE=10\nU')
157             mdb.jobs[linear_job_name].submit(consistencyChecking=OFF)
158             mdb.jobs[linear_job_name].waitForCompletion()
159             session.mdbData.summary()
160             odb = session.openOdb(name=linear_job_name + '.odb')
161             session.viewports['Viewport: 1'].setValues(displayedObject=odb)
162
163             # =====================
164             # Buckling Mode Localization Ratio Calculation
165             # =====================
166             def calculate_localization_ratio(odb, mode):
167                 frame = odb.steps['Step-1'].frames[mode]
168                 displacements = frame.fieldOutputs['U'].values
169                 max_disp = max([math.sqrt(u.data[0]**2 + u.data[1]**2 + u.data
                        ↪ [2]**2) for u in displacements])
170                 avg_disp = sum([math.sqrt(u.data[0]**2 + u.data[1]**2 + u.data
                        ↪ [2]**2) for u in displacements]) / len(displacements)
171                 return max_disp / avg_disp if avg_disp > 0 else 0
172             LOCALIZATION_THRESHOLD = 2.2
173             first_local_mode = None
174             for mode in range(1, 11):
175                 ratio = calculate_localization_ratio(odb, mode)
176                 if ratio > LOCALIZATION_THRESHOLD:
177                     first_local_mode = mode
178                     break
179             odb.close()
180
181             # =====================
182             # Nonlinear Buckling Model Creation
183             # =====================
184             mdb.Model(name=nonlinear_model_name, objectToCopy=mdb.models[
                    ↪ linear_model_name])
185             local_imperfection = (t / 16) * math.sqrt((D/2) / t)
186             global_imperfection = 1.4*L/1000
187             if first_local_mode is None:
188                 imperfection = [(1, global_imperfection)]
189             elif first_local_mode == 1:
190                 imperfection = [(first_local_mode, local_imperfection)]
191             else:
192                 imperfection = [(1, global_imperfection), (first_local_mode,
                        ↪ local_imperfection * 0.7)]
193             imperfection_str = "\n*imperfection,file={0},step=1\n".format(
                    ↪ linear_job_name)
194             for imperf in imperfection:
195                 imperfection_str += "{0},{1}\n".format(imperf[0], imperf[1])
196             mdb.models[nonlinear_model_name].materials['Material-1'].Plastic(
                    ↪ scaleStress=None,
197             table=((yield_stress_1, plastic_strain_1),
198             (yield_stress_2, plastic_strain_2),
```

```
            (yield_stress_3, plastic_strain_3),
            (yield_stress_4, plastic_strain_4)))
            mdb.models[nonlinear_model_name].StaticRiksStep(initialArcInc=
                ↪ initialArcInc,
                maintainAttributes=True, maxArcInc=maxArcInc, maxNumInc=increment,
                    ↪ minArcInc=1e-09,
                name='Step-1', nlgeom=ON, previous='Initial')
            mdb.models[nonlinear_model_name].steps.changeKey(fromName='Step-1',
                ↪ toName='nonlinear')
            mdb.models[nonlinear_model_name].keywordBlock.synchVersions(
                ↪ storeNodesAndElements=False)
            mdb.models[nonlinear_model_name].keywordBlock.insert(37,
                ↪ imperfection_str)
            mdb.saveAs(nonlinear_model_name + '.cae')
            mdb.Job(atTime=None, contactPrint=OFF, description='', echoPrint=OFF,
                ↪ explicitPrecision=SINGLE,
                    getMemoryFromAnalysis=True, historyPrint=OFF, memory=90,
                        ↪ memoryUnits=PERCENTAGE, model=nonlinear_model_name,
                    modelPrint=OFF, multiprocessingMode=DEFAULT, name=
                        ↪ nonlinear_job_name, nodalOutputPrecision=SINGLE, numCpus
                        ↪ =1,
                    numGPUs=0, numThreadsPerMpiProcess=1, queue=None, resultsFormat
                        ↪ =ODB, scratch='', type=ANALYSIS, userSubroutine='',
                    waitHours=0, waitMinutes=0)
            mdb.jobs[nonlinear_job_name].submit(consistencyChecking=OFF)
            mdb.jobs[nonlinear_job_name].waitForCompletion()

            # ======================
            # LPF Extraction and Results Writing
            # ======================
            from odbAccess import openOdb
            from abaqusConstants import *
            odb = openOdb(path=nonlinear_job_name + '.odb')
            try:
                load_factor_data = session.XYDataFromHistory(
                    name='LoadFactor',
                    odb=odb,
                    outputVariableName='Load␣proportionality␣factor:␣LPF␣for␣Whole␣
                        ↪ Model',
                    steps=('nonlinear',)
                )
                max_lpf = max([point[1] for point in load_factor_data])
                print("Analysis␣completed␣for␣D={},␣L={},␣t={}".format(D, L, t))
                print("Max␣LPF:␣{}".format(max_lpf))
                print("First␣local␣mode:␣{}".format(first_local_mode))
                print("-" * 50)
                with open(results_csv_path, mode='a') as results_file:
                    writer = csv.writer(results_file, delimiter=';', lineterminator
                        ↪ ='\n')
                    writer.writerow([D, L, t, first_local_mode, max_lpf])
            except Exception as e:
                print("Error␣in␣analysis␣for␣D={},␣L={},␣t={}:␣{}".format(D, L, t,
                    ↪ str(e)))
                with open(results_csv_path, mode='a') as results_file:
                    writer = csv.writer(results_file, delimiter=';', lineterminator
                        ↪ ='\n')
                    writer.writerow([D, L, t, 'Error', 'Error'])
            finally:
                odb.close()

        except Exception as e:
            print("Error␣in␣analysis␣for␣D={},␣L={},␣t={}:␣{}".format(D, L, t, str(
                ↪ e)))
            with open(results_csv_path, mode='a') as results_file:
                writer = csv.writer(results_file, delimiter=';')
                writer.writerow([D, L, t, 'Error', 'Error'])
            continue
```

Listing A.1: Python script

B

Results of parametric study

Table B.1: Results of parametric study

D [mm]	t [mm]	L [mm]	D/t [-]	CSC [-]	λ_n [-]	$N_{u,\mathrm{FEM}}$ [kN]
100	6	2000	16.7	3	0.79	551
200	6	2000	33.3	3	0.38	1276
220	6	2000	36.7	3	0.35	1403
240	6	2000	40.0	3	0.32	1542
260	6	2000	43.3	3	0.29	1675
280	6	2000	46.7	3	0.27	1809
300	6	2000	50.0	3	0.25	1992
350	6	2000	58.3	3	0.22	2324
355	6	2000	59.2	3	0.21	2350
360	6	2000	60.0	4	0.21	2390
400	6	2000	66.7	4	0.19	2635
500	6	2000	83.3	4	0.15	3274
600	6	2000	100.0	4	0.12	3899
700	6	2000	116.7	4	0.11	4437
800	6	2000	133.3	4	0.09	5071
900	6	2000	150.0	4	0.08	5442
1000	6	2000	166.7	4	0.07	6093
100	6	3000	16.7	3	1.18	372
200	6	3000	33.3	3	0.57	1217
220	6	3000	36.7	3	0.52	1354
240	6	3000	40.0	3	0.47	1493
260	6	3000	43.3	3	0.44	1627
280	6	3000	46.7	3	0.41	1763
300	6	3000	50.0	3	0.38	1906
320	6	3000	53.3	3	0.35	2040
340	6	3000	56.7	3	0.33	2175
350	6	3000	58.3	3	0.32	2241
355	6	3000	59.2	3	0.32	2273
360	6	3000	60.0	4	0.31	2307
365	6	3000	60.8	4	0.31	2339
370	6	3000	61.7	4	0.31	2373
375	6	3000	62.5	4	0.30	2490
380	6	3000	63.3	4	0.30	2524

Continued on next page

Table B.1 – continued from previous page

D [mm]	t [mm]	L [mm]	D/t [-]	CSC [-]	λ_n [-]	$N_{u,\mathrm{FEM}}$ [kN]
400	6	3000	66.7	4	0.28	2655
500	6	3000	83.3	4	0.22	3299
600	6	3000	100.0	4	0.19	3938
700	6	3000	116.7	4	0.16	4558
800	6	3000	133.3	4	0.14	5179
900	6	3000	150.0	4	0.12	5726
1000	6	3000	166.7	4	0.11	6335
100	6	4000	16.7	3	1.57	230
200	6	4000	33.3	3	0.76	1119
300	6	4000	50.0	3	0.50	1845
320	6	4000	53.3	3	0.47	1983
340	6	4000	56.7	3	0.44	2124
350	6	4000	58.3	3	0.43	2198
355	6	4000	59.2	3	0.42	2230
360	6	4000	60.0	4	0.42	2268
380	6	4000	63.3	4	0.40	2402
400	6	4000	66.7	4	0.38	2535
420	6	4000	70.0	4	0.36	2667
440	6	4000	73.3	4	0.34	2798
445	6	4000	74.2	4	0.34	2835
450	6	4000	75.0	4	0.33	2988
455	6	4000	75.8	4	0.33	3021
460	6	4000	76.7	4	0.33	3053
480	6	4000	80.0	4	0.31	3184
500	6	4000	83.3	4	0.30	3311
600	6	4000	100.0	4	0.25	3958
700	6	4000	116.7	4	0.21	4581
800	6	4000	133.3	4	0.19	5190
900	6	4000	150.0	4	0.17	5799
1000	6	4000	166.7	4	0.15	6342
100	6	5000	16.7	3	1.96	154
200	6	5000	33.3	3	0.95	962
300	6	5000	50.0	3	0.63	1789
320	6	5000	53.3	3	0.59	1921
340	6	5000	56.7	3	0.55	2064
350	6	5000	58.3	3	0.54	2124
355	6	5000	59.2	3	0.53	2182
360	6	5000	60.0	4	0.52	2202
380	6	5000	63.3	4	0.49	2367
400	6	5000	66.7	4	0.47	2467
420	6	5000	70.0	4	0.45	2624
440	6	5000	73.3	4	0.43	2759
460	6	5000	76.7	4	0.41	2895
480	6	5000	80.0	4	0.39	3028
500	6	5000	83.3	4	0.37	3162

Continued on next page

Table B.1 – continued from previous page

D [mm]	t [mm]	L [mm]	D/t [-]	CSC [-]	λ_n [-]	$N_{u,\mathrm{FEM}}$ [kN]
520	6	5000	86.7	4	0.36	3442
540	6	5000	90.0	4	0.35	3575
560	6	5000	93.3	4	0.33	3704
580	6	5000	96.7	4	0.32	3831
600	6	5000	100.0	4	0.31	3952
700	6	5000	116.7	4	0.27	4608
800	6	5000	133.3	4	0.23	5227
900	6	5000	150.0	4	0.21	5805
1000	6	5000	166.7	4	0.19	6435
100	6	6000	16.7	3	2.36	111
200	6	6000	33.3	3	1.14	781
300	6	6000	50.0	3	0.76	1685
350	6	6000	58.3	3	0.65	2047
355	6	6000	59.2	3	0.64	2093
360	6	6000	60.0	4	0.63	2130
400	6	6000	66.7	4	0.56	2412
420	6	6000	70.0	4	0.54	2558
440	6	6000	73.3	4	0.52	2701
460	6	6000	76.7	4	0.50	2851
480	6	6000	80.0	4	0.48	2989
500	6	6000	83.3	4	0.46	3127
520	6	6000	86.7	4	0.45	3273
540	6	6000	90.0	4	0.43	3407
560	6	6000	93.3	4	0.41	3539
580	6	6000	96.7	4	0.40	3669
600	6	6000	100.0	4	0.38	3798
700	6	6000	116.7	4	0.33	4454
800	6	6000	133.3	4	0.30	5049
900	6	6000	150.0	4	0.28	5605
1000	6	6000	166.7	4	0.26	6222
100	6	7000	16.7	3	2.75	82
200	6	7000	33.3	3	1.34	618
300	6	7000	50.0	3	0.88	1543
350	6	7000	58.3	3	0.75	1963
355	6	7000	59.2	3	0.74	2003
360	6	7000	60.0	4	0.73	2042
400	6	7000	66.7	4	0.66	2336
420	6	7000	70.0	4	0.63	2504
440	6	7000	73.3	4	0.60	2625
460	6	7000	76.7	4	0.57	2806
480	6	7000	80.0	4	0.55	2934
500	6	7000	83.3	4	0.52	3042
520	6	7000	86.7	4	0.50	3175
540	6	7000	90.0	4	0.49	3338
560	6	7000	93.3	4	0.47	3480

Continued on next page

Table B.1 – continued from previous page

D [mm]	t [mm]	L [mm]	D/t [-]	CSC [-]	λ_n [-]	$N_{u,\mathrm{FEM}}$ [kN]
580	6	7000	96.7	4	0.45	3603
600	6	7000	100.0	4	0.44	3738
620	6	7000	103.3	4	0.42	3873
640	6	7000	106.7	4	0.41	3998
660	6	7000	110.0	4	0.40	4332
680	6	7000	113.3	4	0.38	4477
700	6	7000	116.7	4	0.37	4601
800	6	7000	133.3	4	0.33	5252
900	6	7000	150.0	4	0.29	5848
1000	6	7000	166.7	4	0.26	6504
100	6	8000	16.7	3	3.14	63
200	6	8000	33.3	3	1.53	490
300	6	8000	50.0	3	1.01	1365
350	6	8000	58.3	3	0.86	1813
355	6	8000	59.2	3	0.85	1871
360	6	8000	60.0	4	0.84	1914
400	6	8000	66.7	4	0.75	2250
420	6	8000	70.0	4	0.72	2396
440	6	8000	73.3	4	0.68	2542
460	6	8000	76.7	4	0.65	2715
480	6	8000	80.0	4	0.62	2858
500	6	8000	83.3	4	0.60	3002
520	6	8000	86.7	4	0.58	3116
540	6	8000	90.0	4	0.55	3255
560	6	8000	93.3	4	0.53	3390
580	6	8000	96.7	4	0.52	3540
600	6	8000	100.0	4	0.50	3686
700	6	8000	116.7	4	0.43	4357
720	6	8000	120.0	4	0.41	4738
740	6	8000	123.3	4	0.40	4846
760	6	8000	126.7	4	0.39	4968
780	6	8000	130.0	4	0.38	5111
800	6	8000	133.3	4	0.37	5254
900	6	8000	150.0	4	0.33	5901
1000	6	8000	166.7	4	0.30	6484
100	6	9000	16.7	3	3.54	51
200	6	9000	33.3	3	1.72	398
300	6	9000	50.0	3	1.13	1186
350	6	9000	58.3	3	0.97	1661
355	6	9000	59.2	3	0.95	1708
360	6	9000	60.0	4	0.94	1754
370	6	9000	61.7	4	0.92	1844
380	6	9000	63.3	4	0.89	1927
390	6	9000	65.0	4	0.87	2027
400	6	9000	66.7	4	0.85	2115

Continued on next page

Table B.1 – continued from previous page

D [mm]	t [mm]	L [mm]	D/t [-]	CSC [-]	λ_n [-]	$N_{u,\mathrm{FEM}}$ [kN]
500	6	9000	83.3	4	0.67	2923
520	6	9000	86.7	4	0.65	3055
540	6	9000	90.0	4	0.62	3193
560	6	9000	93.3	4	0.60	3330
580	6	9000	96.7	4	0.58	3462
600	6	9000	100.0	4	0.56	3610
620	6	9000	103.3	4	0.54	3776
640	6	9000	106.7	4	0.53	3880
660	6	9000	110.0	4	0.51	4042
680	6	9000	113.3	4	0.49	4175
700	6	9000	116.7	4	0.48	4309
720	6	9000	120.0	4	0.47	4448
740	6	9000	123.3	4	0.45	4584
760	6	9000	126.7	4	0.44	5002
780	6	9000	130.0	4	0.43	5106
800	6	9000	133.3	4	0.42	5230
900	6	9000	150.0	4	0.37	5878
1000	6	9000	166.7	4	0.34	6510
100	6	10000	16.7	3	3.93	41
200	6	10000	33.3	3	1.91	332
300	6	10000	50.0	3	1.26	1021
350	6	10000	58.3	3	1.08	1478
355	6	10000	59.2	3	1.06	1525
360	6	10000	60.0	4	1.05	1571
370	6	10000	61.7	4	1.02	1664
380	6	10000	63.3	4	0.99	1756
390	6	10000	65.0	4	0.96	1843
400	6	10000	66.7	4	0.94	1954
410	6	10000	68.3	4	0.92	2035
420	6	10000	70.0	4	0.89	2126
500	6	10000	83.3	4	0.75	2804
600	6	10000	100.0	4	0.62	3579
620	6	10000	103.3	4	0.60	3680
640	6	10000	106.7	4	0.58	3844
660	6	10000	110.0	4	0.57	3961
680	6	10000	113.3	4	0.55	4119
700	6	10000	116.7	4	0.53	4260
720	6	10000	120.0	4	0.52	4362
740	6	10000	123.3	4	0.50	4508
760	6	10000	126.7	4	0.49	4656
780	6	10000	130.0	4	0.48	4799
800	6	10000	133.3	4	0.47	4911
820	6	10000	136.7	4	0.45	5375
840	6	10000	140.0	4	0.44	5495
860	6	10000	143.3	4	0.43	5638

Continued on next page

Table B.1 – continued from previous page

D [mm]	t [mm]	L [mm]	D/t [-]	CSC [-]	λ_n [-]	$N_{u,\mathrm{FEM}}$ [kN]
880	6	10000	146.7	4	0.42	5713
900	6	10000	150.0	4	0.41	5858
1000	6	10000	166.7	4	0.37	6534

C

Normalised FEM result against yield strength compared with buckling curves for each length

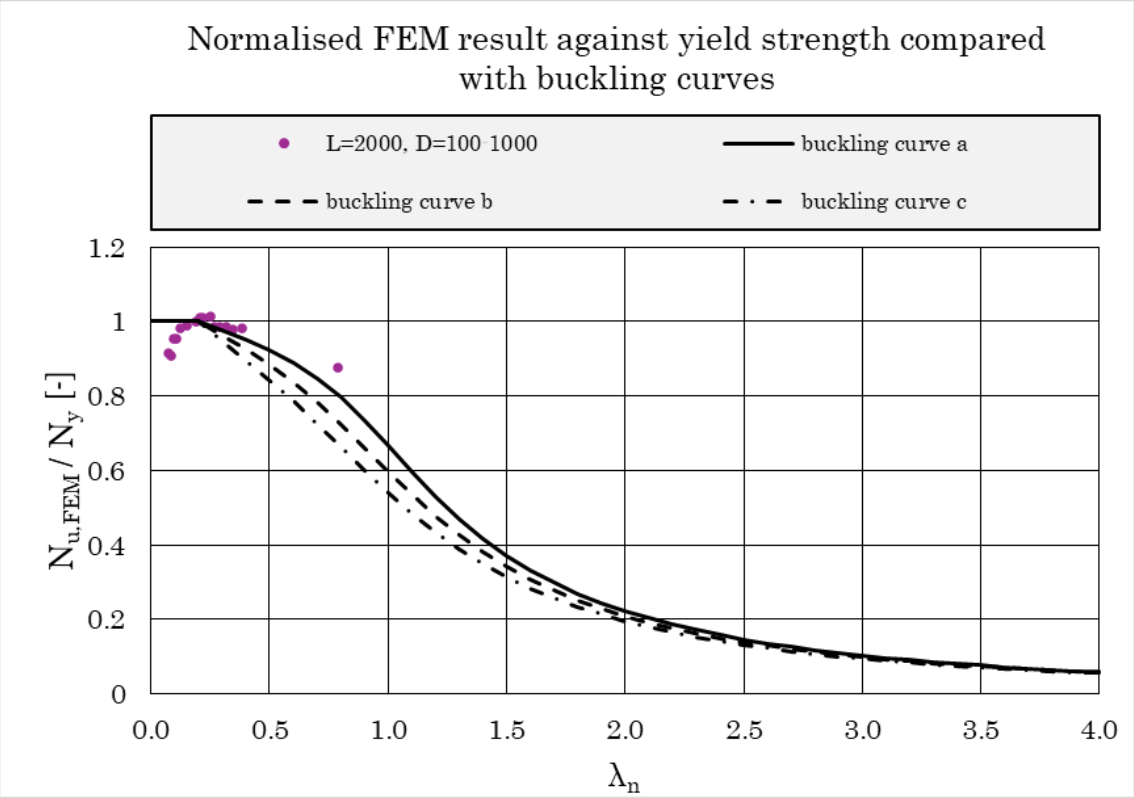

C. Normalised FEM result against yield strength compared with buckling curves for each length

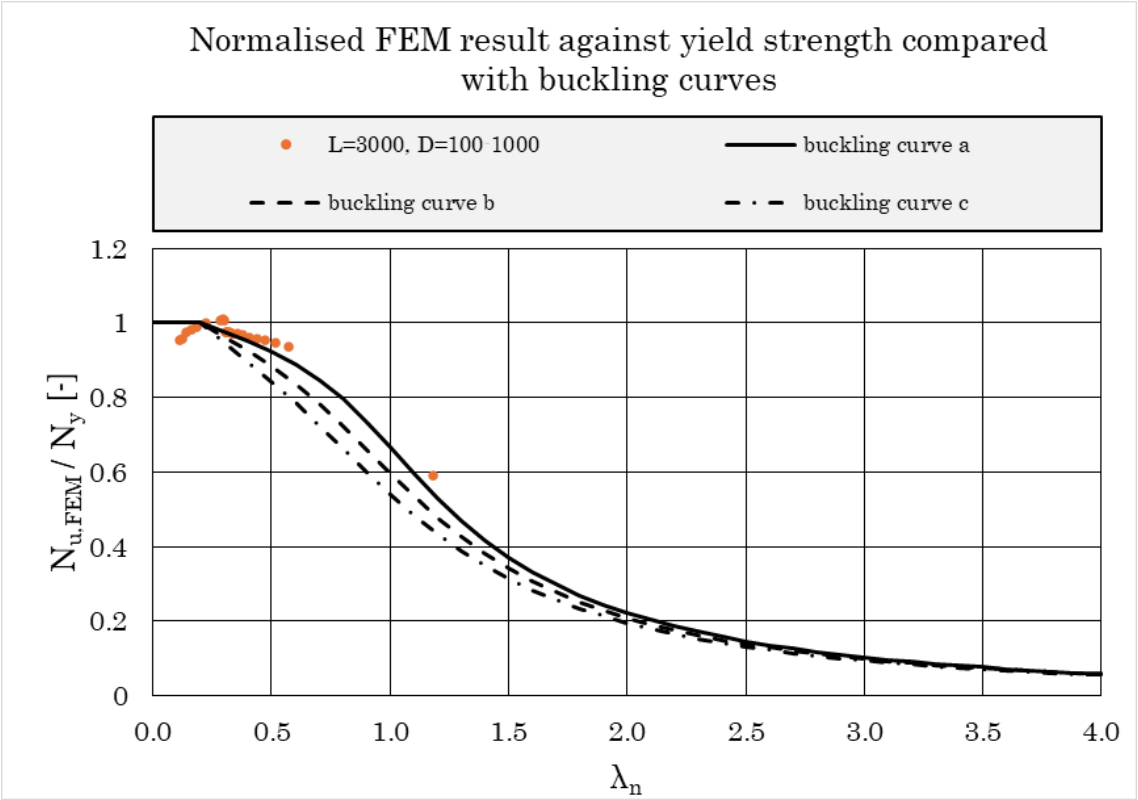

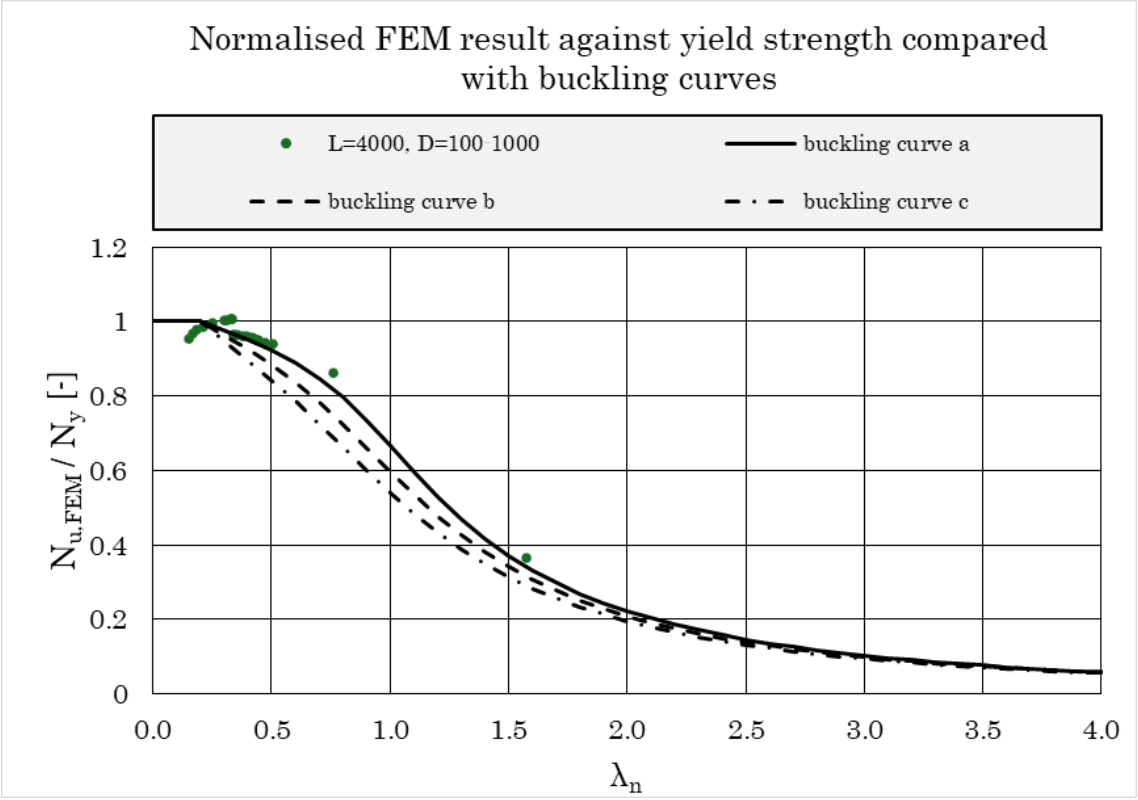

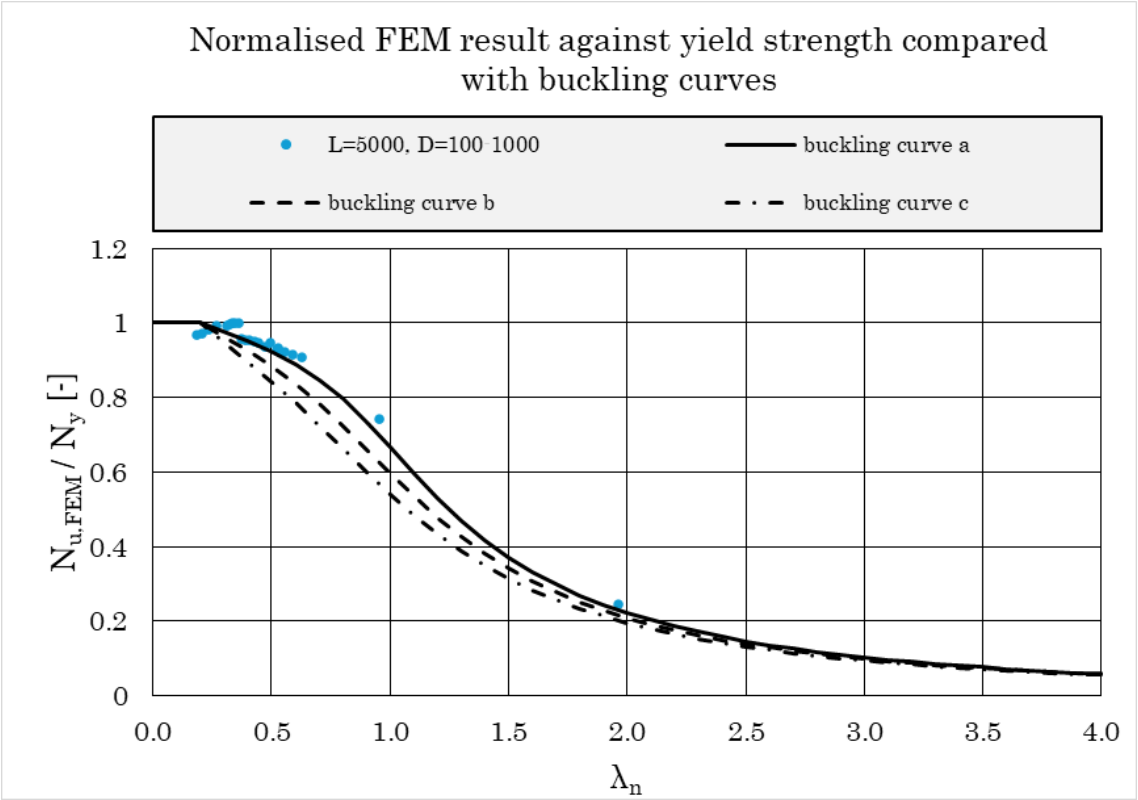
Normalised FEM result against yield strength compared with buckling curves
L=5000, D=100 1000
buckling curve a
buckling curve b
buckling curve c
1.2
1
0.8
0.6
0.4
0.2
0
$N_{u,FEM} / N_y$ [-]
0.0
0.5
1.0
1.5
2.0
2.5
3.0
3.5
4.0
λ_n

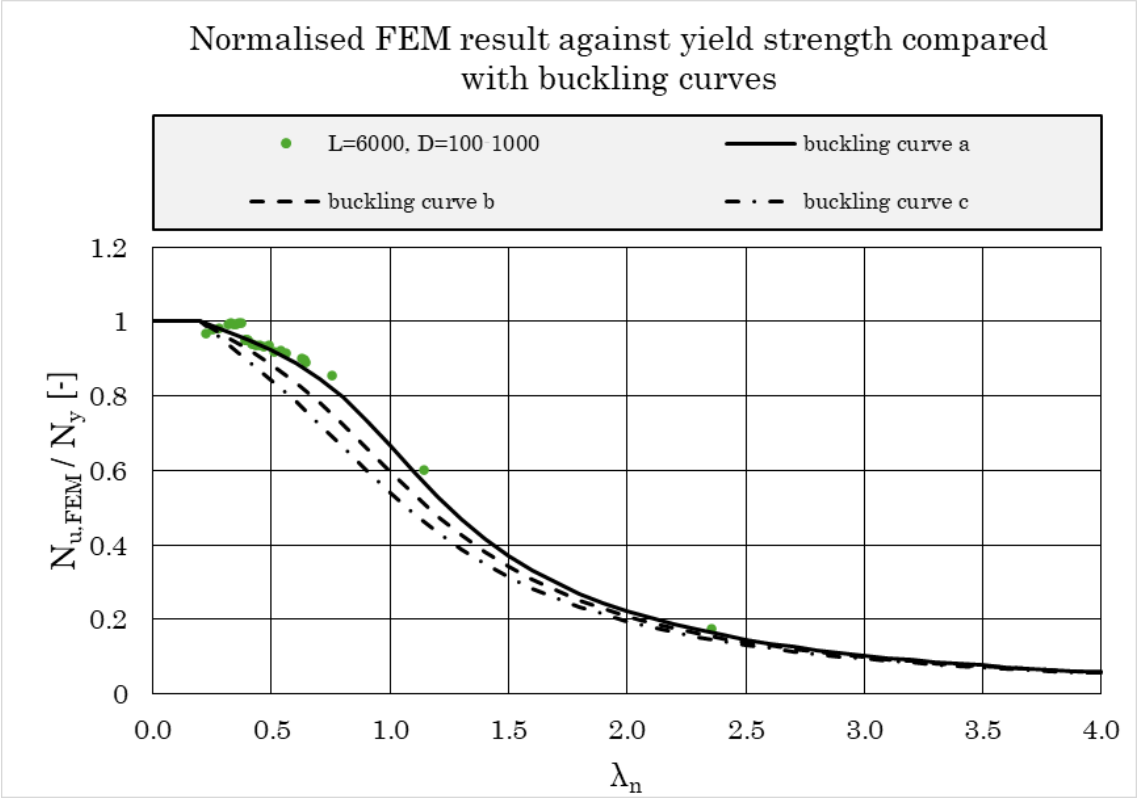
Normalised FEM result against yield strength compared with buckling curves
L=6000, D=100 1000
buckling curve a
buckling curve b
buckling curve c
1.2
1
0.8
0.6
0.4
0.2
0
$N_{u,FEM} / N_y$ [-]
0.0
0.5
1.0
1.5
2.0
2.5
3.0
3.5
4.0
λ_n

C. Normalised FEM result against yield strength compared with buckling curves for each length

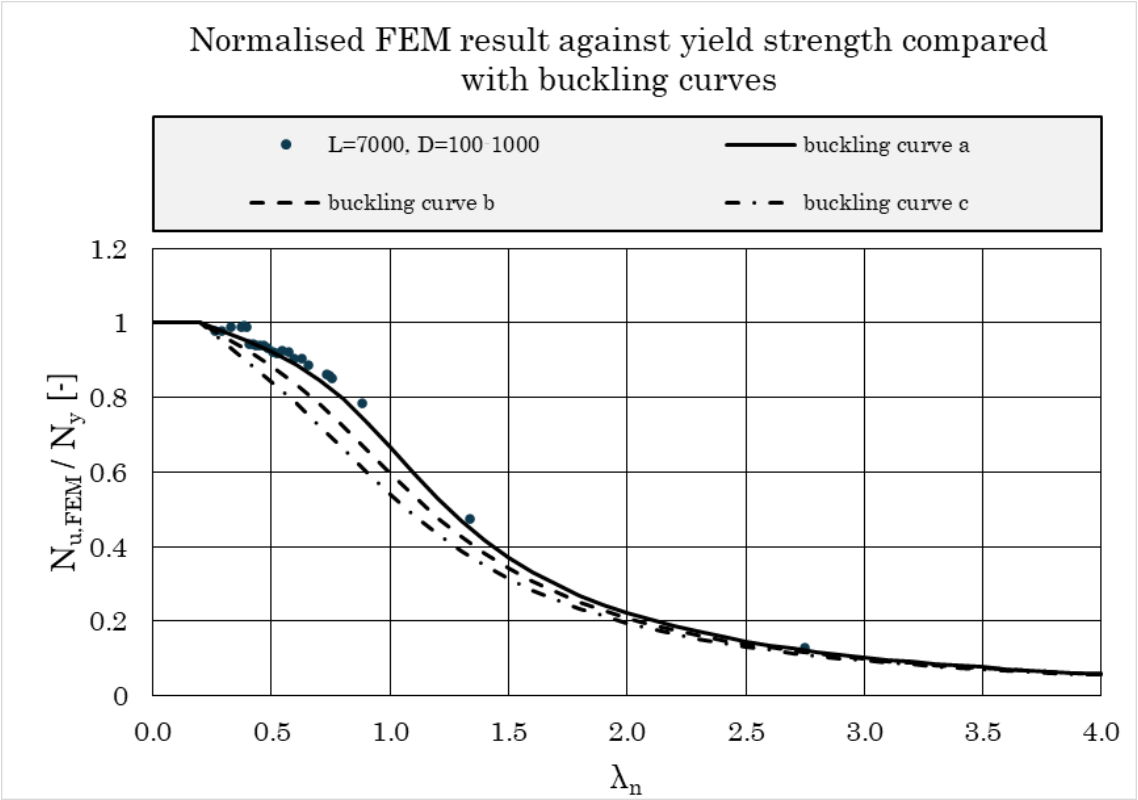

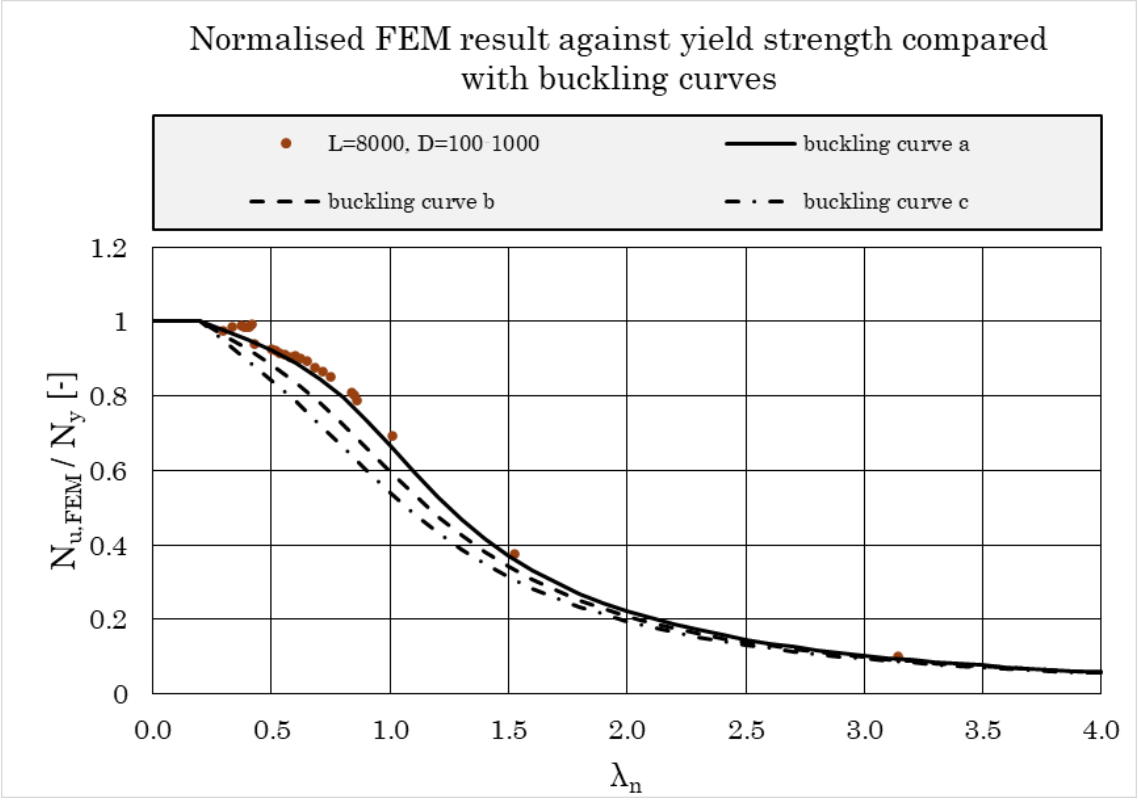

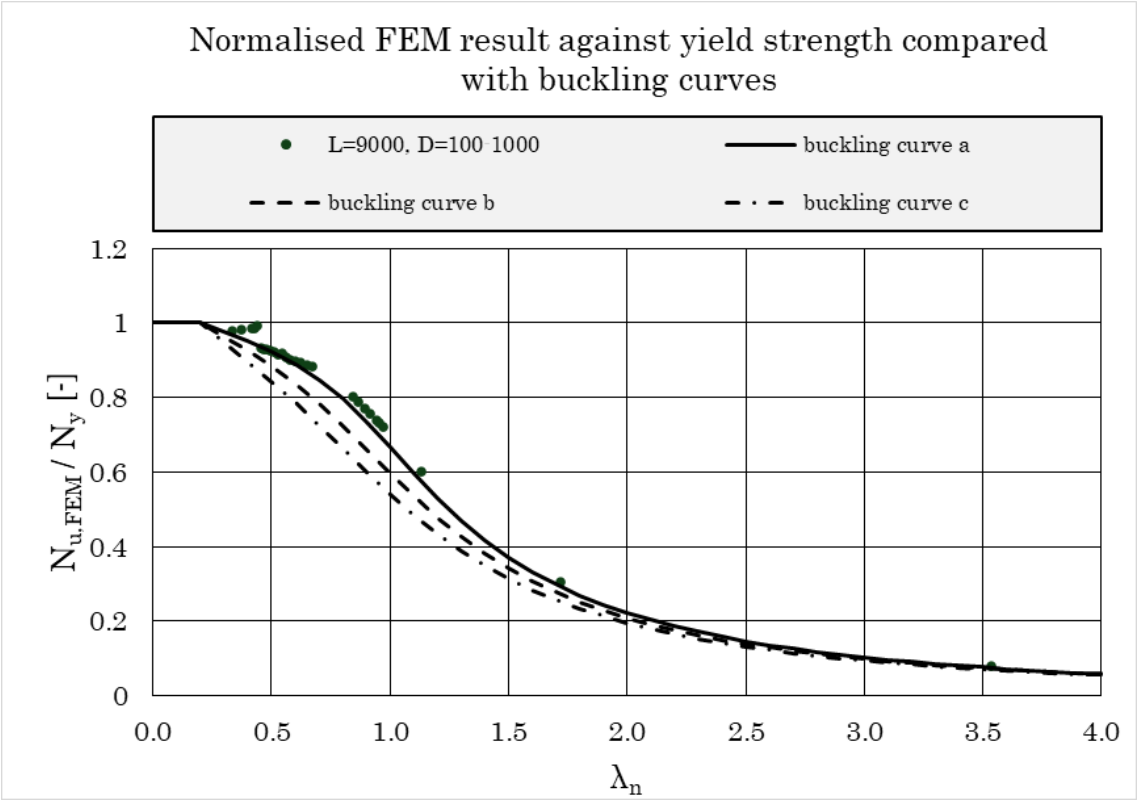
Normalised FEM result against yield strength compared with buckling curves
L=9000, D=100 1000
buckling curve a
buckling curve b
buckling curve c
1.2
1
0.8
0.6
0.4
0.2
0
$N_{u,FEM} / N_y$ [-]
0.0
0.5
1.0
1.5
2.0
2.5
3.0
3.5
4.0
λ_n

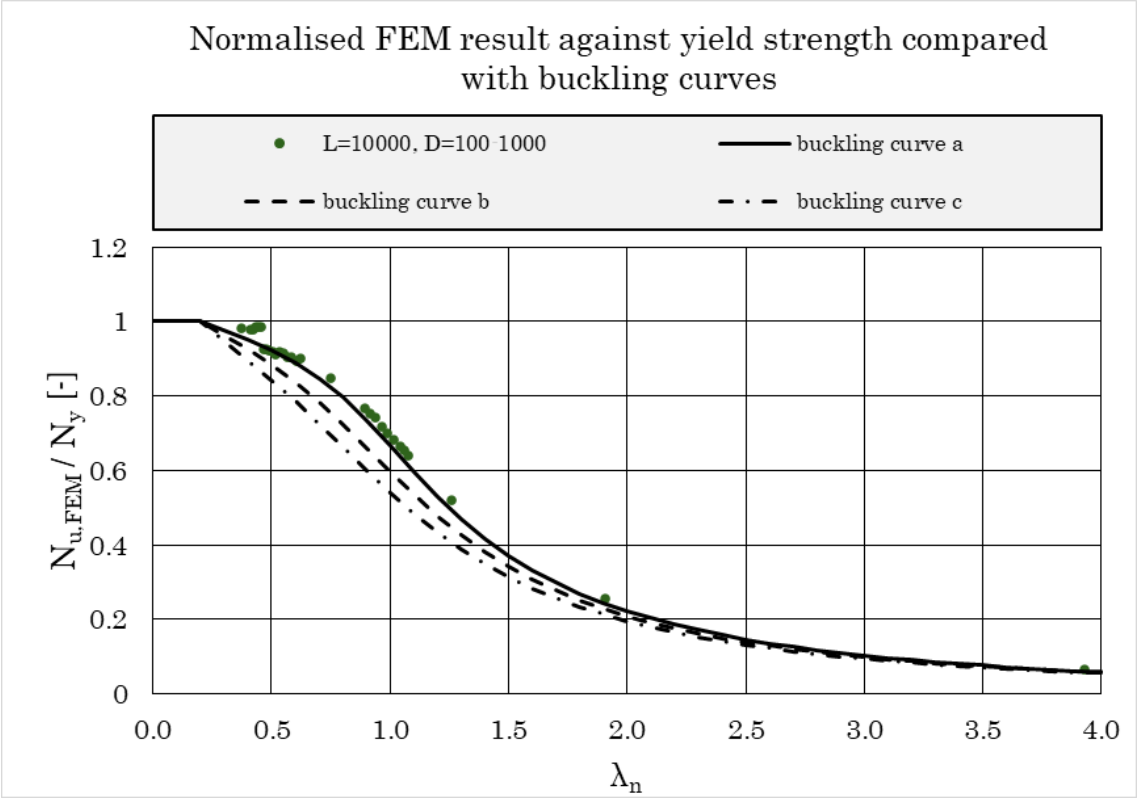
Normalised FEM result against yield strength compared with buckling curves
L=10000, D=100 1000
buckling curve a
buckling curve b
buckling curve c
1.2
1
0.8
0.6
0.4
0.2
0
$N_{u,FEM} / N_y$ [-]
0.0
0.5
1.0
1.5
2.0
2.5
3.0
3.5
4.0
λ_n

D

Normalised FEM results against EN1993-1-1 for CSC 3 and against EN1993-1-6 for CSC 4

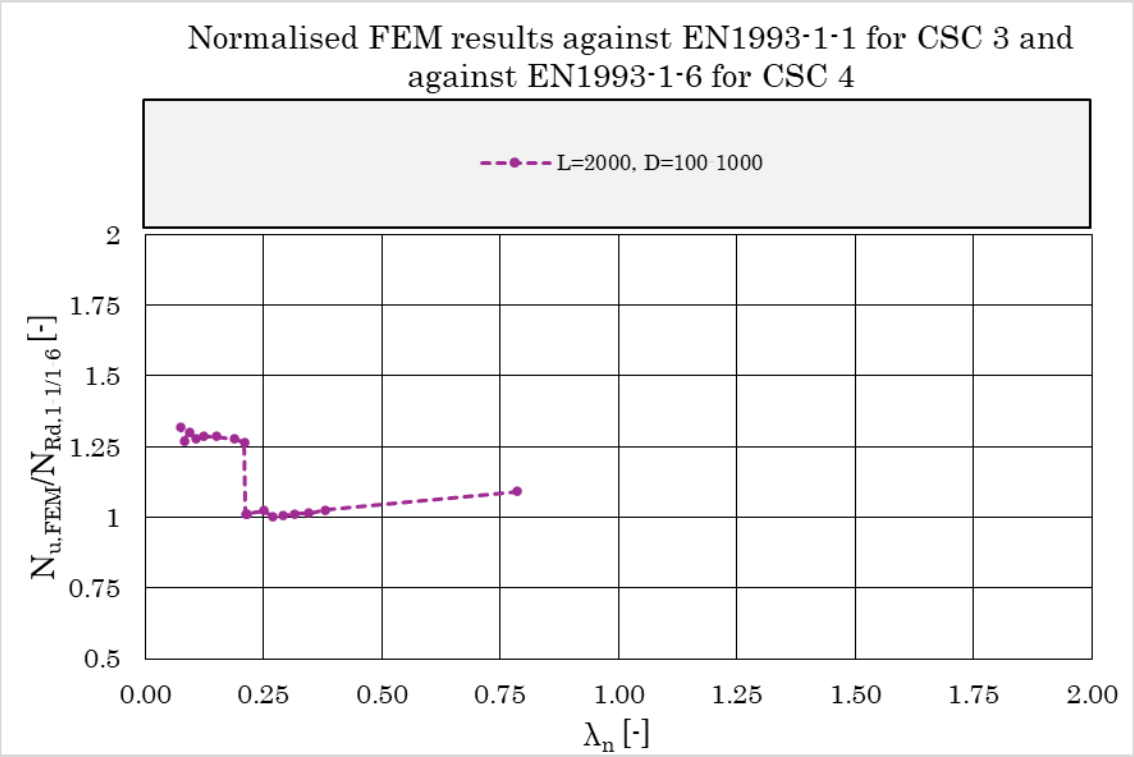

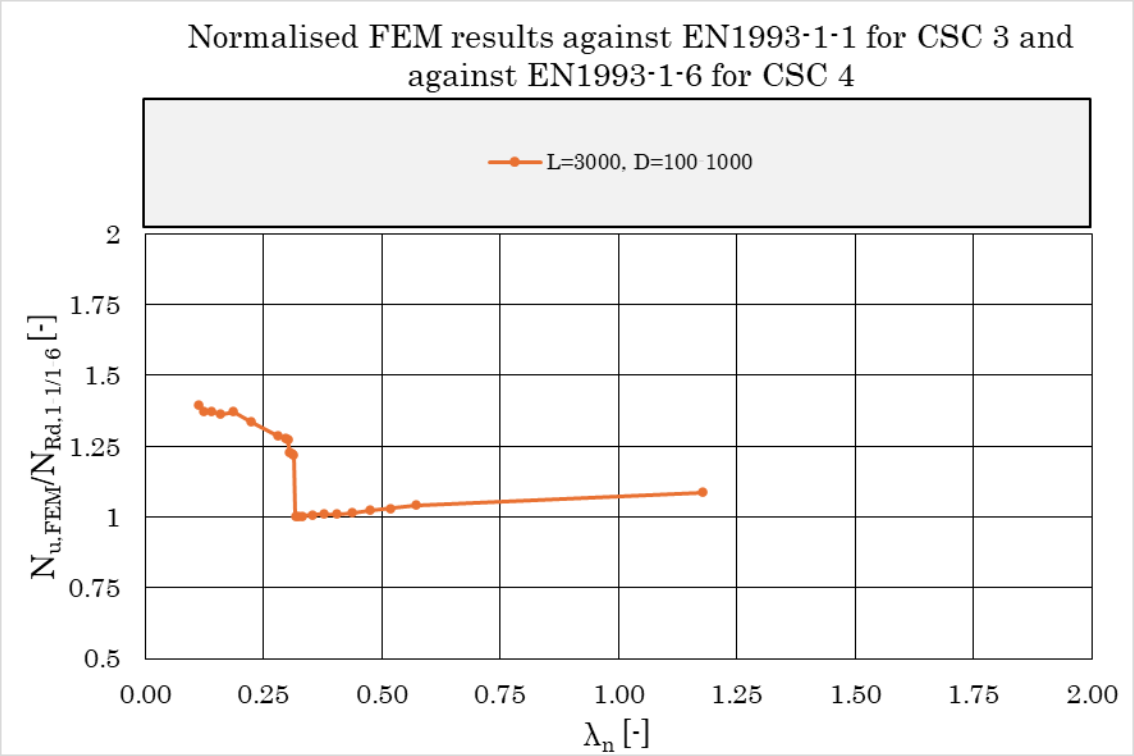
Normalised FEM results against EN1993-1-1 for CSC 3 and against EN1993-1-6 for CSC 4
L=3000, D=100 1000
2
1.75
1.5
1.25
1
0.75
0.5
$N_{u,FEM}/N_{Rd,1\ 1/1\ 6}$ [-]
0.00
0.25
0.50
0.75
1.00
1.25
1.50
1.75
2.00
λ_n [-]

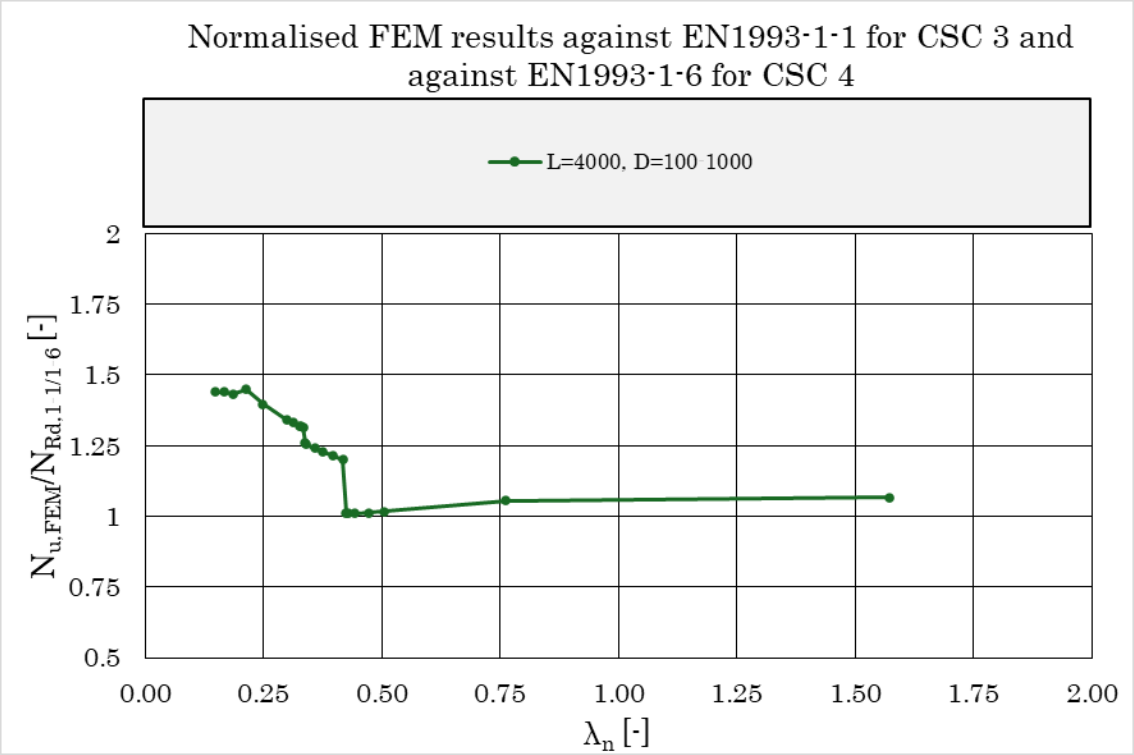
Normalised FEM results against EN1993-1-1 for CSC 3 and against EN1993-1-6 for CSC 4
L=4000, D=100 1000
2
1.75
1.5
1.25
1
0.75
0.5
$N_{u,FEM}/N_{Rd,1\ 1/1\ 6}$ [-]
0.00
0.25
0.50
0.75
1.00
1.25
1.50
1.75
2.00
λ_n [-]

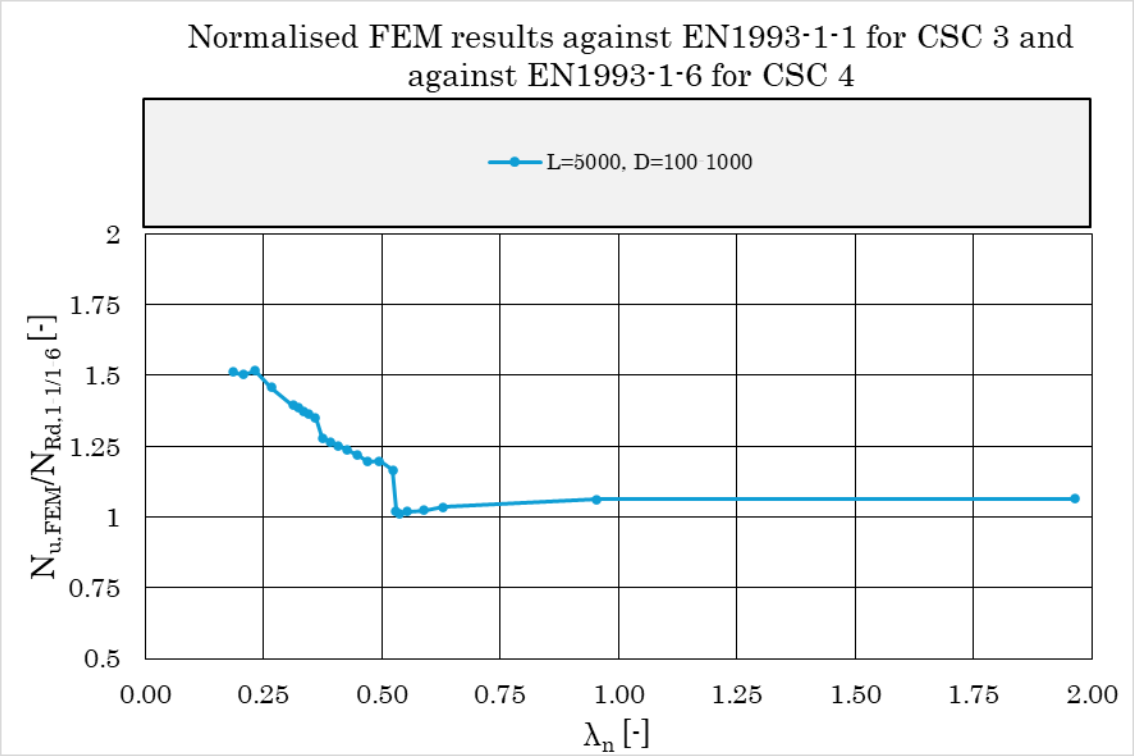
Normalised FEM results against EN1993-1-1 for CSC 3 and against EN1993-1-6 for CSC 4
L=5000, D=100 1000
2
1.75
1.5
1.25
1
0.75
0.5
$N_{u,FEM}/N_{Rd,1\ 1/1\ 6}$ [-]
0.00
0.25
0.50
0.75
1.00
1.25
1.50
1.75
2.00
λ_n [-]

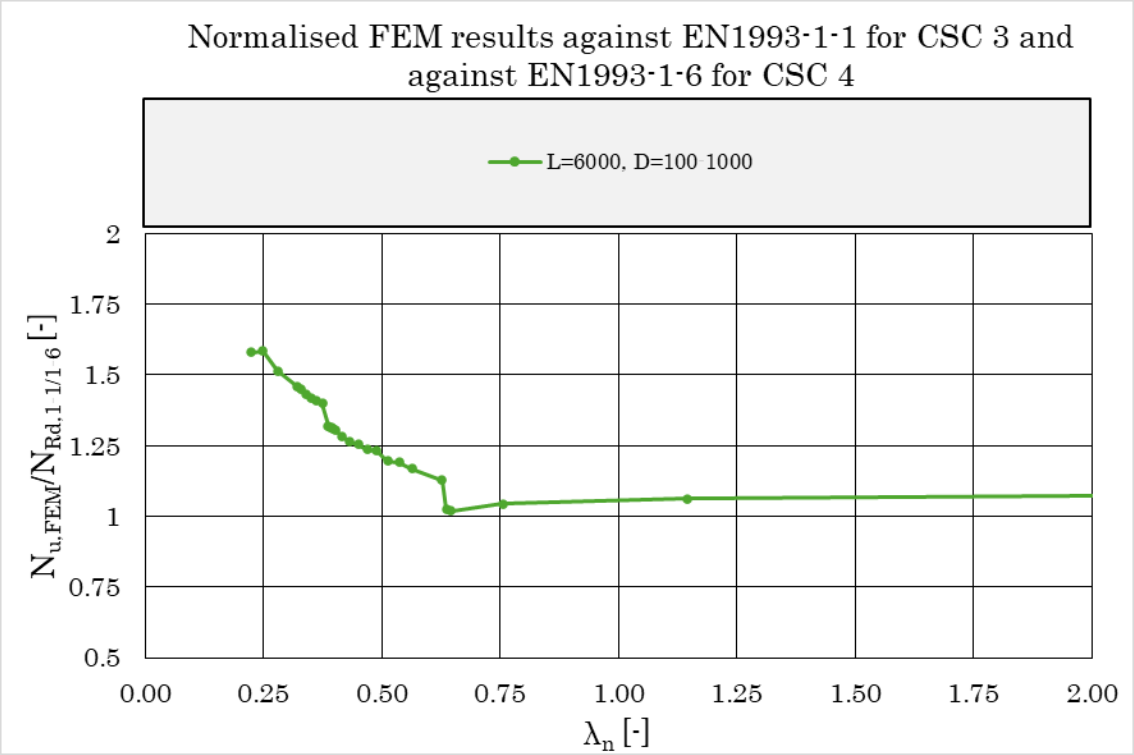
Normalised FEM results against EN1993-1-1 for CSC 3 and against EN1993-1-6 for CSC 4
L=6000, D=100 1000
2
1.75
1.5
1.25
1
0.75
0.5
$N_{u,FEM}/N_{Rd,1\ 1/1\ 6}$ [-]
0.00
0.25
0.50
0.75
1.00
1.25
1.50
1.75
2.00
λ_n [-]

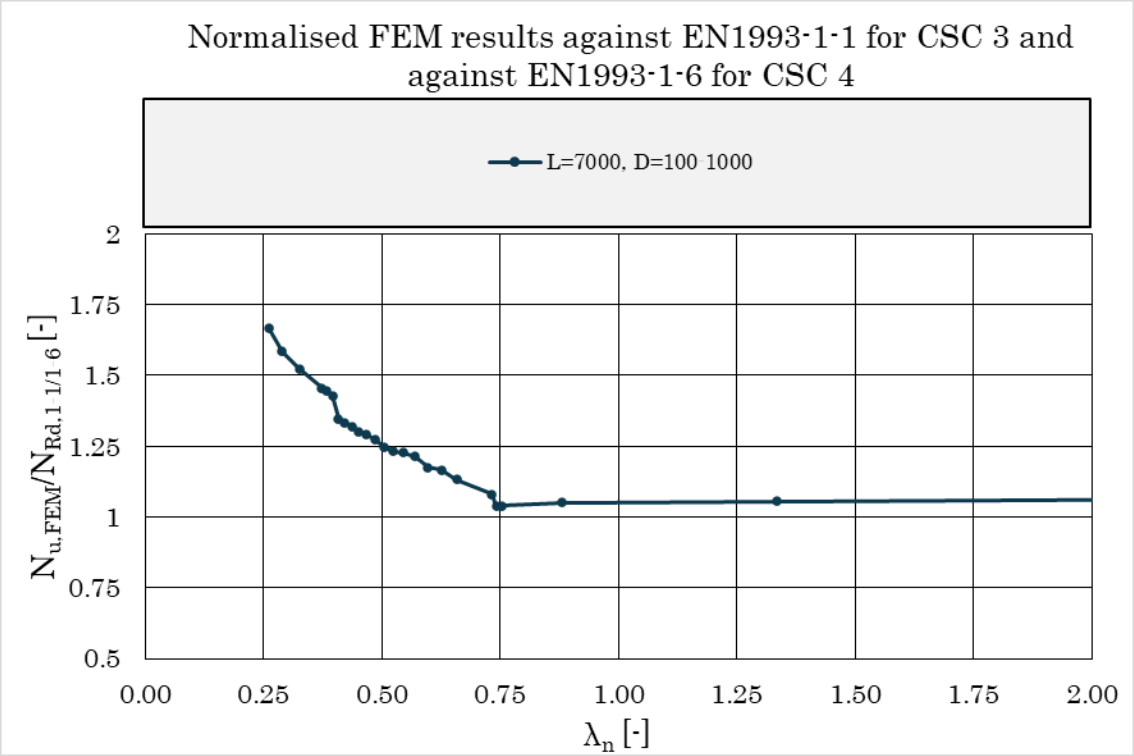
Normalised FEM results against EN1993-1-1 for CSC 3 and against EN1993-1-6 for CSC 4
L=7000, D=100 1000
$N_{u,FEM}/N_{Rd,1\ 1/1\ 6}$ [-]
2
1.75
1.5
1.25
1
0.75
0.5
0.00
0.25
0.50
0.75
1.00
1.25
1.50
1.75
2.00
λ_n [-]

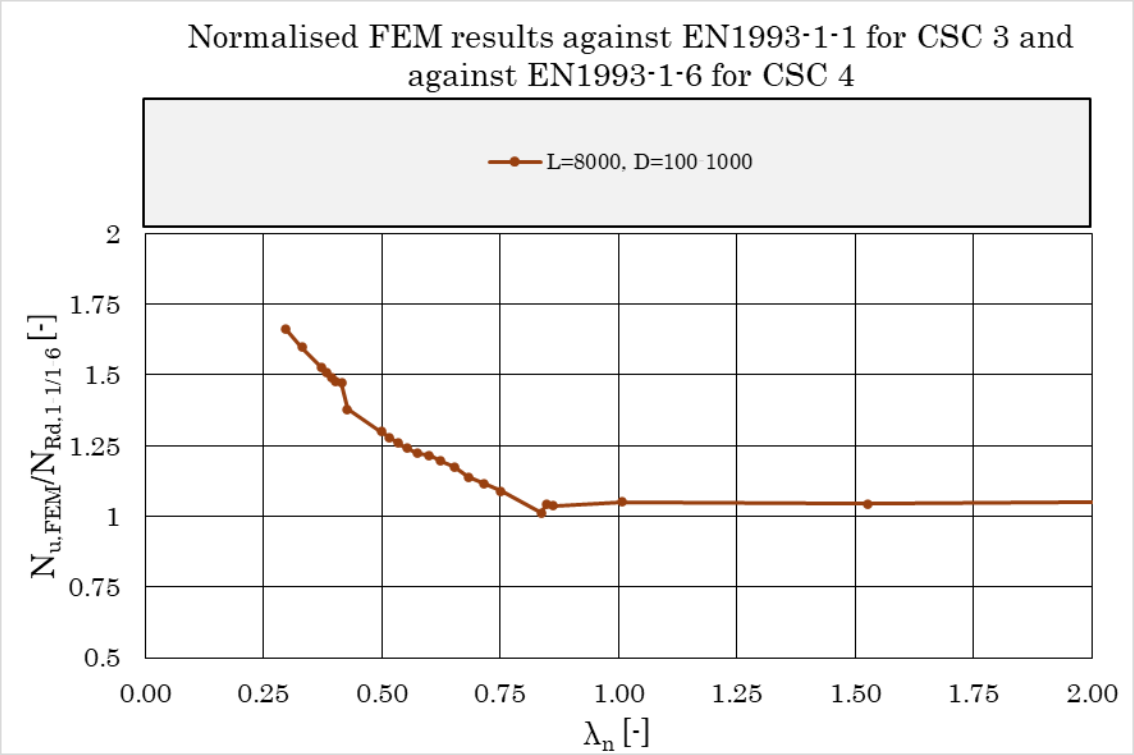
Normalised FEM results against EN1993-1-1 for CSC 3 and against EN1993-1-6 for CSC 4
L=8000, D=100 1000
$N_{u,FEM}/N_{Rd,1\ 1/1\ 6}$ [-]
2
1.75
1.5
1.25
1
0.75
0.5
0.00
0.25
0.50
0.75
1.00
1.25
1.50
1.75
2.00
λ_n [-]

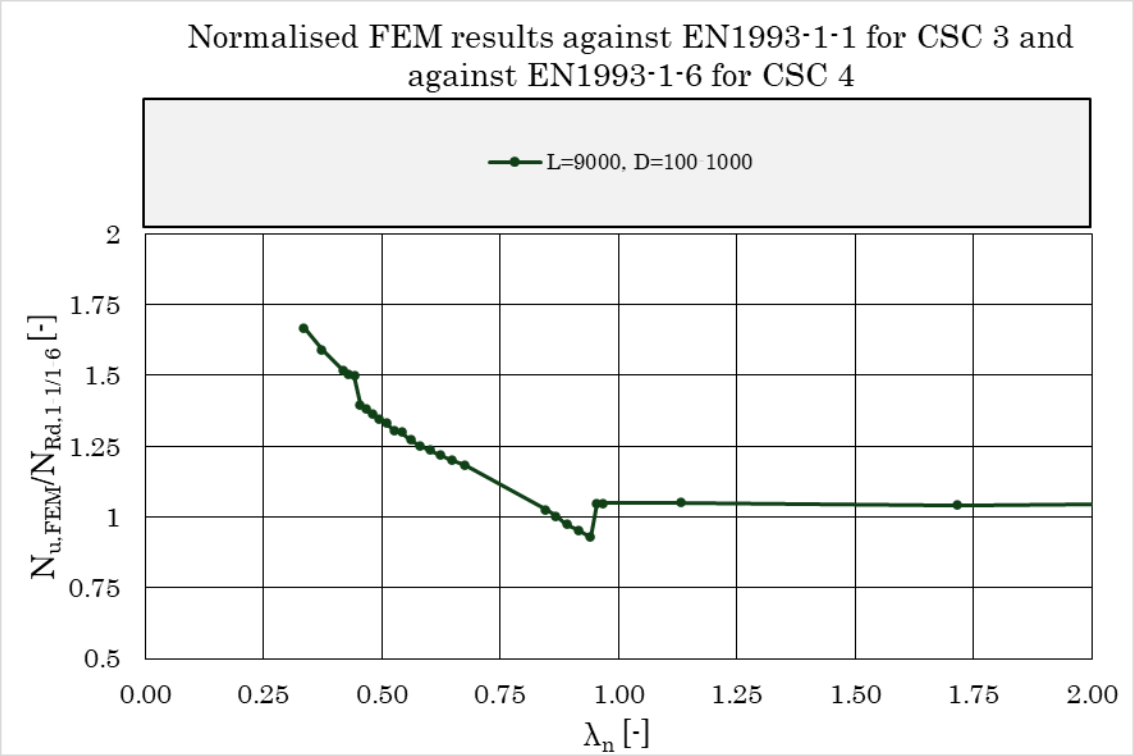
Normalised FEM results against EN1993-1-1 for CSC 3 and against EN1993-1-6 for CSC 4
L=9000, D=100 1000
$N_{u,FEM}/N_{Rd,1\ 1/1\ 6}$ [-]
2
1.75
1.5
1.25
1
0.75
0.5
0.00
0.25
0.50
0.75
1.00
1.25
1.50
1.75
2.00
λ_n [-]

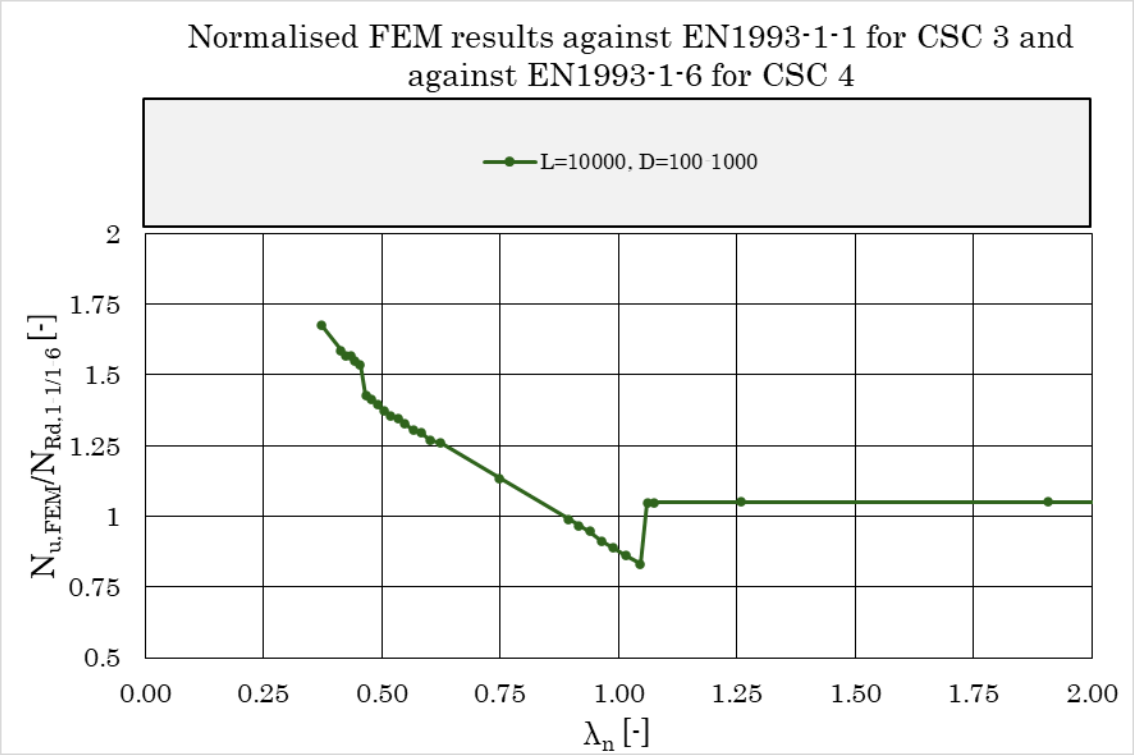
Normalised FEM results against EN1993-1-1 for CSC 3 and against EN1993-1-6 for CSC 4
L=10000, D=100 1000
$N_{u,FEM}/N_{Rd,1\ 1/1\ 6}$ [-]
2
1.75
1.5
1.25
1
0.75
0.5
0.00
0.25
0.50
0.75
1.00
1.25
1.50
1.75
2.00
λ_n [-]

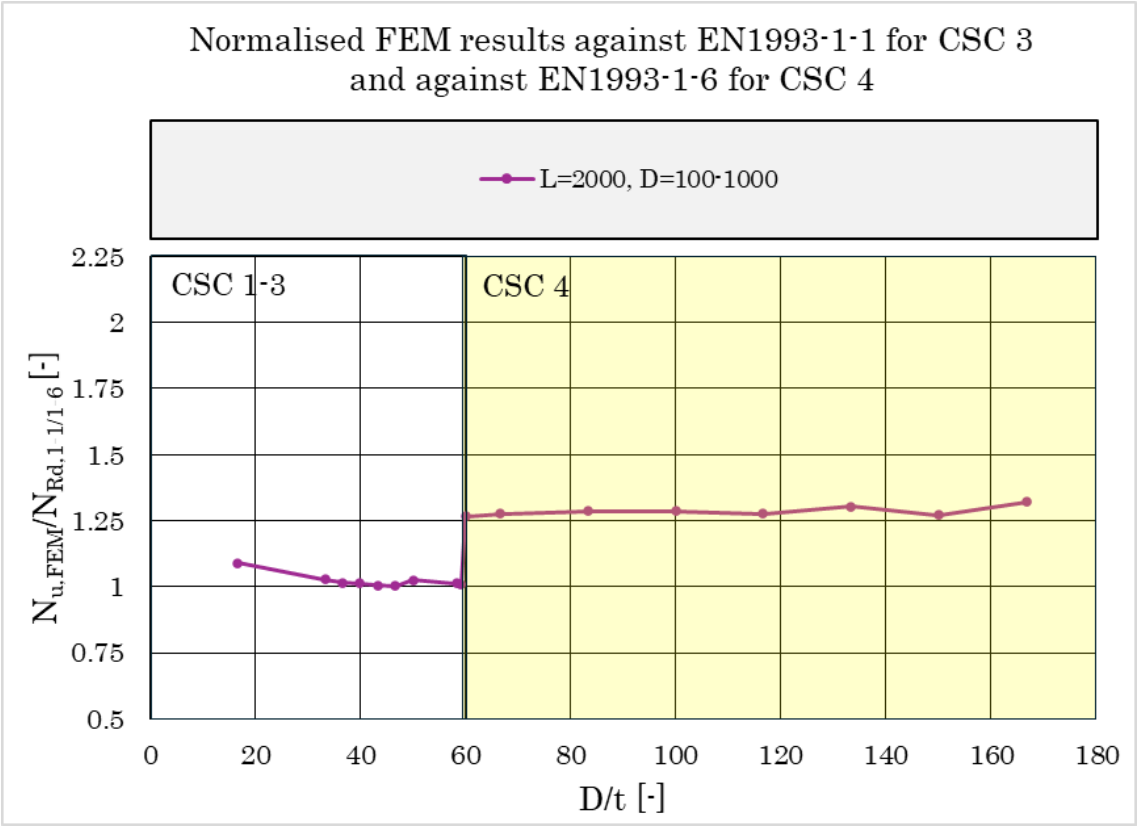
Normalised FEM results against EN1993-1-1 for CSC 3 and against EN1993-1-6 for CSC 4
L=2000, D=100-1000
CSC 1-3
CSC 4
2.25
2
1.75
1.5
1.25
1
0.75
0.5
$N_{u,FEM}/N_{Rd,1\ 1/1\ 6}$ [-]
0
20
40
60
80
100
120
140
160
180
D/t [-]

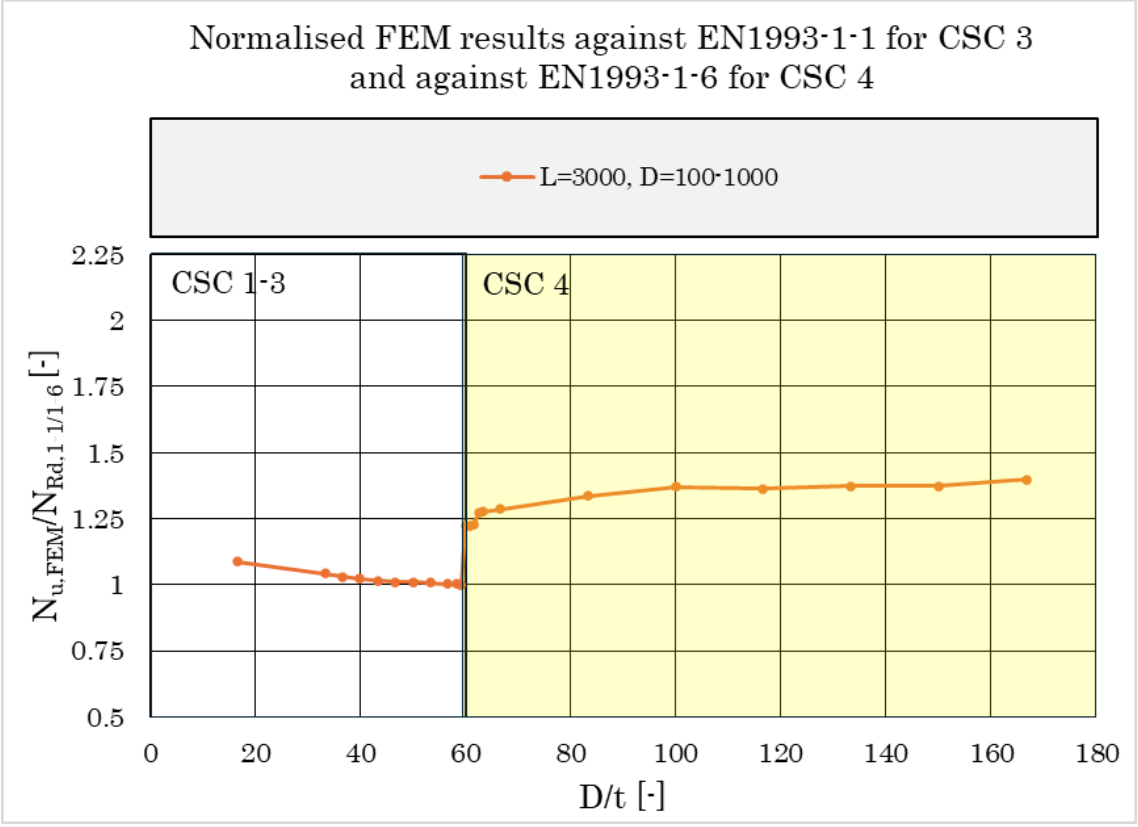
Normalised FEM results against EN1993-1-1 for CSC 3 and against EN1993-1-6 for CSC 4
L=3000, D=100-1000
CSC 1-3
CSC 4
2.25
2
1.75
1.5
1.25
1
0.75
0.5
$N_{u,FEM}/N_{Rd,1\ 1/1\ 6}$ [-]
0
20
40
60
80
100
120
140
160
180
D/t [-]

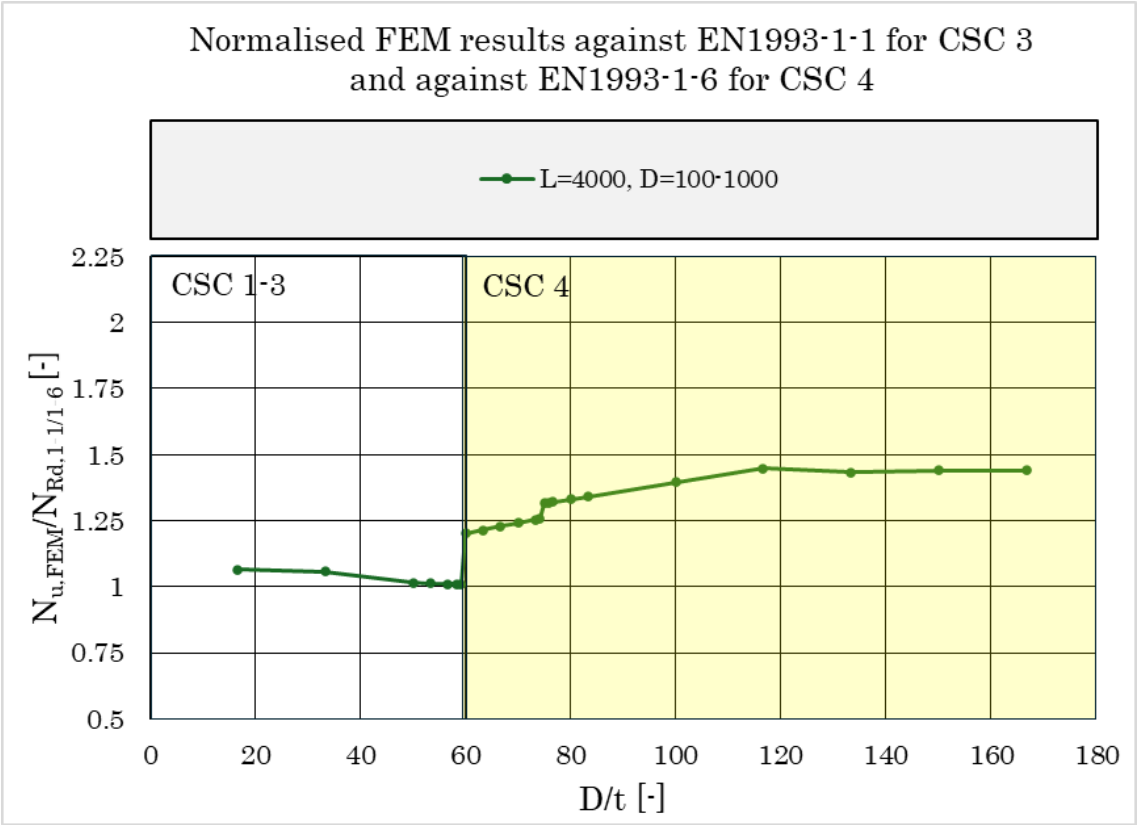
Normalised FEM results against EN1993-1-1 for CSC 3 and against EN1993-1-6 for CSC 4
L=4000, D=100-1000
CSC 1-3
CSC 4
$N_{u,FEM}/N_{Rd,1\ 1/1\ 6}$ [-]
2.25
2
1.75
1.5
1.25
1
0.75
0.5
0
20
40
60
80
100
120
140
160
180
D/t [-]

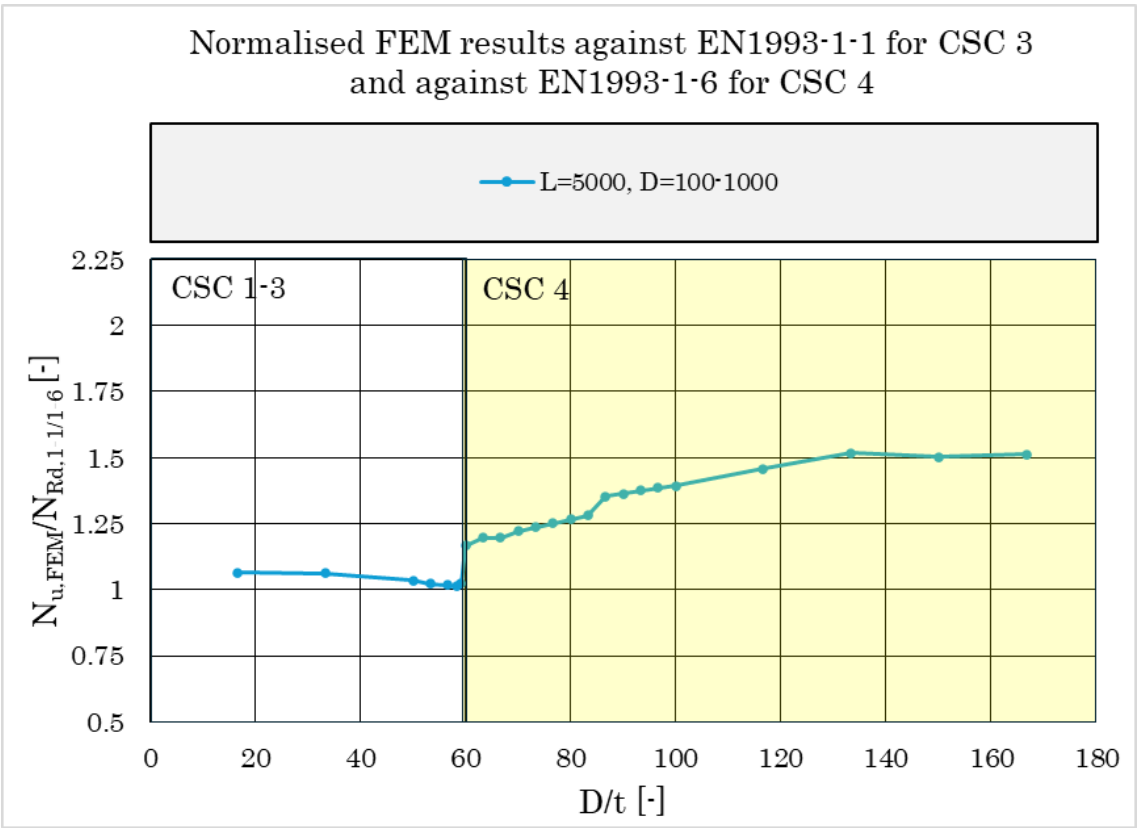
Normalised FEM results against EN1993-1-1 for CSC 3 and against EN1993-1-6 for CSC 4
L=5000, D=100-1000
CSC 1-3
CSC 4
$N_{u,FEM}/N_{Rd,1\ 1/1\ 6}$ [-]
2.25
2
1.75
1.5
1.25
1
0.75
0.5
0
20
40
60
80
100
120
140
160
180
D/t [-]

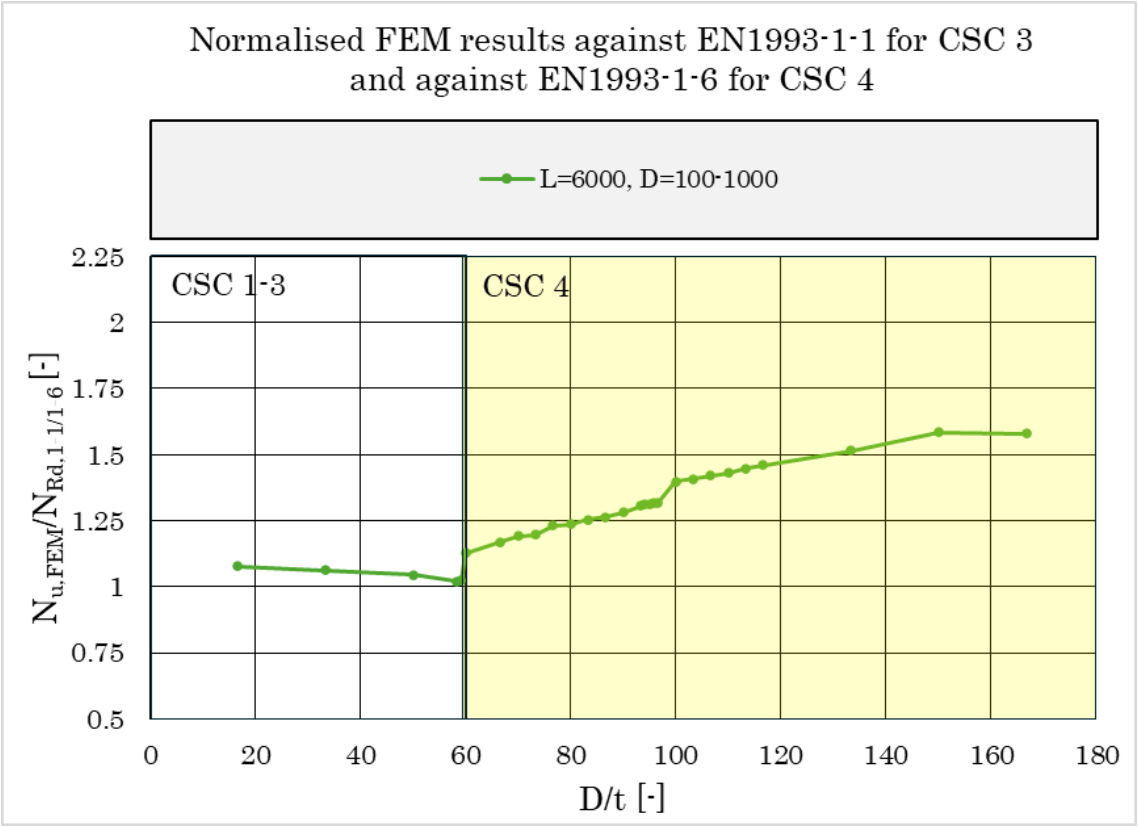
Normalised FEM results against EN1993-1-1 for CSC 3 and against EN1993-1-6 for CSC 4
L=6000, D=100-1000
CSC 1-3
CSC 4
$N_{u,FEM}/N_{Rd,1\ 1/1\ 6}$ [-]
2.25
2
1.75
1.5
1.25
1
0.75
0.5
0
20
40
60
80
100
120
140
160
180
D/t [-]

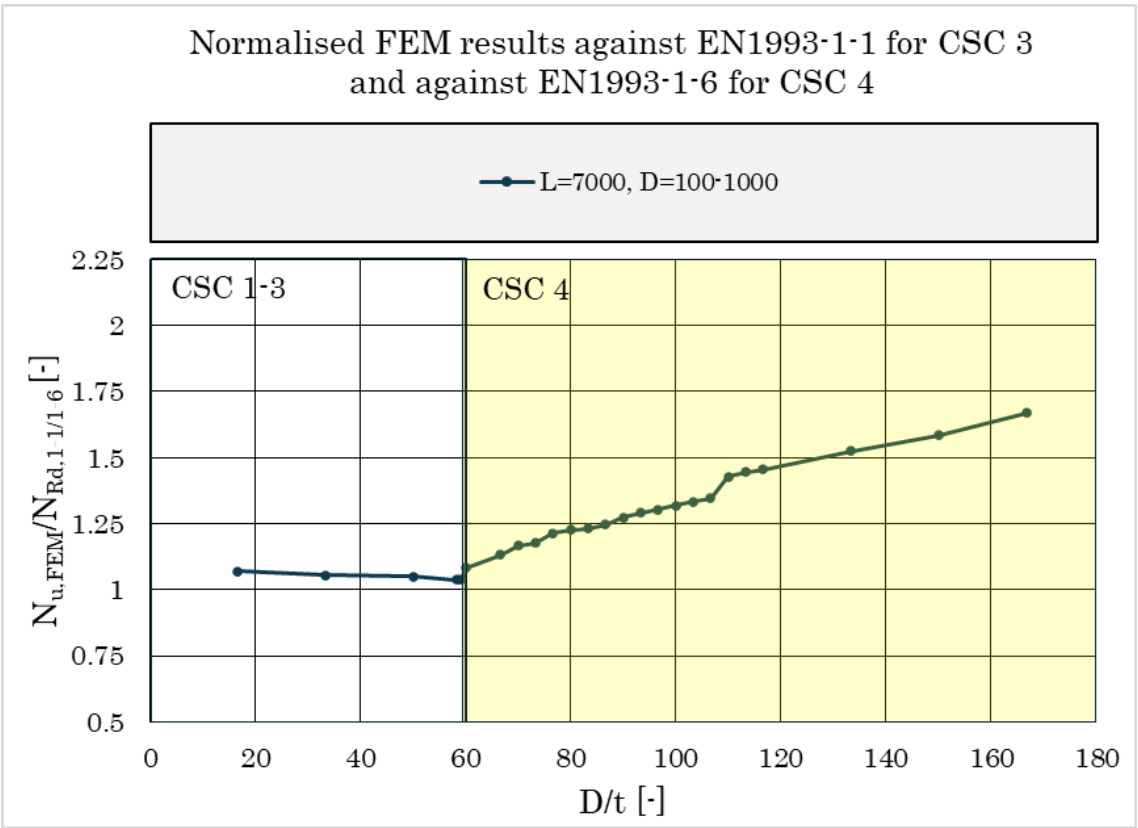
Normalised FEM results against EN1993-1-1 for CSC 3 and against EN1993-1-6 for CSC 4
L=7000, D=100-1000
CSC 1-3
CSC 4
$N_{u,FEM}/N_{Rd,1\ 1/1\ 6}$ [-]
2.25
2
1.75
1.5
1.25
1
0.75
0.5
0
20
40
60
80
100
120
140
160
180
D/t [-]

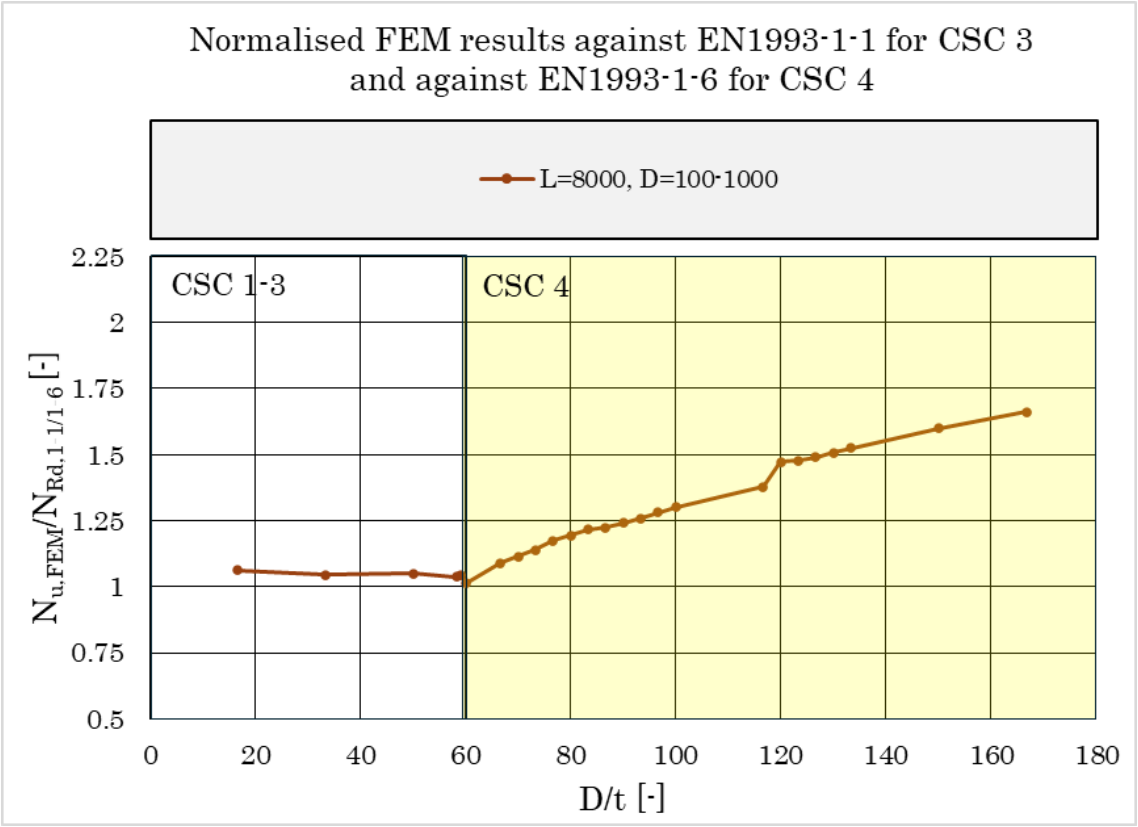
Normalised FEM results against EN1993-1-1 for CSC 3 and against EN1993-1-6 for CSC 4
L=8000, D=100-1000
CSC 1-3
CSC 4
$N_{u,FEM}/N_{Rd,1\ 1/1\ 6}$ [-]
2.25
2
1.75
1.5
1.25
1
0.75
0.5
0
20
40
60
80
100
120
140
160
180
D/t [-]

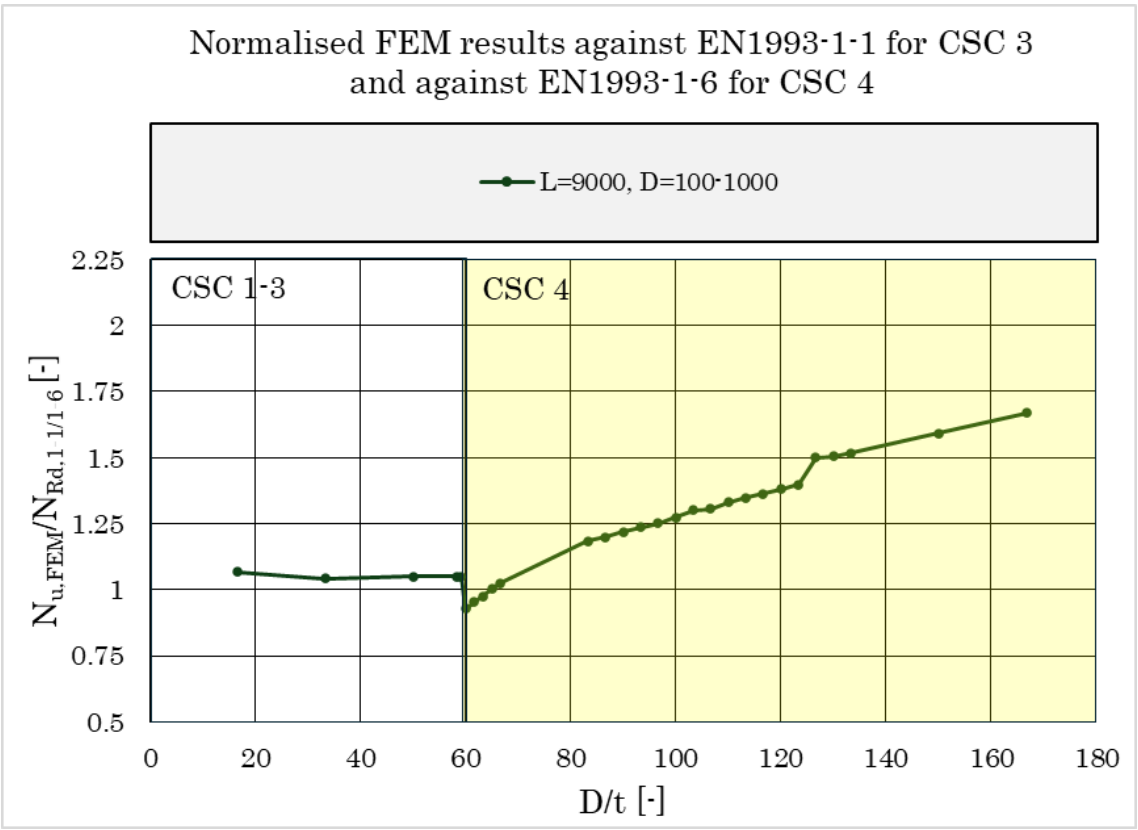
Normalised FEM results against EN1993-1-1 for CSC 3 and against EN1993-1-6 for CSC 4
L=9000, D=100-1000
CSC 1-3
CSC 4
$N_{u,FEM}/N_{Rd,1\ 1/1\ 6}$ [-]
2.25
2
1.75
1.5
1.25
1
0.75
0.5
0
20
40
60
80
100
120
140
160
180
D/t [-]

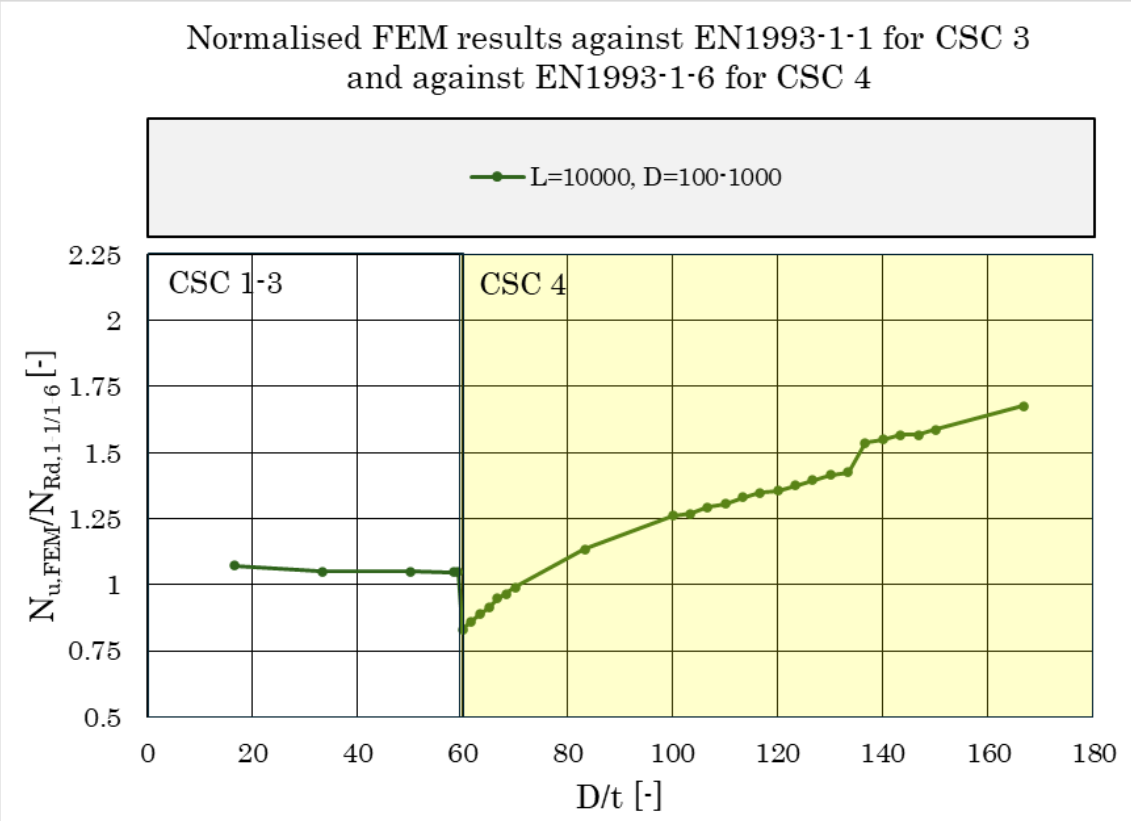
Normalised FEM results against EN1993-1-1 for CSC 3 and against EN1993-1-6 for CSC 4
L=10000, D=100-1000
CSC 1-3
CSC 4
$N_{u,FEM}/N_{Rd,1\ 1/1\ 6}$ [-]
2.25
2
1.75
1.5
1.25
1
0.75
0.5
0
20
40
60
80
100
120
140
160
180
D/t [-]

E

Normalised FEM results against EN1993-1-1 for CSC 3 and against BS5950-1 for CSC 4

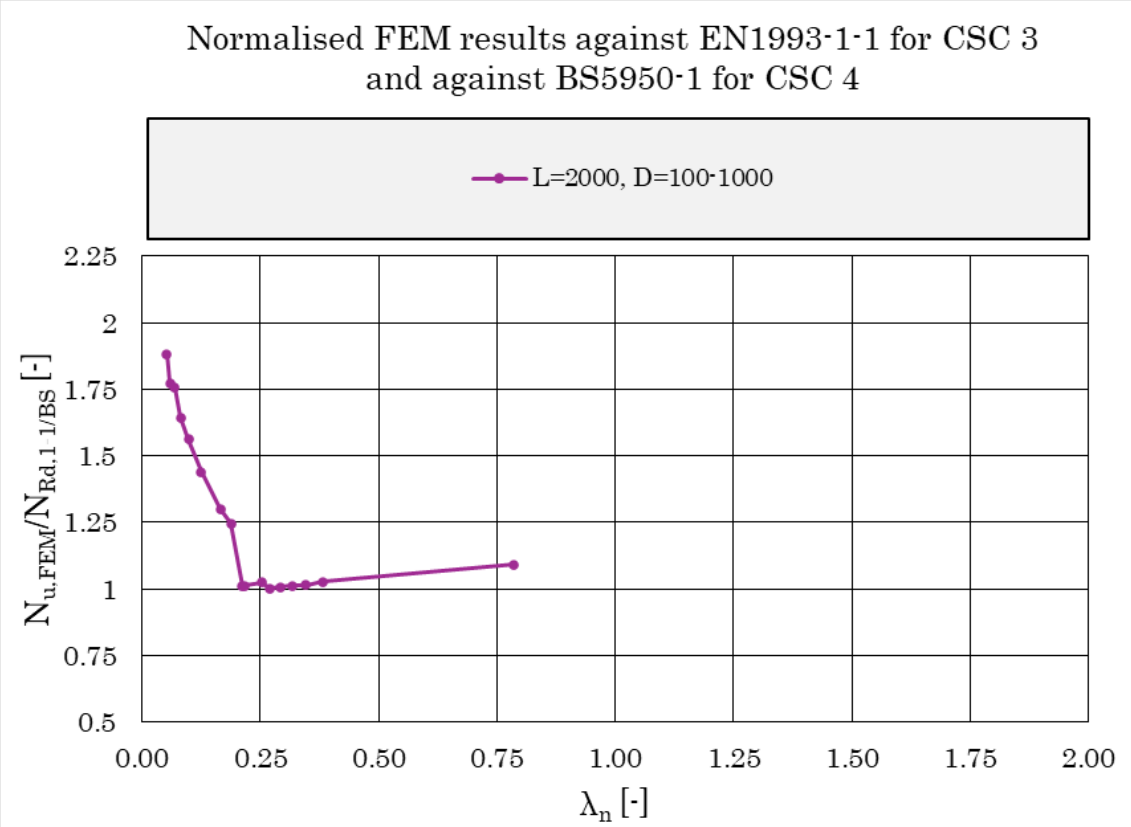

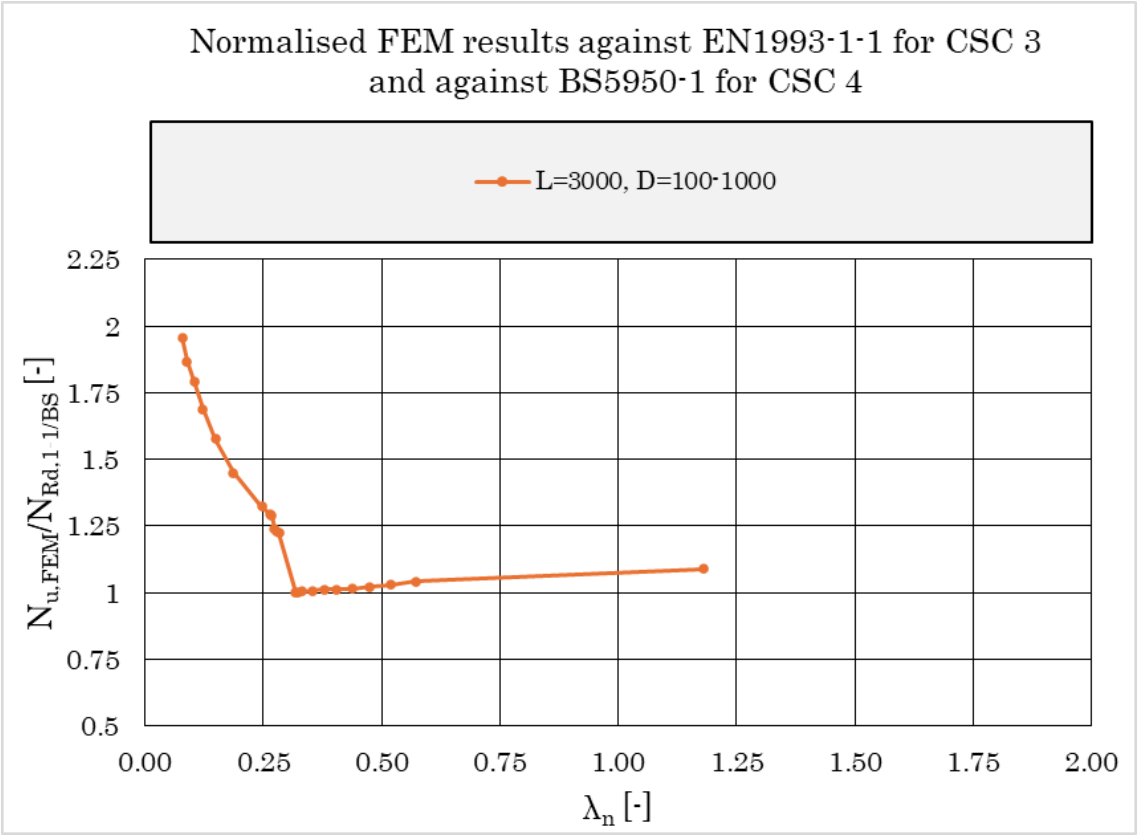
Normalised FEM results against EN1993-1-1 for CSC 3 and against BS5950-1 for CSC 4
L=3000, D=100-1000
2.25
2
1.75
1.5
1.25
1
0.75
0.5
0.00
0.25
0.50
0.75
1.00
1.25
1.50
1.75
2.00
$N_{u,FEM}/N_{Rd,1-1/BS}$ [-]
λ_n [-]

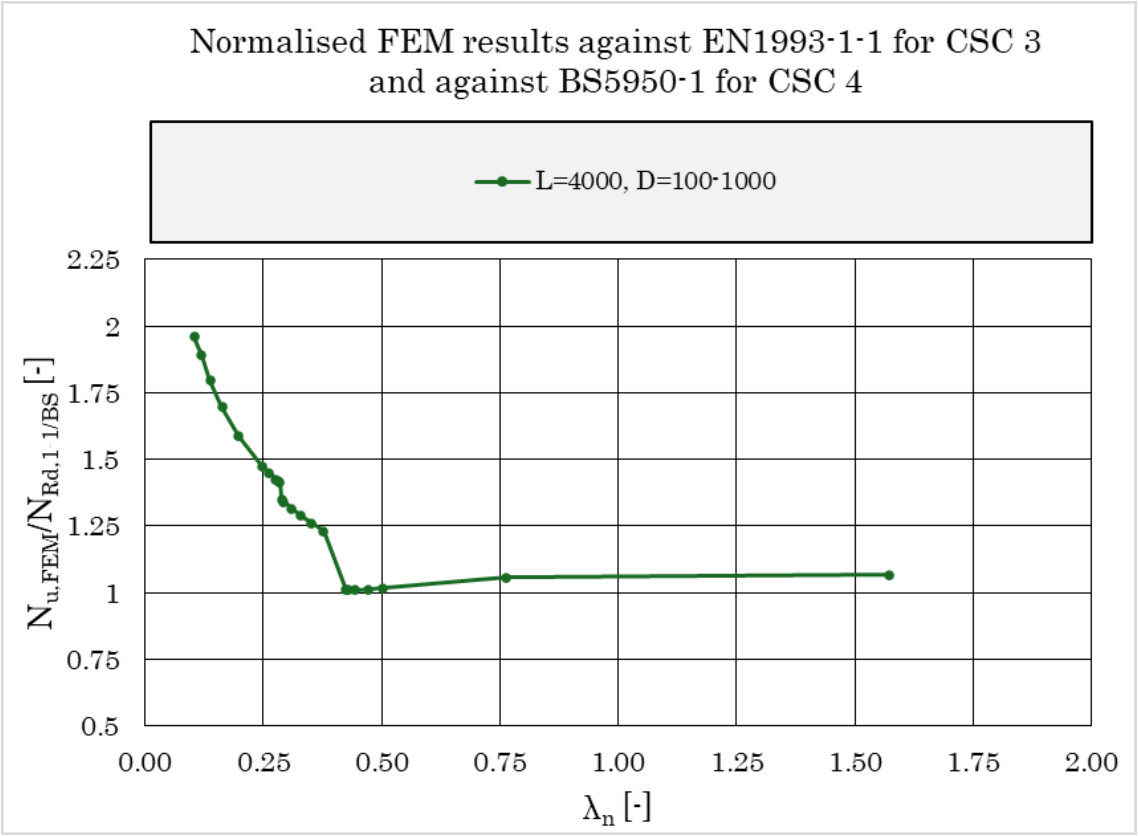
Normalised FEM results against EN1993-1-1 for CSC 3 and against BS5950-1 for CSC 4
L=4000, D=100-1000
2.25
2
1.75
1.5
1.25
1
0.75
0.5
0.00
0.25
0.50
0.75
1.00
1.25
1.50
1.75
2.00
$N_{u,FEM}/N_{Rd,1-1/BS}$ [-]
λ_n [-]

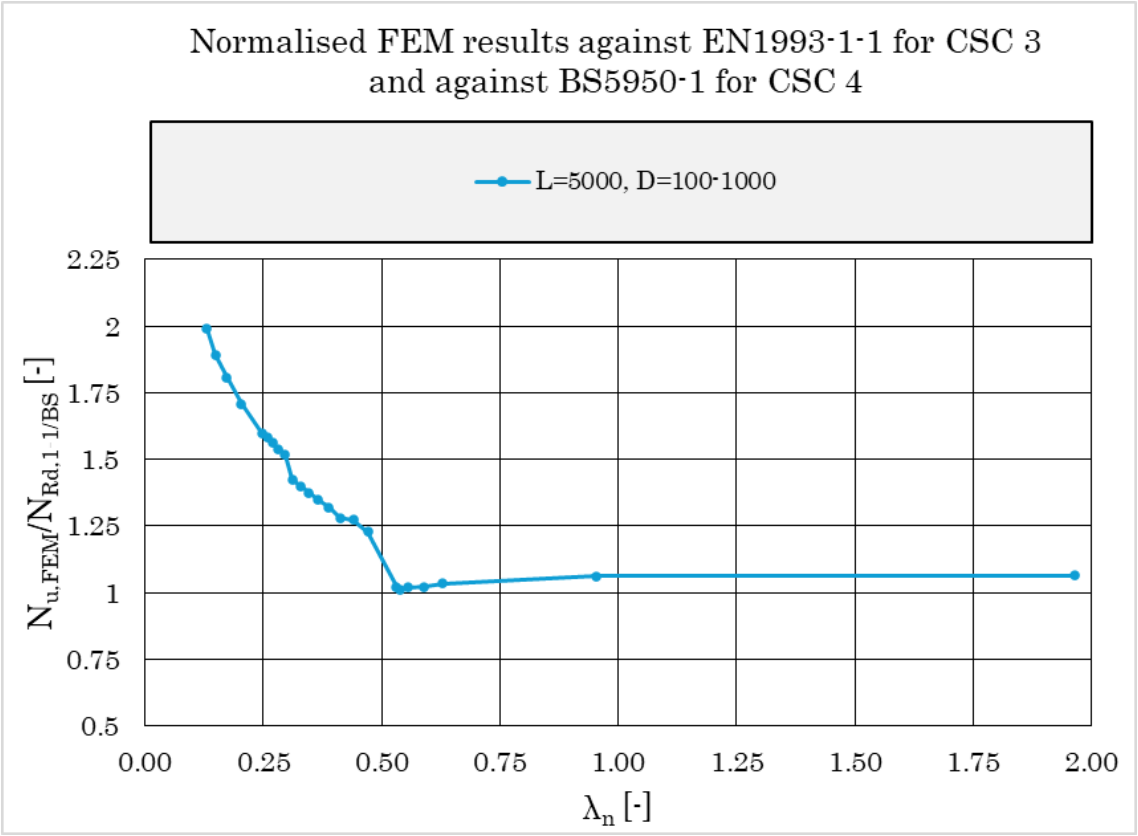
Normalised FEM results against EN1993-1-1 for CSC 3 and against BS5950-1 for CSC 4
L=5000, D=100-1000
2.25
2
1.75
1.5
1.25
1
0.75
0.5
$N_{u,FEM}/N_{Rd,1-1/BS}$ [-]
0.00
0.25
0.50
0.75
1.00
1.25
1.50
1.75
2.00
λ_n [-]

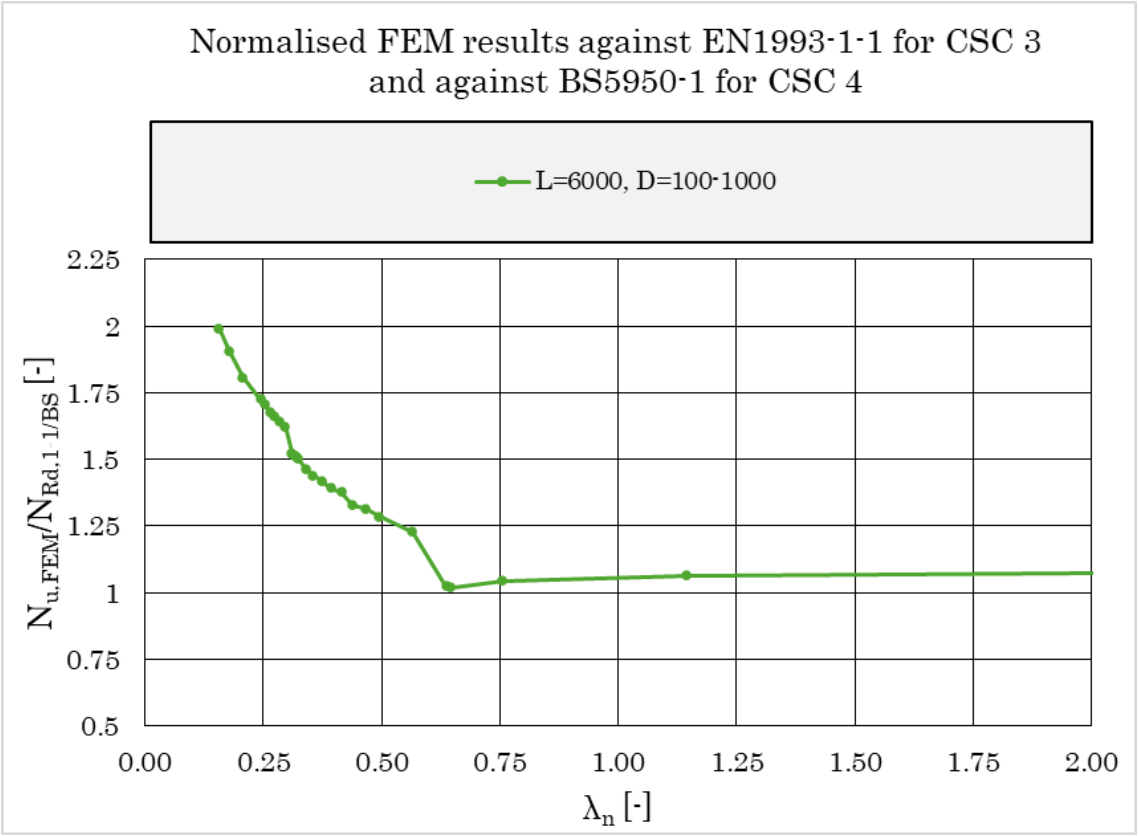
Normalised FEM results against EN1993-1-1 for CSC 3 and against BS5950-1 for CSC 4
L=6000, D=100-1000
2.25
2
1.75
1.5
1.25
1
0.75
0.5
$N_{u,FEM}/N_{Rd,1-1/BS}$ [-]
0.00
0.25
0.50
0.75
1.00
1.25
1.50
1.75
2.00
λ_n [-]

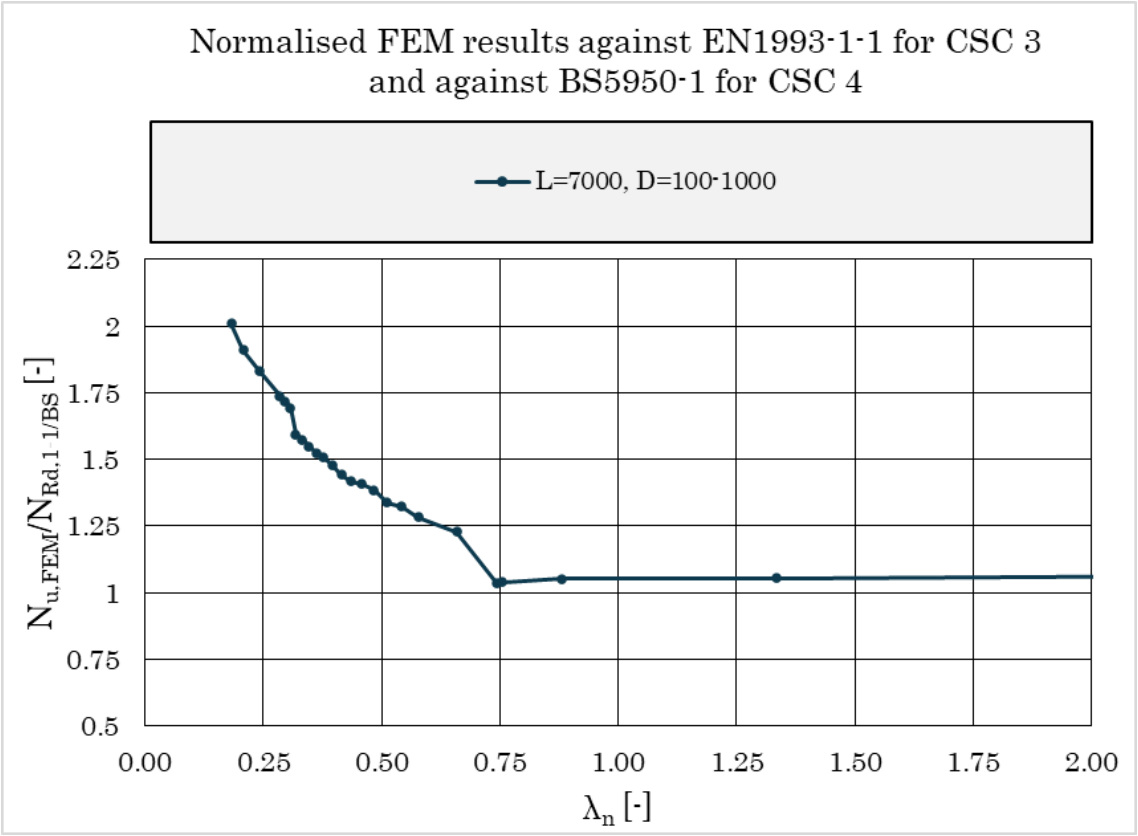
Normalised FEM results against EN1993-1-1 for CSC 3 and against BS5950-1 for CSC 4
L=7000, D=100-1000
$N_{u,FEM}/N_{Rd,1-1/BS}$ [-]
2.25
2
1.75
1.5
1.25
1
0.75
0.5
0.00
0.25
0.50
0.75
1.00
1.25
1.50
1.75
2.00
λ_n [-]

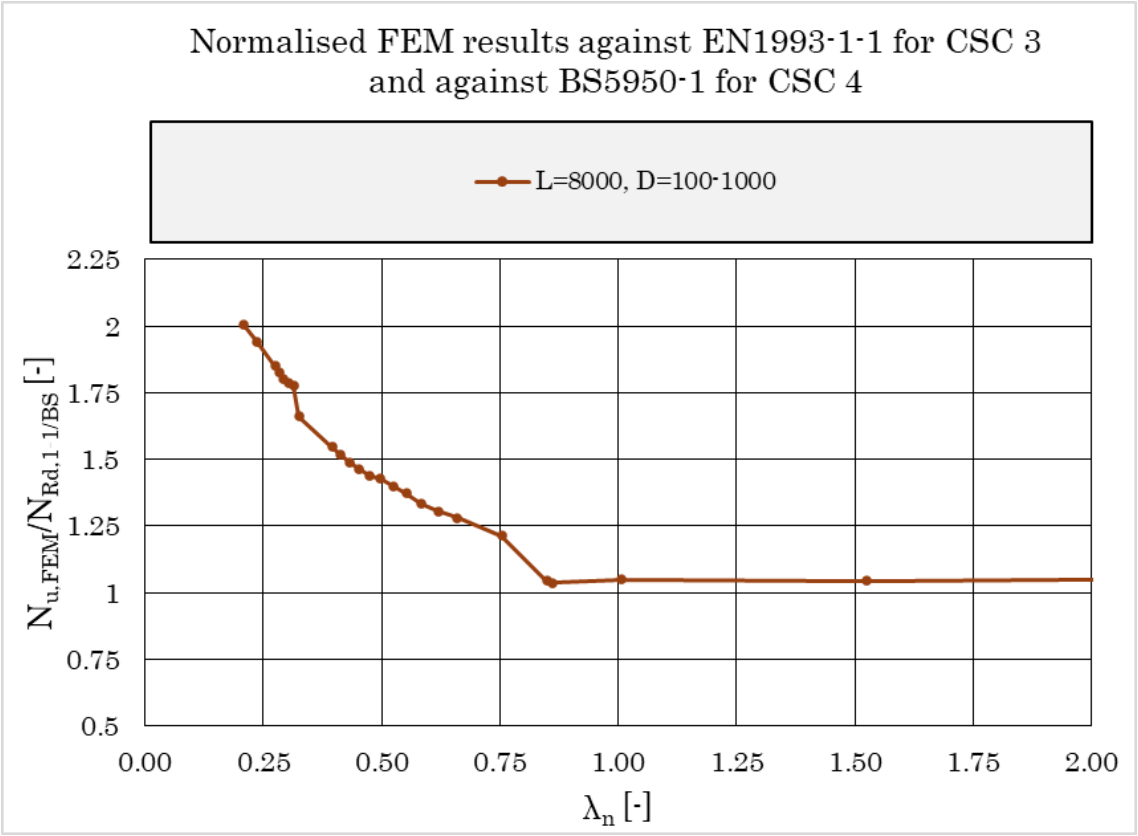
Normalised FEM results against EN1993-1-1 for CSC 3 and against BS5950-1 for CSC 4
L=8000, D=100-1000
$N_{u,FEM}/N_{Rd,1-1/BS}$ [-]
2.25
2
1.75
1.5
1.25
1
0.75
0.5
0.00
0.25
0.50
0.75
1.00
1.25
1.50
1.75
2.00
λ_n [-]

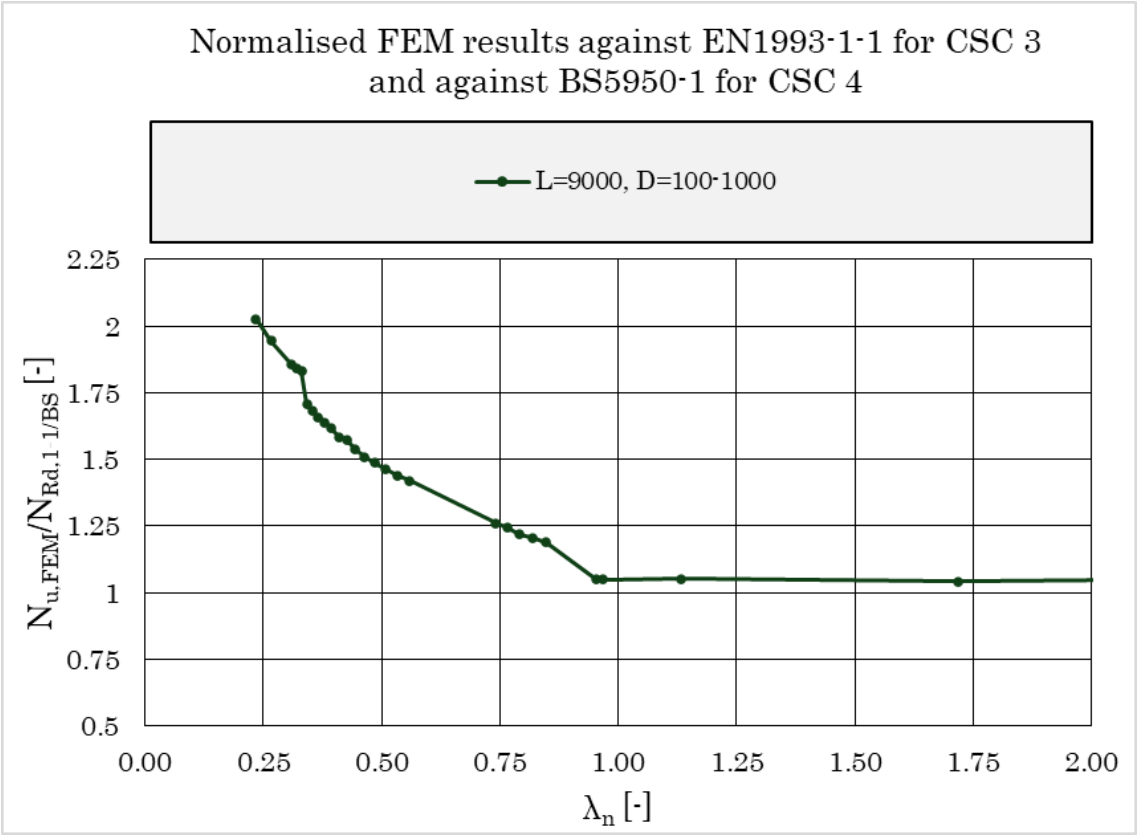
Normalised FEM results against EN1993-1-1 for CSC 3 and against BS5950-1 for CSC 4
L=9000, D=100-1000
$N_{u,FEM}/N_{Rd,1-1/BS}$ [-]
2.25
2
1.75
1.5
1.25
1
0.75
0.5
0.00
0.25
0.50
0.75
1.00
1.25
1.50
1.75
2.00
λ_n [-]

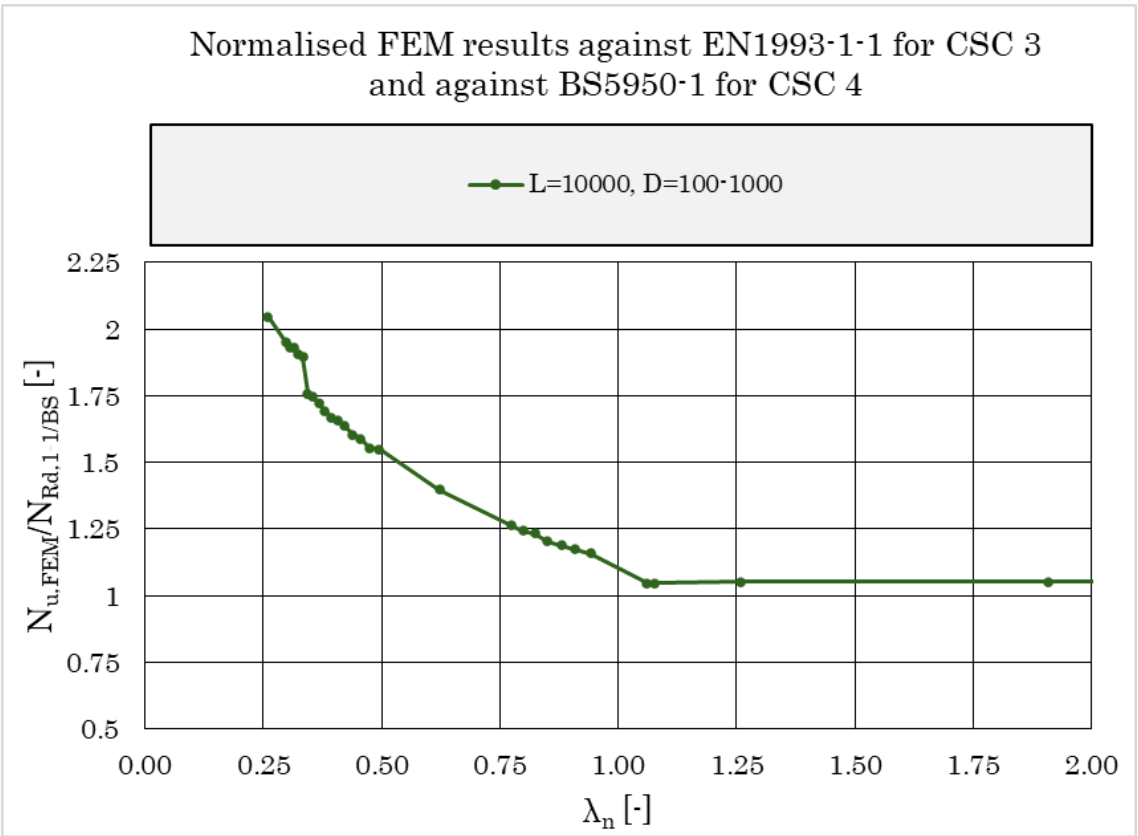
Normalised FEM results against EN1993-1-1 for CSC 3 and against BS5950-1 for CSC 4
L=10000, D=100-1000
$N_{u,FEM}/N_{Rd,1-1/BS}$ [-]
2.25
2
1.75
1.5
1.25
1
0.75
0.5
0.00
0.25
0.50
0.75
1.00
1.25
1.50
1.75
2.00
λ_n [-]

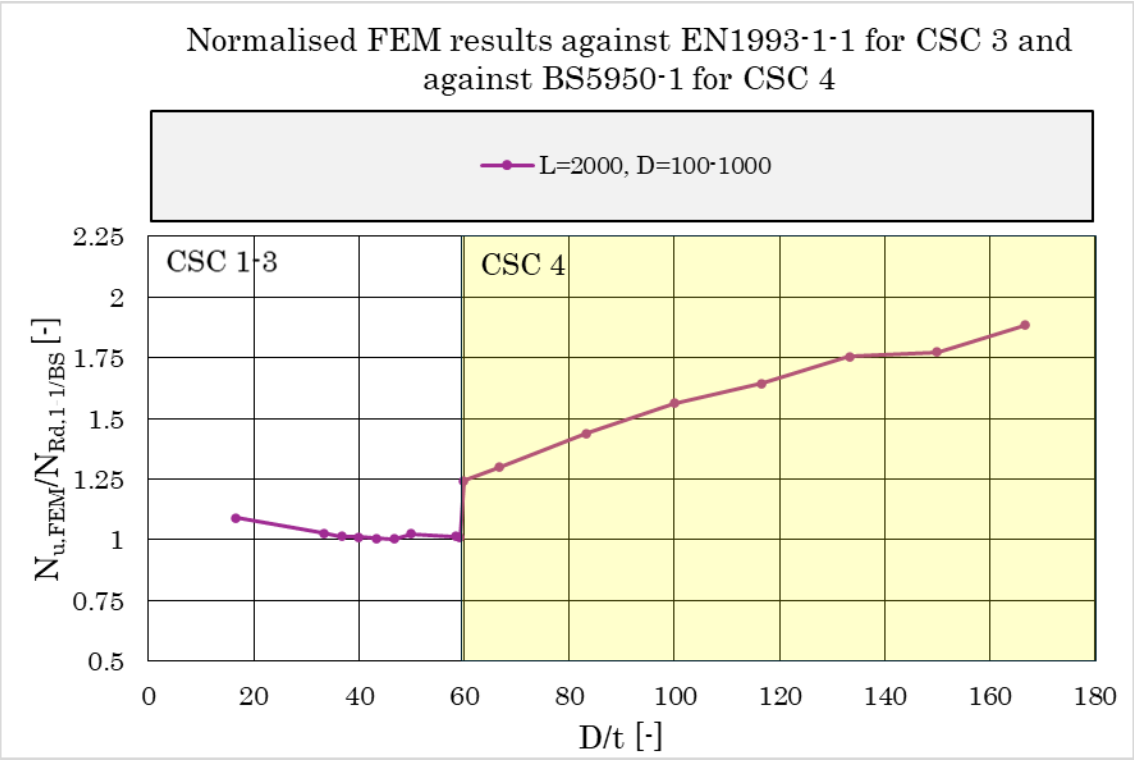
Normalised FEM results against EN1993-1-1 for CSC 3 and against BS5950-1 for CSC 4
L=2000, D=100-1000
CSC 1-3
CSC 4
$N_{u,FEM}/N_{Rd,1\ 1/BS}$ [-]
2.25
2
1.75
1.5
1.25
1
0.75
0.5
0
20
40
60
80
100
120
140
160
180
D/t [-]

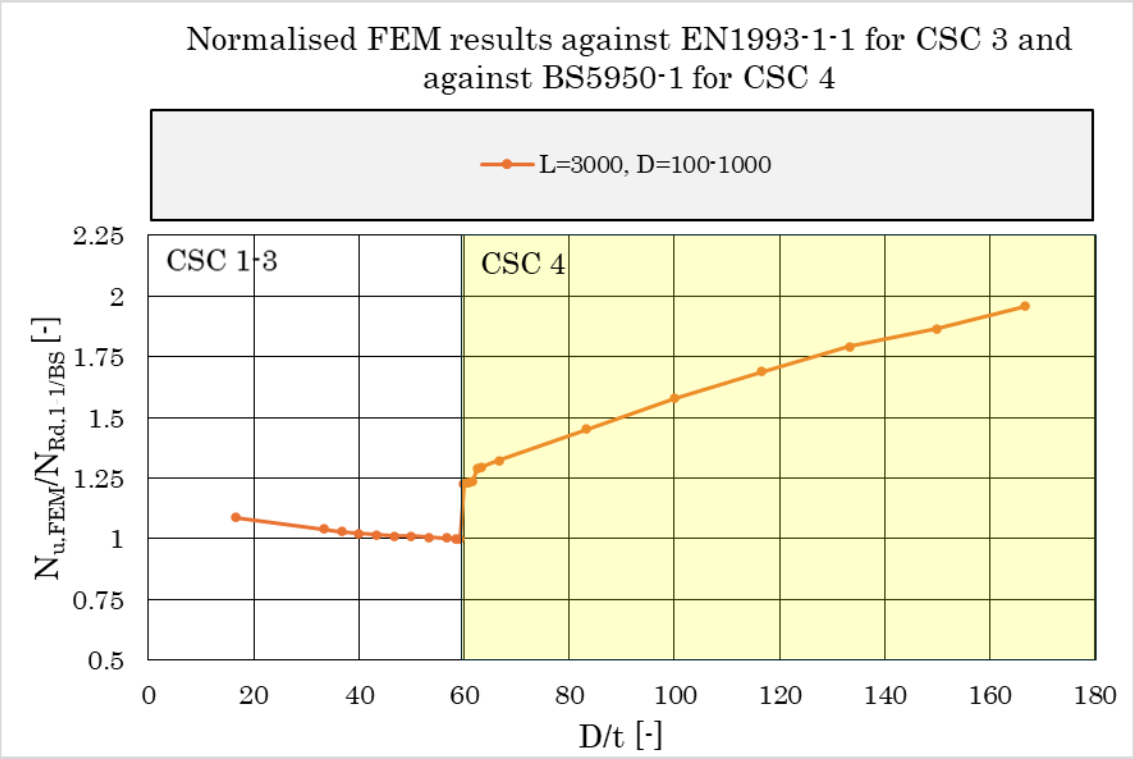
Normalised FEM results against EN1993-1-1 for CSC 3 and against BS5950-1 for CSC 4
L=3000, D=100-1000
CSC 1-3
CSC 4
$N_{u,FEM}/N_{Rd,1\ 1/BS}$ [-]
2.25
2
1.75
1.5
1.25
1
0.75
0.5
0
20
40
60
80
100
120
140
160
180
D/t [-]

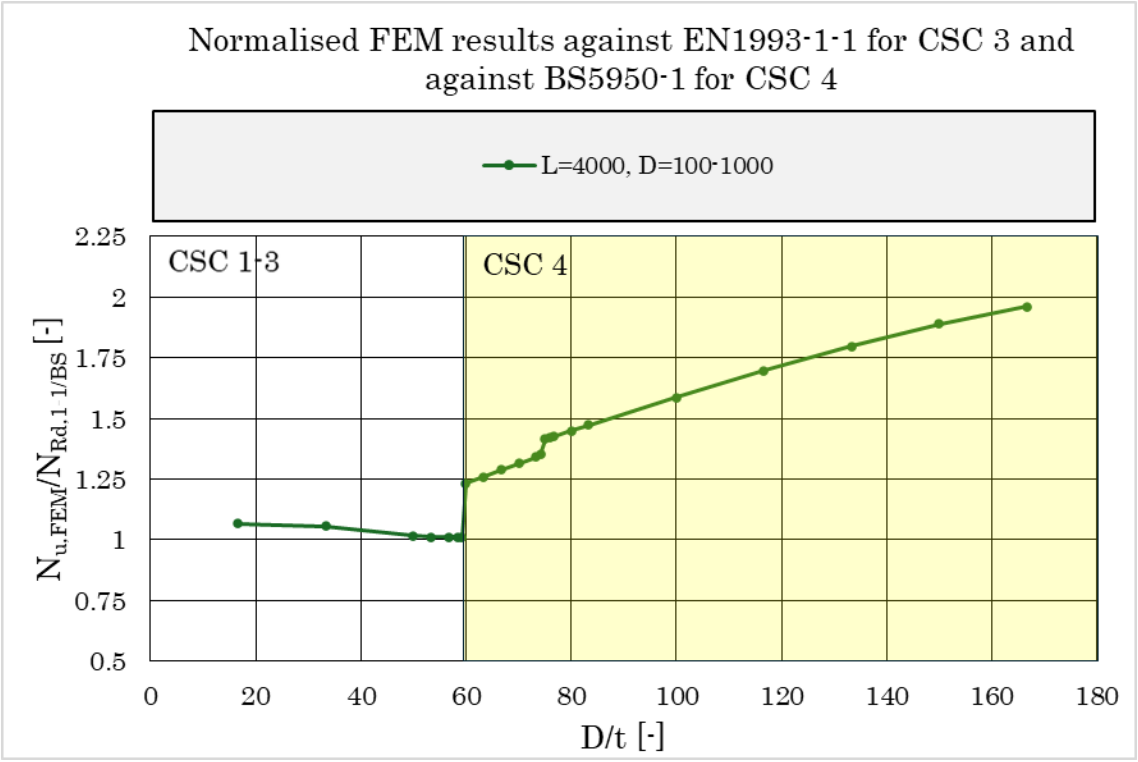
Normalised FEM results against EN1993-1-1 for CSC 3 and against BS5950-1 for CSC 4
L=4000, D=100-1000
CSC 1-3
CSC 4
$N_{u,FEM}/N_{Rd,1\ 1/BS}$ [-]
2.25
2
1.75
1.5
1.25
1
0.75
0.5
0
20
40
60
80
100
120
140
160
180
D/t [-]

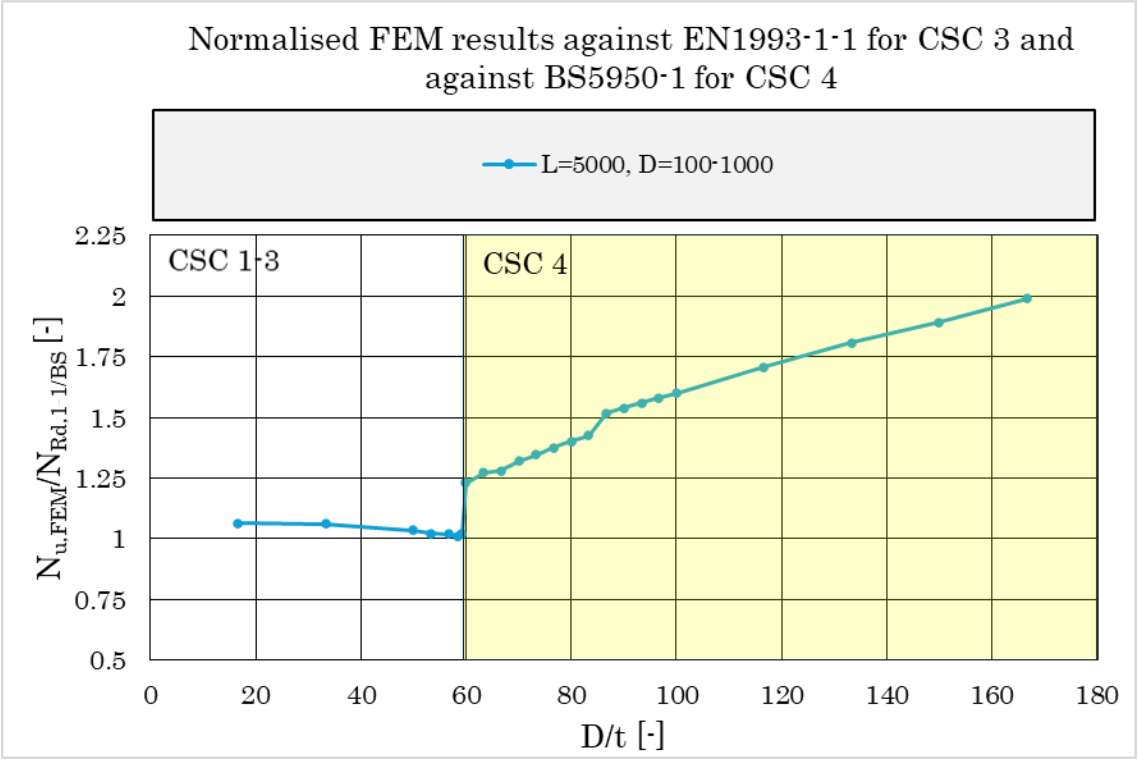
Normalised FEM results against EN1993-1-1 for CSC 3 and against BS5950-1 for CSC 4
L=5000, D=100-1000
CSC 1-3
CSC 4
$N_{u,FEM}/N_{Rd,1\ 1/BS}$ [-]
2.25
2
1.75
1.5
1.25
1
0.75
0.5
0
20
40
60
80
100
120
140
160
180
D/t [-]

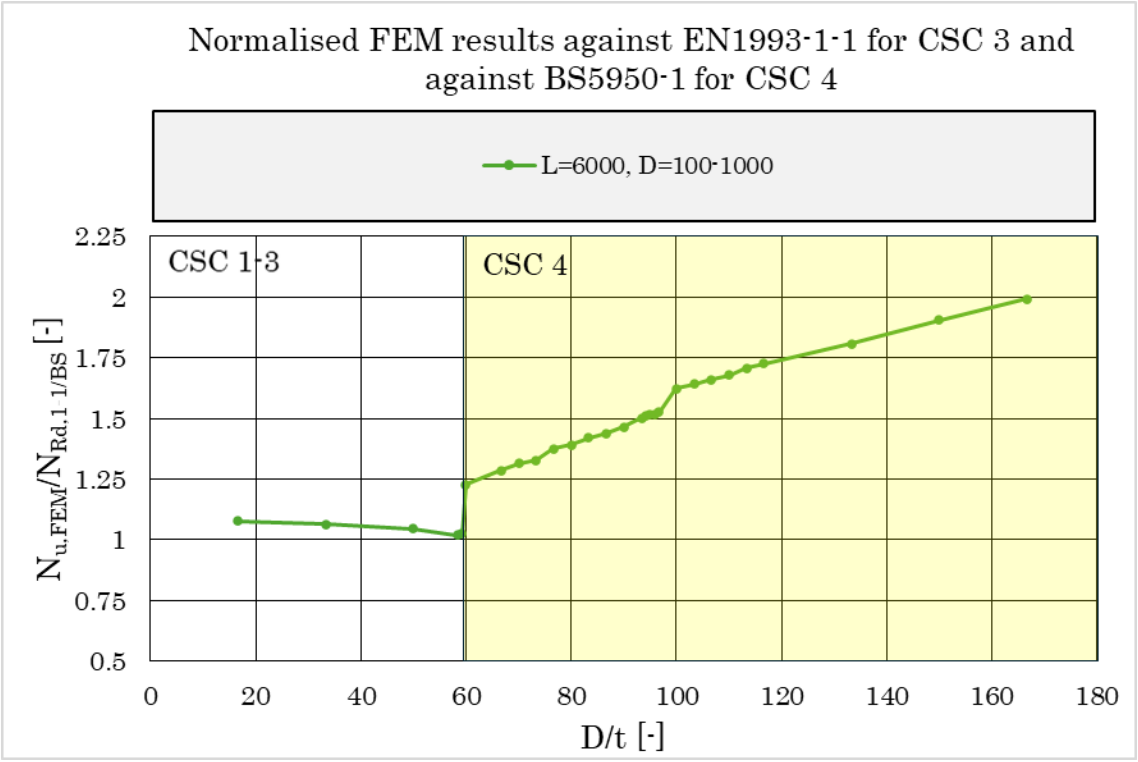
Normalised FEM results against EN1993-1-1 for CSC 3 and against BS5950-1 for CSC 4
L=6000, D=100-1000
CSC 1-3
CSC 4
$N_{u,FEM}/N_{Rd,1\ 1/BS}$ [-]
2.25
2
1.75
1.5
1.25
1
0.75
0.5
0
20
40
60
80
100
120
140
160
180
D/t [-]

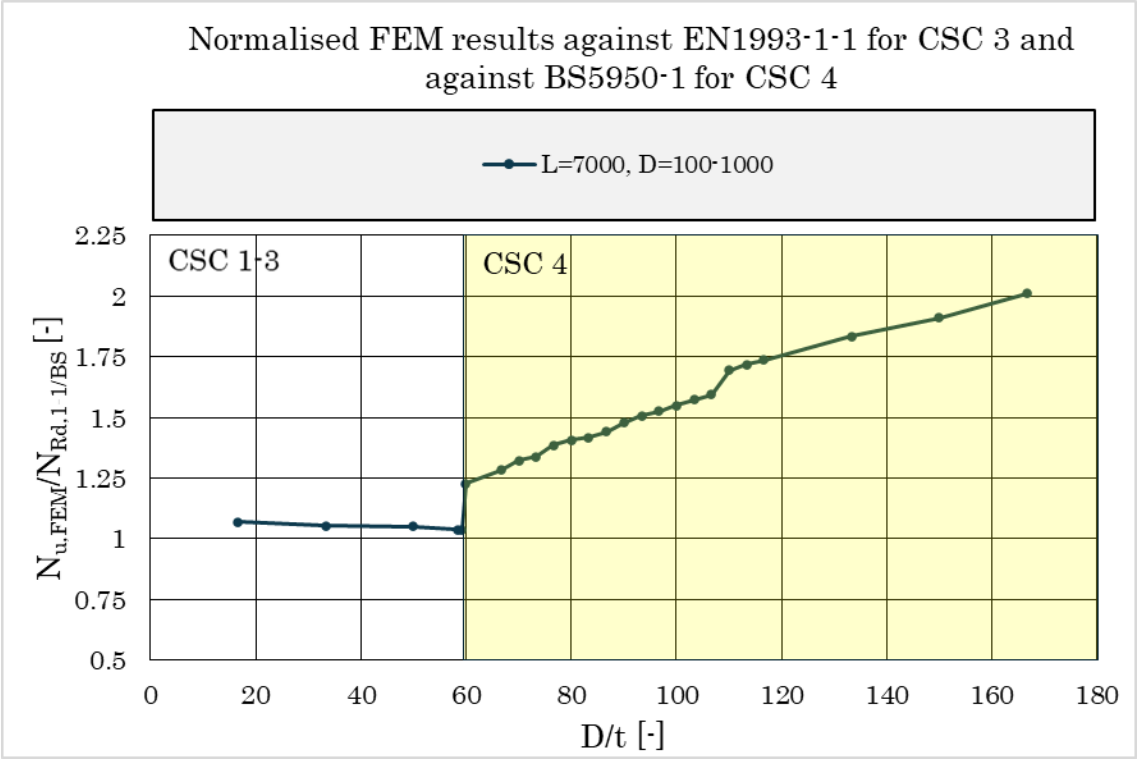
Normalised FEM results against EN1993-1-1 for CSC 3 and against BS5950-1 for CSC 4
L=7000, D=100-1000
CSC 1-3
CSC 4
$N_{u,FEM}/N_{Rd,1\ 1/BS}$ [-]
2.25
2
1.75
1.5
1.25
1
0.75
0.5
0
20
40
60
80
100
120
140
160
180
D/t [-]

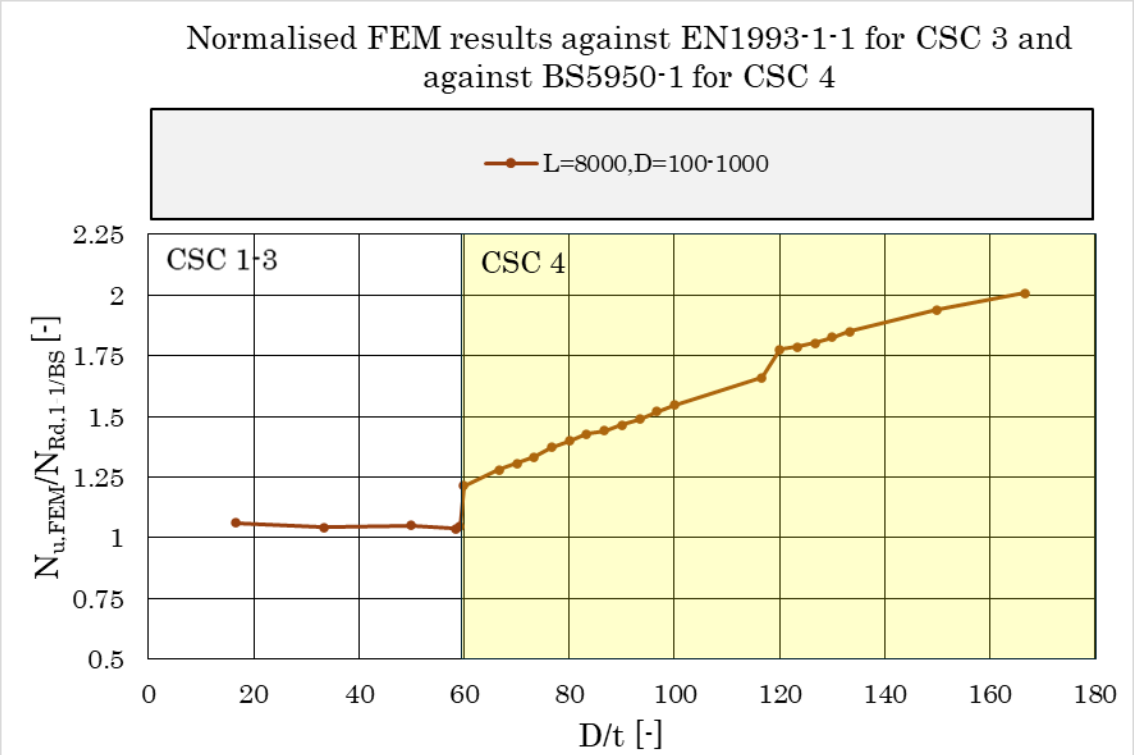
Normalised FEM results against EN1993-1-1 for CSC 3 and against BS5950-1 for CSC 4
L=8000,D=100-1000
CSC 1-3
CSC 4
$N_{u,FEM}/N_{Rd,1\ 1/BS}$ [-]
2.25
2
1.75
1.5
1.25
1
0.75
0.5
0
20
40
60
80
100
120
140
160
180
D/t [-]

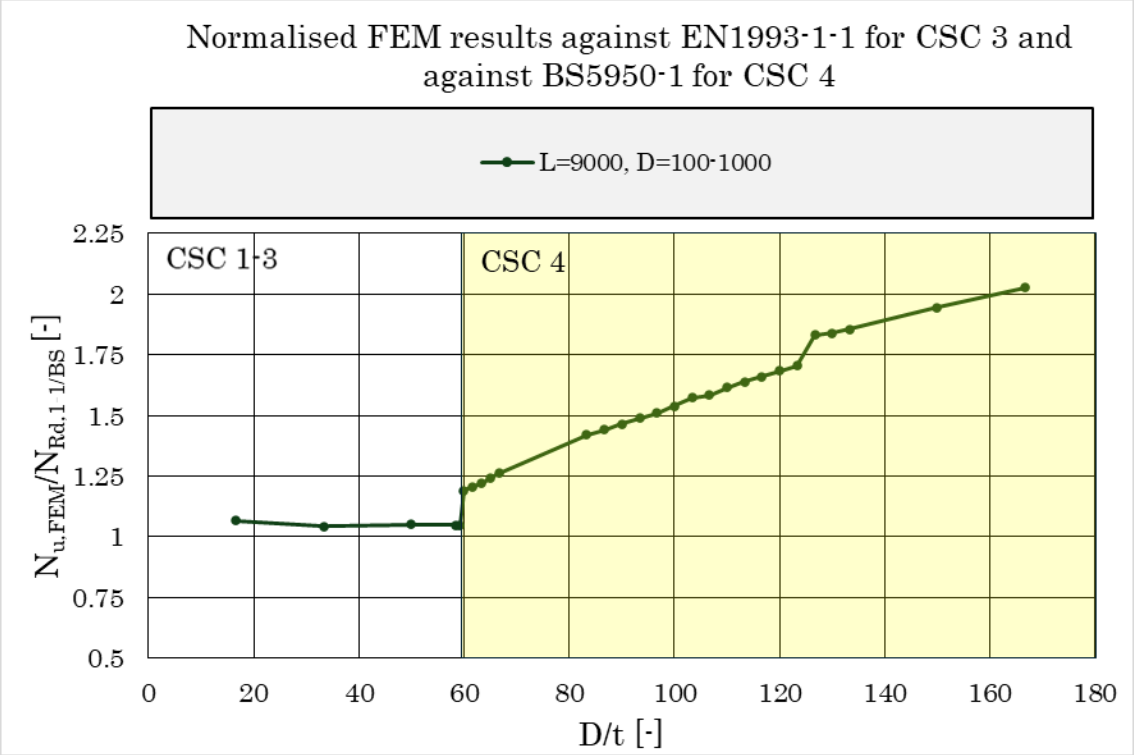
Normalised FEM results against EN1993-1-1 for CSC 3 and against BS5950-1 for CSC 4
L=9000, D=100-1000
CSC 1-3
CSC 4
$N_{u,FEM}/N_{Rd,1\ 1/BS}$ [-]
2.25
2
1.75
1.5
1.25
1
0.75
0.5
0
20
40
60
80
100
120
140
160
180
D/t [-]

E. Normalised FEM results against EN1993-1-1 for CSC 3 and against BS5950-1 for CSC 4

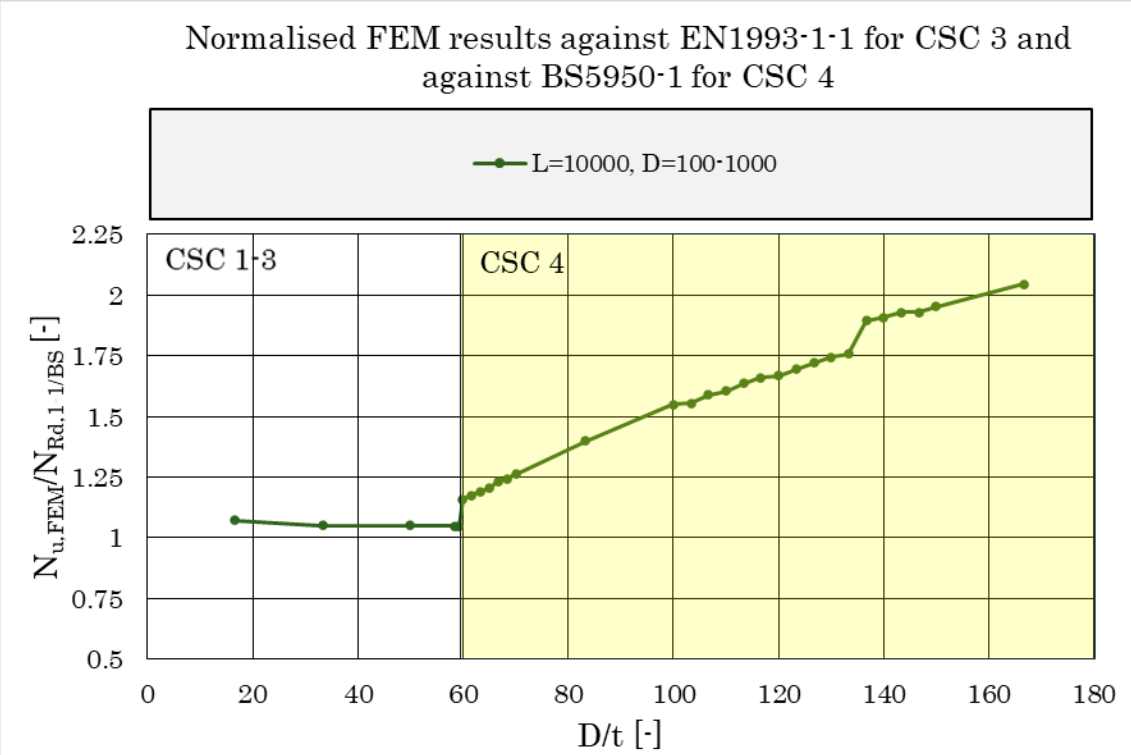

F

Normalised FEM results against EN1993-1-1 introducing a local reduction factor

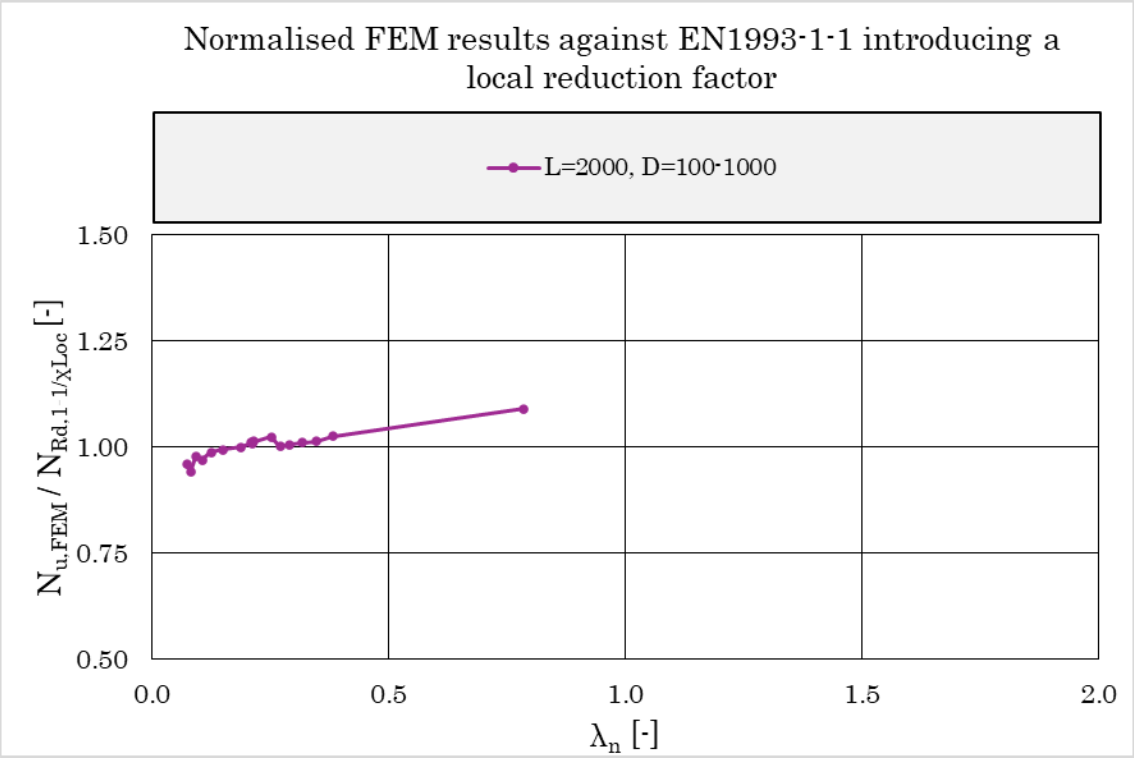

F. Normalised FEM results against EN1993-1-1 introducing a local reduction factor

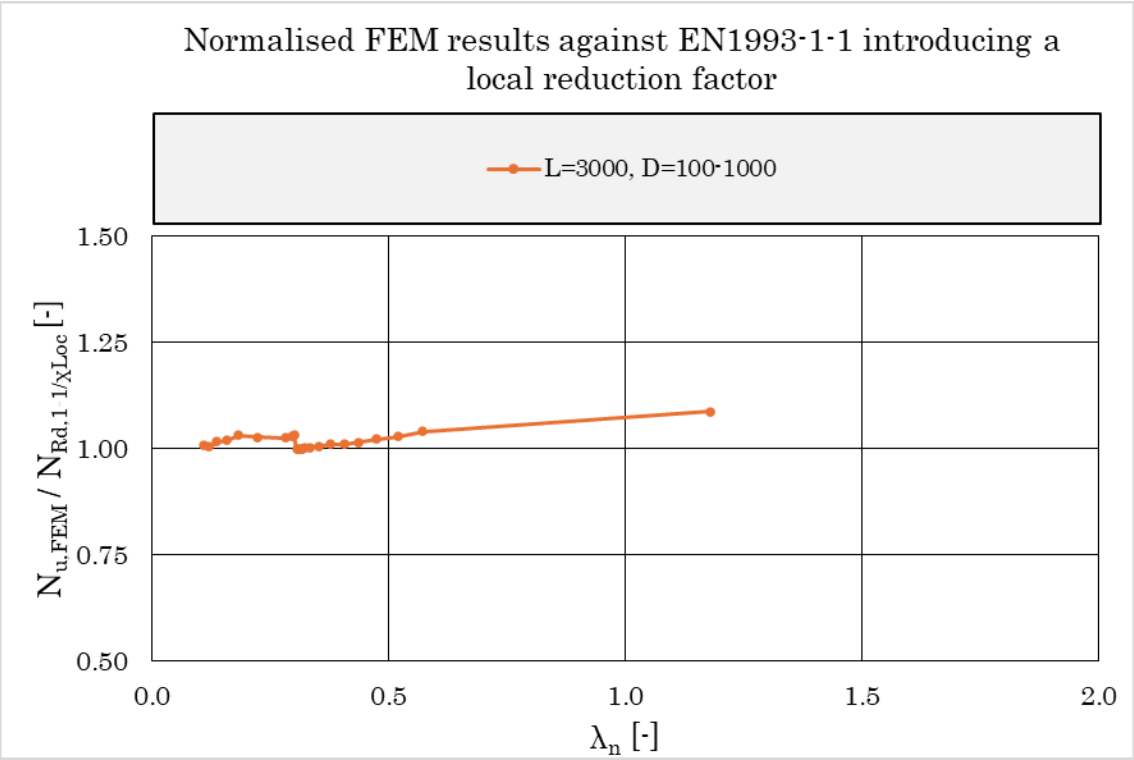

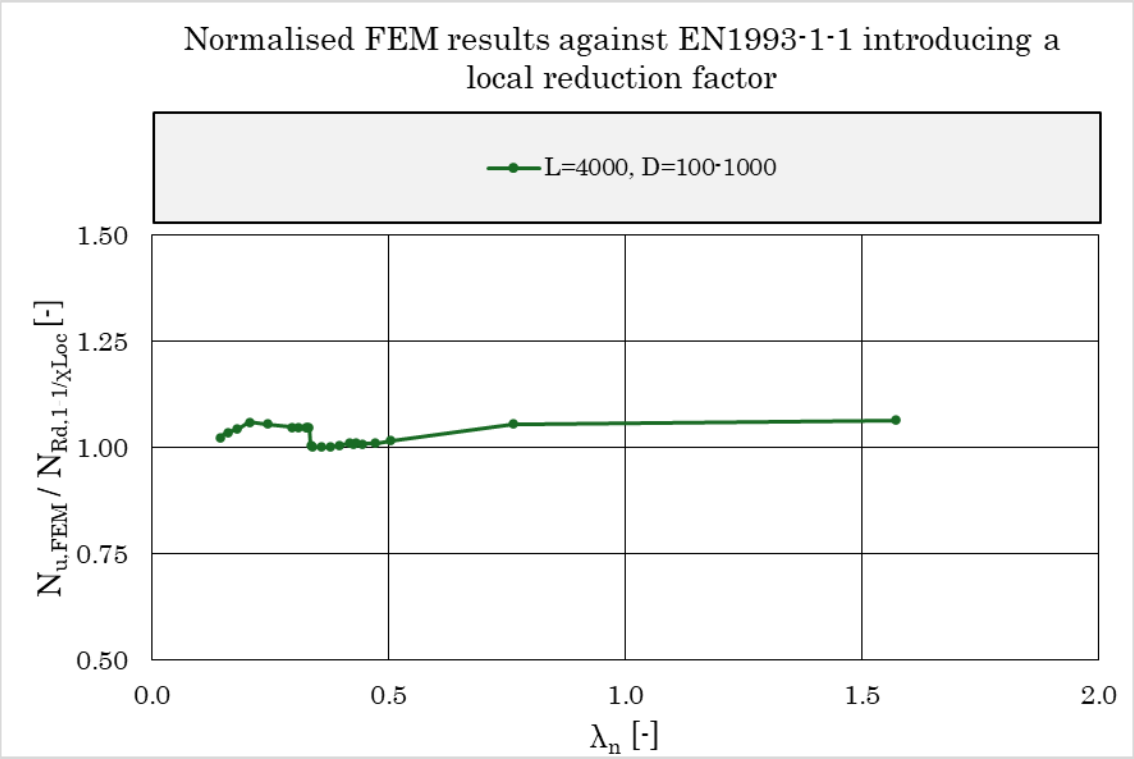

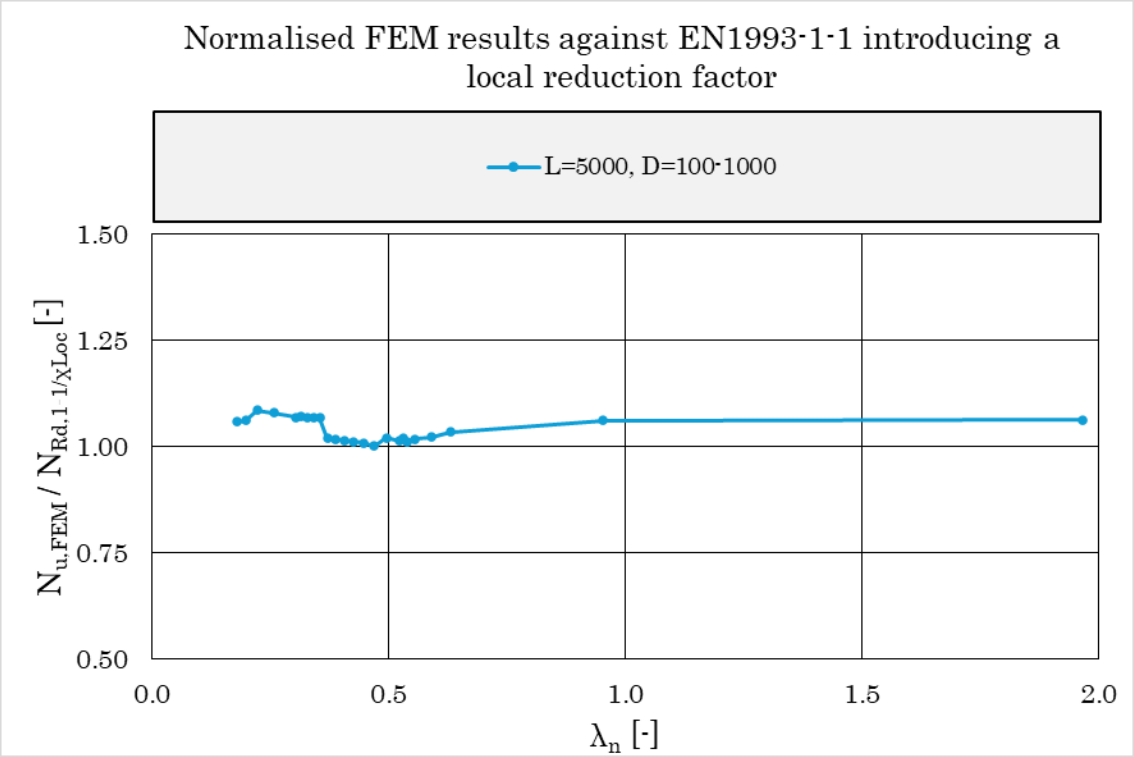
Normalised FEM results against EN1993-1-1 introducing a local reduction factor
L=5000, D=100-1000
1.50
1.25
1.00
0.75
0.50
0.0
0.5
1.0
1.5
2.0
$N_{u,FEM} / N_{Rd,1\ 1/\chi Loc}$ [-]
λ_n [-]

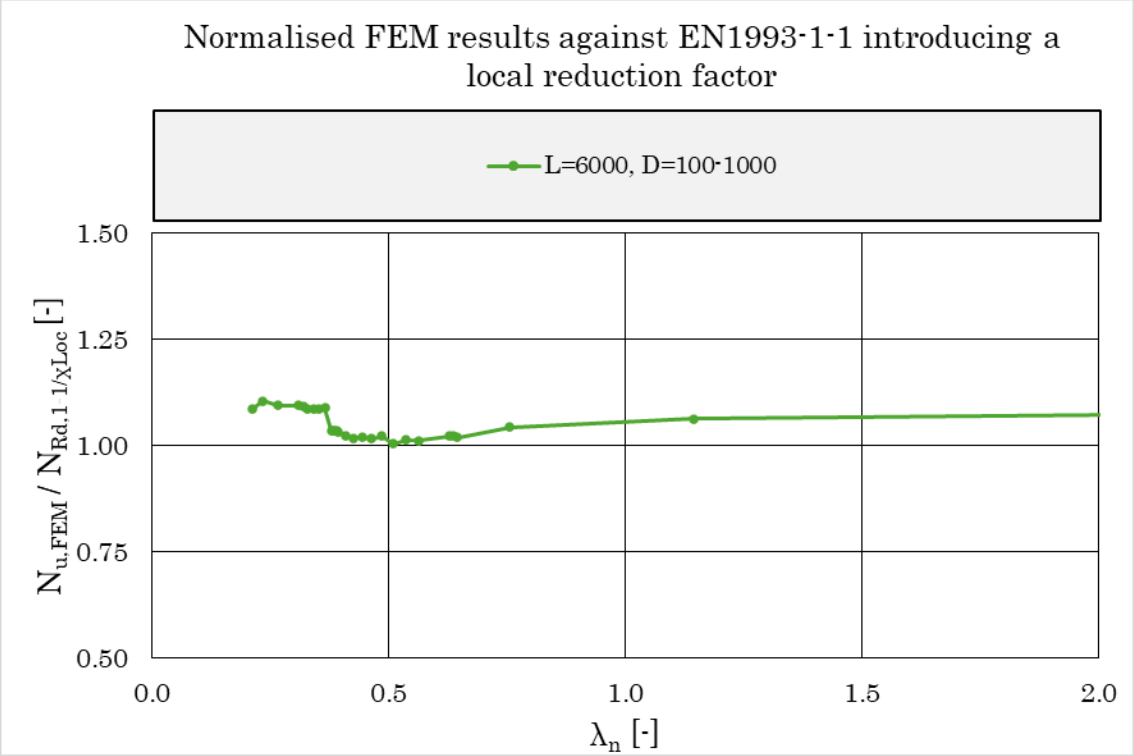
Normalised FEM results against EN1993-1-1 introducing a local reduction factor
L=6000, D=100-1000
1.50
1.25
1.00
0.75
0.50
0.0
0.5
1.0
1.5
2.0
$N_{u,FEM} / N_{Rd,1\ 1/\chi Loc}$ [-]
λ_n [-]

F. Normalised FEM results against EN1993-1-1 introducing a local reduction factor

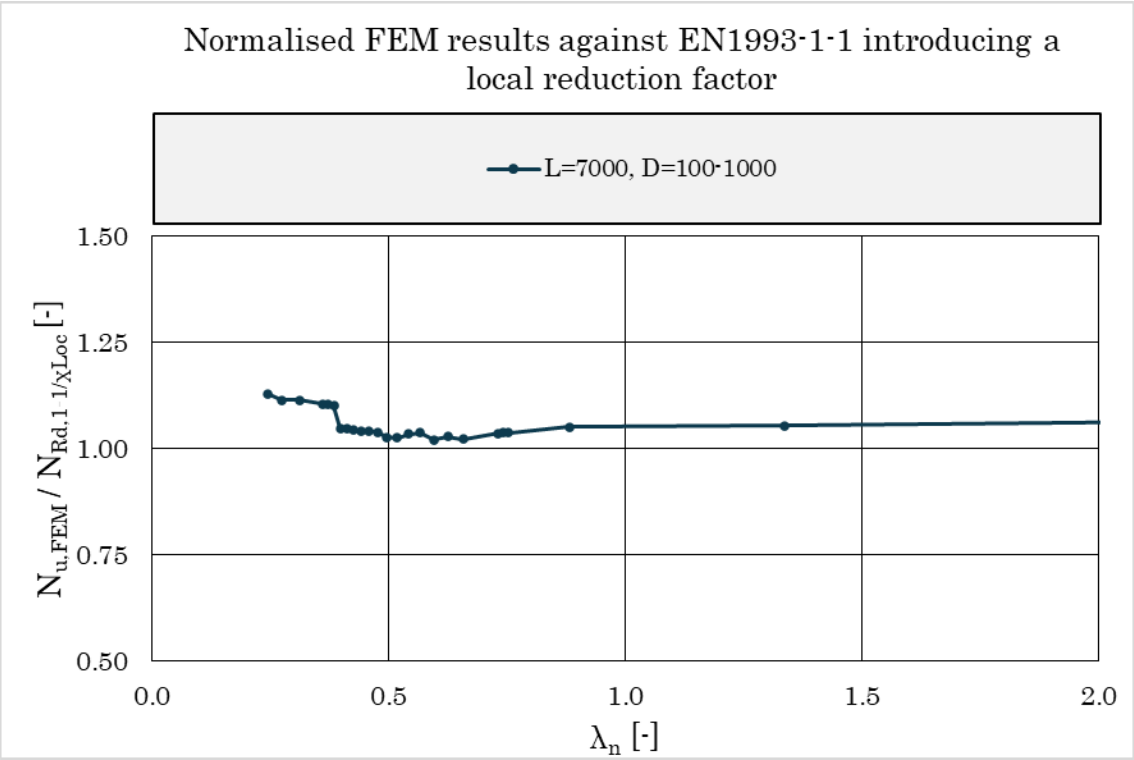

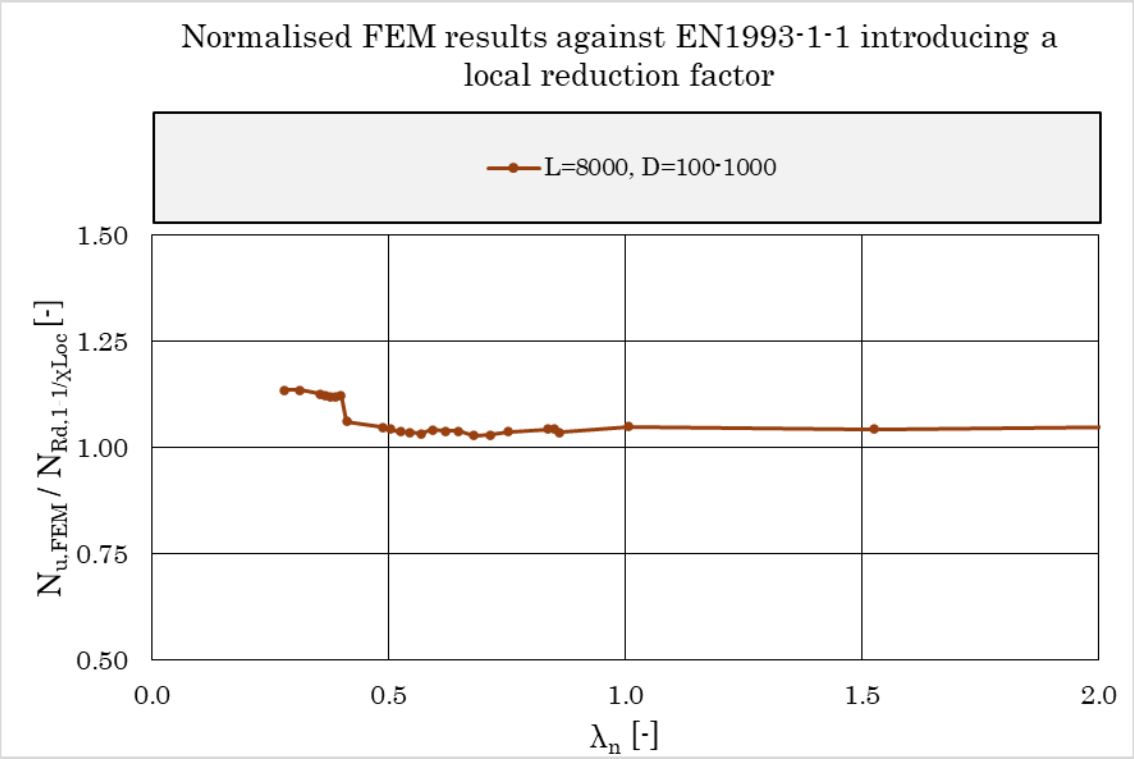

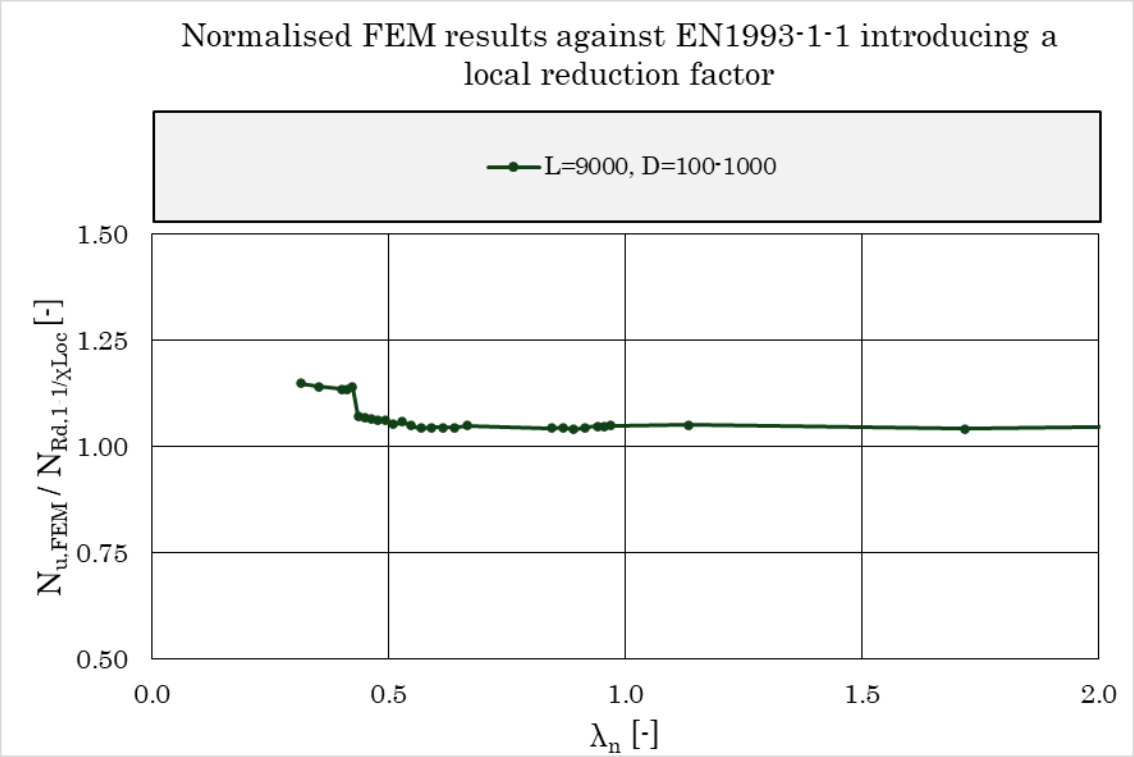
Normalised FEM results against EN1993-1-1 introducing a local reduction factor
L=9000, D=100-1000
1.50
1.25
1.00
0.75
0.50
0.0
0.5
1.0
1.5
2.0
$N_{u,FEM} / N_{Rd,1\ 1/\chi Loc}$ [-]
λ_n [-]

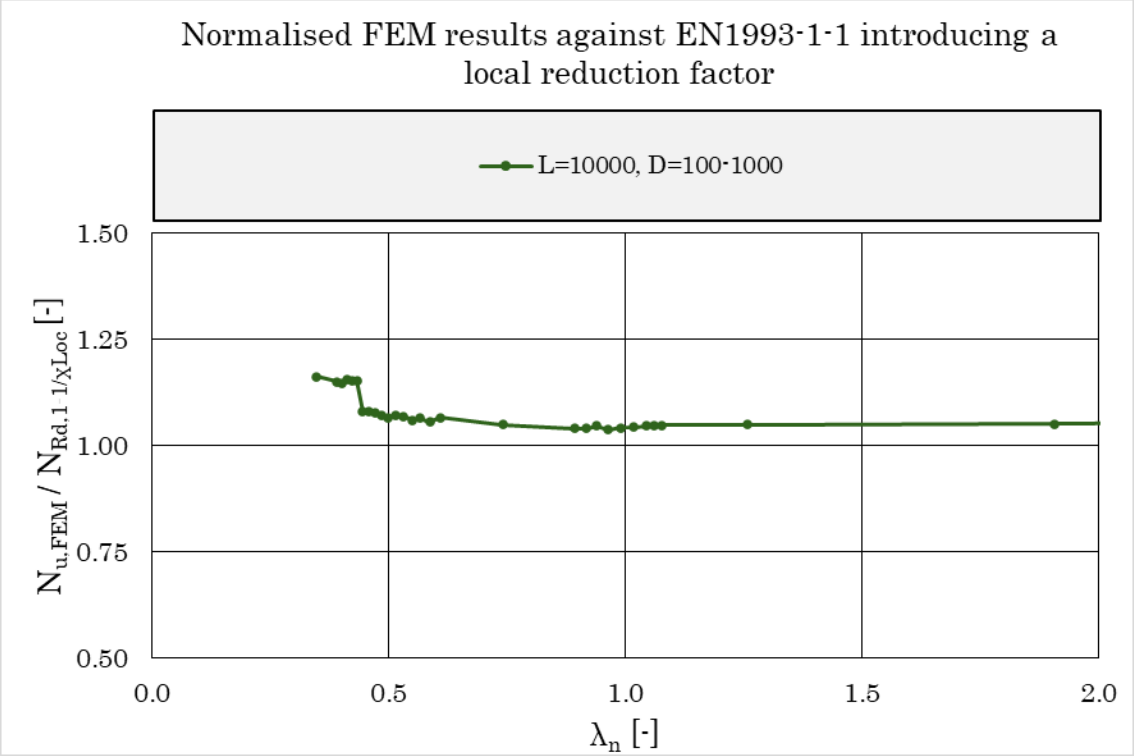
Normalised FEM results against EN1993-1-1 introducing a local reduction factor
L=10000, D=100-1000
1.50
1.25
1.00
0.75
0.50
0.0
0.5
1.0
1.5
2.0
$N_{u,FEM} / N_{Rd,1\ 1/\chi Loc}$ [-]
λ_n [-]

F. Normalised FEM results against EN1993-1-1 introducing a local reduction factor

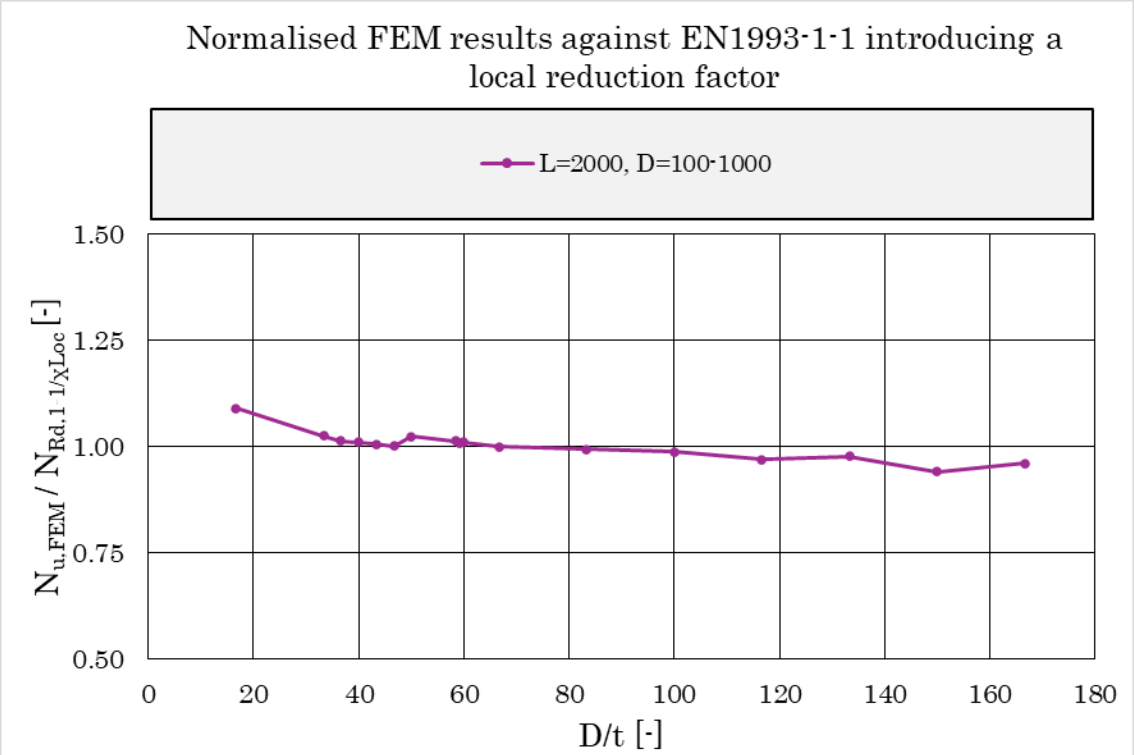

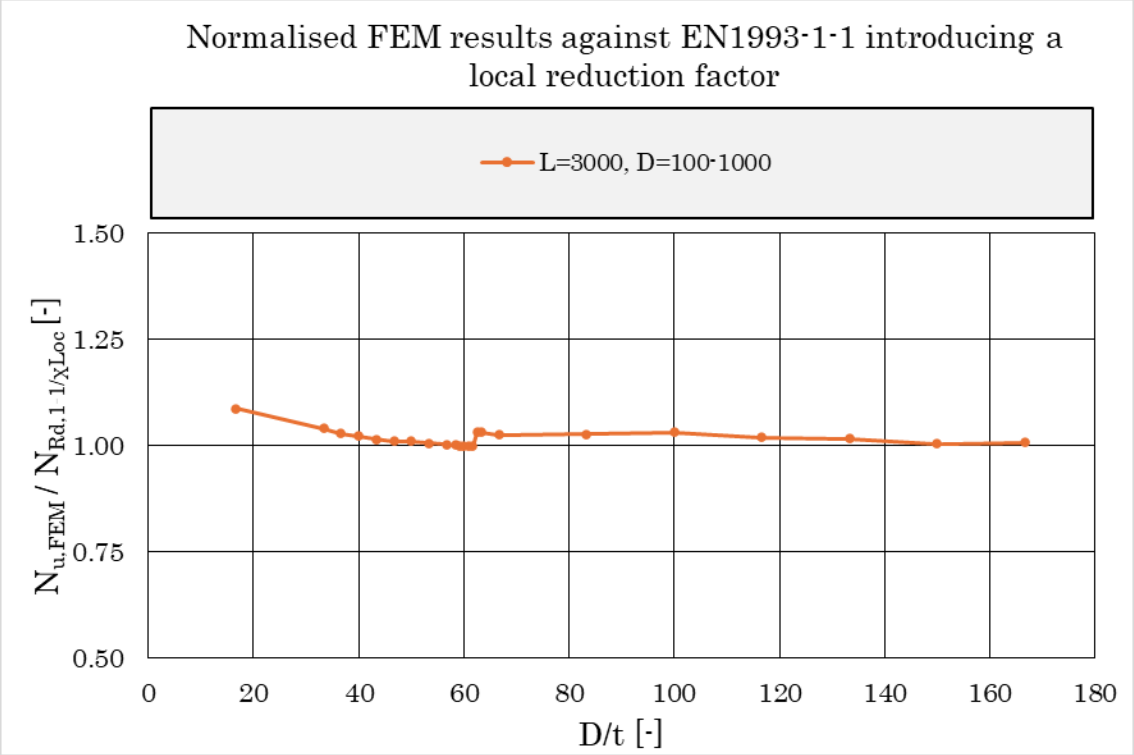

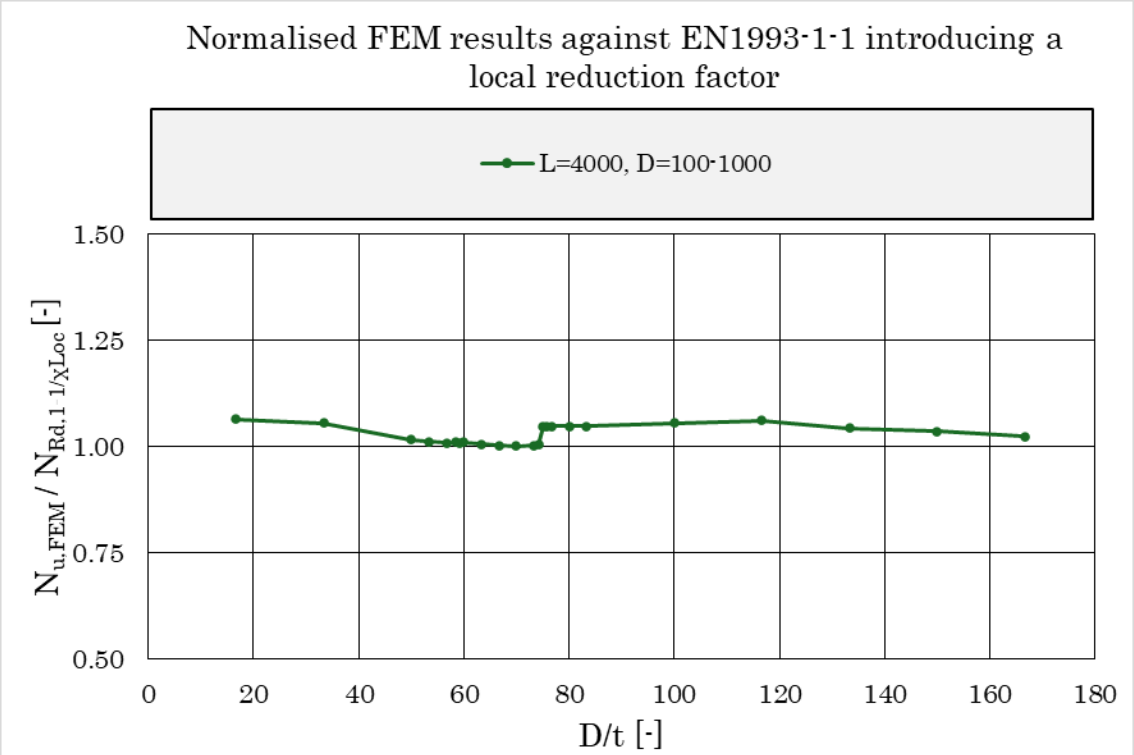
Normalised FEM results against EN1993-1-1 introducing a local reduction factor
L=4000, D=100-1000
1.50
1.25
1.00
0.75
0.50
N_u,FEM / N_Rd,1 1/χLoc [-]
0
20
40
60
80
100
120
140
160
180
D/t [-]

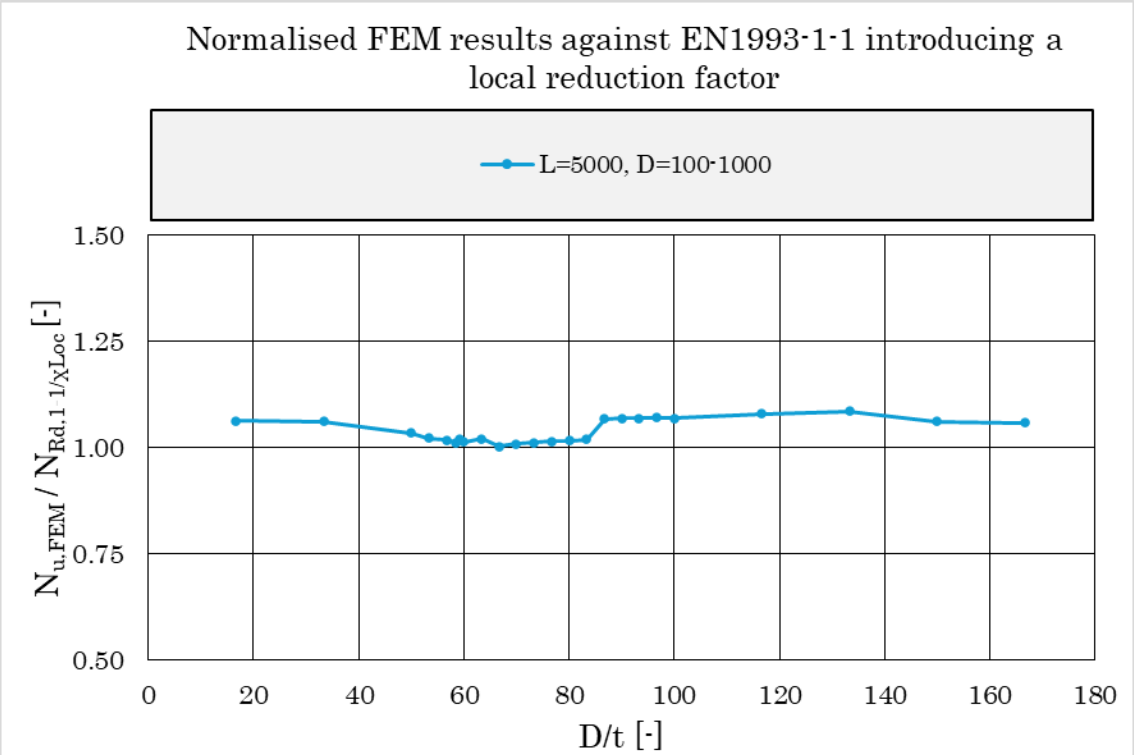
Normalised FEM results against EN1993-1-1 introducing a local reduction factor
L=5000, D=100-1000
1.50
1.25
1.00
0.75
0.50
N_u,FEM / N_Rd,1 1/χLoc [-]
0
20
40
60
80
100
120
140
160
180
D/t [-]

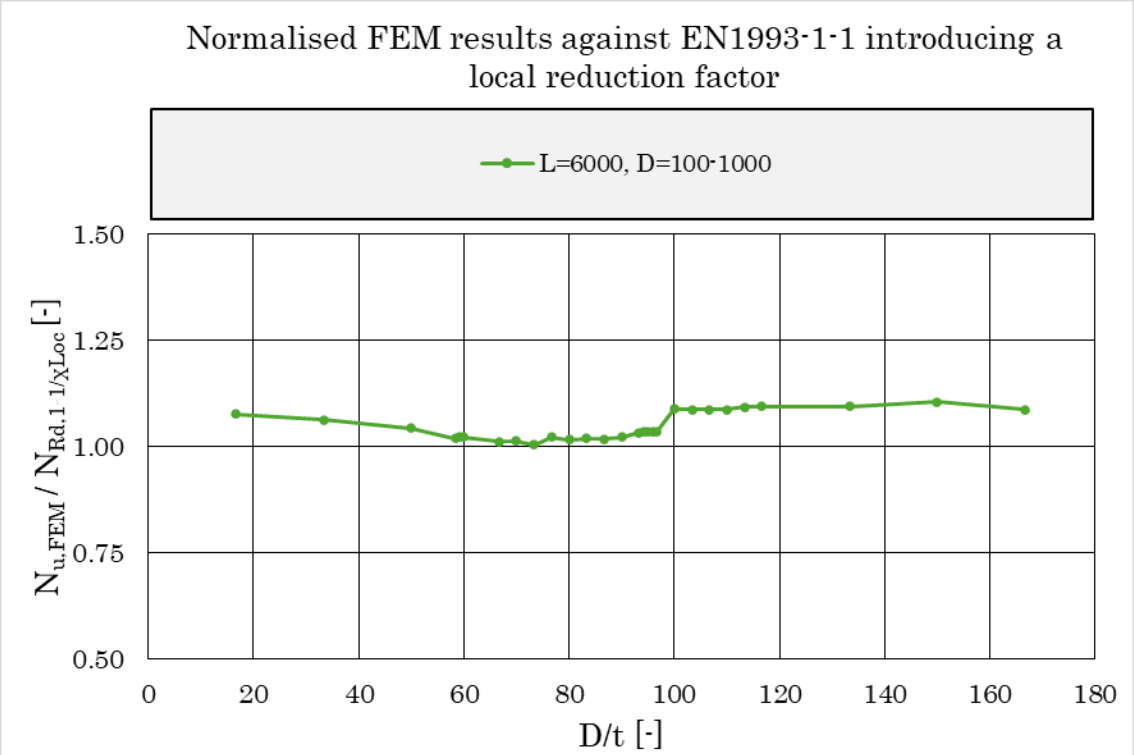
Normalised FEM results against EN1993-1-1 introducing a local reduction factor
L=6000, D=100-1000
1.50
1.25
1.00
0.75
0.50
$N_{u,FEM} / N_{Rd,1\ 1/\chi Loc}$ [-]
0
20
40
60
80
100
120
140
160
180
D/t [-]

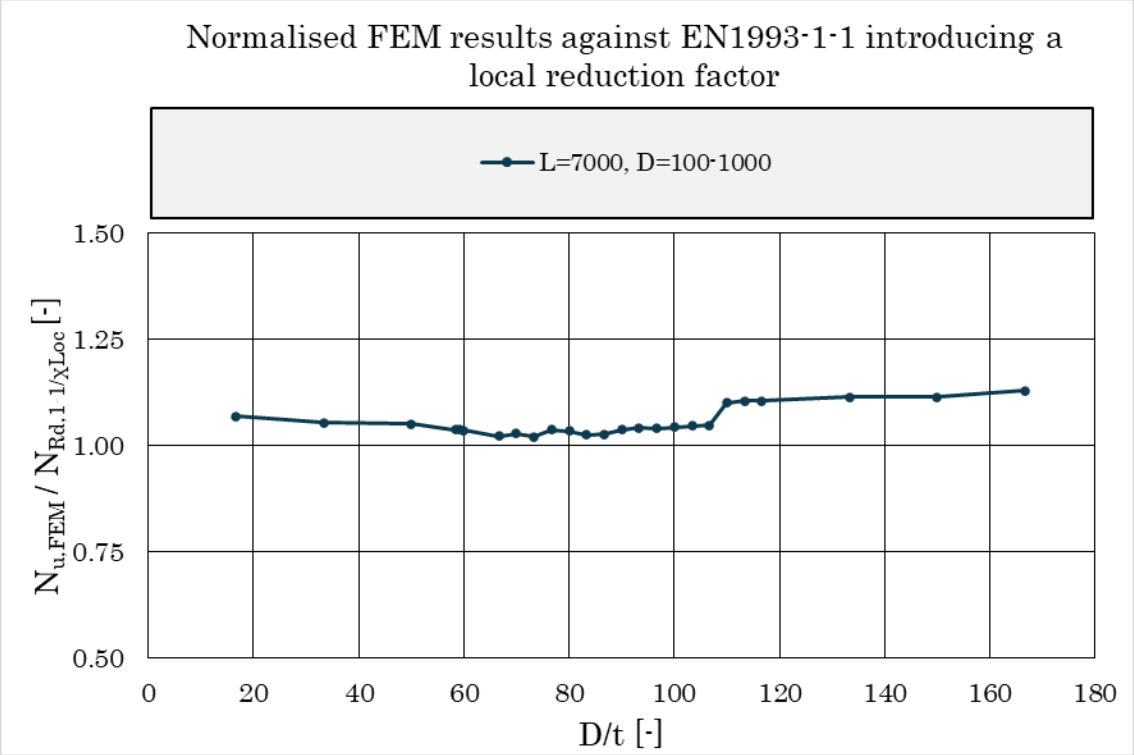
Normalised FEM results against EN1993-1-1 introducing a local reduction factor
L=7000, D=100-1000
1.50
1.25
1.00
0.75
0.50
$N_{u,FEM} / N_{Rd,1\ 1/\chi Loc}$ [-]
0
20
40
60
80
100
120
140
160
180
D/t [-]

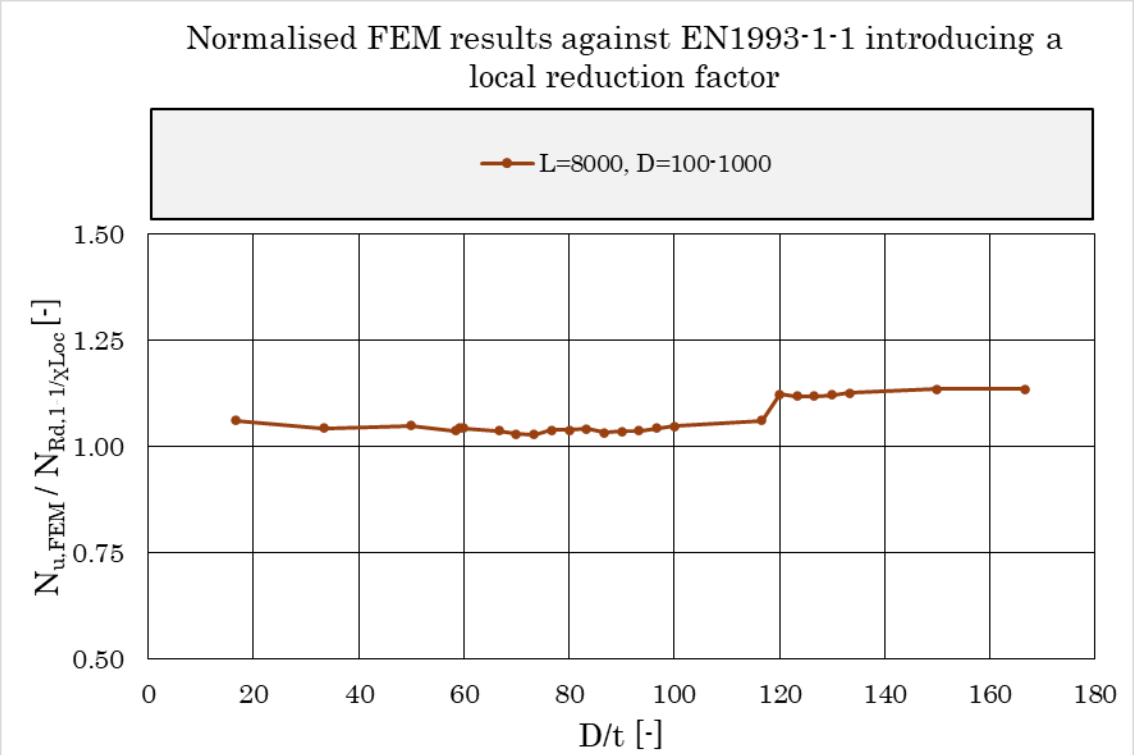
Normalised FEM results against EN1993-1-1 introducing a local reduction factor
L=8000, D=100-1000
1.50
1.25
1.00
0.75
0.50
$N_{u,FEM} / N_{Rd,1\ 1/\chi Loc}$ [-]
0
20
40
60
80
100
120
140
160
180
D/t [-]

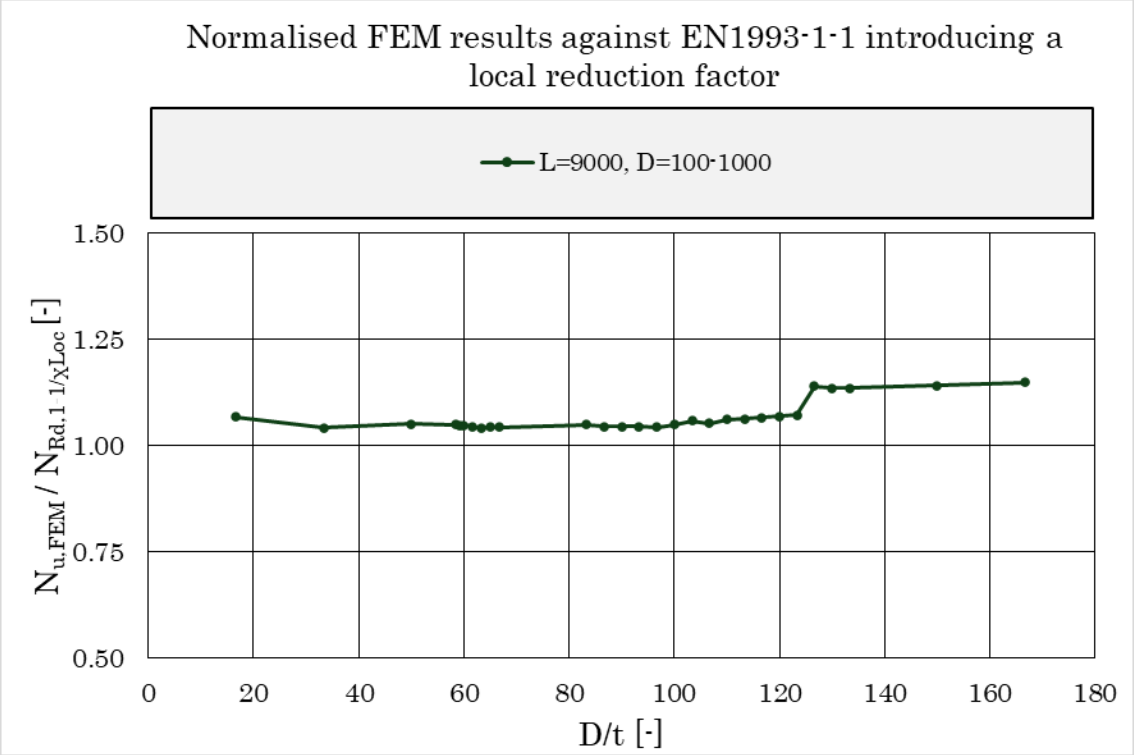
Normalised FEM results against EN1993-1-1 introducing a local reduction factor
L=9000, D=100-1000
1.50
1.25
1.00
0.75
0.50
$N_{u,FEM} / N_{Rd,1\ 1/\chi Loc}$ [-]
0
20
40
60
80
100
120
140
160
180
D/t [-]

F. Normalised FEM results against EN1993-1-1 introducing a local reduction factor

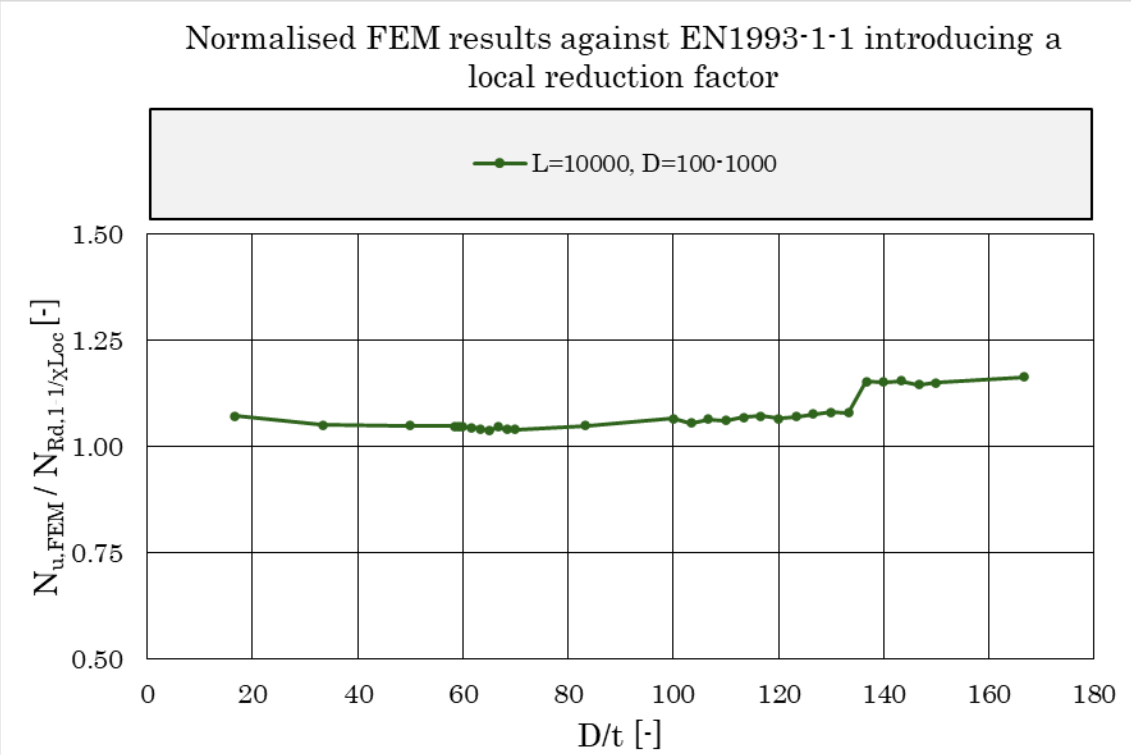

G

Imperfection sensitivity

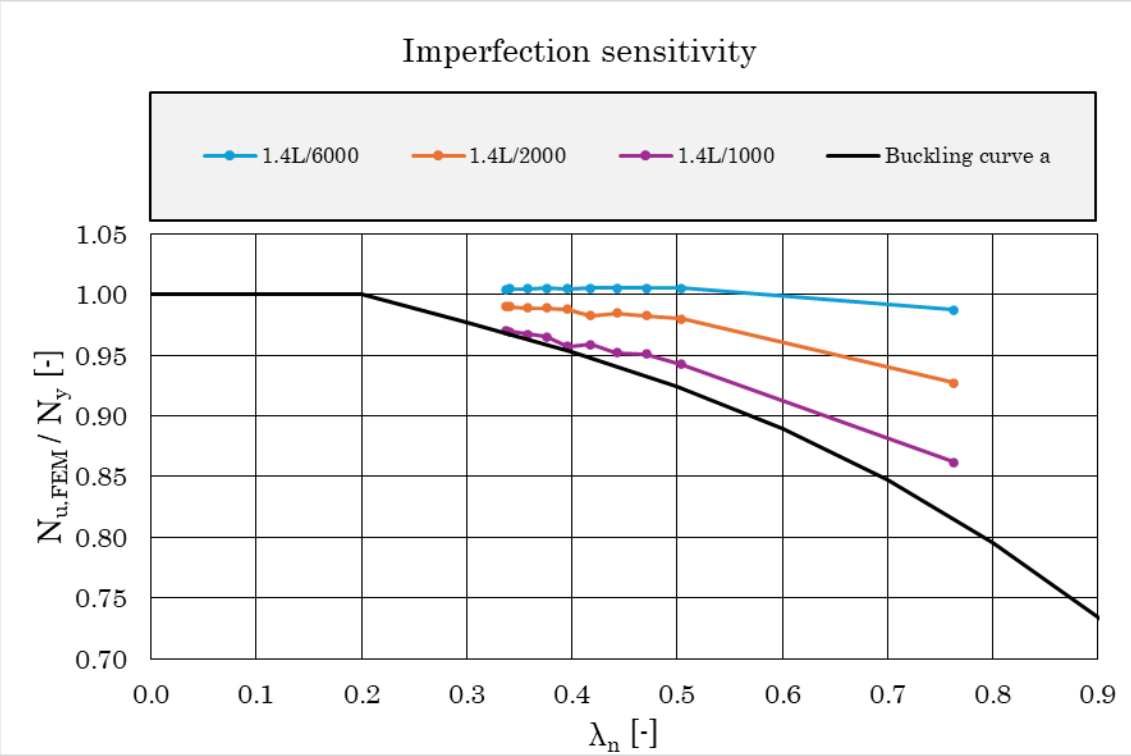

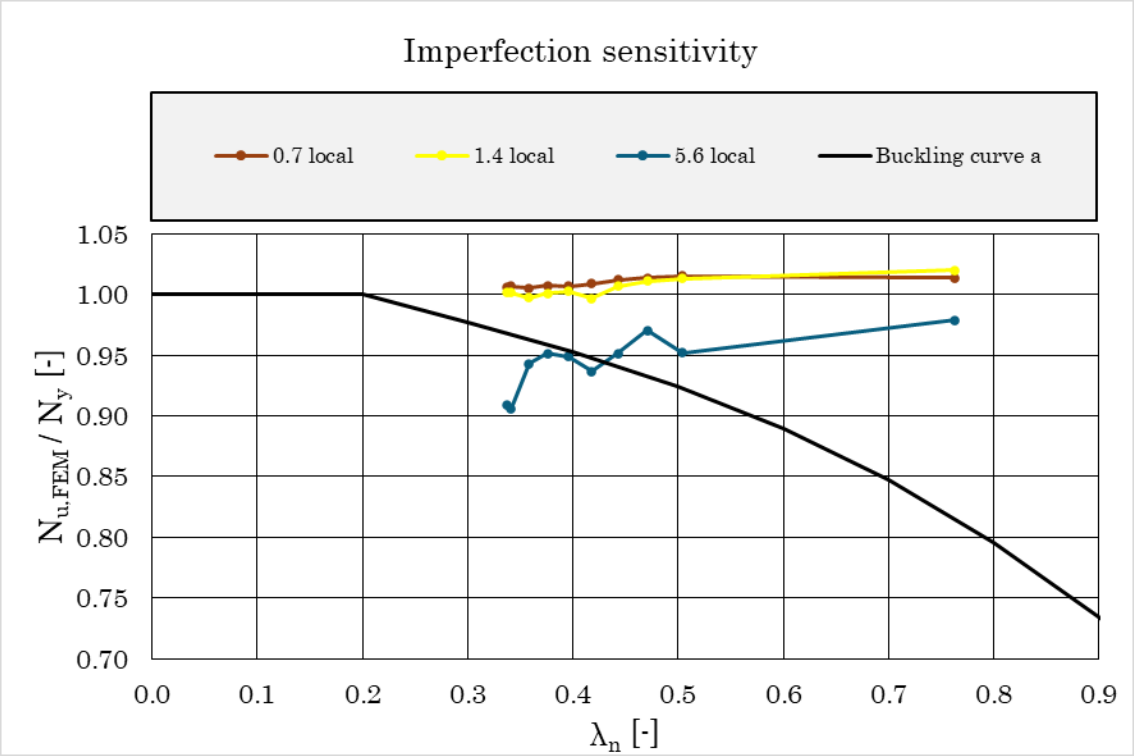
Imperfection sensitivity
0.7 local
1.4 local
5.6 local
Buckling curve a
1.05
1.00
0.95
0.90
0.85
0.80
0.75
0.70
$N_{u,FEM} / N_y$ [-]
0.0
0.1
0.2
0.3
0.4
0.5
0.6
0.7
0.8
0.9
λ_n [-]

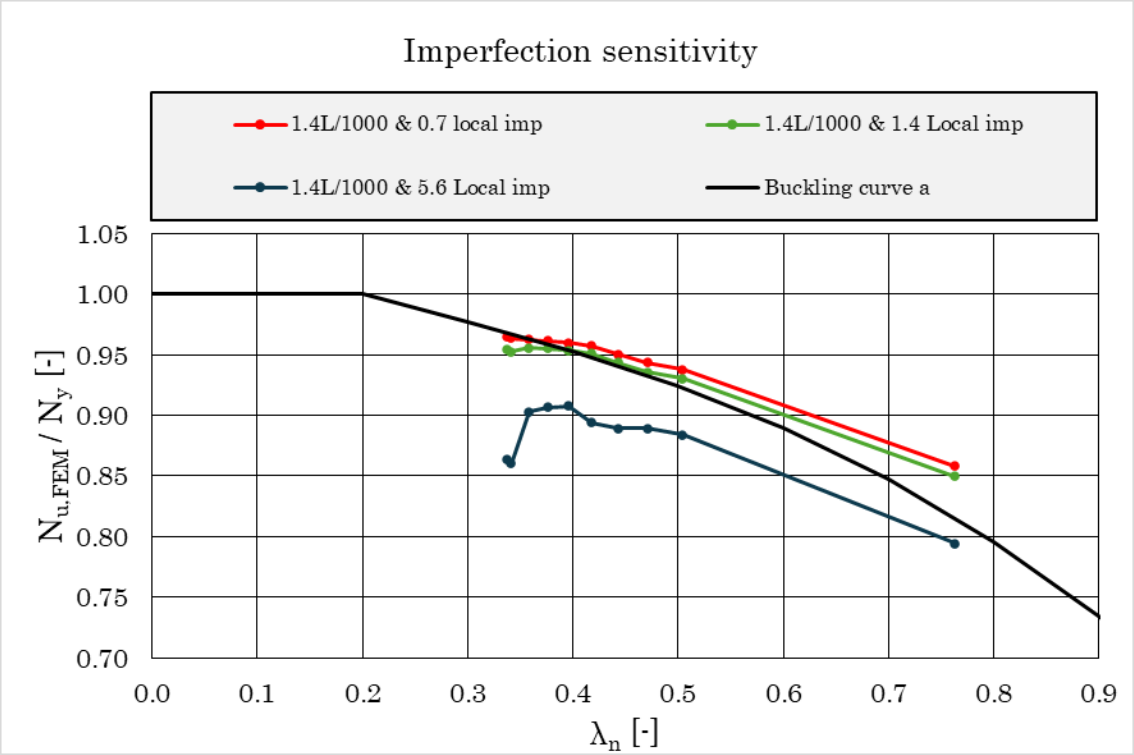
Imperfection sensitivity
1.4L/1000 & 0.7 local imp
1.4L/1000 & 1.4 Local imp
1.4L/1000 & 5.6 Local imp
Buckling curve a
1.05
1.00
0.95
0.90
0.85
0.80
0.75
0.70
$N_{u,FEM} / N_y$ [-]
0.0
0.1
0.2
0.3
0.4
0.5
0.6
0.7
0.8
0.9
λ_n [-]

Imperfection sensitivity									
λ_n	G: **1.4L/1000** **L: 0.7 local imp** [MN]	**G: 1.4L/1000** **L: -** [MN]	G: **1.4L/2000** **L: -** [MN]	G: **1.4L/6000** **L: -** [MN]	G: **1.4L/1000** **L: 1.4 local imp** [MN]	G: **1.4L/1000** **L: 5.6 local imp** [MN]	G: **-** **L: 0.7 local imp** [MN]	G: **-** **L: 1.4 local imp** [MN]	G: **-** **L: 5.6 local imp** [MN]
0.76	1.11	1.12	1.20	1.28	1.10	1.03	1.01	1.020	0.98
0.50	1.85	1.85	1.93	1.98	1.83	1.74	1.02	1.013	0.95
0.47	1.98	2.00	2.07	2.11	1.97	1.87	1.01	1.011	0.97
0.44	2.12	2.13	2.20	2.25	2.11	1.99	1.012	1.01	0.95
0.42	2.27	2.27	2.33	2.38	2.25	2.12	1.01	1.0	0.94
0.40	2.40	2.40	2.47	2.52	2.39	2.27	1.01	1.00	0.95
0.38	2.54	2.55	2.61	2.65	2.52	2.39	1.07	1.00	0.96
0.36	2.67	2.68	2.74	2.78	2.65	2.50	1.01	1.0	0.94
0.34	2.80	2.82	2.88	2.92	2.77	2.50	1.01	1.00	0.91
0.34	2.84	2.85	2.91	2.95	2.80	2.54	1.01	1.00	0.91

Table G.1: Comparison of values for different λ_n and imperfection configurations for L=4000 mm and D=200-445 mm.

DEPARTMENT OF SOME SUBJECT OR TECHNOLOGY
CHALMERS UNIVERSITY OF TECHNOLOGY
Gothenburg, Sweden
www.chalmers.se

CHALMERS
UNIVERSITY OF TECHNOLOGY